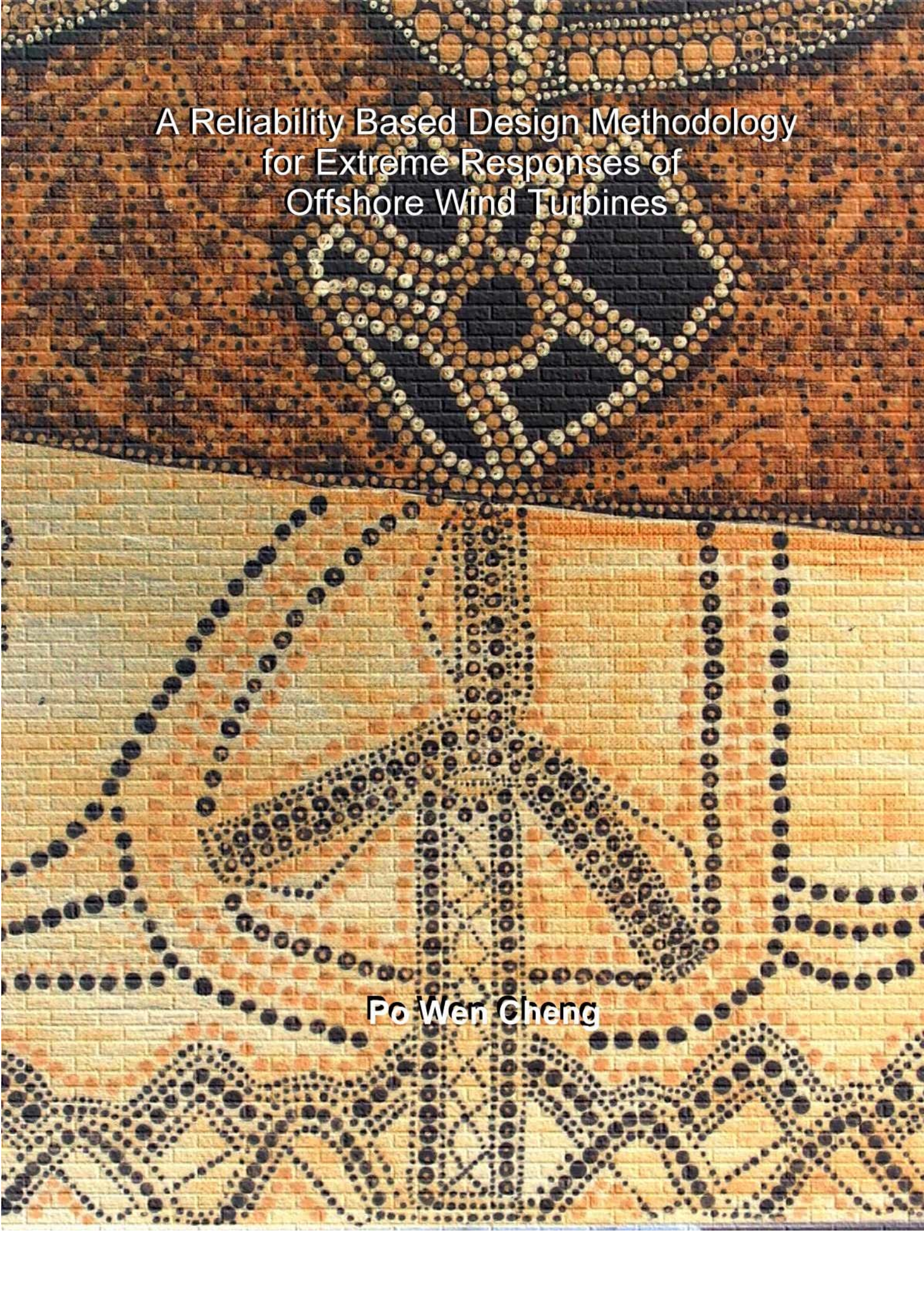
A Reliability Based Design Methodology
for Extreme Responses of
Offshore Wind Turbines
Po Wen Cheng

A RELIABILITY BASED DESIGN METHODOLOGY FOR EXTREME RESPONSES OF OFFSHORE WIND TURBINES

PROEFSCHRIFT

ter verkrijging van de graad van doctor
aan de Technische Universiteit Delft,
op gezag van de Rector Magnificus Prof. dr. ir. J.T. Fokkema,
voorzitter van het College voor Promoties,
in het openbaar te verdedigen op dinsdag 1 oktober 2002 om 13.30 uur

door

Po Wen CHENG

'Diplom-Ingenieur Luft- und Raumfahrt'
Technische Universität Berlin, Duitsland
geboren te Chang-Hua, Taiwan

Dit proefschrift is goedgekeurd door de promotor:

Prof. dr. ir. G.A.M. van Kuik

Toegevoegd promotor

Dr. G.J.W. van Bussel

Samenstelling promotiecommissie

Rector Magnificus, voorzitter,	Technische Universiteit Delft
Prof. dr. ir. G.A.M. van Kuik,	Technische Universiteit Delft
Dr. G.J.W. van Bussel,	Technische Universiteit Delft
Prof. dr. ir. J.H. Vugts,	Technische Universiteit Delft
Prof. ir. A.C.W.M. Vrouwenvelder,	Technische Universiteit Delft
Prof. dr. ir. J.M. van Noortwijk,	Technische Universiteit Delft
Dr. K.O. Ronold,	Det Norske Veritas, Oslo
Dr. P. Tromans,	Peter Tromans Consultancy, Den Haag
Prof. dr. ir. J. Meek	Technische Universiteit Delft, reservelid

ISBN 90-79468-08-7
DUWIND Delft University Wind Energy Research Institute

Keywords: Wind Energy, Offshore, Extreme, Dynamics, Reliability

Published and distributed by:
DUWIND Delft University Wind Energy Research Institute
Stevinweg 1, CN 2628 Delft, The Netherlands

Cover painting and design: Po Wen Cheng

Printed in the Netherlands by Sieca Repro, Delft.

Contents

Summary **v**

Acknowledgement **ix**

Notation **xi**

1 Introduction **1**
1.1 General . . . 1
1.2 Current design practice . . . 2
1.3 Motivation . . . 3
1.4 Approach . . . 5
1.4.1 Response based approach . . . 5
1.4.2 External condition based approach . . . 7
1.5 Structure of the thesis. . . . 7

2 Scope and Limitations **11**
2.1 Current status of the research topic . . . 11
2.2 Scope and limitations . . . 12
2.2.1 Prospects . . . 15

3 Offshore environment **17**
3.1 General description . . . 17
3.2 Wind climate . . . 18
3.2.1 Short-term description of wind . . . 18
3.2.2 Long-term description of wind . . . 20
3.3 Wave climate . . . 21
3.3.1 Short-term description of wave . . . 21
3.3.2 long-term description of wave . . . 22
3.4 Occurrence probability of the sea states . . . 23
3.5 Design Extreme Conditions . . . 29
3.5.1 Extreme wind gust . . . 29
3.5.2 Extreme wave height . . . 30
3.5.3 Combination of the extreme wind gust and the extreme wave height . . . 30

4 Wind turbine concepts **35**
4.1 Wind turbines in general . . . 35
4.2 Subsystems of horizontal axis wind turbines . . . 37
4.3 Operational range of the wind turbine . . . 38
4.4 Pitch controlled turbine . . . 39
4.5 Stall controlled turbine . . . 40

5 Load and Response models **43**
5.1 General Description of Load and Response . . . 43
5.2 Aerodynamic loading . . . 43
5.3 Hydrodynamic loading . . . 44
5.4 Response calculation with DUWECS . . . 46
5.5 Response calculation in the frequency domain . . . 48

6 External load parameters **49**
6.1 Table of the parameters variation . . . 49
6.2 Mean wind speed . . . 50
6.3 Turbulence intensity . . . 50
6.4 Wind shear . . . 52
6.5 Yaw misalignment angle . . . 53
6.6 Significant wave height and wave period . . . 53
6.7 Current speeds . . . 55
6.8 Selection of stochastic variables . . . 55

7 Statistical analysis **57**
7.1 Description of the General Methodology . . . 57
7.2 Extreme value distribution . . . 59
7.3 Distribution of POT models . . . 61
7.3.1 Fitting of the data to the distribution model . . . 62
7.3.2 Goodness of fit test . . . 64

8 MAX models **67**
8.1 summary . . . 67
8.2 Simulation number and simulation length . . . 67
8.2.1 Study of the number of simulations for wind . . . 67
8.2.2 Study of the number of simulations for waves . . . 72
8.2.3 Bootstrap of the simulation results . . . 74
8.2.4 Correlation of the distribution parameters . . . 79
8.2.5 Study of the wind simulation length . . . 81
8.2.6 Study of the wave simulation length . . . 84
8.2.7 Selection of a number of simulations and a simulation length 85
8.3 Statistical uncertainties . . . 86
8.3.1 Bayesian analysis of the uncertainties . . . 86
8.3.2 Uncertainties of the distribution parameters . . . 88
8.3.3 Uncertainties of the choice of distribution . . . 92

8.3.4 Including the two types of statistical uncertainties in the estimates . . . 97
8.3.5 Variation of the estimates caused by different fitting methods . . . 97
8.4 Remarks on this chapter . . . 100

9 Peak Over Threshold (POT) method 101
9.1 Summary . . . 101
9.2 Fitting of the data to POT distribution models . . . 102
9.3 Influence of the number of simulations . . . 103
9.4 Selection of the threshold . . . 106
9.5 Peak counting method . . . 109
9.6 Uncertainties . . . 110
9.6.1 Linear correlation of the neighbouring peaks . . . 110
9.6.2 Combination of POT models with different peak counting methods . . . 111

10 Process model 115
10.1 summary . . . 115
10.2 Gaussian model . . . 116
10.3 Weakly non-Gaussian models . . . 119
10.3.1 Weakly non-Gaussian model with skewness correction . . . 119
10.3.2 Non-Gaussian model with skewness and kurtosis correction 122
10.4 Process models applied to the overturning moment . . . 124
10.5 Selection of the model . . . 125

11 Long-term distributions 127
11.1 Relevant sea states for the long-term distribution . . . 127
11.2 Contributions of the conditional distributions . . . 129
11.3 Variation of the extrapolation parameters . . . 132

12 Constrained simulation 137
12.1 Introduction . . . 137
12.2 Extreme gust response . . . 138
12.2.1 General considerations . . . 138
12.2.2 Deterministic gust model . . . 140
12.2.3 Stochastic gust model . . . 140
12.2.4 Gust response variations due to different gust models . . . 142
12.2.5 Gust response distribution . . . 147
12.2.6 Number of constrained simulations . . . 153
12.2.7 Choice of distribution functions . . . 157
12.3 Extreme wave response distribution . . . 159
12.3.1 Deterministic models of extreme wave . . . 159
12.3.2 Stochastic model of extreme waves . . . 160
12.4 Combination of extremes . . . 163
12.4.1 Combination of the extreme wind gust and waves . . . 163

12.4.2 Comparison of different load combinations 164
12.4.3 Time dealy between the extreme gust and extreme wave . 165
12.5 Application of the constrained simulations 168

13 Application of the methods **169**
13.1 Introduction 169
13.2 Response based models 171
13.2.1 Pitch controlled turbine 171
13.2.2 Stall controlled turbine 173
13.2.3 Choice of Distributions/ Bayesian analysis 175
13.3 External condition based models 179
13.3.1 External conditions: GL approach 179
13.3.2 Model 1/ steady wind 183
13.3.3 Model 2/ IEC gust 183
13.3.4 Model 3/ constrained gust 184
13.3.5 Comparisons of the response based and external condition based approaches 185

14 Conclusions **189**
14.1 General conclusions 189
14.2 Specific conclusions 190
14.3 A proposed approach 192
14.4 Recommendation for future research 193

A Appendix **203**

B Frequency domain response **205**
B.1 Methodology 205
B.2 Application 206
B.2.1 External conditions 206
B.2.2 Load and response 208
B.2.3 Response distributions 209
B.2.4 Frequency Domain or Time Domain method 212

C Wind turbines data **215**

Samenvatting (Dutch) **217**

About the author **221**

Summary

Offshore wind energy has emerged as a viable supplement to onshore wind energy. Large scale offshore wind power plants will contribute significantly to the share of renewable energy in the future energy mix.

The structural design of the offshore wind turbine faces new challenges from the harsh offshore environment of the North Sea. One of the additional design aspects that onshore wind turbines have not been confronted before is the hydrodynamic loading. The combined extreme wind and wave loading can be an important issue for the structural design. It has been shown that an extreme load condition does not necessarily lead to extreme response of the offshore wind turbine. In this study, the emphasis will be on the extreme response of offshore wind turbines.

The environmental contour of the site where the turbine is located is determined using joint statistics of the mean wind speed, significant wave heights and wave periods. The information on the environment is provided by hindcast data. The joint probability density of wind and waves is used to specify extreme load conditions.

The extreme response of the offshore wind turbine to the external load conditions can be determined in the frequency domain and in the time domain. Due to the non-linear response characteristics of the turbine, the time domain approach is to be preferred. The simulation results are analysed with different methods to obtain conditional distributions of the extreme response. These methods use different information from the time series. The MAX approach uses the maximum of each simulation, the POT approach uses the peaks, i.e. local maxima, above a given threshold, and the Process model uses the statistical moments of the time series to determine the extreme response distributions.

The number of stochastic variables has to be limited. The mean wind speed, the significant wave height and the zero up-crossing period are chosen after performing a sensitivity study of the turbine response to the variation of different stochastic variables. The variation of the extreme response distribution to the number of simulations and length of simulations is studied. The recommended number of simulations is 50 and the recommended length of simulations is 40 minutes, for the MAX method. The uncertainties of the distribution models and distribution parameters are taken into account with a Bayesian analysis. The use of non-informative priors does not add significant variation to the estimates. The Bayesian analysis provides a formal criterion for the choice of the distribution

model.

The POT and Process models can yield similar estimates of the extreme response with respect to the MAX method with significantly fewer simulations. To form the long-term distribution of the extreme response, one needs to take into account all the conditional distributions from different sea states. It can be shown, however, that in the presence of few dominating conditional distributions, it is not necessary to take all the sea states into account for long-term estimates of the response, but only those that dominate the tails of the long-term distribution.

The three methods mentioned above are response based, thus the extreme responses with a certain return period are determined by the response distribution. External condition based methods determine the return period of the external conditions (50 year gust, 50 year extreme wave etc.) and assume that the obtained response has an equivalent return period as the external conditions. The two methodologies to obtain extreme responses are applied to two example turbines, one with pitch control and the other one with stall control

The extreme external conditions are currently represented with deterministic models of extreme wind and waves. Stochastic models can be constructed with constrained simulations. In this case, constrained simulations are used to construct extreme wind gust and extreme waves with stochastic properties. The response from constrained gusts and waves are compared to the response obtained with deterministic models. For the pitch regulated turbine analyzed here, the constrained gust does not present a real threat to the turbine, since the controller is able to filter the constrained gust loads. For the stall regulated turbine, the constrained gust and the deterministic gust gave similar estimates of the responses.

The extreme wind gust and extreme wave do not necessarily occur at the same time. A time lag is introduced between the two maxima. The time lag is applied for both deterministic models and constrained gusts and waves. The calculated responses from deterministic models decrease sharply for increasing time lag, while the decrease for constrained models is more gradual. The time lag can have significant influence on the response of the support structure, while it has no effect on the blade response.

The external condition based method does not give an accurate estimate of the extreme response, since the extreme response is not correlated with extreme environmental conditions. For the stall regulated turbine, the external condition based estimates are consistently higher than the response based estimates. Currently, the design codes prescribe extreme external conditions for the determination of the extreme response. Moreover, the extreme mean wind speed prescribed by the design codes is considerably higher than the extreme mean wind speed obtained by a statistical analysis of the hindcast data. The correlation between extreme response and extreme load conditions is evident for the stall controlled turbine but not for the pitch controlled turbine. The extreme response distribution can be used to determine the failure probability of the structure, forming the basis of a risk based design approach.

The load situations considered here exclude special load cases that can arise

during installation, failure of a subcomponent, e.g. the blade pitch mechanism, non-stationary events etc. It is assumed that the turbine is functioning in the normal operation modes. The results obtained are strictly speaking only valid for the chosen turbine configuration and the chosen location, since they determine the response characteristics as well as the external load conditions. The methodology, however, can be applied for different types of offshore wind turbines at different sites.

Acknowledgement

It is probably impossible to thank all the people who have contributed in one way or another to the conclusion of this thesis. To start with I would like to thank my parents who have been very patient and encouraging. After all it took me five different studies in five different universities to realise that it is not about what you study but how you study. My sisters are also very supportive when I decided to study in a foreign country. Thanks to Erika for her continuous support and belief which helped me push through the last stage of this thesis. My house mates from the EduP who gave me a warm welcome when I returned from Berlin.

The environment and the friendly and informal atmosphere at the Section Wind Energy was stimulating and at the same time offers me a lot of freedom for the pursuit of scientific research. My colleagues have to be thanked for in the first place. Wim Bierbooms, who shares the same office with me has been enticing me all these years with the Dutch delicacy, 'drop', is thanked for the fruitful discussions. The work with him during the New Gust project has also contributed to the content of the thesis.

The broad scope of the thesis leads to a scientific supervising team including expertises from wind energy, offshore technology and structural reliability. The cross-fertilisation of the different subjects is very appreciated. Thanks goes to my daily supervisor Dr. Gerard van Bussel and my supervisor Prof. dr.ir. Gijs van Kuik for the constant encouragement. The quality of the thesis has been improved considerably thanks to the scrutinies and comments from Prof. dr. ir. Jan Vugts. The application of structural reliability methods has been greatly facilitated thanks to the expertise offered by Prof ir. Vrouwenvelder.

The members of the examination committee are thanked for their dedication to the examination of the thesis.

Notation

Abbreviations

A-D	Anderson-Darling
CDF	Cumulative distribution function
ESDU	Engineering Science Data Unit
EV	Extreme Values
FD	Frequency Domain
GEV	Generalised Extreme Value (Distribution)
GL	Germanischer Lloyd
GP	Generalised Pareto (Distribution)
IEC	International Electrotechnical Committee
JCSS	Joint Committee Structural Safety
K-S	Kolmogorov-Smirnov
MAX	Maximum
MLE	Maximum Likelihood Estimate
OTM	Overturning Moment
OWT	Offshore Wind Turbine
PDF	Probability density function
POT	Peak over Threshold
Std	Standard deviation
TD	Time Domain

Symbols		unit
A	amplitude	
A^2	Anderson-Darling test value	
C_D	Drag coefficient	
C_M	Inertial coefficient	
D	Kolmogorov-Smirnov test value	
	diameter of tower	m
E	Expectation	
F	Cumulative probability function	
G_0	Gumbel distribution	
G_γ	Generalised extreme value distribution	
G_α	Frechét distribution	
G_k	3 parameter Weibull distribution for the minima	
$H_{\max}$	Maximum wave height	m
H_{s}	Significant wave height	m
I	Turbulence intensity	
M	Response variable	Nm
M_{T}	Full plastic moment	
N_{m}	Number of local maxima	
N_{wave}	Number of waves	
N_0	Number of upcrossings	
N_{10}	Number of 10 minutes period	
P	Probability	
P_{f}	Failure probability	
R	Auto correlation function	
$\dot{R}$	First time derivative of the Auto correlation function	
S	Spectral density function	
T_{z}	Zero upcrossing period	s
$\bar{U}$	Mean wind speed	m/s
U_c	Current speed	m/s
W_0	Exponential distribution	
W_γ	Generalised Pareto Distribution	
X, Y, Z	Process variables	

c	Coefficients of curve fitting	
f	1-Probability density function	
	2-Frequency	Hz
k	1-von Karman constant	
	2-Shape parameter of the Weibull distribution	
m_n	N^{th} spectral moment	
s	Scale parameter	
u	1-Location parameter	
	2-water particle velocity	m/s
u_{cr}	Constrained wind gust speed	m/s
$\dot{u}$	1-Wind acceleration	$\mathrm{m/s^2}$
	2-Water particle acceleration	$\mathrm{m/s^2}$
u'	Gust factor	
$u*$	Friction velocity	m/s
z	Height	m
z_0	Roughness length	m
Γ	Gamma function	
Φ	Standard normal cumulative distribution	
Θ	Parameter set	
χ^2	Chi-Square test value	
α	1-Exponent of the power law	
	2-regularity factor	
β	Skewness	
γ	Shape parameter	
γ_{e}	Euler number	
ϵ	Correction factor	
ζ	Standard normal process	
κ	Kurtosis	
λ	Average number of peaks per time unit	
μ	Mean	
ρ_w	Density of water	$\mathrm{kg/m^3}$
σ	Standard deviation	
σ_{f}	Yield stress	$\mathrm{N/m^2}$
τ	Length of stationary time period	s
ϕ_y	Yaw misalignment angle	degree

Chapter 1

Introduction

1.1 General

Wind energy is going through a period of steady growth The research programs that have been carried out have contributed to the maturing of wind energy technology. The growth is partly induced by positive political signals and financial incentives. There is a clear change in the energy policy toward a higher participation of renewable energy in the overall energy production. Given these favourable conditions wind energy will be able to sustain the growth in the coming years.

In Europe, wind resources on land are becoming more scarce. Specially for large scale wind energy production, suitable locations are more difficult to find. This is specially true for densely populated areas. There is also an audible resistance from some parts of the population and special interest groups who see in the advancement of wind energy a threat to the living environment, hence a deterioration of life quality. The reason can vary from preservation of landscape, protection of the fauna possibly affected by the realisation of large scale wind power projects, to purely esthetical questions. In search of further expansion possibilities of wind energy, offshore locations can be a viable alternative or complement to onshore locations.

There are several reasons to choose offshore locations instead of onshore locations. Firstly, the wind speed is higher and the turbulence intensity is lower because the roughness of the water surface is considerably less than the roughness on a typical land surface. The visual impact is generally not a relevant issue because there will be a minimum distance at which the wind park is situated. The problem of acoustic emission is insignificant given the distance to the populated area. On the other hand there are extra costs involved with the realisation of offshore wind energy. The need of a support structure increases the material costs. Installation and maintenance are more costly due to the transportation and limited access possibilities. Furthermore, the need of an offshore electrical transmission also counterbalances the advantage of higher

energy yield.

To reduce the cost it is necessary to achieve an efficient structural design. In the current design codes for wind turbines, it is required to perform both fatigue and extreme load analysis to ensure that the structure will withstand both types of loads. Ideally, the strength of the structure should match exactly the demand placed by the fatigue and extreme loads. However, there are several uncertainties concerning the external loads, structural response and structural strength. For this reason, the design loads are codified in standards to ensure a consistent treatment of the loads during the design stage.

1.2 Current design practice

The current design practice for onshore and offshore wind turbines concerning the design loads are described briefly in the following paragraphs.

Onshore

The onshore design methodology for wind turbines checks fatigue and extreme loads. For fatigue calculations, stochastic wind fields are generated as input to determine the structural response for a given wind condition Subsequently, the stress amplitudes are counted using, for example, a rainflow algorithm. The frequencies of occurrence of different wind conditions are multiplied with the stress amplitude distribution and the fatigue damage is calculated using the linear damage accumulation law. There are several design codes that describe the procedure to determine the fatigue damage. The IEC [53] and Germanischer Lloyd [44] standards are widely accepted for design calculations of wind turbines, also DNV/RISØ [34] offers guidelines for design calculations of wind turbines.

The extreme load conditions comprise a wide range of situations where extreme loads can occur. There are load cases that are caused by extreme wind conditions such as the extreme wind gust, extreme wind shear, wind directional change etc. The extreme wind gust during operation is modelled with deterministic functions, which do not reflect the random characteristic of the wind turbulence. The main purpose of the deterministic extreme gust is to determine the response of the turbine to a gust with a short rise time.

Offshore

The experience in design of offshore wind turbines and support structures is quite limited. Guideline for design load calculations is still in development. The only guideline specifically written for offshore wind energy is from the Germanischer Lloyd [43]. The approach from the Germanischer Lloyd guideline is described briefly below.

The GL procedure to calculate the fatigue loads is comparable to the procedure used in onshore design. The wave parameters, the significant wave height and the corresponding characteristic wave period, are directly correlated to the wind speeds. This empirical relation of wind and wave parameters is actually a valid approximation only for fully developed sea states. The fatigue loads are partially reduced by the lower turbulence intensity of offshore wind, but on the

other hand the wave excitation adds also a contribution to the fatigue damage. The wind shear, which describes the vertical profile of the mean wind speed, is reduced due to the lower surface roughness, decreasing also the wind shear excitation.

The GL extreme load cases for an offshore wind turbine are comparable to the onshore version. A reduced wave loading is added to almost all of the extreme load cases in the onshore design code. Furthermore, there are two combined extreme load cases of wind and wave. The first one is the combination of 1 minute gust associated with the 50 year mean wind speed and an extreme wave height with a probability of 0.001 for a given significant wave height (e.g. 50 year significant wave height). The second load case considers the 3 second gust associated with the 50 year mean wind speed and a reduced wave height chosen such that it has the same joint cumulative probability as the first load case.

In general, fatigue is the design driver for the rotor blade, because of the material properties of the load carrying material: glass fibres. It has a high ultimate tensile strength but the fatigue strength is lower than the fatigue strength of steel. The slope of the S-N curve is steeper, in comparison to materials like steel. Assuming the same load history, this would result in a higher damage for the composite material (based on the linear damage hypothesis). For fixed offshore structures designed for fossil energy extractions the extreme loading is usually the design driver. This lies in the fact that fixed offshore structures generally have a natural frequency much higher than the peak frequency of the wave load. Furthermore, the wind load plays a less significant role. Hence, the response is dominated by the quasi-static part [88].

1.3 Motivation

For offshore wind turbines (OWT), the extreme response can be a more relevant issue than for onshore wind turbines. The question raised here is how to determine the extreme response of the structure in a rational way. This is necessary to ensure that the structure can withstand extreme loads that can occur during the service life without incurring excessive conservatism in the structural design.

There are several problems related to the above described GL approach to determine extreme responses. First, the deterministic models of extreme wind gust and extreme wave height do not reflect the stochastic nature of the wind and waves. Secondly, the extreme load cases prescribed by Germanischer Lloyd determine the return periods of mean wind speed and significant wave height separately. Thirdly, it is assumed that the response determined in this way corresponds to the return period of the specified external condition. This is in general not valid for dynamic responding structures[1] where the correspondence between the return period of the external condition and the return period of the response does not apply due to the action of the frequency response function.

[1] For statically responding structures this correspondence applies if there is a monotonic relation between the external conditions and the response.

Reliability based design methods are applied to the design of all sorts of offshore structures [70] [36], also in the form of guidelines [33]. The method can also be applied to the design of an Offshore Wind Turbine, OWT[2] [92]. One has to be aware of the differences between conventional offshore structures and an OWT. One significant difference between fixed offshore structures and an OWT, is that the wind turbine has active influences on the load itself. The different operation states (full load, partial load, stand still etc.) of the OWT give rise to different load characteristics. During the energy extraction, the rotating blades reduce the vibration of the support structure through aerodynamic damping. Furthermore, the controller of the system can affect the external loads substantially by actively yawing the nacelle or by pitching the blades, etc.

There are several probabilistic approaches that consider aerodynamic loads and/or hydrodynamic loads for offshore structures. These approaches can be applied to determine the extreme responses of an OWT. For onshore wind turbines there are methods to determine the failure due to fatigue [59][90], and extreme response [73] of the wind turbine using a probabilistic approach. These methods concentrate on the statistical modelling of the measurement data, e.g. extreme flap moment. The advantage of such approaches is that they do include all the extreme responses irrespective of their origin. On the other hand, if the length of measurements is not long enough and do not cover all the wind conditions, the extrapolation from these limited data can incorporate uncertainties to the estimates.

A possible way to get around the limitation of measurements is to obtain the response by simulations. The extreme response can be simulated for a variety of extreme conditions. These extreme conditions are taken from measurement or hindcast data, which usually cover a longer period than the available response measurements. The responses obtained using simulations are analysed statistically and the long-term response distribution can be obtained by extrapolation. This methodology has been applied to the support structure of an OWT in the Opti-OWECS project [58], where the influence of the turbine is taken into account in a simplified way. In this thesis the operating conditions of the wind turbine is considered and different statistical approaches to determine the extreme response are applied.

Another issue addressed in this thesis is the application of stochastic models of extreme wind gusts and extreme waves. The current extreme gust model consists of deterministic functions. The deterministic gust is not based on a physical model but on a number of measurements. The extreme wave model is in general a Stokes wave of higher order (e.g. 5th) [18] or Stream functions [31]. These models produce non-linear waves but these non-linear waves do not contain the random properties of the ocean waves. On the other hand, the stochastic models of extreme wind gust and wave are based on the physical properties of large waves and wind gusts. They can be used to evaluate the response of the OWT to extreme wind gust and extreme waves. The method used here to produce stochastic waves and wind gusts is based on the constrained

[2] In this document, the terminologies from the mentioned reference are used.

simulation. It is an efficient method to produce an extreme wave or an extreme wind gust with stochastic properties without the need of long simulations. The constrained simulation will be discussed in detail in Chapter 12.

1.4 Approach

1.4.1 Response based approach

The pursued approaches can be divided in two parts. A response based approach and an external condition based approach. Figure 1.1 shows schematically the response approach applied here to achieve a rational structural design against the extreme response. The major steps are described briefly below.

- Offshore environment: specification of the external conditions. The distributions of wind and waves are derived from measurements or hindcast data. In general, the short-term conditions of wind and waves are specified by variance spectra with input parameters (e.g. mean wind speed, significant wave height, zero upcrossing period, etc.) that characterise the stochastic process. Long-term wind and wave climates are usually described in distributions of the parameters that characterise the process, for example the mean wind speed, the turbulence intensity, the significant wave height, the zero upcrossing period etc.
- Load response model: generation of stochastic wind and waves from the wind and waves spectra and translation of the wind speed and wave kinematics into aerodynamic and hydrodynamic loads. This can be done in both frequency and time domain. This determines the choice of response model as well. Considering the non-linear response characteristics, the time domain approach is chosen.
- Structural response: translation of the external loads, i.e. aerodynamic and hydrodynamic loads, into structural responses, such as displacements, stresses etc.
- Response statistics: statistical analysis of the response, using the maximum values, the peak over threshold values or the statistical moments of the response time series. For frequency domain analysis, the statistical parameters are extracted from the response spectrum. This step produces conditional statistics: the obtained distributions are conditioned on a given set of sea state parameters. Combining the conditional distributions and the occurrence frequency of the sea state, the response distribution for a random sea state can be obtained.
- Extrapolation of the distribution: Extrapolation of the extreme response distribution for a random sea state to the distribution of the yearly extremes. From this distribution the structural response corresponding to different return periods can be determined. This step of extrapolation is necessary because of the limited data.

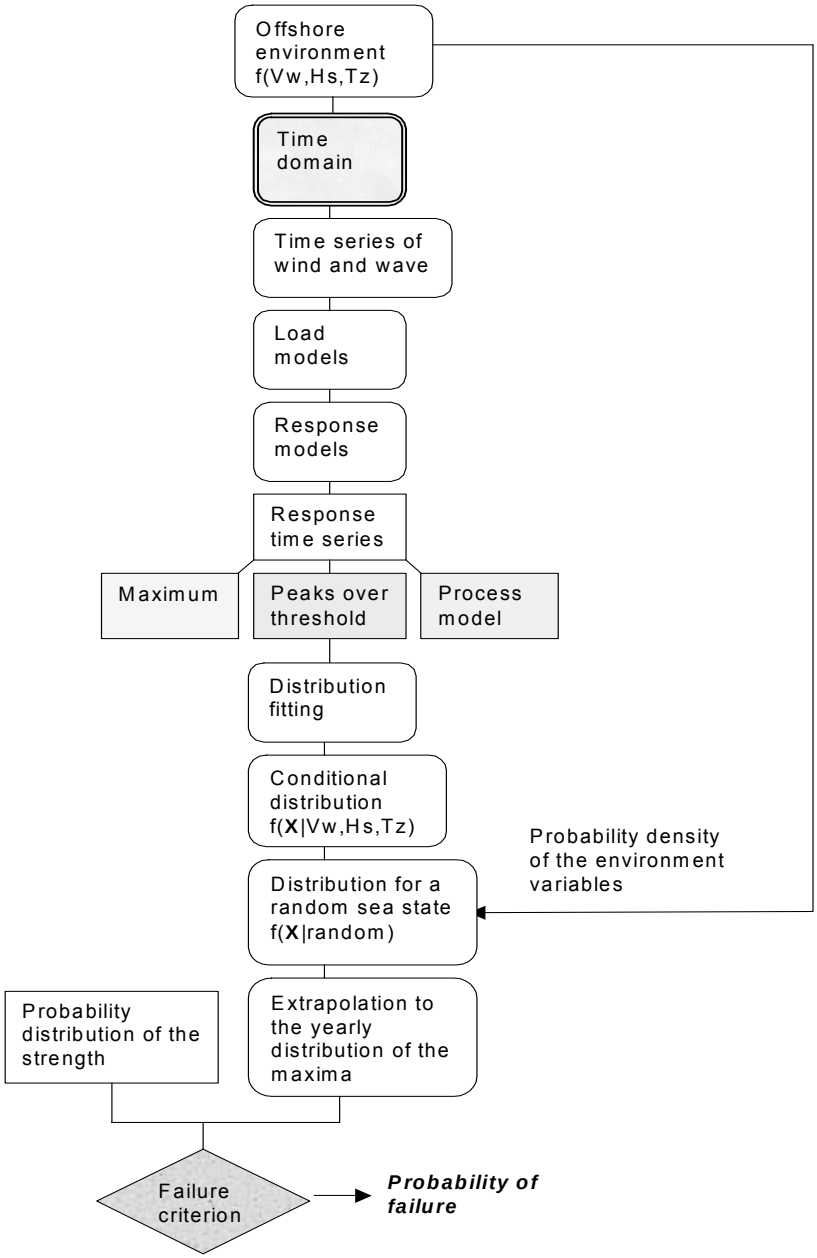

Figure 1.1: Illustration of the proposed methodology

- Failure probability can be determined once the failure criterion is established. The material properties are modelled as constants here, this is acceptable in view of the relatively large uncertainties associated with the response. Whether or not to include the material strength as a stochastic factor depends on the nature of the problem. If the failure probability depends on the local strength, it may be preferrable to take the strength as stochastic variable. In this case, the strength is characterised by a global strength variable which is regarded to have narrower variation than the variation of the response. For further discussion refer to [62].

1.4.2 External condition based approach

The second approach used here to determine extreme responses is based on the external condition. The external condition that corresponds to a return period of, for example 50 years, is determined. The extreme response that corresponds to this external condition is calculated using time domain simulations. It is assumed that the calculated response has the same return period as the return period of the external condition.

The purpose of the external condition based approach is to apply stochastic models of extreme wind gust and waves to determine the response variation due to the randomness of these extreme load models. These stochastic models of extreme wind and wave loads can be an alternative to the currently used deterministic models. Different combinations criteria of the stochastic wave and wind gust are also studied. An example of a stochastic gust and deterministic gust is shown in Figure 1.2

The responses from stochastic models are compared to the responses from deterministic models. The level of risk can be established from the distribution of the extreme responses. Even though the stochastic models have theoretical basis, the use of these models for design calculations needs to be validated with extensive measurements of responses. A preliminary verification of extreme gust responses can be found in [8].

1.5 Structure of the thesis.

Following the introduction, Chapter 2 describes the previous research results relevant to the work presented here, followed by the scopes and limitations of the subjects. Chapter 3 describes the offshore environment, the sea states, extreme wind and wave events and the fitting of joint distributions of wind and waves. The extreme load conditions from design codes are specified. Chapter 4 describes the OWT concepts and the turbines used in this study. Chapter 5 gives a brief account of the load and response modelling of an OWT. Chapter 6 deals with the reduction of the stochastic variables that govern the external conditions, eliminating those which have less influence on the response.The statistical analysis of extremes is described briefly in Chapter 7, together with the fitting methods and the statistical tests. Study of the length and number of

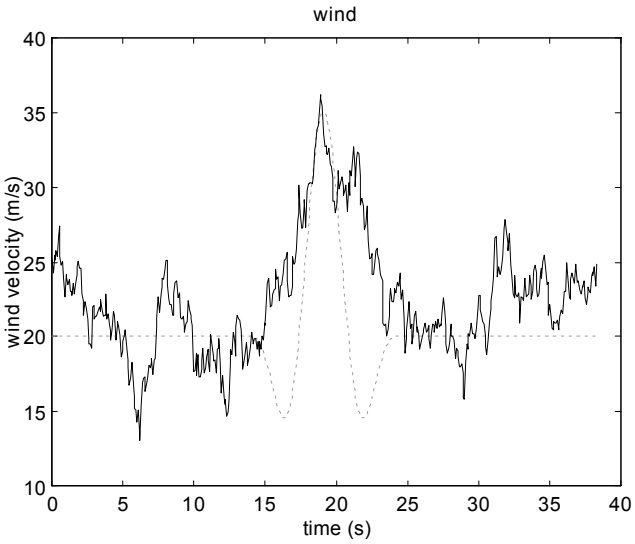

Figure 1.2: A random realisation of a stochastic gust (solid) together with the deterministic gust (dash-dot)

simulations necessary for a reliable estimate of the response distribution can be found in Chapter 8. The uncertainties of the distribution choice and distribution parameters, are analysed with Bayesian analysis. This analysis is carried out for the MAX model, where only the maximum response of each simulation run is used.

Instead of using only the maximum of each simulation run the peak values over a certain threshold (POT) are also suitable for the analysis of extreme responses. In Chapter 9, different POT models are fitted to the sample peak distribution. The uncertainties concerning the peak counting and the level of the threshold are investigated. Extrapolation of the peak response distribution is performed to determine the extreme response of different return periods. Apart from the maximum and peak values, one can also use the statistical moments of the simulated time series to predict extreme responses. This random process model is described in Chapter 10. First a Gaussian model is used and then a weakly non-Gaussian model, which is based on a correction of the Gaussian process where the correction is applied to obtain the non-Gaussian skewness and kurtosis of the extreme response distribution. The long-term distributions of the extreme responses are determined in Chapter 11.

Chapter 12 concerns constrained simulations. The constrained gust and wave models are described. The influence of the different gust models on the response is studied, including variations of the gust centre. The number of constrained simulations necessary to obtain a reliable distribution of the gust responses is studied. The combination of constrained waves and wind gusts is treated in

the same chapter using both deterministic and stochastic models. Different combination criteria are applied. Chapter 13 is dedicated to the comparison and application of the methods described above and finally conclusions and recommendations for further research are given in Chapter 14.

Chapter 2

Scope and Limitations

2.1 Current status of the research topic

There are not many references in the area of structural reliability applied directly to offshore wind turbines. One of the first studies on offshore wind turbines using random wind and waves can be found in [71], where a simple turbine with a support structure model has been developed. In the "Study of Offshore Wind Energy in the EU" [66], the combination of wind and wave load cases are determined based on statistical criteria. It contains numerous extreme load cases closely related to the cases specified in the design code of GL offshore. However, in the design code a deterministic method is applied to obtain the extreme response of the OWT using, for example, Stream functions and steady wind. In another study entitled 'Structural and Economic Optimisation of Bottom-Mounted Offshore Wind Energy Converters, Opti-OWECS, [58], a probabilistic method has been applied to the support structure using state of the art programs for the design of offshore structures.

Conditional distributions of the response of the support structure during a storm are determined. The long-term distributions of the responses are obtained from a convolution and extrapolation procedure. The storm-based approach has the advantage that the storms can be considered as independent events [58]. For the Opti-OWECS study, the wind loads are simplified as a tower top force.

Kühn [57] has analysed different extreme load cases for an OWT using deterministic models. Measurements of OWT response are scarce and in many cases wind speeds and wave heights are not measured simultaneously. Measurements of extreme responses of a modern onshore wind turbine with a pitch control [60] have shown that the extreme flap moment during a very severe storm is still lower than the flap moment around rated mean wind speed. For the support structure of an OWT, however, this may not necessarily be the case. But it does show that the contribution of the aerodynamic forces during operations to the blade response is considerably higher than during stand still, for a pitch regulated wind turbine.

Madsen et al [65] have carried out calculations of extreme response of the blade and the yaw bearing moments. Statistical analysis is applied to the simulation results. An experimental onshore wind turbine model is used for the calculation. A semi-analytical approach based on the Davenport [30] and the Hermite model, proposed by Winterstein [99], [101], has been applied. The results from the simulations show a good agreement between the conventional approach, which uses an extreme value distribution to fit the extreme values of the simulations, with the semi-analytical approach. Fitzwater & Winterstein [39] also applied the quadratic Weibull model to fit extreme flap moments from measurements data. If the data follow a Weibull distribution then the data will appear as a straight line when plotted in the Weibull scale. The quadratic model is more flexible than the Weibull distribution because it can follow the curvature of the data if the data is not strictly Weibull distributed.

A Process method based on Volterra series is also applied to determine the maximum response of the blade. In many cases the distribution of the maxima shows little scatter so that the mean value of the distribution can be used as a good approximation [30]. A similar study based on the Hermite model and applied to the ultimate load of the rotor blade can be found in [76].

There are numerous publications regarding the probabilistic treatment of fatigue loads and fatigue damages, [59],[90] and [14], all of them concerning onshore wind turbines. The basic idea is to find the load amplitude distributions for a given combination of mean wind speed and turbulence intensity. The fatigue strength of the material is usually represented by the S-N curve. The parameters of the S-N curve are modelled as stochastic variables. Knowing the distribution of the stress that depends on the the external condition (i.e. mean wind speed and turbulence intensity), the distribution of the external condition and the distribution of the strength parameters, one can proceed to calculate the fatigue failure, given a failure criterion.

The other topic of this thesis is the modelling of extreme wind gusts and waves using contrained simulations. The constrained simulation of waves is based on the concept of New Wave [87], which gives the expected profile of an extreme wave. By superposing the New Wave to a stochastic wave [49], one can create extreme waves with stochastic properties without long simulations. The variability of the response due to wave forces has been studied with constrained simulations [48]. The constrained simulation of wind was applied to onshore wind turbines in [9]. A modified expression of New Wave exists [42], which includes an extra parameter of an instantaneous frequency instead of the mean frequency assumed in the derivation of New Wave.

2.2 Scope and limitations

The past works mentioned in the previous section have been objects of separate research with very different application areas. Hence, the object of this thesis is to formulate a general methodology to apply the probabilistic design approach to an offshore wind turbine.

The subjects of offshore climates, aerodynamics, hydrodynamics, structural dynamics, structural reliability etc. cover very broad areas of research. Given this large number of subjects treated here, one needs to define a boundary around the relevant objectives and specify the limitations.

The main purpose of the thesis is to develop a risk-based design methodology for an OWT, where the emphasis is placed on the extreme response. The method is then applied to an OWT model to determine the extreme responses using time domain simulations. The method should be general enough so that it can be applied to different kinds of OWT configurations, that is, different wind turbine concepts or different support structure concepts etc. At the same time, it should address the specific issues of an OWT, such as the combination of wind and wave loads.

The response treated here refers to two global response variables of the structure. One is the flap moment at the blade root and the other one is the overturning moment of the support structure. However, the methodology can be applied to displacements, stresses, strains, forces etc., depending on the application purpose.

External condition: The external condition is taken from the NESS/NEXT hindcast database [72] for a location in the North Sea close to the Dutch coast. The same location was used in the Opti-OWECS study. This database contains the partial correlation of the mean wind speed with wave parameters (This correlation is in fact inherent to the hindcast model itself, however, verifications with measurements have shown good agreement with the measured data). The external conditions given here can be described by stationary parameters such as the mean wind speed and the significant wave height etc. Short and non-stationary events (e.g. extreme wind shear simultaneously with extreme change of wind direction) can induce extreme responses as well, but these events are not retrievable from hindcast database. Since these events do not occur very frequently, there is not enough data available for a statistical description of such events at the moment. For this reason, these non-stationary events are not considered.

The scatter diagram is built from the hindcast database. A scatter diagram is a discrete representation of the probability density of the sea state parameters. In the offshore terminology, sea state is characterised by two parameters, the significant wave height and the corresponding characteristic wave period. In this thesis, the word "sea state" is used in a broader sense, to include other parameters that describe the offshore environment, in particular, the mean wind speed.

The minimum number of sea state parameters that needs to be considered is investigated. This reduction of parameters is necessary since the computational effort increases exponentially with the number of stochastic parameters. The stochastic wind field is generated with SWING3 [5], only the horizontal components of the wind speed is considered. The wave is generated with a random phase model. The spatial variation of the wave field is not considered, that is, the cross correlation of the water elevation between two points is not taken into account. The stochastic wave is generated using linear wave theory, while the

deterministic extreme wave is modelled with Stream functions.

Load models: The aerodynamic loads and hydrodynamic loads are calculated using load models implemented in the simulation code DUWECS [102]. The core of the aerodynamic load model is the blade element momentum theory, with correction factors for 3D effects, turbulent wake states, dynamic inflow etc. Comparisons of DUWECS features and other state of the art simulation codes can be found in [57],[68]. The hydrodynamic loads are based on the Morison equation [78]. To calculate the hydrodynamic loads, it is necessary to determine the kinematics of the particles. The kinematics of the water particles depends on the wave theory. For random waves, the linear wave theory (Airy) is used, while for extreme deterministic waves Stream functions are used.

Response models: The response is obtained with the time domain simulation code DUWECS . It is capable of performing non-linear simulations. The OWT is comprised of different sub-models that are interconnected. The rotor is modelled as a rigid blade with hinge flexibilities in the flap and lead-lag direction. The support structure is a finite element model. The physical degrees of freedom are replaced by the modal degrees of freedom. To improve the calculation of the quasi-static part of the response, higher modes are added to the simulation as static modes.

The response of the wind turbine is also influenced by the generator and the gearbox. Therefore, a generator and a gearbox are also included in the simulation code.The modelling of the controller is a crucial part because of the influence it exerts on the loads. For this study, two generic wind turbines and one support structure concept are used. The wind turbine concepts are a stall controlled wind turbine and a pitch controlled wind turbine. The support structure concept for both turbines is the monopile.

Operational conditions: The operational condition of the wind turbine affects the response significantly. The wind turbine is assumed to operate under normal conditions, that is, without failure in any of the components that can affect the response characteristics. Abnormal load conditions are classified as special load cases. They include for example, operation with failure of the controller, yaw mechanism, pitch mechanism etc. Evidently, these operation conditions can induce extreme responses as well. However, the chance of occurrence of these events is largely unknown and as a consequence they are not included in the probabilistic methodology proposed here.

In the near future the design of wind turbines with respect to extreme responses still needs to be checked against these special load cases. If the probabilities of these rare extreme events can be determined with more certitudes, it can be easily incorporated into the probabilistic method. Another class of special load cases not considered here are the loads during the transport and erection phase.

Statistical analysis: The response time series are analysed with statistical methods using different amounts and kinds of information. This information can be the maximum of each simulation run, the peak values over a certain threshold or the statistical moments of the complete time series. The selected response are fitted to different parametrical distributions. The goodness of fit

is verified with different statistical tests.

The distributions are conditioned on the environmental parameters. Multiplying the probabilities of the environmental parameters with the respective distribution and sum over the considered ranges of the environmental parameters gives the response distribution for a random environmental condition. The extrapolation of the distribution for a random external condition to a yearly distribution of extreme responses depends on the number of occurrences of the external conditions which can be considered as independent. Thus, this number is an uncertain parameter. However, one study [100] shows that even for highly correlated adjacent periods, it has little effect on the upper tail of the extreme value distribution.

The uncertainties concerning the choice of distributions can be treated with a Bayesian analysis, whose result indicates the percentage of participation for the different distribution functions. The uncertainties of the distribution parameters can be treated analogously. Although the treatment of the uncertainties with Bayesian is not completely objective, it offers a formal and useful procedure to take these uncertainties into account.

Combined extremes: The combination of extreme wind and waves is an important aspect of the OWT design. Using the response approach this is automatically taken into account by the scatter diagram. For the external condition based approach, this combination need to be specified. Currently, the combination of wind and waves are not precisely specified in the design standards. the most conservative assumption is that the maximum of the wind and wave occurs at the same time. In addition, the constrained simulations of wind gusts and waves are applied to determine the variability of the extreme response of an OWT. Different combination possibilities are studied including time delays between the maximum of the wind speed and the wave.height. The study of time delay has been accomplished for deterministic models and stochastic models of extreme gust and extreme waves.

Structural reliability: The failure probability of the structure will be calculated based on a fixed strength of the material. In reality the strength of the structure is also stochastic, due to the variation of geometrical properties, ultimate stress etc. The use of a fixed strength model is justified by the fact that the load and response of the structure has much larger variation, hence a much broader distribution. Furthermore, the material strength is represented by a global strength parameter, hence the local variations of the material strength are smoothed out.

One important thing to keep in mind is that the response characteristic is specific to the OWT configuration while the external conditions are site specific For this reason one needs to exercise caution when attempting to generalise the results to different OWT configurations or locations.

2.2.1 Prospects

To conclude this chapter, one can say that the probabilistic method is an useful tool to gain insight into the variability of extreme responses. The response

based methods determine the long-term extreme response from the distribution of responses and not from the distribution of external conditions.

However, the large amount of simulations required by the response based method is the major obstacle for a widespread use of it. The constrained simulation procedure represents an alternative model to the deterministic models. The constrained simulations consider the stochastic property of the wind turbulence and waves in a shorter simulation length.

Theoretically, the estimated response distribution can be used for structural reliability analysis leading to a more efficient structural design of the OWT. But for the structural optimisation of an offshore wind turbine, it means a large number of iterations to calculate the response distribution. Every time a structural parameter is changed, all the responses need to be recalculated using the time domain simulations. Hence, for the moment this method can not be used for optimisation. However, this method can be used to calibrate the safety factors for the extreme loads, contributing to a more rational design process.

Chapter 3

Offshore environment

3.1 General description

In this chapter the statistical characterisation of the wind and wave climates for offshore locations are described. The focus is on the extreme wind and wave conditions. Different statistical characterisations are used for different time scales. Short-term refers to a time scale associated with the stationary period, while long-term refers to time scale larger than the stationary period, e.g. one month, one year etc.

The occurrence probability of the sea states[1] is determined from the hindcast data. The hindcast data are extracted from the NESS/NEXT (North European Storm Study) database [72]. The database contains numerous parameters that characterise the metocean conditions, from which three are used here, the mean wind speed, the significant wave height and the zero up-crossing wave period. The database covers a large part of the North Sea with a 30 km by 30 km grid. The chosen location is in the North Sea, about 20 km off the Dutch coast, the same location as used in the Opti-Owecs study.

Furthermore, the hindcast data can be used to determine design wind and waves conditions, to determine energy yields and establish weather windows for maintenance [7]. An analytical approach to determine the joint distribution of wind and wave parameters is also applied to the metocean data, to be more precise, the mean wind speed, the significant wave height and the zero upcrossing wave period. This approach enables the extrapolation of the sea state parameters to return periods that are longer than the length of the data. The joint probability density can be used to determine, for example, the environmental contour of the 100 year sea state.

In this chapter, it is simply stated that the data will be fitted to a cumulative probabilty distribution. The fitting method used is the least squares method.

[1] As mentioned in the Scope and Limitations, the term sea state is used here in a broader sense than in the offshore engineering, to include the mean wind speed as a characteristic variable.

The details of different fitting procedures will be discussed in Chapter 8. The extreme offshore environment which are determined in this chapter does not necessarily produce the largest response of an OWT.

3.2 Wind climate

3.2.1 Short-term description of wind

With the term wind, one usually refers to the wind speed. The short-term distribution of the wind speed refers to periods associated with the stationary period of the wind. The stationary period of the wind varies from 10 minutes to 1 hour. The wind speed is then divided into a constant term, the mean wind speed, and a fluctuating term, the turbulence. A measure to characterise the turbulence is the turbulence intensity I_t

$$I_t = \sigma/\bar{U} \tag{3.1}$$

where σ is the standard deviation of the process and $\bar{U}$ is the mean wind speed.

The turbulence is generally assumed to be a Gaussian process, although the actual turbulence can deviate considerably from the Gaussian assumption depending on the terrain conditions and stability conditions [51]. For offshore wind climate the GL Offshore guideline defines a 12% turbulence intensity for all the mean wind speeds. In an offshore wind park the turbulence intensity is higher due to the park effect. The park effect refers to the increase of the turbulence intensity due to the fact that many wind turbines will operate in the wakes of the other wind turbines. To account for the park effect of the turbulence intensity in a park, the Danish offshore guideline has specified a turbulence intensity of 19.2%, if the distance between the turbines is more than five times the diameter of the rotor [29]. It has to be noticed that the turbulence intensity usually decreases with the wind speed and is in fact a stochastic variable.

The turbulence is described by a variance spectrum. The spectrum used here is the von Karman spectrum. From the variance spectrum, a stochastic wind series at one location can be generated using a random phase model. For the load calculation this is not sufficient since it does not take the spatial variation into account. This is described by the cross spectrum. In general, the cross spectrum is complex, containing an in-phase and an out-of-phase component. In this case, only the in-phase part is taken into account, the so-called co-spectrum. This can be expressed in terms of the variance spectrum and the coherence function. One of the commonly used coherence functions is the exponential coherence. Other coherence models with non-elementary functions can be found in [37].

Using the random phase simulation technique developed by Shinozuka [81] a (Gaussian) stochastic wind field can be obtained using the variance spectrum and the cross spectrum. In this thesis, the wind simulations are produced with the program SWING 3 [5]. In contrast with other wind simulation programs, it generates times series of wind speed attached to the blade. Thus, the generated signals are wind speeds as seen by a rotating blade. This input spectrum of the

turbulence has a rotational sampling effect, with peaks in the frequencies which are multiples of the rotation frequency. The advantage is that only points 'seen' by the blades are generated, reducing the simulation effort and data to a minimum. A disadvantage with this approach is that to transform the irrotational spectrum to a rotational spectrum, the rotation speed of the blade has to be known in advance. Thus, it can not be used for variable speed wind turbines. This problem is solved by using azimuthal decomposition in the newer version of the simulation program SWING 4 [6].

The variation of the mean wind speed with the height is described by the wind shear or vertical wind profile. The theoretical description of the wind profile is based on the shear stress within the boundary layer. The shear stress reaches the maximum at the surface and approaches zero in the free atmosphere. The wind shear can be described by the Prandtl logarithmic law as

$$\bar{U}(z) = \frac{u_*}{k} \ln\left(\frac{z}{z_0}\right) \tag{3.2}$$

where $\bar{U}(z)$ is the mean wind speed at height z, u_* is the friction velocity which can be written as $u_* = \frac{U(z_{ref})}{2.5 \ln(z_{ref}/z_0)}$, k is the von Karman constant, which is approximately equal to 0.4 and z_0 is the roughness length determined by the condition of the surface. The friction velocity u_* changes with the surface roughness and the mean wind speed. For practical reasons, Equation 3.2 is written in terms of a reference mean wind speed $\bar{U}(z_{ref})$ at a reference height z_{ref}

$$\bar{U}(z) = \bar{U}(z_{ref}) \cdot \frac{\ln(z/z_0)}{\ln(z_{ref}/z_0)} \tag{3.3}$$

Given a reference mean wind speed $\bar{U}(z_{ref})$ at a reference height z_{ref}, one can determine the mean wind speed profile if the roughness length z_0 is also given. For the open sea the roughness length depends on the wave surface elevation, thus it depends indirectly also on the mean wind speed. The most common relation used to model the roughness dependency is the Charnock relation, which relates the friction velocity and the roughness length to a constant, the Charnock constant [66]. Solving the Equation 3.3 and the Charnock relation iteratively one can obtain the wind speed profile over the height. An accepted mean value of the roughness length for the open sea condition is 0.0002 m [93], the Joint Committee on Structural Safety (JCSS) code [54] recommends a roughness length of 0.003 m for the open sea. The usual range of variation[2] is between 0.0001 m and 0.0005 m. The fact is that the roughness length can not be determined directly and there is a large discrepancy in the calculation of the roughness length. However, within the given variation of the roughness length,

[2] The real roughness length varies with the sea state parameters. The values given here are characteristic values which are calculated with different methods, therefore the large spreading of the values. However, the large variation of the roughness length does not affect the mean wind speed profile significantly.

the mean wind speed profile does not vay significantly. In the JCSS code an extension of the logarithmic law is given for height > 200 m.

In most of the design codes of wind turbines, an empirical model is used. It is based on a power law. It is important to note that the power law has no physical foundations, however, it often describes the vertical variation of the mean wind speed accurately for engineering applications. The power law of the wind speed profile is written as

$$\bar{U}(z) = \bar{U}(z_{ref}) \cdot \left(\frac{z}{z_{ref}}\right)^{\alpha} \tag{3.4}$$

where α is an exponent determined by measurements. The GL offshore guideline prescribes a value of 0.11, independent of the external conditions. It is possible to relate the power law exponent to the roughness length using an exponential model for the range of z_0 of interest [41]

$$z_0 = 15.25\ m \cdot \exp(-1/\alpha) \tag{3.5}$$

3.2.2 Long-term description of wind

The long-term distribution refers here to the distribution of the mean wind speed. The Weibull distribution is widely used to model the distribution of the mean wind speed, with an averaging period of 10 minutes to 1 hour. The mean wind speeds can be taken from the hindcast database. In some cases, the wind speeds of interest are wind speeds of rare occurrence, the extreme wind speed. The extreme wind speed has a different distribution than the Weibull distribution. Assuming that the Weibull distribution is the parent distribution then the extreme mean wind speed follows the extreme value distribution type I (EV I or Gumbel distribution).

The EV I distribution is asymptotically exact given a parent distribution of an Exponential distribution. The estimate of extreme wind speeds with long return period, say 50-100 years, depends on the number of independent periods. Assuming that all the hourly mean wind speeds are independent, that is, there is no correlation between the mean wind speeds, the number of independent periods is 8766, which is the number of hours in one year.

However, it has been shown that using the number of hours in one year as the number of independent periods leads to an overestimate of the extreme wind speed. It has been estimated that the number of independent periods are approximately $n \sim 100$ [50].

The extreme wind speed distribution can be obtained via extrapolation of the parent distribution or fitting of the year extremes with a Gumbel distribution. Given a Weibull parent distribution with shape factor larger than 1, the Gumbel approach gives an overestimate of the extreme mean wind speed, while for parent distributions with shape factor smaller than 1 the Gumbel distribution underestimates the extreme mean wind speed [26].

The uncertainty concerning the number of independent periods of the mean wind speed makes a direct estimate of the annual extreme wind speed via extrapolation difficult. The difference in the estimate can be considerable. The mean wind speed with a return period of 100 years is estimated from an extrapolation of the Weibull parent distribution, using a number of independent periods (in one year) of 100 and 8766. The estimates differ considerably, about 15%.

Although the maximum number of independent periods, 8776, may seem too conservative, it is not a relevant issue here for the demonstration of the methodology. Furthermore, the number of independent periods is not the only factor that can affect the estimate of extreme wind speeds, other factors such as terrain characteristic, type of wind climate etc., can have influences on the estimate as well.

Alternatively, one can fit the annual extreme mean wind speeds to an extreme value distribution. The advantage is that the yearly extremes can be regarded as independent. However, the number of data points is limited to the number of years, in which data are available. Since the number of years is less than 20, the outcome can be uncertain. In this study, the extreme mean wind speed is determined from the extrapolation of the parent distribution.

3.3 Wave climate

3.3.1 Short-term description of wave

The waves are considered to be a stationary process for a period between 1 to 6 hours. Moreover, the wave elevation is usually considered as a zero mean Gaussian process. As with the wind, the Gaussian assumption is an approximation. To characterise the wave, different parameters are used. One is the significant wave height, which is defined as the mean value of the highest 1/3 of the waves. In a spectral description, the significant wave height is related to the standard deviation of the process through the definition.

$$H_s = 4\sqrt{m_0} \tag{3.6}$$

where m_0 is the zero-th spectral moment. The n-th spectral moment is defined as

$$m_n = \int f^n S(f) df \tag{3.7}$$

The zero-th spectral moment represents the total energy content of the wave spectrum. The other wave parameter is the wave period. The one used here is the mean zero-upcrossing period T_z, which is defined by the ratio between the length of the record (in seconds) and the number of zero up-crossings. The zero-upcrossing period is also defined in term of the spectral moments [18]

$$T_z = \sqrt{\frac{m_0}{m_2}} \tag{3.8}$$

There are other characteristic wave periods such as the peak period, which is the period where the wave spectrum has a maximum. In this study, the wave period refers to the mean zero-upcrossing period, if it is not explicitly specified.

The wave in a sea state can be described with a variance spectrum. There are numerous spectral representations of the wave. The classical spectrum of Pierson-Moskowitz (P-M) describes a fully developed sea state. For a partially developed sea state, the JONSWAP [3] spectrum is usually applied. In general, one can say that the P-M spectrum has a larger spreading of the wave energy, while the JONSWAP spectrum has a more pronounced spectral peak. This peak can be of importance for the response if the fundamental frequency of the support structure is close to the peak frequency.

The choice of the spectrum certainly has effect on the extreme response, though in many cases the choice can not be done on an entirely objective basis. It has to be considered from case to case. For this application the P-M spectrum is chosen. This choice does not mean that the P-M spectrum is considered as the most appropriate wave spectrum for this shallow water site. It is also a variable in the design process. The final choice of the spectrum is left to the designer who applies this probabilistic methodology.

3.3.2 long-term description of wave

The long term description of waves is similar to that of the wind. The significant wave heights H_s extracted from the hindcast database are used to determine the cumulative distribution. The relationship between significant wave height and wave period, T_z is not deterministic. Thus, the wave elevation has a two dimensional probability distribution. In the following section the issue on the joint probability distribution will be discussed. In any case, if in situ data are available then the measured data should be used.

The significant wave height can be fitted to the Weibull distribution. This can be the two parameter Weibull distribution or the three parameter Weibull distribution (which contains an extra location parameter). The return period of the extreme H_s is determined in an analogous way as the extreme mean wind speed. The fitted Weibull distribution is the parent distribution of the significant wave height. The parent distribution can be extrapolated given a number of independent periods. The extrapolation of the significant wave height faces the same dilemma concerning the number of independent periods as the extrapolation of the parent distribution of the mean wind speed. The stationary period of waves can vary between 1 to 6 hours. This means also that the number of independent periods can differ. In this case, the number of independent period is chosen as 8766/3, assuming a stationary period of 3 hours for the waves.

An alternative to the extrapolation model is the fitting of the annual extreme H_s. The annual extreme H_s can be fitted to an EV type I distribution (Gumbel

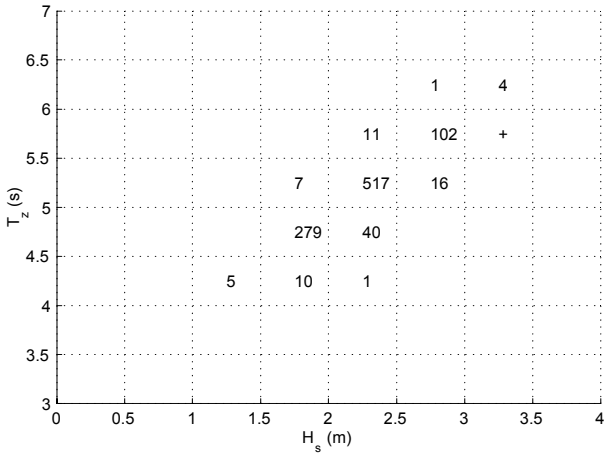

Figure 3.1: Scatter diagram of significant wave height and zero upcrossing period (part per thousand) with a stationary length of 3 hours, for a mean wind speed of 13 m/s (+ represents part that is less than 1).

distribution). The advantages and disadvantages are the same as for the fitting of the annual extreme mean wind speeds.

In this thesis, the extreme H_s is determined from extrapolation of the parent distribution. This is done at the expense of bearing the uncertainty of the number of independent periods. However, the influence of the number of independent periods is less significant for long return periods, e.g. 50 or 100 years [100].

3.4 Occurrence probability of the sea states

In the previous sections, the mean wind speed and significant wave height are treated separately. In reality, a certain correlation exists between the two variables. To obtain a joint occurrence probability of the sea states, the hindcast data can be treated in two different ways. The sea states can be sorted into bins according to the mean wind speed, significant wave height and wave period. This discrete presentation of the sea states is visualised as a scatter diagram. Figure 3.1 shows a scatter diagram for a given mean wind speed, depicting different combinations of the significant wave heights and wave periods. Observe that the term sea state is used in a broader sense to include the mean wind speed as a parameter.

For a continuous distribution of the sea state parameters, a statistical procedure has to be applied to the hindcast data in order to obtain a joint probability density of the mean wind speed, significant wave height and wave period. Different procedures exist using different distributions and dependencies structures

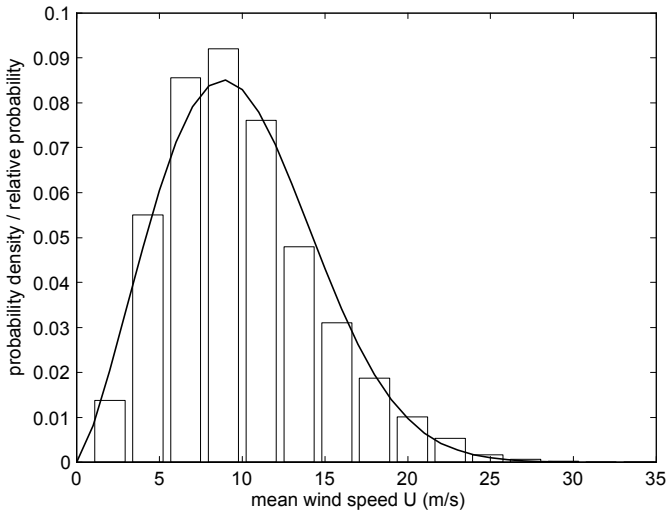

Figure 3.2: Histogram of the mean wind speeds and the a Weibull PDF corresponding to the fitted CDF.

(see [10], [104] and [56]). Here, the conditional distribution approach shown in [56] is applied to the hindcast data. The basic idea is that the joint probability density function can be written as a product of the conditional Probability Density Functions (PDF), namely

$$f(\bar{U}, H_s, T_z) = f(\bar{U}) \cdot f(H_s|\bar{U}) \cdot f(T_z|\bar{U}, H_s) \tag{3.9}$$

where $f(U)$ is the marginal distribution of the mean wind speed $\bar{U}$, $f(H_s|\bar{U})$ is the conditional distribution of the significant wave height for a given mean wind speed and $f(T_z|\bar{U}, H_s)$ is the conditional distribution of the wave period (in this case it is the mean upcrossing period) conditioned on the mean wind speed and the significant wave height. The marginal distribution of the mean wind speed is obtained by fitting all the mean wind speeds in the data to a cumulative distribution function (CDF). In this case, the 2 parameter Weibull distribution is chosen. The 2 parameter Weibull distribution is defined as

$$F(x) = 1 - e^{-\left(\frac{x}{s}\right)^k} \tag{3.10}$$

s is a scale parameter and k is a shape parameter. Figure 3.2 shows the histogram of the mean wind speed together with the corresponding Weibull PDF[3].

Every mean wind speed is divided into classes of 2 m/s width. The significant wave heights that corresponds to each wind class is fitted to a 2 parameter

[3]The mean wind speed is fitted to a Cumulative Distribution Function(CDF). From the fitted CDF, the corresponding PDF is obtained.

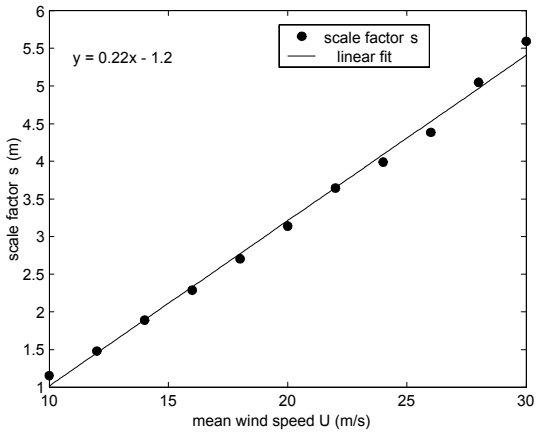

Figure 3.3: Scale factors of the conditional distribution of H_s.

Weibull distribution. From the Weibull plot of the significant wave heights (not shown here), it shows that the significant wave heights can be modelled with a two parameter Weibull distribution. The H_s plotted in the Weibull scale forms nearly a straight line, especially for H_s which corresponds to higher mean wind speeds. The distribution parameters can be written as a function of the mean wind speed. By doing this, a continuous description of the conditional distribution of the H_s can be obtained. Figure 3.3 shows the scale parameter and Figure 3.4 shows the shape parameter of the Weibull distribution of the H_s as function of the mean wind speed.

Dots in the figures represent the fitted values of the distribution, the straight line is the regression curve. In [56] a power law for the regression curve was suggested; in this case a linear regression is sufficient. The resulting equation of the linear regression is also shown in the plot. The scatter of the shape parameter is comparatively larger than the scatter of the scale parameter. Nevertheless, the regression curve captures the trend of the shape factor satisfactorily. One can improve the regression behaviour by adding a quadratic term. In this case, the difference of the estimates of higher fractiles is, however, negligible.

The distribution of the zero upcrossing period can be usually described by a Log-Normal distribution. The mean and standard deviation of the T_z is parameterised by the mean wind speed and significant wave height. In this case, it is observed that the scatter around the mean wind speed and wave height is small for high wind speeds. For this reason the mean zero upcrossing period is determined by the mean wind speed and significant wave height through a linear regression. The following model is used

$$T_z = c_0 + c_{\bar{u}}\bar{U} + c_{H_s}H_s \tag{3.11}$$

c_o, $c_{\bar{u}}$ and c_{H_s} are the regression parameters. Indeed, Equation 3.11 ignores

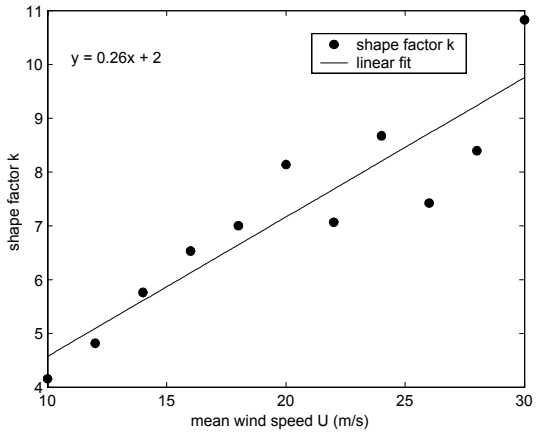

Figure 3.4: Shape factors of the conditional distribution of H_s.

the variability of the T_z, for a given combination of H_s and $\bar{U}$, but this variation is relatively small as can be seen in Figures 3.5 and 3.6. Since the areas of interest for the extrapolation are the high wind speeds, only the data in which the mean wind speed is higher than 20 m/s is used for the regression. Figure 3.5 shows the predicted T_z versus the T_z of the data for all the sea states with a mean wind speed above 20 m/s. It can be seen that the regression model captures the T_z in a satisfactory way.

Figure 3.6 shows the same as the previous figure but for all the significant wave heights above 4 m. It can be seen that the predicted value of T_z is usually lower than the data. This is caused by the fact that not all the sea states with H_s higher than 4 m do correspond to the strong wind situations. If the extreme response of the wind turbine is likely to occur during strong wind, (but not only during strong wind situations), the linear regression model of the T_z can be regarded as sufficient.

The joint probability density of the mean wind speed and significant wave height is transformed into a standard normal space of uncorrelated variables using Rosenblatt transformation [77]. The 100 year contour line describes a circle in this normalised space. The radius r of the circle is determined by

$$\Phi(r) = 1 - \frac{1}{N_{100}} \tag{3.12}$$

where, Φ is the standard normal distribution and N_{100} is the total number of sea states in 100 years. The contour in the physical space can be determined by transforming the standard normal variables back to the physical variables. Figure 3.7 shows the 50 year environmental contour line. Assuming that the response is proportional to the wind speed and wave height then the maximum response is likely to occur at sea states between the maximum mean wind speed

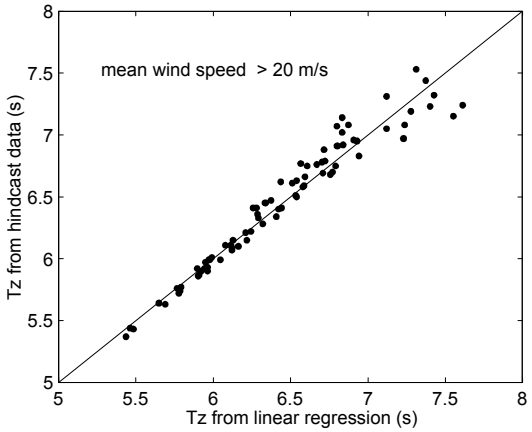

Figure 3.5: Predicted T_z from linear regression and data (mean wind speed >20 m/s).

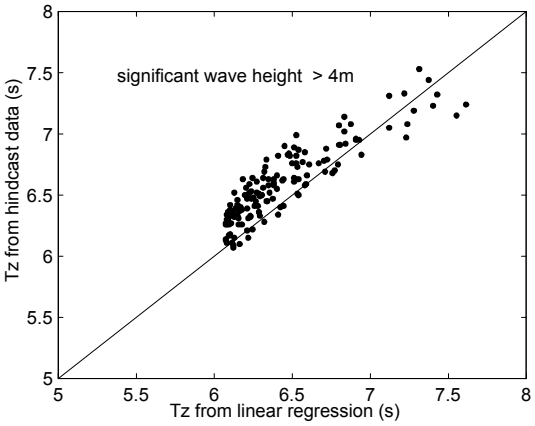

Figure 3.6: Predicted T_z from linear regression and data (significant wave height > 4 m).

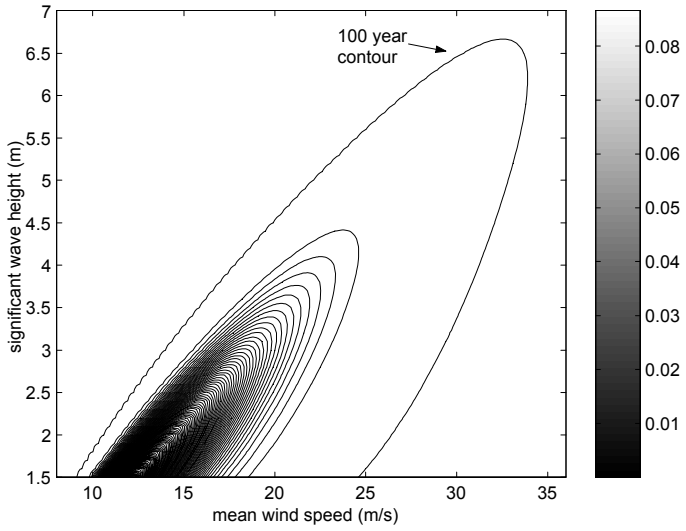

Figure 3.7: Contour plot of the joint PDF of the mean wind speed and significant wave height.

with the associated wave height and the maximum significant wave height with the associated wind speed.

One can determine the 100 year mean wind speed and significant wave height from the marginal distributions of the mean wind speed and significant wave height. However, the correlation between the wind and wave is neglected in that case. Alternatively, a 100 year environmental contour can be determined from the joint probability density function of the mean wind speed and significant wave height. The 100 year contour contains an infinite number of combinations between the mean wind speed and the significant wave height. Table 3.1 shows two special combinations from the contour line, one that corresponds to the maximum mean wind speed with the respective significant wave height and the other one to the maximum significant wave height with the respective mean wind speed.

This table is needed later when the deterministic load condition has to be determined from the 100 year sea state parameters. It can be seen that by taking into account the correlation between wind and waves, the estimates of the 100 year sea state parameters are not significantly different from the estimates using the marginal distributions. Moreover, the joint probability density gives even a higher estimate of the significant wave height than the marginal one. The reason is that the Equation 3.9 preserves the marginal distribution of the independent variable. Here, the mean wind speed is chosen as the independent variable. The marginal distribution of the significant wave height is not preserved. The overestimate has also to do with the fact that the regression curve predicts a

Table 3.1: 100 year mean wind speed and significant wave height estimated from marginal and joint distributions

	$\bar{U}$ (m/s)	H_s (m)	T_z (s)
Marginal distribution	34.5	6.30	7.68
Joint PDF max wind	34.5	6.45	7.78
Joint PDF max wave	32.7	6.70	7.95

smaller shape parameter than the fitted one (see Figure 3.4). A smaller shape parameter leads to a larger estimate of the extreme values of the distribution (see also Figure 8.12).

In this case, the joint probability density approach has not shown substantial benefits compared to the marginal distribution approach, partly because there is a strong correlation between the extreme mean wind speed and the extreme significant wave height. This can be observed in Figure 3.7.

3.5 Design Extreme Conditions

3.5.1 Extreme wind gust

The previous section deals with the long-term probability (e.g. 100 year sea state parameters). However, the deterministic design condition is usually specified in terms of a maximum wind speed averaged over a short period, e.g. 3 seconds, and a maximum wave height with a given probability of exceedence and the associated period. These design parameters can be determined from the short-term statistics if the sea state parameters are known.

For the extreme design conditions, gust speeds of different averaging period are determined. The gust factor is determined as [97]

$$u' = 0.42 \ln(T_1/T_2) \tag{3.13}$$

T_1 is the averaging period of the mean wind speed (10 minutes to 1 hour) and T_2 is the gust averaging period (3 seconds to 1 minute). Thus, the mean wind speed for an averaging period of T_1 can be converted to wind gust speeds of an averaging period of T_2, taken into account that the relationship between the gust factor u', the turbulence intensity I_t and the mean wind speed $\bar{U}$. The wind speed of shorter averaging period u is

$$u = (u' \cdot I_t + 1)\bar{U} \tag{3.14}$$

The extreme mean wind speed can be determined using the approach outlined in the preceding section. The calculated extreme mean wind speed with a return period of 50 or 100 years is different from location to location. The GL offshore guideline has specified the extreme mean wind speeds according to wind turbine classes. For example, the wind turbine class one has a 50 year

extreme mean wind speed of 50 m/s with an averaging period of 10 minutes. Wind turbine class one has the most demanding design mean wind speed.

This mean wind speed is much higher than the one shown in Table 3.1. However, the difference will decrease slightly if one takes into account the fact that the hindcast mean wind speeds have an averaging period of 1 hour. This can be converted to a 10 minute mean wind speed by an increase of approximately 10% according to the GL guideline. Furthermore, the extrapolation of the extreme mean wind speed depends strongly on the data used to fit the joint distributions.

3.5.2 Extreme wave height

For the deterministic extreme wave model, the maximum wave height has to be determined. The following distribution of the maximum wave height was proposed [40]:

$$F_{H_{\max}|H_{s_{\max}}}(H_{\max}|H_{s_{\max}}) = \exp(-N_{wave} \cdot \exp[-\delta \cdot (H_{\max}/H_{s_{\max}})^k]) \quad (3.15)$$

with the distribution parameter $\delta = 2.26$, $k = 2.13$. $H_{s_{\max}}$ is the significant wave height of the sea state considered, in this case the 100 year sea state. N_{wave} is the number of waves defined by

$$N_{wave} = \frac{\tau}{T_z|H_{s_{\max}}} \quad (3.16)$$

where τ is the length of the stationary period of the sea state (in this case, it is assumed to be 3 hours) and $T_z|H_{s_{\max}}$ is the zero upcrossing period for a given significant wave height. Equation 3.15 gives the probability of the largest wave in a stationary period, in contrast with the Rayleigh distribution of the individual wave height within a stationary period used in [43]. The Rayleigh distribution gives the exceedence probability of a given wave height, while Equation 3.15 gives the probability of the largest wave within a stationary period.

The design wave height can be defined, for example, as the wave height with an exceedence probability of 1%. A less severe design wave is the most probable wave height (the maximum of the probability density function). In this thesis, the former criterion of the design wave is applied. The associated wave period to the extreme wave height can be estimated as [33]

$$T_{H_{\max}} = 1.2 \cdot T_z \quad (3.17)$$

Another alternative to detemine the extreme wave height and the wave period from a joint distribution of these two variables [85].

3.5.3 Combination of the extreme wind gust and the extreme wave height

For the external condition based method, the extreme condition is often expressed in terms of an extreme gust speed with an extreme wave height. Ob-

Table 3.2: Load combination of the individual extreme wind and waves specified in the GL design codes

Load case	**Wind speed**	**Wave height**	**Wave period**
case 1	50 year, 3 second gust	$1.32 \cdot H_s$ (50 year)	$1.2 \cdot T_z$
case 2	50 year, 1 minute gust	$1.86 \cdot H_s$ (50 year)	$1.2 \cdot T_z$

viously the chance that the maximum of an extreme wind gust occurs simultaneously with the maximum of an extreme wave is not very big, however, often there is no better alternative than the assumption of simultaneous occurrence.

Two combination cases have been suggested in [66]. These two combination cases are listed in Table 3.2.

Case 1, the 3 second averaged gust speed with a return period of 50 years is combined with a reduced wave height. Case 2, the one minute averaged gust wind speed is combined with an extreme wave height with an exceedence probability of 0.1%. The reduced wave height has been obtained by taking that both load cases have the same joint cumulative probability.

It is assumed that the wind and waves are independent processes within the stationary period. Thus, the joint cumulative probability function is simply the product of the cumulative distribution of the wind speed (i.e. the turbulent part) and the cumulative distribution of the individual wave height. It is to be noticed that the joint cumulative probability has not the illustrative interpretation as the one dimensional cumulative probability. In a one dimensional CDF, a cumulative probability of 0.99 can be interpreted as an event with 1% exceedence chance. If the CDF is the distribution of annual extremes, the 1% exceedence corresponds to a return period of 100 years. For the joint cumulative probability, the 0.99 probability represents the product of the cumulative probabilities of the wind speed and wave heights without much information on the exceedence probability.

For example, to produce a joint cumulative probability of 0.99, one can choose a cumulative probability of a wind speed of 0.99 and a cumulative probability of a wave height of $0.\overline{99}$ (the bar denote a repetition till infinity). This means that one can choose a wave height of infinitively large return period and still the joint cumulative probability remains 0.99. Apparently this information obtained from the joint cumulative probability is not very useful. For this reason, it is more illustrative to work with the joint probability density function which gives more useful information concerning the joint occurrence of the wind and waves.

Using the GL combination criteria, the numerical values of the two extreme load combinations can be determined. Instead of a 50 year mean wind speed, a 100 year mean wind speed is used. The mean wind speeds (and significant wave heights) need to be converted to the same return period. The 100 year mean wind speed is approximately 3% higher than the 50 year mean wind speed. These two 100 year combined load cases are specified in Table 3.3 using the extreme mean wind speed of the wind turbine type class I from the GL Offshore

Table 3.3: Two different combinations of the extreme wave height and wind speed of a 100 year return period sea state, using the parameters given by GL wind turbine class I

	Extreme load combinations	
	1	2
wind speed	63.3 m/s	54.7 m/s
wave height	8.31 m	11.71 m
wave period	9.22 s	9.22 s

Wind Turbine guideline and a turbulence intensity of 12%.

The other alternative to specify the two extreme load combinations is to use the mean wind speed and the significant wave height determined from the 100 year contour of the joint probability density function (see Table 3.1) .In this case, there are 4 different combinations as shown in Table 3.4. The turbulence intensity used here is also 12%.

As can be seen, the difference in the extreme gust speed is quite considerable for this location. On the one hand, the specification of the extreme mean wind speed from the GL guideline is more on the conservative side because it should be applicable to different site conditions. On the other hand, the uncertainties can be considerable in the determination of the 100 year mean wind speed using the joint probability density function. This is because of the limited amount of data (in this case less than 10 years), from which the 100 year mean wind speed is extrapolated. This applies to the extrapolation of the extreme wave height as well.

The discrepancy between the extreme wave heights in Table 3.4 and Table 3.3 can be explained by the distribution functions used to determine the extreme (individual) wave height. In this thesis, a probability of exceedence of 1% for the largest wave in a stationary period is chosen. In the GL case, a probability of exceedence of 0.1% is chosen for the distribution of all the local maxima of the waves. More specifically, GL uses a Rayleigh distribution for the probability of local maxima of the wave heights while Equation 3.15 refers to the probability of the largest wave height in a given stationary period. For this reason these two design wave heights are not directly comparable.

To make a comparison, one can extrapolate the Rayleigh distribution of the wave maxima with the number of waves defined in Equation 3.16. By doing this, the probability of exceedence of the wave heights in Table 3.3 within a stationary period of 1 hour can be determined. Given a wave height of 11.7 m, the probability of exceedence is 0.35. This means that the chance that the largest wave in the stationary period is higher than 11.7 m (see Table 3.3) is 35%. Therefore, the choice of 0.1% exceedence for the distribution of local maxima of the wave height seems to underestimate the maximum wave height in a stationary period.

The reason is that Rayleigh distribution is more conservative because it represents the distribution of local maxima of a narrow band process. Hence it

Table 3.4: Two different combinations of the extreme wave height and wind speeds using the 100 year environmental contour of the joint PDF

	100 year sea state 1		**100 year sea state 2**	
	LC 2	LC 1	LC 2	LC 1
wind speed	46.9 m/s	41.5 m/s	44.4 m/s	39.3 m/s
wave height	10.2 m	13.4 m	10.6 m	13.9 m
wave period	9.2 s	9.4 s	9.2 s	9.4 s

LC: load combination

is preferable to use Equation 3.15, which specifies the distribution of the largest wave in a stationary period.

Another possibility for the combination of extreme wind and waves is the Turkstra rule [64]. It assumes that the maximum of the combined load condition is the maximum value of one process (e.g. wind speed) with an arbitrary value of the other process (e.g. wave height). For example, if wind is the dominant load then a combined load case can be a 100 year, 3 second gust, with random waves corresponding to a 100 year significant wave height. The random wave height gives an arbitrary value at the instant that the maximum gust speed occurs. Although, tt has to be noticed that the Turkstra rule gives an lower bound of the load combination, i.e. it can underestimate the actual combined loads.

It is not possible to determine beforehand the load combination that will present the most severe load situation to the wind turbine. The combinations given here are based on the assumption that an extreme wind gust and/or extreme wave will induce an extreme response in the OWT.

Chapter 4

Wind turbine concepts

4.1 Wind turbines in general

The wind turbine concepts that have been conceived are very diverse. In general, there are two basic concepts, the vertical axis wind turbine and the horizontal axis wind turbine. The main advantage of a vertical axis wind turbine is that the operation is independent of the wind direction. Furthermore, the machinery is usually located at the tower base and are easily accessible for maintenance. However, the stability and dynamic problems associated with large vertical axis wind turbines have hindered this concept to be commercially successful. Nevertheless, the vertical axis wind turbine is still popular among small wind turbines.

Most of the wind turbines manufactured today for the electricity production are horizontal axis wind turbines. The advance of the horizontal axis wind turbines has profited from the researches of helicopter aerodynamics making it a more efficient concept than the vertical axis wind turbines. Moreover, the early success of the Danish concept (horizontal axis, stall regulated power control, constant speed, asynchronous generator with direct grid connection) has contributed to the present market dominance of horizontal axis wind turbines. The main advantages of the horizontal axis wind turbine are the simplicity and robustness and a disadvantage is that a horizontal wind turbine needs an auxiliary yaw system to position the wind turbine in the wind direction.

One can also divide the wind turbine concepts according to the functioning principle, a lift concept and a drag concept. Lift based wind turbines use the lift forces of the rotor to drive the shaft. They are more efficient than wind turbines that use the drag forces. Drag based machines are usually low speed and high torque, which makes them less suitable for electricity generation.

The two example turbines considered here are horizontal axis wind turbines. They use two different power regulation concepts. An active power control is the pitch control, which regulates the power by pitching the blades. A passive control is the stall control, it uses the stall effect to reduce the lift forces. Figure 4.1 shows different configurations of wind turbines using lift and drag principles.

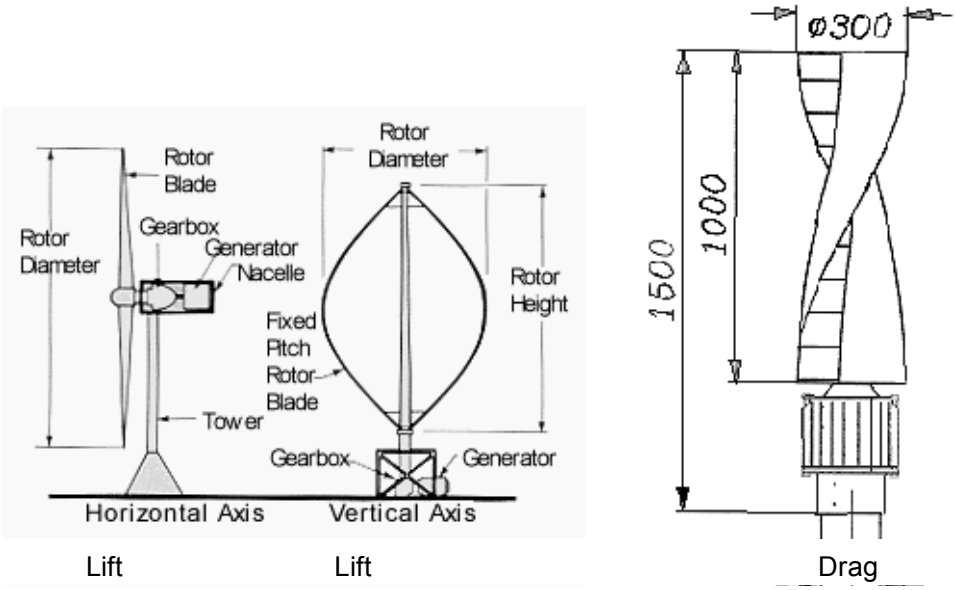

Figure 4.1: Different configurations of wind turbines from left to the right, horizontal axis lift, vertical axis lift (© 1998 by the American Wind Energy Association) and vertical drag (© 1998 by the Windside Production Ltd.)

4.2 Subsystems of horizontal axis wind turbines

A typical horizontal axis wind turbine consists of the following subsystems:

Rotor

The rotor is the interface between the kinetic energy of the wind and the mechanical power of the shaft. The rotor of wind turbines for electricity production usually consists of 2 or 3 blades, although a 1 blade design does exist as well but is not widely used. The main material for the rotor blades is glass fibres or carbon fibres reinforced plastics. Wood is also used for the blade production, which is a more environmentally friendly material.

Drive train

The drive train contains the low speed shaft driven by the rotor, a gearbox and the high speed shaft connected to the generator. The gearbox transforms the high torque low speed rotation to low torque high speed rotation to meet the generator frequency.

Electrical system

The main component of the electrical system is the generator. It converts the mechanical energy into electrical energy. There are direct drive systems that connect the low speed shaft directly to a low speed generator, eliminating the need of gearboxes.

Yaw system

Horizontal axis wind turbines need a yaw system to move the turbine in the wind direction. For large wind turbines, an active yaw motor moves the turbine to the wind direction. Passive yaw systems can be used for smaller wind turbines. The misalignment of the wind direction with the rotation axis of the turbine blades induces extra structural loads and reduces the efficiency of the wind turbine as well. The degree of misalignment is defined here in yaw angles.

Nacelle

The nacelle accommodates the machiney and prevents the direct exposure of the machinery to the environment. It also transfers the loads from the rotor to the tower.

Tower/ support structures

The tower transfers the load from the nacelle to the foundation. For offshore wind turbines, the support structure comprises the tower and the foundation. Typical designs of onshore towers are tubular towers or lattice towers. Typical support structures are monotower, tripod, lattice tower, with gravity based or piled foundations.

Power control systems

The main purpose of the control system is to limit the energy output. There are two basic concepts to regulate the power production [41]. The active one, pitch control, regulates the power output through pitching of the blade, i.e. decreasing the angles of attack at a constant rotational speed. Hence it changes also the aerodynamic forces on the blade. The passive control concept uses the stall principle. By keeping a constant rotational speed of the rotor regardless of the mean wind speed, the angle of attack will increase with the mean wind

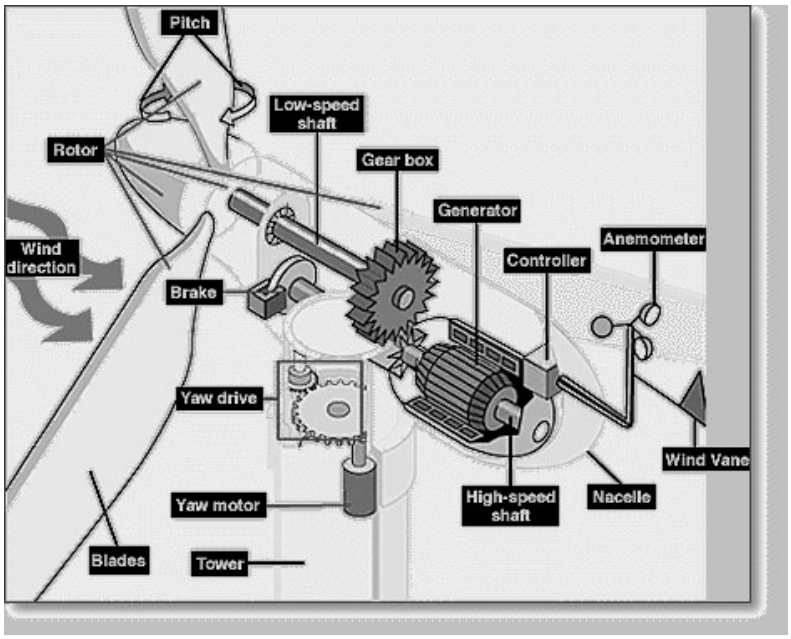

Figure 4.2: Different subsystems of a typical horizontal axis wind turbine. (©1997 DOE)

speed. The idea is to achieve a controlled stall of the flow above the nominal mean wind speed, increasing the drag forces, thus limiting the power output. Between these two basic concepts there is a whole range of hybrid concepts. In this case only these two basic concepts are taken into account. Figure 4.2 shows the schematic illustration of the different subsystems of a wind turbine.

4.3 Operational range of the wind turbine

The operational range of the wind turbine is defined by two wind speeds. The cut-in wind speed, which is the minimum wind speed at which a wind turbine starts producing energy, and the cut-out wind speed, which is the maximum wind speed at which a wind turbine can operate. Another characteristic wind speed is the rated wind speed. It is the wind speed at which the nominal power of a wind turbine is reached. These three wind speeds are shown in two power curves (see Figure 4.3) of two types of wind turbines.

The wind turbine starts operating at the cut-in wind speed, the power output increases with the third power of the wind speed. The nominal power output is reached at the rated wind speed. Until this point both types of wind turbines behave in a similar way. The difference lies in the higher wind speed regions where the power output has to be limited. The pitch controlled wind turbine

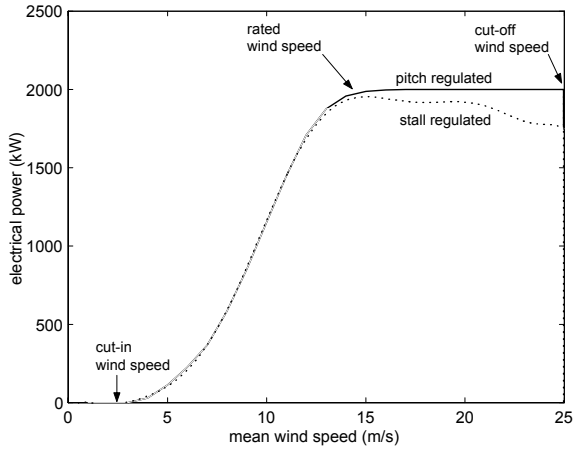

Figure 4.3: Power curves of a pitch regulated and a stall regulated wind turbine.

usually pitches the blade in the positive direction reducing the angle of attack, hence decreasing also the lift force and torque. This type of power control is more precise because the flow is still attached to the airfoil and the forces can be predicted with fair accuracy.

The passive stall control keeps the rotational speed constant, thus the angle of attack increases with the wind speed. At higher wind speeds (higher angles of attack), stall occurs, the flow is no longer attached to the airfoil and the lift forces collapse. The problem with a passive stall control is that stall is a highly non-linear unsteady phenomenon, thus the power output control becomes rather erratic because the forces can not be predicted accurately. Figure 4.3 shows idealised power curves, while in reality the fluctuation of the electrical power output is much larger.

The two types of power regulation also give rise to different load characteristics. Figure 4.4 shows the thrust forces of a pitch regulated and a stall regulated turbine, taken from [16]. As can be seen the thrust force of a stall regulated turbine increases monotonously with the wind speed. It has no possibility to reduce the aerodynamic loads. Furthermore, due to the stall, the blade damping is lower than pitch regulated blades. In contrast with the stall regulated turbines, the pitch regulated turbines can adjust the blade pitch angle to reduce the aerodynamic loads, hence reducing the thrust forces.

4.4 Pitch controlled turbine

Two specific turbines are used throughout this thesis. The reference pitch regulated turbine is a design wind turbine for offshore application, developed by Kvaerner Turbin and Kvaerner Oil & Gas Limited [38]. The turbine has two

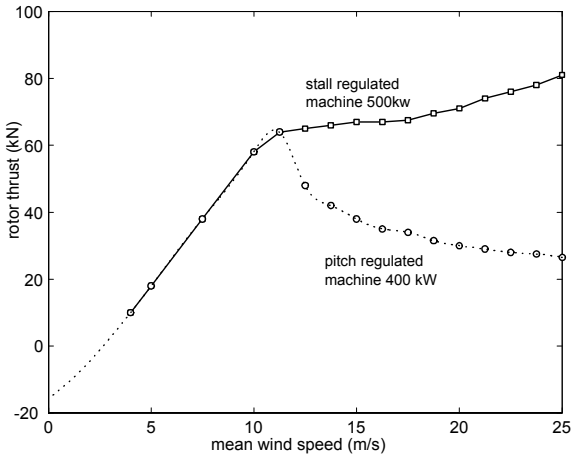

Figure 4.4: Rotor thrust forces of a pitch regulated and a stall regulated wind turbine.

blades with a rotor diameter of 80 m. The rated wind speed is 13.7 m/s. The blades are pitch controlled above the rated wind speed. The turbine has a rated power of 3 MW. The support structure consists of a monopile directly connected to a monotower through a flange. The water depth of the location is 20 m, see Figure 4.5

After cut-out wind speeds, the blades are pitched in a position to reduce the drag forces of the blade during storms. This means that the aerodynamic forces do not contribute in a significant way to the tower bending during extreme wind conditions.

In this thesis, it will be simply referred to as the pitch regulated wind turbine.

4.5 Stall controlled turbine

Besides the pitch controlled turbine, a reference stall turbine is also used for comparison of different turbine concepts. The stalled regulated turbine has a rated power of 1 MW with a rated mean wind speed of 16 m/s. The rotor diameter is 54 m and it has a hub height of 48 m. The support structure is of the monotower type with a monopile foundation. The water depth is 20 m. The cut-in wind speed is 3.5 m/s and the cut-out wind speed is 25 m/s.

One should note that the absolute comparison of responses from these two turbines is not relevant because the size of the these two turbines is not the same. The main purpose is simply to identify the fundamental differences in extreme responses dealing with two different control concepts. Observe that the stall turbine does not have the possibilities of reducing the thrust forces during a storm by blade pitching. This has an influence on the extreme response for the

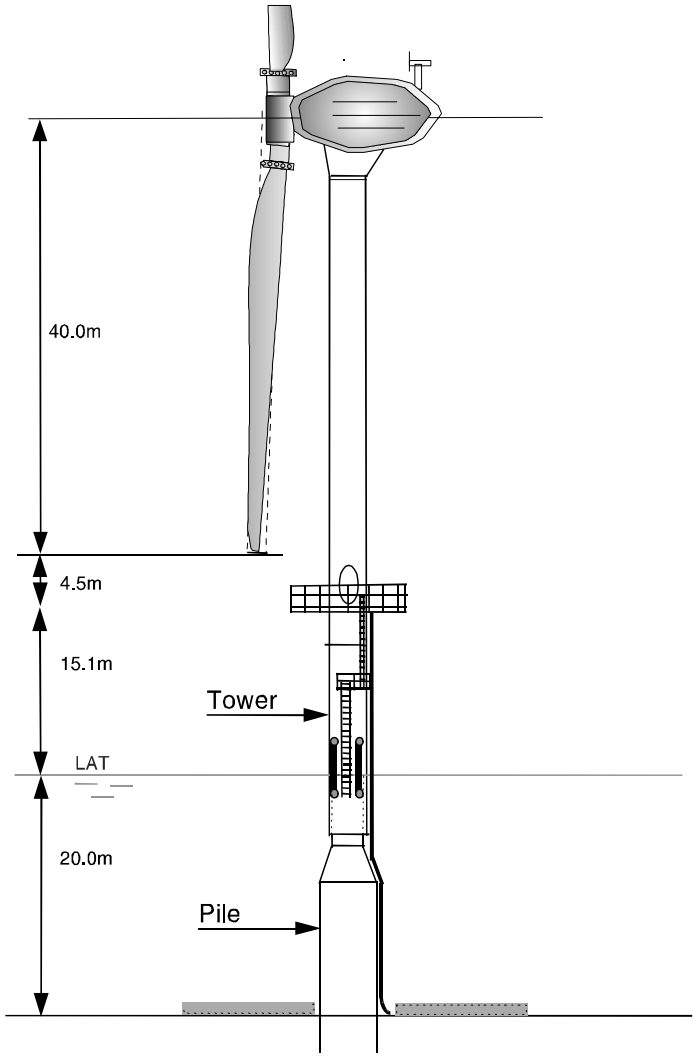

Figure 4.5: The dimensions of the pitch controlled turbine.

support structure, since the contribution of the aerodynamic thrust is relatively high compared to the pitch controlled turbine mentioned above.

In this thesis, it will be simply referred to as the stall regulated wind turbine. Main data of the pitch regulated and stall regulated wind turbine are listed in Appendix C.

Chapter 5

Load and Response models

5.1 General Description of Load and Response

Load models define mathematically the external loads perceived by the structure. The main sources of external loads are the fluctuating wind and wave loads. The load models usually connect the kinematic variables of the external processes (e.g. wind speed, water particle velocity, acceleration etc.) to external loads (e.g. pressures, distributed forces, moments etc.).

The response model describes how the structure reacts to the external loads, in terms of displacement, strain, stress etc. In this chapter, a short account is given of the load models used in the simulation program. The load and response models are based on engineering models widely used for design of wind turbines. It is assumed that the load and response models used here are accurate enough to predict the structural response. The uncertainties concerning the load and response models are not taken into account.

5.2 Aerodynamic loading

The wind load has a component originating from the wind speed and another component from the acceleration of the wind. However, for the blade response the acceleration term is negligible because the frequencies from the acceleration excitation are very high compared to the blade natural frequencies.

The classical blade momentum theory [98] forms the basis of the calculation of the blade loads. The flow passing an airfoil will produce lift and drag forces. The lift and drag forces are proportional to the relative velocity of the flow. The relative velocity of the flow is determined by the incoming undisturbed wind speed, the rotational speed of the rotor, the structural motion of the rotor and the induced velocity. The induced velocity is a disturbance velocity induced by the wind load on the rotor disk.

The lift and drag forces are also proportional to coefficients that characterise the variation of the lift and drag forces with the angle of attack. The

aerodynamic coefficients of the airfoils are determined from two dimensional wind tunnel tests for a fixed blade section. Corrections of these coefficients have been proposed for three dimensional flows on rotating blades.The main effect of the correction is that the lift coefficients are higher than the prediction from the two dimensional measurement for a calculated angle of attack. For a more detailed description of the 3D effects see [82] [86].

The aerodynamics of unsteady flow conditions is still under continuous investigation. The dynamic inflow model implemented in the simulation program DUWECS, applies a first order differential equation to account for the unsteady aerodynamic effects. Stall is another highly nonlinear phenomenon. An overview of the current status of the research on the rotor aerodynamics can be found in [83].

The uncertainty concerning the calculation of the aerodynamic loading is difficult to quantify. Especially during operation, the blade load and blade response are affected largely by non-linear phenomena. During storms, when the rotor is parked, the aerodynamic forces usually can be predicted with sufficient accuracy. For the present study it is assumed that the current models implemented in the simulation code predicts the aerodynamic loads satisfactorily.

5.3 Hydrodynamic loading

To compute the wave forces on the support structure, the wave kinematics must be determined. The water particle kinematics can be calculated using different theories. One can divide waves in two different categories, regular waves and random waves.

Regular waves

Regular waves are waves that have a defined period and are repeated periodically. Within regular waves, one can distinguish between linear and non-lnear waves. The linear wave theory is valid for waves of infinitely small amplitudes, e.g. Airy linear wave theory. For finite amplitude waves, non-linear waves theories apply, e.g. Stokes waves or Stream functions. The main characteristic of non-linear waves is that the crest is higher and sharper while the trough is rounder, compared to linear waves.

Random waves

Ocean waves have random characters and do not have a defined period. Within random waves one can distinguish also between linear and non-linear waves. The linear wave theory can be applied to generate random waves. The basic idea is that the summation of a large number of linear regular waves with random phases can reproduce random water waves. The enegy of different frequency components is determined from a discretisation of the wave spectrum.

Non-linear random waves have a higher order correction of the non-linear boundary conditions. The wave height distribution becomes non-Gaussian. The non-linear random wave is numerically more cumbersome to implement [55]. For descriptions and comparisons concerning simulations of ocean waves refer to [12].

In this thesis, the random wave kinematics are calculated using the Airy linear wave theory and regular non-linear waves are calculated using the Stream functions. The hydrodynamic loading is caused by the water particle velocity and acceleration. The forces that the moving water particles cause on a slender structure can be described by the Morison equation. The Morison equation assumes that the total wave forces consist of a linear addition of an inertial component and a drag component.

$$f = C_M \rho_w \frac{\pi D^2}{4} \frac{\partial u}{\partial t} + C_D \rho_w \frac{D}{2} |u| \, u \tag{5.1}$$

f is the total force per unit length of the cylinder, ρ_w is the water density. D is the cylinder diameter, u is the water particle velocity and $\frac{\partial u}{\partial t}$.is the local acceleration of the water particles. C_M is an inertial coefficient and C_D is a drag coefficient. These coefficients are determined from laboratory tests. The coefficients are functions of different parameters, the K-C (Keulegan-Carpenter) number, Reynold number, and roughness parameter etc.[78].

The Morison equation is applicable for hydrodynamically transparent structure, that is, the diameter of the structure is small compared to the wave length. For hydrodynamically compact structures, such as gravity based towers, diffraction theory has to be used [18]. Since only slender monopiles are considered for the support structure, the use of the Morison equation is sufficient to model the hydrodynamic loading. Current speed is not taken into account.

The integration of the hydrodynamic forces is carried out up to the mean sea level throughout this study. The linear wave theory implemented in the simulation program supports also Wheeler stretching [96]. Wheeler stretching assumes that the kinematics of the water particles at the instantaneous free surface are identical to those originally calculated at the still water level.

For the OWT in the coastal zone, the phenomena of breaking waves can be an important design factor. The impact load of breaking waves can excite the response from higher natural frequencies of the structure. However, the quantification of breaking wave loads still needs further study. In the study "Offshore Wind in the EC" [66] some simulation studies have been done on the sensitivity of the structural response of the support structure to different breaking wave models.

Two models were used, one based on the momentum theory and the other one based on laboratory measurements. The impact force on the structure is modelled as a triangular impulse. The result shows that the structural response is much lower than the external load integrated over the structure. The reason is that the short duration of the impact load does not have a large effect on the dynamic response of the structure. In a technical report [95] of the study "Offshore Wind in the EC", 5 and 10 modes for the support structure are used in the calculation of the dynamic response. However, the difference between the responses calculated using 5 and 10 dynamic modes is insignificant.

Nevertheless, the uncertainties concerning the modelling of breaking wave loads are large. The breaking process is certainly not deterministic and the idealisation of the breaking wave loads as impact loads, the modelling of the

impact loads with triangular impulses etc., have an influence on the breaking wave response. In the study "Offshore wind in the EC", it has been shown that the higher modes do not increase the response. However, this conclusion assumes that the breaking wave forces are modelled accurately. A probabilistic description of the breaking wave loads is necessary to integrate the variation of the breaking wave response into the extreme response analysis. For the time being this is not considered in this thesis.

5.4 Response calculation with DUWECS

DUWECS is a time domain simulation program that is capable of simulating the response of an offshore wind turbine. It includes the dynamics of the different components of an OWT. The major components and their interactions are illustrated in Figure 5.1 The tower model in DUWECS is a modal representation of the physical model built with the finite element program ANSYS. The modal analysis also includes the soil properties modelled as distributed springs and dampers.

It has to be noticed that the modal decomposition is efficient for calculation of dynamic response. The structural response of the support structure has a considerable quasi-static part. In the modelling of the support structure 20 modes are used, 10 dynamic modes and 10 static modes. The static modes are included for a better capture of the quasi-static part of the response

The rotor is modelled as a hub with hinged blades with flap and lead-lag flexibilities. This means that the blade itself is rigid and the flexibilities are concentrated on the hinge springs at the hub. This implies that estimates of the blade tip displacement using the hinge model may not be accurate enough because the flexibilities are distributed along the blade and not concentrated. However, for estimates of the blade root bending moment, the hinge model is sufficiently accurate, taken into account the uncertainties of the aerodynamic loads [15]. Moreover, comparison of 8 European wind turbine design codes have shown that using more advanced blade models (based on multibody dynamics or modal models, etc.) does not necessarily improve the blade response calculation compared to field measurements [80].

The controller has a crucial influence on the response of the rotor. It provides an active feedback of the rotor to a change in the external conditions in order to maximise the energy output and minimise the structural loads. For an overview of the DUWECS features and modules see [102].

The equations of motion are solved using a Runge Kutta time marching scheme and the results are stored in Matlab files. The outputs that are used here in the statistical analysis are the flap moment at the blade root and the overturning moment at the sea bottom.

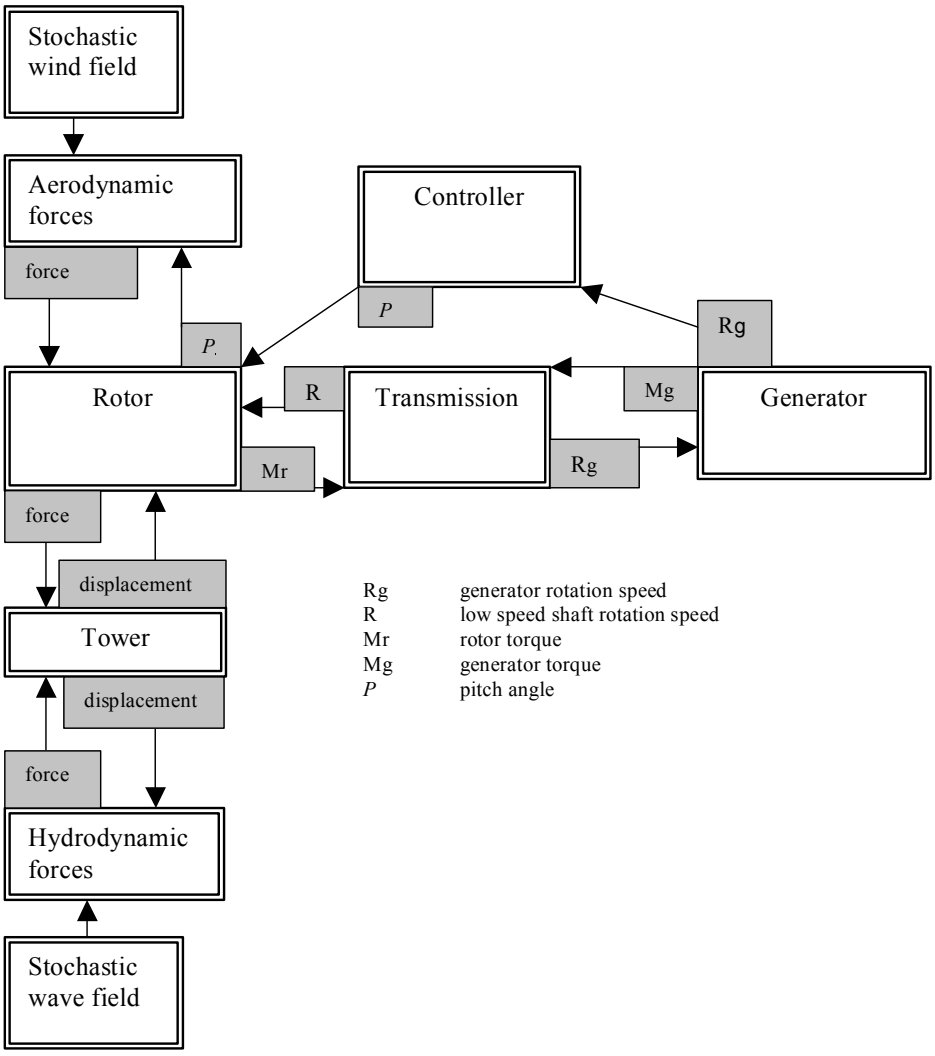

Figure 5.1: Interaction of the subsystems in DUWECS, modified after [57].

5.5 Response calculation in the frequency domain

The extreme response of an offshore wind turbine can be calculated in the frequency domain using linear models. The reason for using the frequency domain approach is because it requires less computational effort than the time domain approach.

However, it has its limitations as well. A simple calculation in frequency domain is limited to linear models with linear response characteristics. A usual assumption is that the input load is Gaussian, consequently the response is also Gaussian, due to the linearity of the structure and the load models. In many cases this means linearisations of the input loads, hence lnearised structural responses.

The presence of non-proportional damping, e.g. from the foundation or the rotation of the blade structure, requires further simplifications of the equations of motion. The resulting structural response is Gaussian.

The frequency domain method can be extended for non-linear problems. However, the simplicity and elegance of the method is overshadowed by the required mathematical manipulations. In spite of the limitations, it is a fast way to obtain a rough estimate of the response required for the preliminary design.

In Appendix B, the frequency domain method is applied to a stall controlled wind turbine to obtain the extreme responses during standstill.

Chapter 6

External load parameters

6.1 Table of the parameters variation

The number of external load parameters is numerous. To determine which of them have to be taken into account as stochastic variables, it is necessary to study the influence of these parameters on the response. The stochastic variables considered here are listed in Table 6.1 with the variable's range specified in it. The ranges specified are values that can occur in service life conditions. The choice of stochastic variables is limited and partially arbitrary, assuming that those chosen ones can have significant influence on the response variation. The pitch controlled turbine is used here to study the variation of the response.

The reference values of the load conditions is also specified in Table 6.1. The response of the reference load condition is compared to the response produced by the variation of the stochastic variables. Only one variable is changed at one time, while the rest of the variables maintains the reference value. In this way the relative influence of the stochastic variables can be quantified. All the load cases are limited to the normal operational range of the turbine, i.e. the wind speed is between the cut-in and cut-out wind speed. The reason is that the extreme response for this pitch controlled turbine occurs during operating conditions. The reference mean wind speed is 13 m/s because the response characteristic at this wind speed is similar to a stall controlled turbine. Thus, the conclusions drawn from here can be applied partially to the stall controlled wind turbine as well. The simulation length is 10 minutes and for every variation 10 simulations are carried out.

From every simulation the maximum responses, the flap moment and the OTM, are determined. Subsequently the mean value of the 10 maximum responses are calculated. The mean values of the maximum responses are normalised with the mean values of the maximum responses of the reference load condition. This ratio is used to indicate the influence of the stochastic variable on the the extreme response.

Table 6.1: Variation ranges and reference values of the stochastic variables

Stochastic variables	**Variation range**	**Reference value**
Mean wind speed U	8 m/s to 24 m/s	13 m/s
Turbulence intensity I_t	10 % to 20 %	12%
Wind shear exponent α	0.11 to 0.16	0.11
Yaw misalignment angle ϕ_y	–30 degrees to 30 degrees	0 degree
Significant wave height H_s	0.75 m to 6.75 m	2.27 m
Zero upcrossing period T_z	3.5 s to 8.5 s	5.5 s
Current speed U_c	0 m/s to 1.6m/s	0 m/s

6.2 Mean wind speed

Figure 6.1 shows the variation of the extreme flap moment and the overturning moment of the support structure at the sea bottom. The mean values of the maximum value from the maxima of 10 simulations are shown. The values shown are normalised with respect to the reference response at 13 m/s. As one may presume beforehand, the mean wind speed exerts a significant influence on the load. For a non-rotating and passive structure the axial load induced by the wind speed increases as the mean wind speed increases. However, the active influence of the wind turbine on the load itself through the controller changes the load characteristic of a wind turbine.

In this case the load increases with the mean wind speed till the rated wind speed. The load maximum is located near the rated wind speed. At higher wind speeds, the load decreases to a level comparable to those of the below rated wind speed (Figure 6.1). As comparison, Figure 4.4 shows the thrust forces of a pitch regulated and a stall regulated wind turbine. The thrust forces of the stall regulated turbine increase monotonically with the mean wind speed. The flap moment of the blade of a stall regulated wind turbine has qualitatively the same behaviour as the thrust force. This means that even though the controller is not a stochastic variable, the influence of the controller can not be neglected.

For the support structure the mean wind speed also plays a relevant role. The influence from the rotor can be clearly seen. The variation of the response of the support structure follows the variation of the rotor response. There is a slight difference at higher wind speeds; for the support structure the decrease in response is less pronounced. The controller effectively reduces the rotor flap moment by pitching, but the total thrust of the rotor is not reduced as significantly as the flap moment. This component contributes significantly to the bending of the support structure.

6.3 Turbulence intensity

The second parameter considered here is the turbulence intensity. The offshore wind measurements showed that the turbulence intensity fluctuates with the

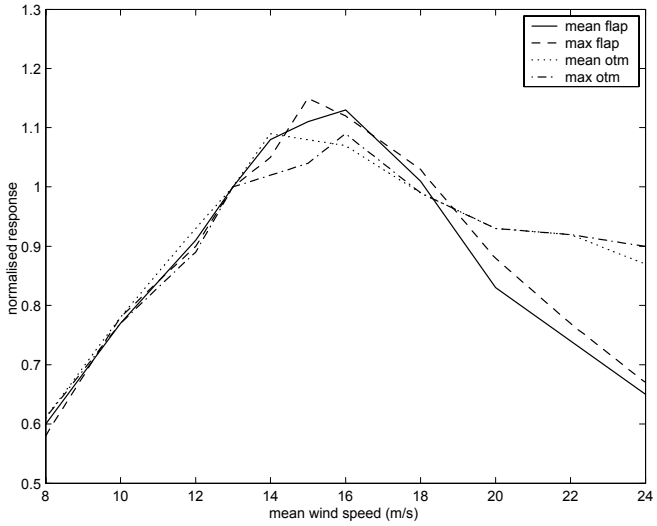

Figure 6.1: Variation of the maximum response with respect to the mean wind speed.

mean wind speed. The mean turbulence intensity generally increases with the mean wind speed, as the roughness of the sea surface is a function of the mean wind speed. However, measurements in the Danish North Sea have shown that at low wind speeds the turbulence intensity can be high, it decreases with the mean wind speed up to about 10 m/s and then increases again with the mean wind speed [47].

The measured turbulence intensity varies also for a given mean wind speed. This spreading of the turbulence intensity is smaller at high wind speeds and larger at low wind speeds. Generally, it is assumed that the offshore wind has a lower turbulence intensity than the onshore wind. Measurements have shown averaged values of the turbulence intensity of around 10% . The offshore wind turbine guideline from Germanischer Lloyd prescribes a turbulence intensity of 12%. For a turbine in a wind farm, the level of turbulence can increase due to the wake effect to 20%.

Figure 6.2 shows the variation of the extreme responses of the turbine with different turbulence intensities. The mean, and maximum of the flap moment and OTM are normalised with respect to the response with a turbulence intensity of 12%. The maximum increase in response is around 10 % compared to the reference response. The effect of the turbulence increase is more evident for the blade than for the support structure. The mean OTM does not increase much as the turbulence intensity increases from 10% to 20%. The maximum of the OTM has a significant increase at a turbulence intensity of 20%.

One has to be aware of the fact that for higher mean wind speeds, the effect of the turbulence can be more significant because the wind speed fluctuation is

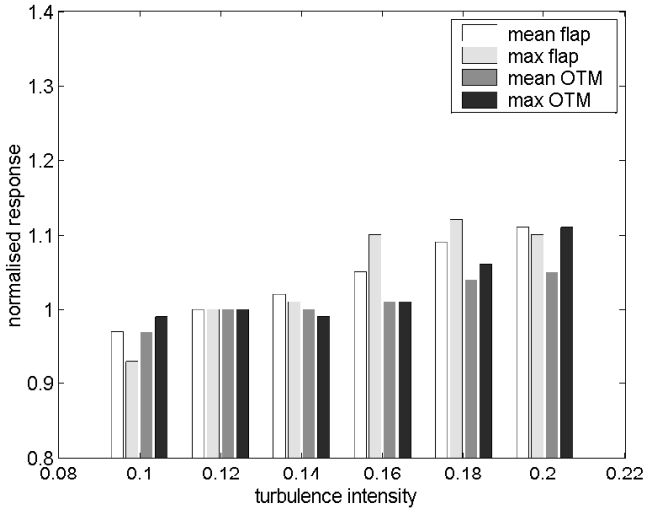

Figure 6.2: Variation of the mean of the extreme responses with the turbulence intensity; normalised with the mean of the extreme responses of the reference load condition.

increased in absolute terms even with a constant turbulence intensity. Instead of assuming a constant turbulence, the effect of the turbulence can be taken into account by taking the turbulence intensity as a function of the mean wind speed. In this case, a mean turbulence intensity is used because the variation of the turbulence intensity for a given mean wind speed is not taken into account.

6.4 Wind shear

The mean wind speed is a function of the height and the mean wind speed profile can be described by the power law (see Equation 3.4). As mentioned before the power law is an empirical formulation without physical background. Instead of varying the roughness length itself, the exponent of the power law is chosen as a variable. The exponent is a function of the surface roughness. For the open sea, the surface roughness is dependent on the sea state, thus it is not a constant value. However, most of the guidelines use a fixed value for the roughness length. The Germanischer Lloyd guideline suggests a wind shear exponent of 0.11 for offshore and 0.16 for onshore locations. The variation of the extreme response is studied for wind shear exponents between 10% and 20%.

From the response calculations, it becomes clear that the change in wind shear exponent has almost no effect on the extreme responses of the rotor and of the support structure. This is not surprising, since the maximum difference in the mean wind speed at the rotor tip is less than 5 percent of the mean wind speed at hub height within the variation range of the wind shear exponent [23].

However, it has to be noticed that for very large wind turbines, the problem may not be the variation of the wind shear exponent but rather about the validity of the wind shear model. The dimension of the rotor may exceed the internal boundary layer [52] and the wind profile assumed here may not apply. For the time being, the variation of the wind shear can be neglected.

6.5 Yaw misalignment angle

Ideally the wind turbine would operate without any yaw angle, that is, there is no misalignment between the incoming wind direction and the rotation axis of the rotor. However, due to the randomness of the wind, a certain misalignment always exists. The influence of this yaw angle on extreme response is studied here with angles from –30 degree to 30 degree.

The yaw angle changes the inflow condition due to the change in the tangential components of the wind speed. In this case the negative yaw angles increases the inflow angle and the angles of attack, the contribution of the drag to the flap moment also increases. For a positive yaw angle, the drag force is decreased, though the lift forces increase. Figure 6.3 shows the variation of the response for different yaw angles. The mean value and the maximum of the response are normalised with respect to the response with zero misalignment. For this specific turbine, the negative yaw angle considerably increases the blade response of the turbine, while at positive yaw angles the maximum blade response remains almost unchanged. The support structure is less susceptible to the misalignment and the response even decreases for positive angles. In the simulation code DUWECS a continuous sinusoidal variation of the yaw misalignment angle is implemented. Thus, this influence is partially taken into account, although not in a stochastic way.

6.6 Significant wave height and wave period

The design practice of the offshore industry characterises the offshore environment with two parameters, significant wave height, H_s, and a characteristic wave period, in this case the mean zero upcrossing period T_z. The two parameters (H_s and T_z) are estimates of visual observations, measurements or hindcast data. These parameters are usually represented in the form of a scatter diagram, which contains the number of observations of the sea states, providing the occurrence frequency of the sea states.

The H_s and T_z are not totally independent variables, this can be seen in the scatter diagram (see Figure 3.1). In this case the interest lies in the variation of the extreme response due to the variation of the significant wave heights and wave periods. For this reason the influence of these two parameters on the extreme response is studied without regarding the probability of occurrence of the sea states. The hydrodynamic environment exerts little influence on the rotor response. The maximum variation of the flap moment caused by the

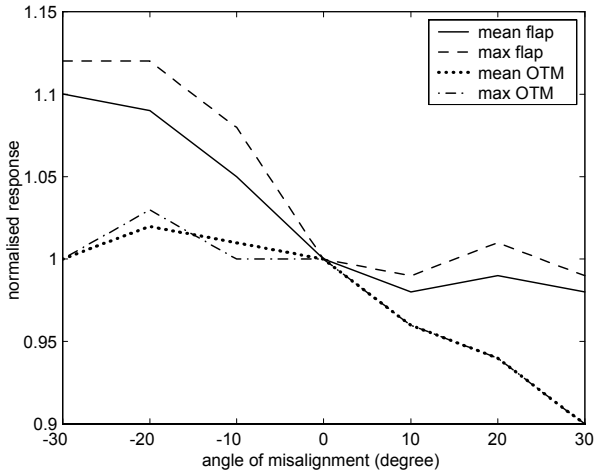

Figure 6.3: Variation of the response with respect to the misalignment of the wind.

variation of the significant wave height and wave periods is less than 3%. The little influence of the hydrodynamics parameters on the rotor has to do with the fact that the rotor has relatively high natural frequencies compared to the wave periods where the wave energy is concentrated.

In contrast to the rotor, the support structure perceives the change of the significant wave height and wave period with the respective change in the response. At low significant wave height the influences of the wave period is less evident. With increasing wave height the influence of the wave period becomes more visible. The maximum ratio of the response occurs at the maximum significant wave height with a wave period, that is very close to the first natural period of the support structure. The maximum increase of the response ratio is about 15%. The response ratio is the ratio between the mean of the maxima (of the flap moment or the OTM) with varying H_s and T_z and the mean of the maxima from the reference load condition (see Table 6.1).

The influence of the wind load on the response of the support structure is quite considerable, since the large increase of the significant wave height (from 0.75 up t0 6.75 m) leads only to a response increase of 15%. Remember that the variation applies to the H_s and T_z and the mean wind speed remains 13 m/s. On the other side, the period plays also an important role, because the response ratio of the OTM increases rapidly in the neighbourhood of wave periods that are close to the natural period of the support structure. The wave parameters play an important role for the dynamic response of an OWT and can not be neglected [23].

6.7 Current speeds

The sea current interacts with the wave altering the water kinematics. Many models exist to account for the interaction of waves and currents but the simple superposition method in which wave and current kinematics are computed separately and added together in the Morison equation is often used. The presence of current contributes to the drag forces, but the contribution is rather insignificant in the cases considered here. Both for the rotor and the support structure. For this reason it is not necessary to take the current as a stochastic parameter, unless the current speeds of the location have a much higher value than the current speeds considered here.

6.8 Selection of stochastic variables

From the parameters studied, the variation of the maximum response within the range of values specified in Table 6.1 are compared. It can be seen that for the rotor, aerodynamic parameters prevail. For extreme load during the turbine operation one can effectively disregard the hydrodynamic influences, while turbulence intensity and the flow misalignment angle can have considerable influence on the extreme response. The problem that prevents these variables being included in a probabilistic analysis is the lack of data. The hindcast database does not contain information on the turbulence intensity. In case data are available they can be incorporated in the probabilistic analysis, using the methodology outlined in this thesis.

An alternative to a constant turbulence intensity is the formulation of turbulence intensity that varies with the mean wind speed. This has been done for onshore design code [53].The misalignment of the wind flow is partially taken into account in the simulation code as a continuous sinusoidal variation of the yaw misalignment angle.

For the support structure both the aerodynamic and hydrodynamic parameters are relevant. At relatively 'calm' sea states it is possible to neglect the scatter of the significant wave height and the mean zero up-crossing period, since their influence on the response is marginal. Considering the amount of simulations and the stochastic modelling of the load environment, the mean wind speed can be seen as the most important parameter, followed by the hydrodynamic parameters H_s and T_z.

Other stochastic variables exist but they are not treated here. It is assumed that the chosen parameters have greater influence on the response, though the relevancy of the parameters can differ from location to location and from turbine concept to turbine concept. For example, for non-rotationally symmetrical structures the directionality of waves can affect the response characteristic. The hydrodynamic coefficients are also subject to considerable fluctuations associated with marine growth etc. The spreading in the foundation properties can change the dynamic behaviour of the wind turbine [103].

It has to be noticed that it is not always possible to have a statistical char-

acterisation for uncertain parameters, due to lack of information. The emphasis here is on the methodology, which remains the same with the inclusion of more stochastic variables. At the present, the mean wind speed, the significant wave height and the zero upcrossing wave period are considered as stochastic variables.

Chapter 7

Statistical analysis of the extreme responses

7.1 Description of the General Methodology

This section describes globally how the distribution of the extreme response from time domain simulations can be obtained. More details on the extreme response distribution can be found in Chapter 8 and 9. Two different methods to model the extremes are used. The MAX model, which only takes the maximum of each time series into account and the POT (peaks over threshold) model, which considers peaks over a certain threshold. These two methods fit the data to different distribution functions.

A third method, the Process method is not included in this chapter because the assumptions are different from the MAX and POT methods. Different fitting methods which can be applied to fit the distribution functions are given. The influence of the different fitting methods on the distribution is studied

The response of every sea state is analysed separately to determine the conditional distribution of the maximum response for that sea state. Every simulation of the structural response to a random sea state is different. Thus, after carrying out a series of simulations, the conditional response distribution for that sea state can be determined. This conditional distribution of the response for a given set of sea state parameters is often termed a short-term distribution.

The sea states are associated with certain occurrence probabilities. In a continuous description of the sea state occurrence probabilities, the CDF of the extreme response for a random sea state is given as

$$F(m)_{\text{rand om}} = \iiint F(m|\bar{U}, H_s, T_z) \cdot f(\bar{U}, H_s, T_z) d\bar{U} dH_s dT_z \tag{7.1}$$

The conditional distributions of the response variable m is multiplied by the joint probability density of the parameters $\bar{U}, H_s$ and T_z and integrated

over the possible variation of these parameters. In practice, the sea state has a discrete description, thus, the conditional distributions are 'weighted' with the occurrence probabilities of the corresponding sea state and the sum of all the weighted contributions represents the distribution of the extreme response for a random sea state. This distribution that takes into account the contribution from different conditional distributions are also called the long-term distribution.

To extrapolate the response distribution to a longer period, one usually assumes the independence of the sea states and then the distribution is simply the distribution for a random sea state elevated to the power of N, where N is the number of independent sea states in a period of, e.g.one year. The probability of non-exceedence $F_N(m)$ for a maximum response m in N sea states is then defined as

$$F_N(m) = (F(m)_{\mathrm{rand\,om}})^N \tag{7.2}$$

In fact, the assumption that all the sea states are independent can lead to a conservative estimate. To achieve the assumption of independence of events different approaches can be applied. The approach applied to the support structure in the Opti-OWECS project was to model the storms as independent events and then derive the distribution of the extreme response due to storms of random occurrence. Such an approach may not be applicable to the rotor, since normal operating conditions may induce more severe response to the rotor than during the storms. However, it has been shown that the number of independent sea states is less relevant if the response of interest corresponds to a large return period, e.g. 50 year [100]. Because the extreme response increases only slowly for large number of independent sea states N.

In case N is the number of sea states in one year, the distribution obtained is a distribution that describes the cumulative distribution of the year maxima. Often an extreme response is characterised by a return period T , this can be defined as

$$T = \frac{1}{1 - F_{1\ year}} \tag{7.3}$$

where $F_{1\ year}$ is the cumulative distribution of the year maxima. For example if $F_{1\ year} = 0.99$ then the return period is 100 years. By using the inverse of the cumulative distribution of the year maxima one can obtain the extreme response of the corresponding return period.

The long-term distribution of the determined extreme response is assumed to completely describe the variations of the extreme response. The question now is what is the chance that a structure will withstand the extreme loads to be encountered during its service life. If the strength of the structure is considered to be deterministic and a critical value of the strength can be determined, the probability of failure is simply the probability that the response is higher than the critical strength. In reality the strength of the structure is not deterministic,

but for this problem, the only failure mode considered is the exceedence of the yield stress.

The yield stress has a much narrower variation than the structural response, so that the assumption of deterministic strength can be justified. However, it depends on the type of problem; for example, for foundation analysis, the uncertainty of the strength can be considerably larger than the variation of the loads or responses. Again, this has to be put in perspective because for large gravity base offshore structures, the local variations of the soil strength are more or less averaged out over a large volume and in such cases the variability of the loads becomes significant. For smaller foundations, this spatial averaging effect will be less pronounced and the variation in the local soil strength becomes important in a reliability analysis.

Of course, there are other extreme load situations that do not depend on the external conditions only, such as an occurrence of faults. When a fault exists in combination with unfavourable external conditions, extreme responses can occur. The probability of such kind of events are largely unknown. A set of extreme load cases that can occur during the service life are listed in the IEC code[53] and the structure is expected to withstand these kinds of extreme loads.

7.2 Extreme value distribution

The commonly applied distribution models to fit the extreme response are briefly described. The different types of extreme distributions correspond to different types of parent distributions. The wind input is Gaussian but non-linearity of the response and load models make the response non-Gaussian. However, if the response is nearly Gaussian, the maxima of the response should belong to the attraction domain of one of the theoretical extreme value distributions.

For distributions of the exponential type, asymptotic expressions exist for the largest values. There are three extreme value distributions that describe this domain of attraction. The Gumbel, the Fréchet and the reverse Weibull distribution. The unifying description of these extreme value distributions is given by [75] in the following parametrisation,

$$G_0(x) = \exp(-\exp(-(x-u)/s)), \qquad \gamma = 0 \tag{7.4}$$

$$G_\gamma(x) = \exp\left(-\left(1+\gamma\frac{x-u}{s}\right)^{\frac{-1}{\gamma}}\right), \qquad 1+\gamma(x-u)/s > 0,\ \gamma \neq 0. \tag{7.5}$$

where u is a location parameter, s is a scale parameter and γ is a shape parameter. Equation 7.4 is the limiting form of the equation 7.5 for $\gamma \to 0$. It can be noticed that

- $G_0(x)$ is the Gumbel distribution (i.e. $\gamma \to 0$)
- $G_\gamma(x)$ is the Frechét distribution for $\gamma > 0$

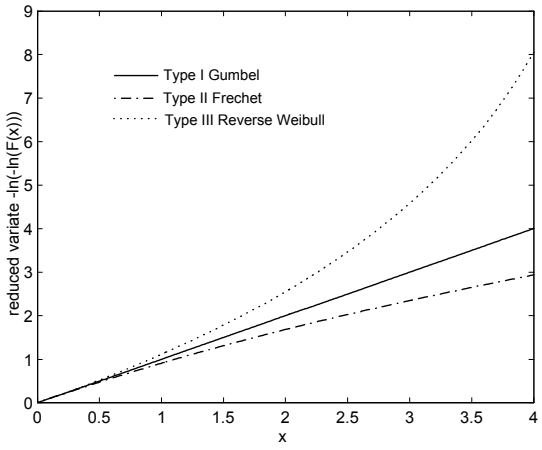

Figure 7.1: The three types of the extreme value distribution.

- $G_\gamma(x)$ is the reverse Weibull distribution for $\gamma < 0$

For the Fréchet distribution there is a left end point equal to $-s/\gamma + u$. The right end point for the reverse Weibull distribution is $s/|\gamma| + u$. Equation 7.5 can pose a problem for the extrapolation of the extreme responses if the shape factor γ is negative. The existence of a right end point means that there is an upper limit to the maximum response. The establishment of an upper limit to the extreme flap moment or the overturning moment is difficult to be justified physically with the limited simulation data. For this reason, GEV distribution with a negative shape parameter is not used.

Figure 7.1 shows the three extreme value distributions, the shape parameters for the Frechét and reverse Weibull distribution are 0.2 and -0.2 respectively. The Gumbel distribution is a straight line on this scale, the reverse Weibull has a curvature toward the right end point of the distribution. The Frechét distribution has the heaviest tail of all the three distributions and is slightly curved in this plotting scale.

As an alternative, one can force a positive shape factor of the GEV distribution by fitting the data to a Frechét distribution using an α parametrisation, which can be written as

$$G_\alpha(x) = \exp\left(-\left(\frac{x-u}{s}\right)^{-\alpha}\right), \qquad \mathrm{x} \geq u \tag{7.6}$$

The Fréchet distribution has a heavier tail than the Gumbel distribution. Another useful distribution which is used for the modelling of the smallest n random variables is the three parameter Weibull distribution

$$G_k(x) = 1 - \exp\left(-\left(\frac{x-u}{s}\right)^k\right), \qquad \text{x} \geq u \tag{7.7}$$

To differentiate it from the largest value distributions, k is used to denote the shape factor instead of γ. This distribution has a left end point at $x = u$ and the tail of this distribution is less heavy than the Fréchet distribution. Other suitable distributions that can be used to fit the extremes responses of an OWT are: the Normal distribution, Gamma distribution, Rayleigh distribution etc. For a list of the distributions used in this study see Appendix A.

7.3 Distribution of POT models

It has been shown [74] that the peaks over a certain threshold values follow a Generalised Pareto distribution if the parent distribution belongs to the attraction domains of the Extreme Value distributions. Examples of such parent distributions are the Normal, Gamma, and Exponential distributions etc. For each of the Extreme Value distributions, there is a correspondence with one of the POT distributions. The Generalised Pareto distribution has the following parametrised form

$$W_\gamma = 1 - \left(1 + \gamma\frac{x-u}{s}\right)^{\frac{-1}{\gamma}} \text{ for } \left\{ \begin{array}{ll} 0 < x & \gamma > 0 \\ & if \\ 0 < x < 1/|\gamma| & \gamma < 0 \end{array} \right\} \tag{7.8}$$

$$W_0 = 1 - \exp\left(-\frac{x-u}{s}\right) \text{ for } \gamma = 0 \tag{7.9}$$

u is the location parameter, s is the scale parameter and γ is the shape parameter. W_0 is the limiting form of the Generalised Pareto distribution for $\gamma = 0$. The correspondence with the Extreme value distribution can be seen clearly

- $W_0(x)$ is the Exponential distribution (i.e. $\gamma \to 0$)
- $W_\gamma(x)$ is the Pareto distribution for $\gamma > 0$
- $W_\gamma(x)$ is the Beta distribution for $\gamma < 0$

Observe again that the Beta distribution has a right end point, thus, such a distribution can not be used to extrapolate the extreme peak values, because the existence of such boundary can not be determined using only limited data from simulations.

The Pareto distribution offers an optimal fit if the parent distribution corresponds to the attraction domain of the Fréchet distribution. The Exponential distribution is a suitable distribution if the parent distribution belongs to the attraction domain of the Gumbel distribution. One can see that the Exponential distribution is the three parameter Weibull distribution with the shape parameter $\gamma = 1$. Thus, the use of the three parameter Weibull distribution may offer more advantage due to the extra flexibility of the shape parameter.

7.3.1 Fitting of the data to the distribution model

There are different methods to fit the data to the distribution models presented in the previous sections. Three methods are described here. These methods are: the method of moments, the least squares fit and the maximum likelihood estimate.

The method of moments

The method of moments consists of matching the statistical moments of the data to the statistical moments of the distribution function. The Gumbel distribution is taken here as an example. The Gumbel distribution has two parameters. Hence, with the first two statistical moments, the distribution parameters can be determined. The expected value μ_x of the Gumbel distribution is defined as

$$\mu_x = u + \gamma_e \cdot s \tag{7.10}$$

where γ_e is the Euler constant. The standard deviation σ_x is defined as

$$\sigma_x = \frac{s\pi}{\sqrt[2]{6}} \tag{7.11}$$

By matching the sample statistical moments to the statistical moment of the distribution, one can determine the two distribution parameters u and s. The Gumbel distribution is positively skewed and the skewness is independent of the two distribution parameters. The skewness β of the Gumbel distribution is 1.1396.

The reverse Weibull distribution is not considered because of the existence of the right end point of the distribution. The existence of the statistical moments of the Fréchet distribution depends on the shape factor α, the j-th moment does exist if $j < \alpha$. This makes the parameter estimation with the method of moments unpractical, because the existence of the statistical moments is not guaranteed.

Since the Gumbel distribution has a fixed skewness, it offers also less flexibility to match the data skewness. The three parameter Weibull distribution can be a suitable distribution. The first three statistical moments of the Weibull distribution can be used to match the sample statistical moments. Solving the three equations simultaneously one can obtain the estimates of the distribution parameters. The moments of the Weibull distribution are [67]

$$\mu_x = E[x] = u + \sigma \cdot \Gamma\left(1 + \frac{1}{k}\right) \tag{7.12}$$

$$\sigma_x = E[(x - \mu_x)^2] = \sigma \cdot \sqrt{\Gamma\left(1 + \frac{2}{k}\right) - \Gamma^2\left(1 + \frac{1}{k}\right)} \tag{7.13}$$

$$E[x^3] = \sum_{n=0}^{3} \binom{3}{n} \cdot u^{3-n} \cdot \sigma^n \cdot \Gamma\left(1 + \frac{n}{k}\right) \tag{7.14}$$

where Γ is the Gamma function. The solution of these three equations are not as straightforward as for the Gumbel distribution, since it involves the solution of nonlinear equations. These equations can be solved numerically.

The least squares method

The least squares method consists of finding a set of distribution parameters that yields a minimum deviation between the distribution function and the sample data. The measure used here is the square distance between the distribution function and the emprical distribution function. The empirical function is obtained by ordering the data x such that $x_{i+1} > x_i$. The empirical cumulative probability $\hat{F}$, corresponding to x_i is

$$\hat{F}(x_i) = \frac{r_i}{1+N} \tag{7.15}$$

where r_i is the rank of the data point x_i and N is the total number of data points. If x_i is the minum then $r_i = 1$, conversely if x_i is the maximum then $r_i = N$. Equation 7.15 is the so called Gumbel plotting position. There are other plotting positions that can be used. For example, in conjunction with the least squares fit and the Gumbel plotting position a small bias is introduced when each data point is given an equal weightage [27]. Gringorten has suggested a different plotting position [45] to remove the bias.

The distribution parameters $\boldsymbol{\theta}_{lsq}$ determined by the least squares method can be expressed as

$$\boldsymbol{\theta}_{lsq} = \min\{\sum \Big(F(x_i|\boldsymbol{\theta}) - \hat{F}(x_i)\Big)^2\} \tag{7.16}$$

$\boldsymbol{\theta}$ is the vector of the distribution parameters, $F(x_i|\boldsymbol{\theta})$ is the conditional distribution function and $\hat{F}(x_i)$ is the empirical distribution. In many cases the minimisation problem can be simplified through a transformation of the data.

For example, the Gumbel distribution has a double exponential form. Through a double logarithmic transformation, the right hand side of the Gumbel distribution will become a linear equation of the form $Ax + B$. The distribution parameters can be derived from the coefficients of the linear equation. For three parameter distributions the Equation 7.16 is solved using a non-linear minimisation method.

Maximum Likelihood Estimate (MLE).

The third method employed here is the MLE. The essential element of this method is the conditional density function $f(x_i|\boldsymbol{\theta})$. The likelihood function $\prod f(x_i|\boldsymbol{\theta})$ is the product of the conditional density functions. The likelihood function is a function of the distribution parameters. The maximum likelihood estimate of the distribution parameters $\boldsymbol{\theta}_{mle}$ is defined as

$$\boldsymbol{\theta}_{mle} = \max\Big\{\prod f(x_i|\boldsymbol{\theta})\Big\} \tag{7.17}$$

Basically, it is a selection criterion. The best distribution parameters are those that correspond to the maximum of the likelihood function.

In many cases the log-likelihood is used, since the product of the conditional density would become a sum, which is easier for mathematical computations. As with other numerical estimates, a local maximum can be computed instead of the global maximum. For a good estimate of the the initial values for the numerical iteration, one can compute the initial distribution parameters with other methods such as the method of moments. Fortunately, this usually happens only for multi-modal data, which is not the case here.

7.3.2 Goodness of fit test

In order to judge how well the chosen distribution fits to the data, a goodness of fit test is applied to the fitted distribution. There are many different tests depending on the purpose of such a test. A graphical method is a simple method of check. Usually the distribution function can be transformed in such way that it can be written as a linear function in logarithmic scale. The sample CDF is then plotted using this scale. The fitted distribution will appear as a straight line. Depending on how the sample distribution deviates from this straight line, one can accept or reject the fit.

A starting point of the hypothesis testing is a hypothesis about a certain characteristic of the data called the null hypothesis. In this case, the null hypothesis is concerned with the fact whether the distribution function fit the data or not. The acceptance or rejection of the null hypothesis is determined in light of the data. If there is a large difference between the data and the chosen distribution model, then the null hypothesis is rejected. The quantitative criterion to reject the null hythothesis is given the goodness of fits test. Notice that a failure to reject the null hypothesis is not the same thing as accepting the null hypothesis.

For a less subjective judgement one can use the χ^2 test. In this test, the data are arranged into a discrete number of bins that span the interval. The number of data points in each bin is then compared to the expected number of data points predicted by the fitted distribution function. The expected number can be obtained by integrating the CDF over the interval limits and multiplying by the number of data. The χ^2 test is in fact less subjective than the visual test but it is not entirely objective either.

The outcome of the statistics depends on the number of bins and the size of the bins. There are no universally accepted rules for choosing these parameters; however, it is recommended to use equiprobable bin sizes (i.e. the probability in each bin is the same) with the expected number in each interval being five or more [61]. Since the number of data is not large (around 50), this would lead to a large bin size. In all the subsequent tests, bins of equal size are used. The χ^2 statistics is defined as

$$\chi^2 = \sum_{j=1}^{k} \frac{(N_j - np_j)^2}{np_j} \tag{7.18}$$

where N_j is equal to the number of data points in the bin j, n is the total

number of the samples and p_j is the probability density integrated between the limits of the bin j. The χ^2 is then checked against the critical value of the χ^2 distribution for the given number of degrees of freedom and a significance level. If the χ^2 is lower than the critical value, then the null hypothesis is not rejected, thus the chosen distribution with its distribution parameters can be considered a probable fit.

Another category of test is based on the sample distribution function. The deviation of the fitted distribution function is a measure for the goodness of fit. A popular test in this category is the Kolmogorov-Smirnov test. It measures the largest vertical difference between the sample distribution function and the fitted distribution function:

$$D = \sup_x |F_n(x) - F(x)| \tag{7.19}$$

where, $F_n(x)$ is the sample distribution function. If the sample size is small then the Kolmogorov-Smirnov test is to be preferred to the χ^2 test. Another powerful class of tests is the quadratic statistics, where the square of the deviation is taken as a measure. The Cramer-von Mises test measures essentially the sum of the square deviations and the Anderson-Darling statistics is a weighted sum of the deviations, with more weight given to the tails of the distribution. Since the goal here is to predict extreme responses, the tail of the distribution will play an important role. For this reason the Anderson-Darling test is to be preferred to the Cramer-von Mises test because of its ability to detect deviations in the tails. The Anderson-Darling test can be written as

$$A^2 = -\frac{1}{n}\sum\{(2i-1)\ln[F(x_i)(1-F(x_{n-i+1}))]\} - n \tag{7.20}$$

In this case the data are ordered in an ascending order, that is $x_1 < x_2 ..... < x_n$. The choice of test depends on which part of the distribution is more important for the response estimate. A test that is good for measuring deviations of the mean values may not detect deviations of the tail and vice versa. For more details on the testing procedure see [28].

In many cases, the formalism of the test still can not replace a visual inspection of the data. A practical approach is to plot the data on different probability papers and check if data appear as a straightline. The suitability of the distribution models can then be confirmed by goodness of fit test.

Chapter 8

MAX models

8.1 summary

The methodology described in this chapter is applied to the response of the pitch regulated wind turbine, i.e. flap moment and the overturning moment. The maximum of the response is extracted for each simulation. These values are fitted to an extreme value distribution, which is a quite straightforward approach. A disadvantage of this method is that many simulations are necessary, since from each simulation only the maximum value is used.

In the first place, the influence of the number of simulations and of the length of the simulations on the fitted distribution are investigated. It is necessary to determine beforehand how many simulations are necessary and how long the simulation length should be in order to achieve a reliable fit of the distribution. In addition, a Bayesian analysis [13], that incorporates the uncertainties of the choice of the distribution and of the distribution parameters into the estimate of the extreme response, is applied. Furthermore, the variation of the estimates of the extreme responses that are caused by different fitting methods and the chosen parametric models are studied.

The study of simulation length and simulation number is applied to the MAX model. The estimate of the extreme response from the MAX approach will be used as a reference value for the estimates obtained using the POT and Process models in the following two chapters.

8.2 Simulation number and simulation length

8.2.1 Study of the number of simulations for wind

Obviously the quality of the long-term estimate of the response depends on the amount of information available. One can simulate, let's say, 20 years and estimate the extreme response distribution from, for example, the annual extremes or monthly peaks over a certain threshold. The advantage of using the annual

extremes is that they can be considered independent, although the amount of data is still limited. Even with 20 year simulation data, there are only 20 data points. For this reason, one can use other information of the data, such as peaks over threshold or statistical moments etc.

Using simulations of a long period such as 20 years is not a practical approach because it would take a lot of simulation time even with today's high performance computers. Thus, the influence that the limited information exerts on the estimates has to be analysed. The two variables analysed here are the number of simulations and the length of simulations.

Using the MAX model the distribution of the extreme response during a given sea state is determined. The question is how many simulations are needed and how long the simulation should be. The expectation is that there will be a limit where more simulations do not change the estimates of the extreme values, or at least the extra information from simulations is marginal to justify the extra computational effort.

To analyse the influence of the number of simulations on the statistical parameters, *100 simulations* have been carried out. Hence, the population size from which all the random drawings take place, is 100. The simulation length is *10 minutes* and the *mean wind speed is 13 m/s*. The turbulence intensity is *0.12* and the turbulence spectrum used is the *von Karman spectrum*[1]. From the 100 maxima, N samples are randomly drawn. This random drawing is repeated many times. The sample size[2] of the random drawing varies from 10 to 90.

Figure 8.1 shows the fluctuation of the mean value for 100 drawings with different sample sizes N. From the 100 maxima obtained by time domain simulations, 10, 30 and 60 maxima are randomly drawn. The mean values of these randomly drawn maxima (10, 30, 60) are calculated. The mean values are normalised with the reference mean value of the 100 maxima obtained by simulations. The random drawing is repeated for 100 times (the horizontal axis).

It can be seen that the variability of the mean values is rather small. Even with 10 maxima the variation of the mean value is no more than plus or minus 3 percent. Figure 8.2 shows the variation of the standard deviation for different sample sizes. The variation of the standard deviation is much larger. The samples are the same as those drawn for Figure 8.1. The standard deviation is normalised with the reference standard deviation from the 100 maxima obtained by simulations.

The variation can vary as much as plus or minus 50% from the reference value. It is evident that the variation range of the mean value and the standard deviation decreases with an increasing number of simulations

Figure 8.3 shows the variation of the mean values and of the standard deviation of the randomly drawn maxima of different sizes N. To be more precise, 100 random drawings are performed. Each random drawing consists of N max-

[1] See also Table C.3 for the parameters of the time domain simulations. If they are not explicitly mentioned, these parameters are used.

[2] In this context, the sample size, the number of simulations and the number of maxima, all of them refer to the number of randomly drawn maxima from a total population of 100 maxima obtained from simulations.

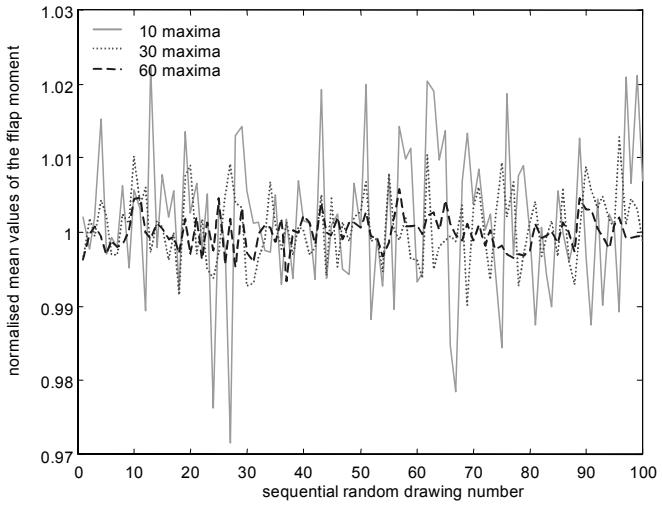

Figure 8.1: Variation of the mean value of the randomly drawn maxima of the flap moments with 3 different numbers of maxima, normalised with the mean value from the 100 maxima.

ima with N varying from 10 to 90. The measure of variation of the mean values is defined as the ratio between the standard deviations of the mean values of the randomly drawn maxima and the mean value of the 100 maxima. The variation of the standard deviation is defined as the ratio between the standard deviations of the standard deviations of the randomly drawn maxima and the standard deviation of the 100 maxima (see also Table 8.1).

As mentioned before the variation of the mean values is very small compared to the variation of the standard deviation. The decrease of the variation of the standard deviation is nearly linear with the number of maxima. The standard deviation of the mean values and the standard deviation of the standard deviations are listed in Table 8.1. The variations of the mean values and standard deviations approach zero since the random drawings are carried out without replacement[3].

The histogram of the 100 maxima obtained from simulations is plotted in Figure 8.4 and a Normal probability density function is also shown. The fit is obtained by fitting the sample CDF. The skewness of the 100 maxima is 0.2 and kurtosis is 3.47. The skewness and the kurtosis show that the extreme flap moment has a slightly heavier distribution tail than the Normal distribution and the upper tail is slightly larger than the lower tail.

From the variation of the statistical descriptors, it is difficult to judge how

[3]Without replacement means in this context that every random drawing consists of N elements and these N elements are drawn without replacement. For the next random drawing these N elements are returned to the population. This is in fact a variation of bootstrap.

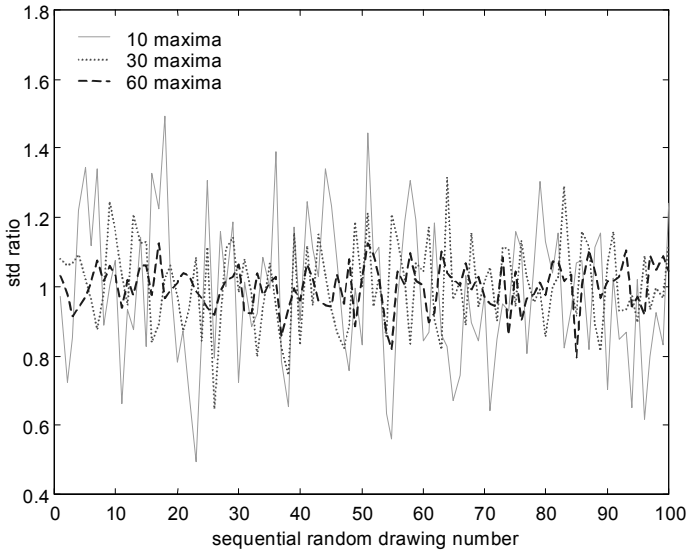

Figure 8.2: Variation of the standard deviations of the randomly drawn maxima of the flap moments with 3 different numbers of maxima, normalised with the standard deviation from the 100 maxima.

Table 8.1: variation of the mean and standard deviation of the maxima of the flap moment with the number of simulations

number of simulations	$\frac{\sigma_\mu}{\mu_{ref}}$ in %	$\frac{\sigma_\sigma}{\sigma_{ref}}$ in %
10	0.99	21.2
20	0.59	15.8
30	0.47	12.5
40	0.33	10.6
50	0.28	7.5
60	0.23	6.6
70	0.20	4.5
80	0.14	4.4
90	0.10	2.2
σ_μ is the standard deviation of the mean values of the maxima	μ_{ref} is the mean value of 100 maxima	
σ_σ is the standard deviation of the standard deviation of the maxima	σ_{ref} is the standard deviation of 100 maxima	

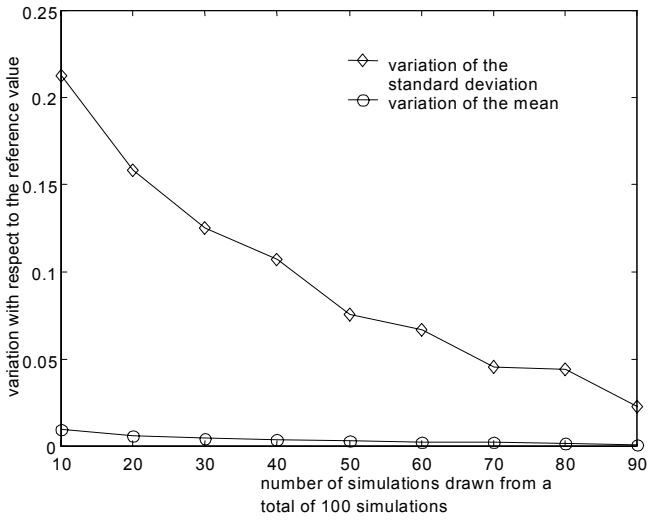

Figure 8.3: COV of the mean and of the standard deviation of the flap moment maxima from randomly drawn samples for different sample sizes.

many simulations, i.e. maxima, are needed to enable a good estimate of the distribution of the extreme response. For this reason the randomly drawn maxima are fitted to a 3 parameter Weibull distribution using the least squares fitting method. The variation of the distribution parameters with the number of maxima is analysed.

Cumulative distribution functions (CDF) are used to fit the sample CDF. The disadvantage of fitting a CDF is that an over-smoothing effect is taking place, so that details of the data distribution are lost, for example a multimodal distribution can not be easily recognised in the sample CDF. In such case, one can use histogram to visualise the details of the distribution.

The variation of the distribution parameters with the number of simulations is non-Normal, thus, the standard deviation may not give a good picture of the parameter fluctuation. Instead, the maximum range of the variation is chosen as an alternative indicator, which gives the maximum and the minimum variation of the distribution parameters. Furthermore, the 99 percentile of the distribution of the extreme flap moment is also shown. Figure 8.5 shows the variation of the distribution parameters and the 99 percentile of the distribution.

For all the distribution parameters, the boundaries of the 95% and 5 % of the distribution are also given, assuming that the variation of the distribution parameters follows a Normal distribution. This interval is much smaller than the variation of the range defined by the maximum and the minimum of the fitted distribution parameters. This may suggest that the range values are strongly influenced by outliers. This is a by-product of the least squares fitting method. The fitting of the 3 parameter Weibull distribution can produce uncommon

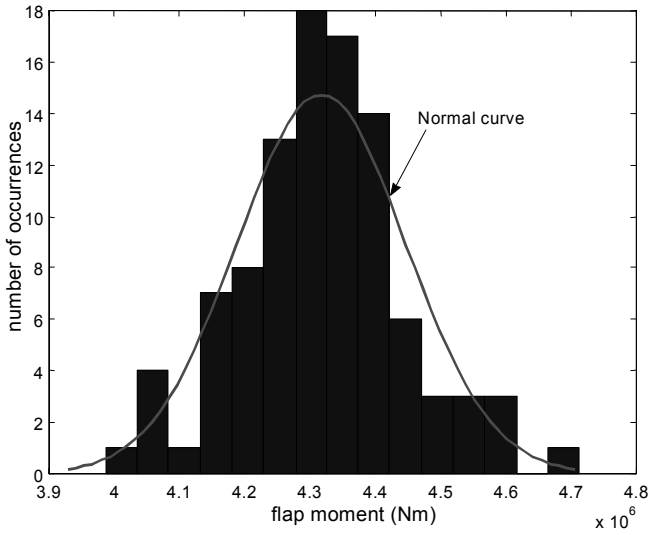

Figure 8.4: Histogram of the maxima of the flap moments from 100 simulations.

parameter combinations. In such cases, the scaling parameter s can be larger than the location parameter u. Thus, the interval bounded by the 95% and 5% of the distribution gives a more realistic picture of the parameter variation than the ranges.

The number of uncommon combinations of parameters decreases as the number of simulations increases. It can be seen that the range defined by the maximum and the minumum converges to the 95% and 5% boundaries. The variation of the estimated response decreases rapidly till the simulation numbers reaches 50 and after that it decreases slowly. It can be assumed that if the number of simulations is around 50, then the estimated distribution parameters do not deviate significantly from the reference one. The 99 percentile of the distribution of the extreme flap moment confirms this trend. The reference distribution parameters are the parameters estimated from 100 simulations. The variation in the predicted extreme values can deviate considerably if the number of simulations used to fit the response distribution is low. With 50 simulations, the maximum and the minimum of the 99 percentile of the distribution differ no more than 15% from each other (see Figure 8.5, lower right).

8.2.2 Study of the number of simulations for waves

The overturning moment of the support structure is strongly influenced by the wave loading. The number of simulations required for the fitting of the extreme flap moment distribution is not necessarily applicable to the overturning moment. For this reason, the overturning moments are analysed here with the same methodology as with the flap moment. 100 simulations have been carried

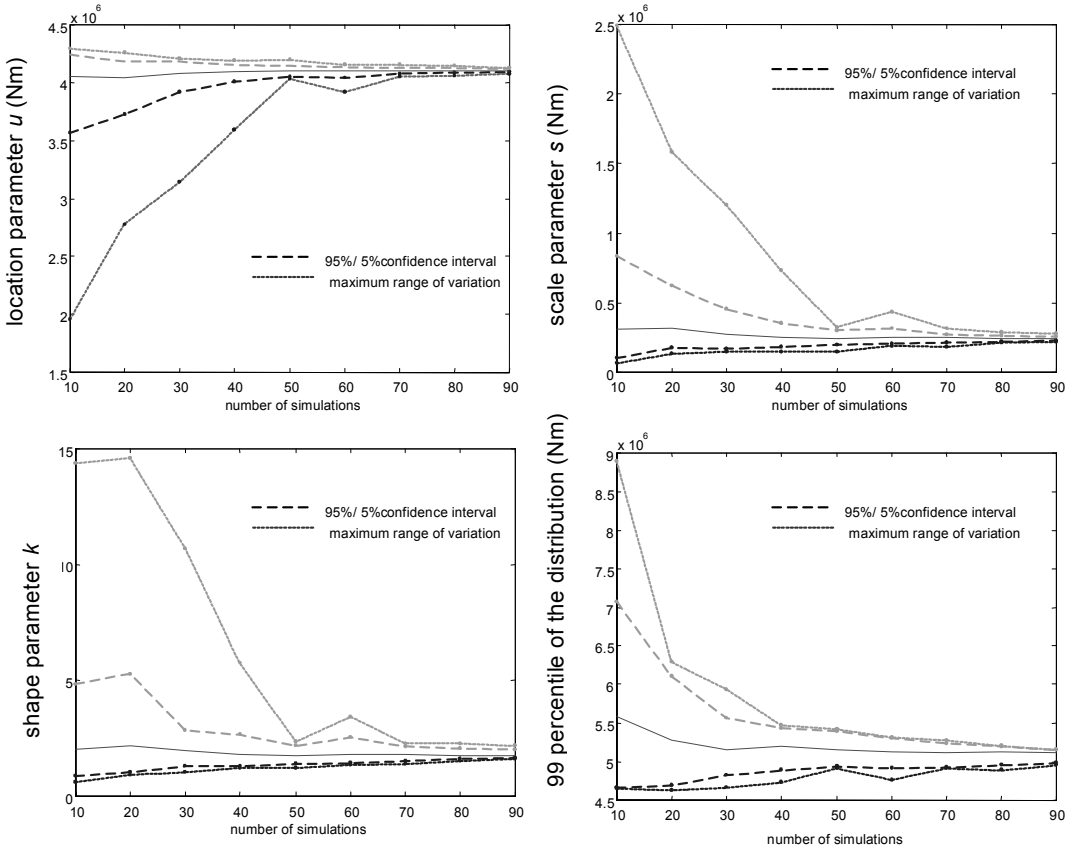

Figure 8.5: from upper left clockwise, variation of the distribution parameters u, s , k of the Weibull distribution and the 99 percentile of the distribution of the maximum flap moment.

out with a significant wave height of 6.9 m and a zero upcrossing period of 7.7 m/s. The choice of this set of wave parameters is based on the assumption that the extreme response of the support structure without wind loading occurs in an extreme sea state. Thus, the required number of simulations will be determined by an extreme sea state and not a mild sea state.

Wind loading is not present in order to exclude the influence of the wind. The simulation length is 10 minutes. Indeed, this length is not long enough for wave simulations, however, it is assumed that the number of simulations and the length of simulations can be determined separately. The issue concerning the length of simulations is treated later in this chapter.

The overturning moment is treated with the same methodology as with the flap moment. Random drawings are performed from the 100 OTM's obtained by time domain simulations. The sample size of the random drawings varies from 10 to 90. For each sample size 50 random drawings are carried out. The randomly drawn OTM's are fitted to a 3 parameter Weibull distribution.

Figure 8.6 shows the variation of the 99 percentile of the OTM distribution for different sample sizes, that is, the number of simulations used to fit the 3 parameter Weibull distribution. The vertical axis is normalised with the 99 percentile of the OTM distribution obtained using 100 simulations. As can be observed, the variation of the 99 percentiles decreases with the number of simulations. The mean estimates of the 99 percentiles lies consistently above the reference 99 percentile and the minimum of the 99 percentile estimate varies significantly less than the maximum of the 99 percentiles. It also means that the chance is much bigger that a random estimate of the 99 percentile is more likely to be above rather than below the reference value (from 100 simulations).

Using 50 simulations, the maximum and the minimum of the 99 percentiles are between 1.21 and 0.95 of the reference 99 percentile. Further increase in the simulation number has less impact on the reduction of the spreading of the 99 percentiles. Thus, 50 can also be regarded as a reasonable number of simulations required to obtain a reliable fit of the OTM distribution. The variation of the distribution parameters of the overturning moment (not shown here) is similar to the variation of the distribution parameters of the flap moment shown in Figure 8.5. The ranges of variations of the distribution parameters are much larger than the ranges of variations of the 99 percentiles of the distribution. Since the objective is to determine extreme responses of long return periods, Figure 8.6 gives a better indication of the required number of simulations than the variations of the distribution parameters.

8.2.3 Bootstrap of the simulation results

Flap moment:

The question, whether 100 simulations can be regarded as sufficient so that the conclusion drawn from the previous section can be supported, can be raised. First, the bootstrap method [35] is applied to investigate the variability of the statistical parameters given 100 simulations. The main idea of bootstrap is that the real distribution is unknown, but the empirical distribution from the 100

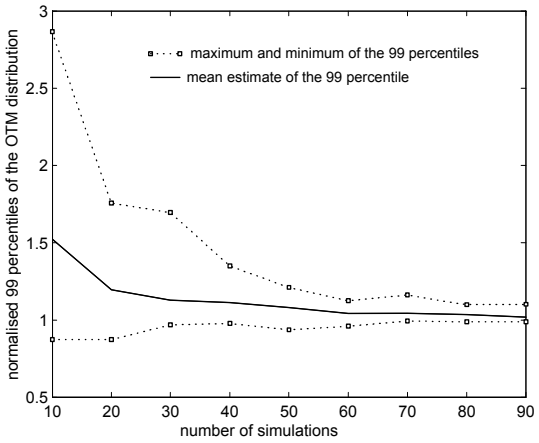

Figure 8.6: Variations of the 99 percentiles of the overturning moment distribution with different number of simulations.

simulations is a good approximation of the true unknown distribution. Resampling the empirical distribution one can have an idea of the intervals where the true unknown statistical parameters are located.

The resampling of the empirical distribution is carried out by random drawings. Data are randomly drawn from the original population (i.e. 100) and returned to the population so that repeated values are possible (bootstrap with replacement). The size of the sampled data is equal to the size of the original data, i.e. 100 samples. This procedure is repeated 1000 times and the variability of the distribution parameters is studied.

From Figure 8.7 it can be seen that the distributions of the parameters are not Gaussian. The spreading is smaller than the standard deviation of the Gaussian distribution. The 99 percent upper bound and the 1 percent lower bound of the distribution are shown in Table 8.2. For every bootstrap sample the 99 percentile of distribution is determined and its variation is illustrated in Figure 8.7 (lower right).

The variation of the 99 percentiles is quite close to a Normal distribution and the maximum and the minimum of the 99 percentiles differ about +/-5 % from the mean estimate of the 99 percentile. Given other uncertainties that influence the estimation of the extreme value, this variation can be regarded as acceptable. Thus, it can be said that the variation of the distribution parameters is not very significant from the 'actual' parameters.

The ultimate question of whether 100 simulations are sufficient to support the conclusions drawn above can not be answered unambiguously. On the one hand, one needs to know the true distribution, which remains unknown, in order to judge the number of simulations required for a reliable estimate of the response distribution. On the other hand, the aim of this analysis of the

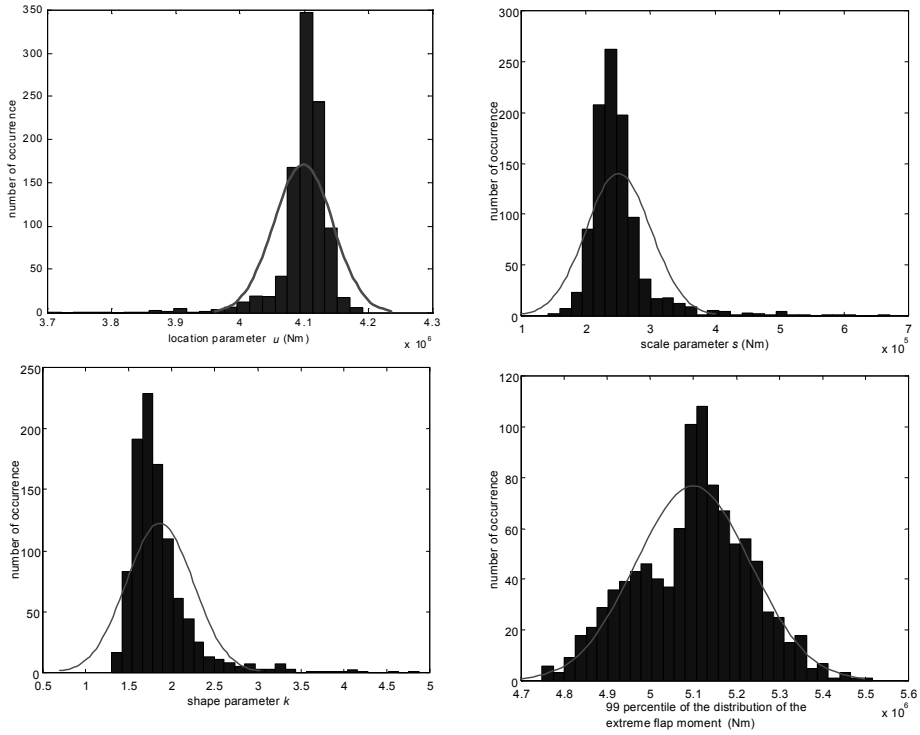

Figure 8.7: histogram of the variation of the distribution parameters (clockwise from upper left) u, s, k, and 99 percentile of the distribution from 1000 bootstraps

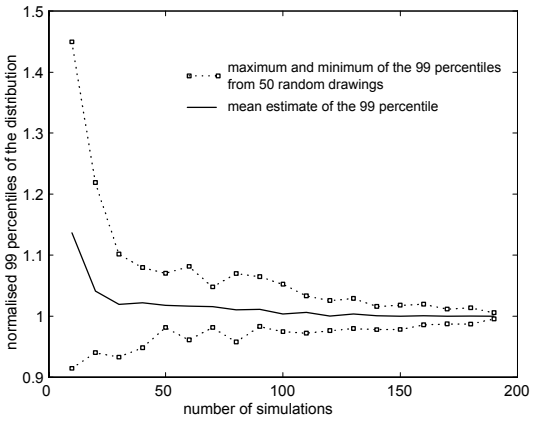

Figure 8.8: 99 percentile of the flap moment distribution obtained using different numbers of simulations, normalised with the 99 percentile of the distribution using 200 simulations.

simulation number is to reduce the simulation number instead of simulating for, say, 100 years.

A theoretical justification is not investigated instead a practical criterion is used here. The reasoning is that if 50 simulations are really sufficient then the convergence of the estimates shown for a population size of 100 (see Figure 8.5) will be observed also for larger population sizes. For this reason, the population size is increased to 200 and the variation of the 99 percentile of the distribution is studied for different numbers of simulations, varying from 10 to 190. For each number of simulations 50 random drawings are carried out.

Figure 8.8 shows that with 50 simulations, the variation of the 99 percentile is within 10% of the 99 percentile estimated using 200 simulations. With a population size of 100 and 200 simulations, the convergence behaviour is very similar. The spreading is sharply reduced until the number of simulations reaches 50. Further increase in the number of simulations reduces the spreading but the rate of reduction is rather slow and insufficient to justify the extra computational effort. Therefore one can assume that the choice of 50 simulations is independent of the population size.

Overturning moment:

The same question posed for the flap moment applies also to the OTM. Figure 8.9 shows the 99 percentiles of the OTM from 1000 bootstraps. The 99 percentiles are normalised with the 99 percentile obtained using the original 100 simulations. It can be seen that the maximum variations are 5% above and 5% below the reference values. Thus, regarding the limited variation one can say that the 100 simulations are representative and the 99 percentile obtained using 100 simulations is close to the actual unknown value of the 99 percentile.

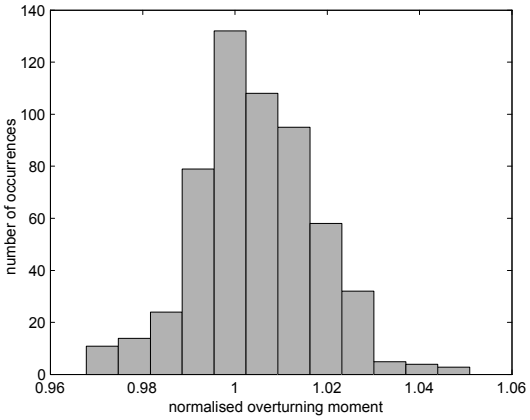

Figure 8.9: The histogram of the 99 percentile of the OTM distribution from 1000 bootstraps.

The variation of the distribution parameters of the OTM distribution exhibits approximately the same behaviour as the variation of the distribution parameters of the flap moment. The ranges of variations of the distribution parameters of the OTM (not shown here) are much larger than those of the flap moment (Figure 8.7). But as mentioned before, for this application the 99 percentile is a better indicator than the distribution parameters.

The question whether a conclusion drawn from 100 simulations is valid is also raised for the overturning moments. The total number of simulations is increased to 200 and random drawings are carried out with different sample sizes, varying from 10 to 190. Figure 8.10 shows the variation of the 99 percentile of the distribution with different numbers of simulations. The 99 percentiles are normalised with the 99 percentilie obtained from 200 simulations.

As can be seen, the convergence behaviour is very similar whether 100 or 200 simulations are used as population size. The spreading decreased rapidly until the number of simulations reaches 50. Above 50 the rate of the reduction of the spreading is slow. In absolute terms, the variation of the 99 percentiles of the OTM with the number of simulation is more significant than the flap moment. With 50 simulations the maximum estimate from 50 random drawings is about 25% higher than the reference value and the minimum is about 6% lower than the reference value. Thus, the chance of making an unconservative estimate is lower because the chance that the 99 percentile estimated from 50 simulations will be higher than the reference value from 200 simulations is bigger. Therefore one can assume that the choice of 50 simulations is a reasonable choice.

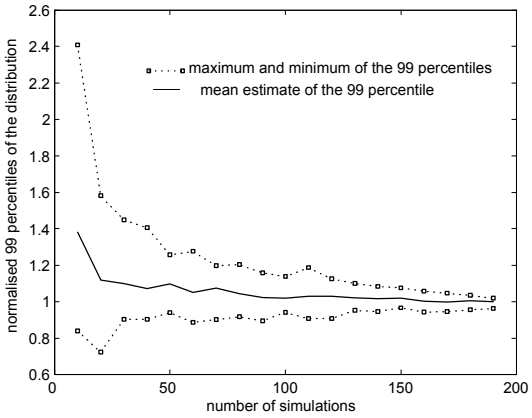

Figure 8.10: 99 percentile of the overturning moment distribution obtained using different numbers of simulations, normalised with the 99 percentile of the distribution using 200 simulations.

8.2.4 Correlation of the distribution parameters

As can be seen in Table 8.2, the shape and scale parameters of the maximum flap moment distribution can have large variations. However, the effect on the 99 percentile of the distribution is rather small compared to the magnitude of variation of the distribution parameters. The large variation of the scale parameter and the shape parameter can be explained by the correlation of these two parameters. The 3 parameter Weibull distribution can be written in a general form, defining the normalised variable $\tilde{x} = (x - u)/s$, then the Weibull distribution of the response for one random sea state becomes

$$F(\tilde{x}) = 1 - \exp(-\tilde{x}^k) \tag{8.1}$$

For the distribution of the one year extreme response, one can assume that all the sea states are independent and the one year distribution of the extreme response can be calculated using the extrapolation formula, where N is the number of independent sea states. Thus, $F(\tilde{x})_{1year} = F(\tilde{x})^N$. Taking this into account and using Equation 8.1, one can write the inverse of the CDF as

$$\tilde{x} = \left[-\ln\left(1 - \sqrt[N]{F_{1year}}\right)\right]^{\frac{1}{k}} \tag{8.2}$$

$\tilde{x}$ can be interpreted as a 'gust' factor which expresses the extreme value with a certain exceedence probability in term of the scale parameter s (since $x = u + s\tilde{x}$). Figure 8.11 shows the variation of this 'gust' factor for different time periods T in years and for different shape factors k. It is simply assumed that all the sea states are independent and the sea state duration is 3 hours, thus T can be easily converted to N.

Table 8.2: variation of the distribution parameters and fractile values

	Lower bound ($F_{low} = 0.01$)	**Upper bound** ($F_{up} = 0.99$)	$\frac{up-low}{median}$
u location factor	$3.88 \cdot 10^6$	$4.16 \cdot 10^6$	0.07
s scale factor	$0.18 \cdot 10^6$	$0.48 \cdot 10^6$	1.27
k shape factor	1.37	3.41	1.15
99 percentile	$4.81 \cdot 10^6$	$5.39 \cdot 10^6$	0.11

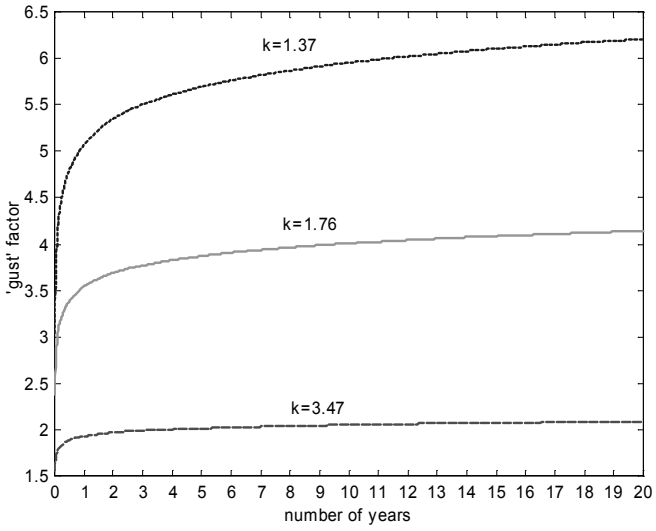

Figure 8.11: variation of the gust factor (see Equation 8.2)with the shape factor k and number of years for the distribution of the maximum flap moment.

As can be seen, the larger the shape factor, the faster it converges to an upper limit value. The three shape factors shown here are the 1 percent lower bound, the median, and the 99 percent upper bound values from the variation computed with the bootstrap (Figure 8.7).

From Figure 8.11 it can be seen that the 'gust' factor can have a large range of variation. However, this scale of variation is not translated to the 99 percentile of the extreme flap moment. From the three distribution parameters, only the location parameter u has a limited variation range. The scale and shape parameter can have very large variations. However, the tail values of the extreme distribution that were shown here have a reasonably limited variation. This can be attributed to the fact that the scale factors and shape factors do have a certain correlation. Figure 8.12 shows the scatter plot of the scale factor and the shape factor obtained from fitting of the bootstrap samples.

From Figure 8.12 it can be seen that the scale factor and shape factor are positively correlated. The linear correlation coefficient is in the order of 0.9. For

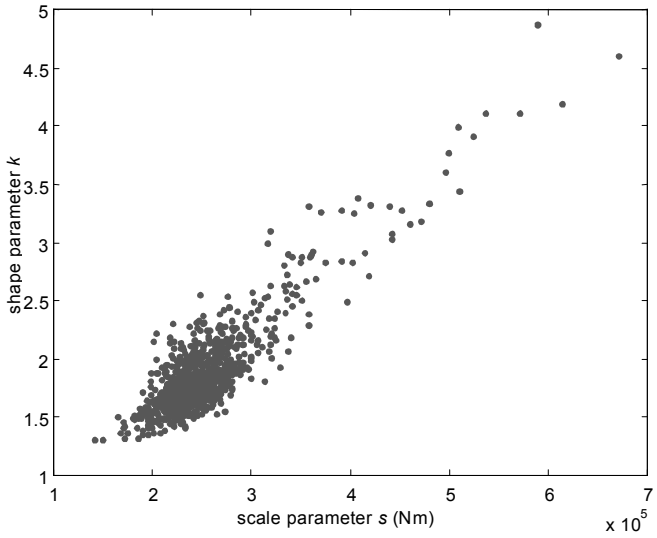

Figure 8.12: correlation of the shape parameter k with scale parameter s of the distribution of the maximum flap moment.

larger scale factors, which means larger standard deviation, the shape factor is also large. A large shape factor means a smaller 'gust' factor, thus the variation of the product $\tilde{x}s$ is smaller than the individual variation of $\tilde{x}$ or s. There may not be a physical reason for that but rather a by-product of the fitting procedure. The three parameter Weibull distribution has more degrees of freedom than, for example, the Rayleigh distribution, but the choice of the scale factor and shape factor is not totally independent of each other.

Another plot that illustrates the influence of the randomness of the extreme response is Figure 8.13, which shows the scatter plot of the maximum wind speed with the maximum flap moment in each simulation. The peak gust speed is uncorrelated with the peak flap moment, due to the stochastic properties of the wind. On the other hand, there can be other properties of the stochastic wind that are more influential on the extreme response, such as the acceleration of the wind, which can produce wind gusts of very small rise time. For this reason, deterministic models that take the maximum wind speed as the wind load parameter can have a very different estimate of the extreme flap moment than the MAX method.

8.2.5 Study of the wind simulation length

In this section the influence of the wind simulation length on the extreme blade response is analysed. For this purpose a large number of 10 minutes simulations have been carried out. The external conditions for the simulation are the same as the external conditions used in the analysis of the number of simulations. The

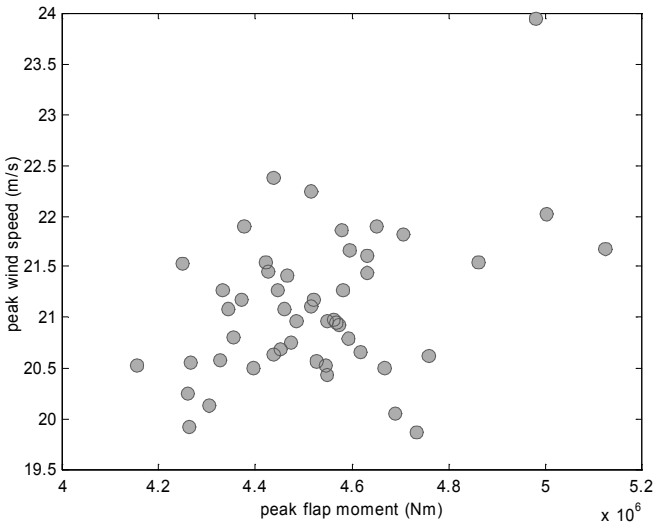

Figure 8.13: Correlation of the peak gust speed with the peak flap moment.

10 minutes simulations are grouped to represent simulations of longer length. The simulation length can vary from 10 minutes to 1 hour since the stationary period of the wind is assumed to be somewhere between 10 minutes to 1 hour. The reason for the grouping is that the simulation method of wind (and waves) used here requires a spectral discretisation and the spectral discretisation depends on the length of the simulation. A longer simulation length means a finer discretisation of the spectrum. For this reason only 10 minutes simulations are used to ensure uniform discretisation for all the simulation lengths, so that the extreme responses of different simulation lengths can be compared.

The maxima are selected from the grouped simulations. The number of maxima for all the simulation lengths is 50, which is the number suggested by the analysis of the previous section. These maxima are fitted to a 3 parameter Weibull distribution. The variation of the distribution parameters is depicted in Figure 8.14. The distribution parameters are normalised with the mean value of the distribution parameters from the 1 hour simulations. To quantify the variation of the distribution parameters within a given simulation length, the simulations are randomly grouped and the distribution parameters are then determined. This random regrouping and parameter estimation are performed 50 times for each simulation length. The standard deviations of the parameter variation are obtained for each simulation length. The variation of the distribution parameters for a given simulation length is shown with error bars of 1 standard deviation.

As can be seen from Figure 8.14, the variation of the parameters decreases with the increasing simulation length. The variation of the location parameter is limited in relation to the 1 hour estimate, while the scale and shape parameters

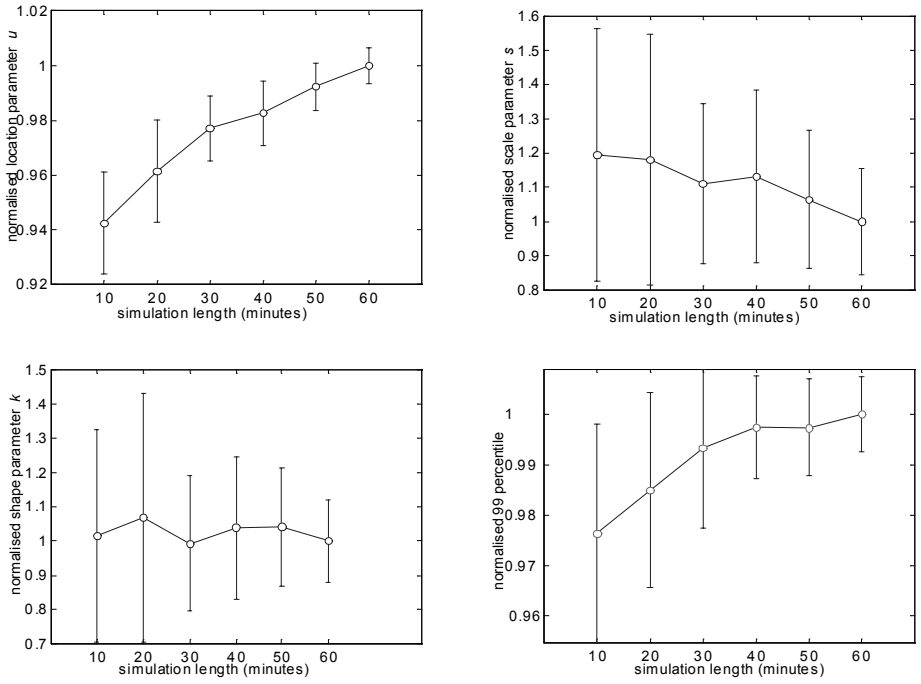

Figure 8.14: Weibull distribution parameters and the 99 percentiles of the distribution of the maximum flap moment for different simulation lengths of wind; error bars show one standard deviation.

can have larger fluctuations. The values of the location parameter increase with the simulation length. The reason is that the longer the simulation length the narrower the distribution, because only the largest values are included in the distribution. The large variation of the scale and shape parameter does not result in a large variation of the 99 percentiles (see Figure 8.14, lower right) of the distribution, which is due to the correlation of these two parameters.

From the given result one can say that with 40 minutes as simulation length, an optimal reduction of the spreading of the estimate is achieved, at the same time further increase of the simulation length does not have substantial effects on the estimate of the 99 percentiles. Moreover, the 1 standard deviations of the 99 percentile of the distribution for all the different simulation lengths does not exceed 10% of the 99 percentile of the 1 hour estimate. From a practical point of view, one can say that for the estimate of extreme blade responses, 40 minutes wind simulation would be sufficient.

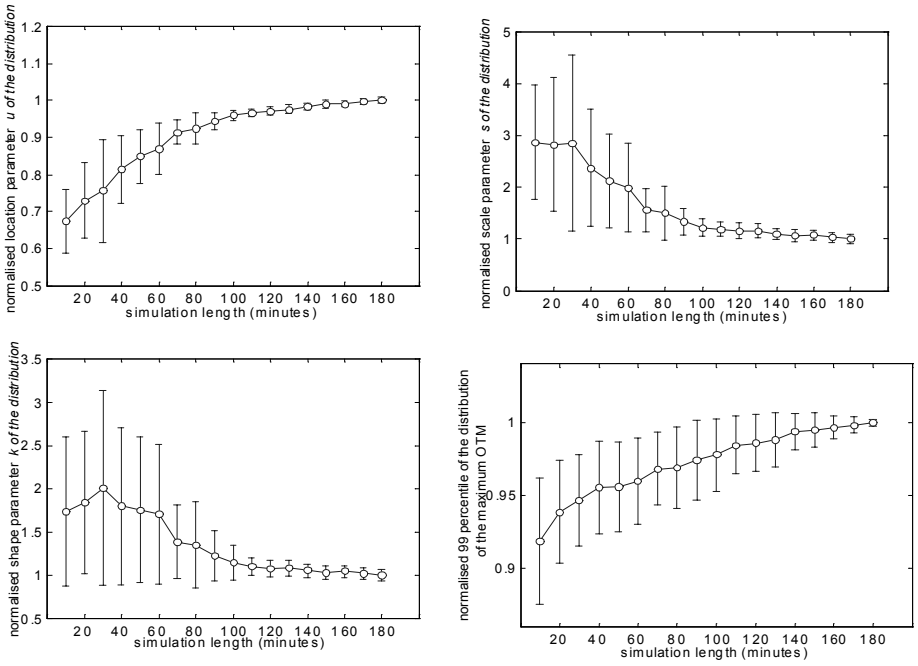

Figure 8.15: Weibull distribution parameters and the 99 percentiles of the OTM maxima for different simulation lengths of the waves; shown with error bars of one standard deviation.

8.2.6 Study of the wave simulation length

The requirement for the wave simulation length can be rather different from the wind simulation length. The stationary period of waves can vary from 1 to 6 hours. For the design of offshore structures a stationary period of 3 hours is commonly used. The influence of the wave simulation length on the extreme response of the support structure is analysed in a similar manner as the influence of the wind simulation length on the blade response. In this case 900 simulations with a length of 10 minutes were performed. The 10 minute responses are then grouped to represent simulations of different lengths. Again, random grouping is made to study the variability of the statistical parameters within different simulation lengths. From the random groupings the standard deviations are obtained for each simulation length.

The overturning moment of the support structure is taken as the response indicator. The studied simulation lengths range from 10 minutes to 3 hours. The number of simulations is 50. There is no wind input, so that an interference of the two stochastic processes is excluded. The sea state parameters used here are, a significant wave heigt of 6.9 m and a zero upcrossing period of 7.7 s.

The maxima from the grouped responses are fitted to a 3 parameter Weibull

distribution and the variation of the distribution parameters is shown in Figure 8.15. The distribution parameters are normalised with the reference values obtained from 3 hours simulation length. From the results shown, it can be seen that the distribution parameters converge rapidly towards the end value. This is observed for simulation lengths up to 80 minutes. Then the convergence rate decreases, approaching slowly the reference value. Judging from the fluctuation of the distribution parameters, one could have expected that the 99 percentiles of the distribution would have larger variations. The 99 percentiles in Figure 8.15 (lower right) shows in fact a much more limited variation than the distribution parameters. This has already been observed for the study of the wind simulation length. It can also be noticed that the convergence of the 99 percentiles is much slower than the convergence of the distribution parameters, although the relative variation with respect to the reference value is considerably smaller.

The 99 percentiles increase with the simulation length. Roughly one can distinguish two linear trends. From 10 to 40 minutes the slope of the curve suggests a more rapid increase of the 99 percentile estimates than from 50 minutes to 3 hours. From a practical point of view one would choose a shorter simulation length because of the computational time. In this case 40 minutes would be a compromise between computational effort and accuracy. With a simulation length of 40 minutes, 90% of the estimates of the 99 percentiles will differ no more than 10% of the mean estimate of the 99 percentiles. Hence, this can be seen as an acceptable deviation

8.2.7 Selection of a number of simulations and a simulation length

The choice of the number of simulations can be made based on the analysis in the previous sections. It has been shown that 50 can give a satisfactory estimate of the response distributions. However, in absolute terms the error incurred in using a limited number of simulations is bigger for the overturning moment than for the flap moment. Partly, because the length of the stationary period for waves is longer and in that analysis only 10 minute simulations are used. Nevertheless, both the flap moment and the overturning moment show a rapid convergence with 50 simulations, further increase in the number of simulations has less significant improvement on the estimate.

It is more difficult to choose the length of the wave simulation because the convergence of the OTM distribution is not manifested in such way that a clear limit can be established as with the number of simulations. There is always a trade-off between computation time and degree of accuracy. For this reason one can justify the choice of 40 minutes as simulation length because of the convergence rate and the fact that the mean estimate of the overturning moment is only 5 % below the 3 hour estimate.

For the wind simulations, 40 minutes is also an ideal length regarding the convergence of the 99 percentile of the flap moment distribution. With 40 minutes simulation, the mean estimate of the 99 percentiles is less than 1%

below that of 1 hour. For combined simulations of wind and wave 40 minutes simulation is recommended.

Moreover, the simulation length will depends on other factors such as the relative contribution of the wind and wave loads to the total response or the local wind and wave climate. For the pitch regulated turbine considered here, the wind load is dominant for the extreme response, hence performing a longer wave load simulation would not affect the estimate of the extreme response significantly.

8.3 Statistical uncertainties

8.3.1 Bayesian analysis of the uncertainties

The estimate of the extreme response beyond the data length is loaded with uncertainties. There are many types of uncertainties present in the whole process of response estimation. In this context only the statistical uncertainties that arise from fitting of the parametric models, such as uncertainties of the distribution, parameters of the distributions are considered. The influence of the uncertainties can be taken into account using a Bayesian analysis [13]. The influence of the fitting methods on the parameter estimation is also studied.

The results of the simulations are subject to a statistical analysis. The uncertainties that are associated with the statistical analysis are: the choice of the distribution type and the parameters of the distribution. The choice of the distribution can not be determined unambiguously in most cases, thus a subjective choice has to be made. The uncertainties concerning the parameters of the distribution can then be considered using the Bayesian analysis. The core of the Bayesian analysis is the Bayes theorem [94]

$$P(A|B) = \frac{P(B|A) \cdot P(A)}{P(B)} \tag{8.3}$$

where $P(A|B)$ denotes the conditional probability of A given B. The subjectivity of the Bayesian analysis lies in the term $P(A)$ which represents the prior probability of the parameters. The $P(A|B)$ is the so called posterior probability. The choice of the prior probability can be rather arbitrary. It is usually based on a subjective judgement about the character of the distribution (through experience, expert opinions etc.). However, in engineering problems the likelihood function usually dominates, thus the subjective prior probability will have less relevance on the posterior probability. In an engineering approach where the decision making process can not always be based on an objective judgement because of lack of information, Bayesian analysis is a useful tool to include statistical uncertainties.

As an illustration of the method, the Bayesian analysis is applied to 50 maxima of the flap moment of the blade, obtained from 50 simulations of 10 minutes. The maxima of the flap moment are fitted to a 3 parameter Weibull distribution. The Bayesian theorem can be written as

$$f''(\boldsymbol{\theta}) = C \cdot \prod f(x_i|\boldsymbol{\theta}) \cdot f'(\boldsymbol{\theta}) \tag{8.4}$$

f'' is the posterior and f' is the prior probability density of the Weibull distribution parameters. $\boldsymbol{\theta}$ represents the vector of the distribution parameters and C is a normalisation factor to be determined. $\prod f(x_i|\boldsymbol{\theta})$ is the so called data likelihood function and x_i are the data obtained by simulations, e.g. maximum flap moments. The data likelihood function is also used to determine the distribution parameters in the maximum likelihood estimate, see Equation 7.17

$\boldsymbol{\theta}_{mle}$ determines the maximum likelihood estimate (MLE) of the distribution parameters, where the likelihood function has a maximum. In the case of a 3 parameter Weibull distribution, a three dimensional probability density function of the distribution parameters is obtained and the hyper-volume of the function is normalised to unity by the constant C .

The uncertainties of the distribution parameters can be taken into account through the total probability theorem,

$$F(x) = \iiint F(x|\boldsymbol{\theta}) f''(\boldsymbol{\theta}) \mathbf{d}\boldsymbol{\theta} \tag{8.5}$$

$F(x|\boldsymbol{\theta})$ is in this case the conditional distribution of the peak flap moment given a set of distribution parameters.

In the same manner that the uncertainties of the parameters are dealt with, the Bayesian analysis can be applied to the uncertainties of the choice of distribution models. Instead of the continuous density distribution of the parameters, a prior set of weighting factors for different types of distributions is given.

$$f''(\mathbf{F}_i) = C \cdot f(x_i|\mathbf{F}_i) \cdot f'(\mathbf{F}_i) \tag{8.6}$$

$\mathbf{F}_i$ represents the different distribution types taken into consideration. The term $f(x_i|\mathbf{F}_i)$ is calculated using the following integral [91]

$$f(x_i|\mathbf{F}_i) = \mathbf{K}_i = \int f_i(x_i|\boldsymbol{\theta}) f'(\boldsymbol{\theta}) \mathbf{d}\boldsymbol{\theta} \tag{8.7}$$

There is no information available that indicates a certain distribution is more likely than the others. Hence, a uniform prior is used, the prior weights of the distributions, $f'(\mathbf{F}_i)$, are equally divided among the distributions. In this case the normalisation factor is simply $C = \frac{1}{\sum_i f'(\mathbf{F}_i) \cdot \mathbf{K}_i}$. Using Equation 8.6 the posterior weighting factors for the different distributions functions are obtained. The posterior weighting factors are taken into account analogously as described in Equation 8.5, where the summation sign replaces the integration sign.

$$F(x) = \sum_i F(x|\mathbf{F}_i) f''(\mathbf{F}_i) \tag{8.8}$$

Notice that Equation 8.5 takes into account all the possible variations of the distribution parameters while Equation 8.8 can only take a finite number of distribution functions into account. This implies also that the end result strongly

depends on the selection of the distribution functions. Thus, one should make visualisations of the simulation data in a probability scale, e.g. Normal plot, Weibull plot, to verify that the chosen distributions provide a good coverage of the data in the probability space.

8.3.2 Uncertainties of the distribution parameters

In this section the uncertainties of the distribution parameters are examined. The Bayesian analysis is applied to treat the uncertainties of the distribution parameters. The distribution functions used here are, 3 parameter Weibull, Gumbel and Normal distribution. These 3 CDF's are used to model the maxima of the flap moment. The maxima are obtained from 50 simulations of a 40 minutes length. The mean wind speed is 15 m/s[4].

First the data likelihood function defined in the Equation 7.17 is obtained. The 3 parameter Weibull distribution has a data likelihood that is a function of three variables. Figure 8.16 shows the data likelihood function for different combinations of the three parameters (that is, one parameter is held as constant). In principle, one needs to integrate the data likelihood function over all the possible parameter values. However, the likelihood function decays rapidly towards zero, hence for numerical integrations only a limited region needs to be considered.

The slight dependency between the two parameters s and k can be seen by following the maximum of the likelihood function for a given location parameter u (Figure 8.16 top left). It seems rather symmetrical along a constant value of s and k but actually the symmetrical axis is slightly oblique. A larger scale factor s corresponds to a larger shape factor k and vice versa. For constant k and s there is also a slight symmetry between the two parameters. As can be seen the shape factor and the scale factor decrease for increasing location factor.

The posterior distribution of the distribution parameters needs to be determined. In this case a constant distribution of the prior, a non-informative prior, is assumed. The posterior probability density of the parameters is proportional to the data likelihood function with a constant normalisation factor C. Using the total probability theorem (Equation 8.5), the distribution of the extreme flap response that includes the uncertainties of the distribution parameters can be obtained. After the distribution of the maximum flap moment is determined, the fractile values that are relevant for the structural design can be calculated. In this case, the extreme flap moment with a return period of 100 years can be determined.

To avoid the triple integration, the integral of Equation 8.5 is split in a double and a single integral. First the data likelihood function is integrated over the s and k domain, which gives the marginal distribution of the location parameter u.

[4]The choice of the mean wind speed of 15 m/s is that at this mean wind speed, the most severe response of the pitch regulated wind turbine is expected, this is shown later in Section 11.2.

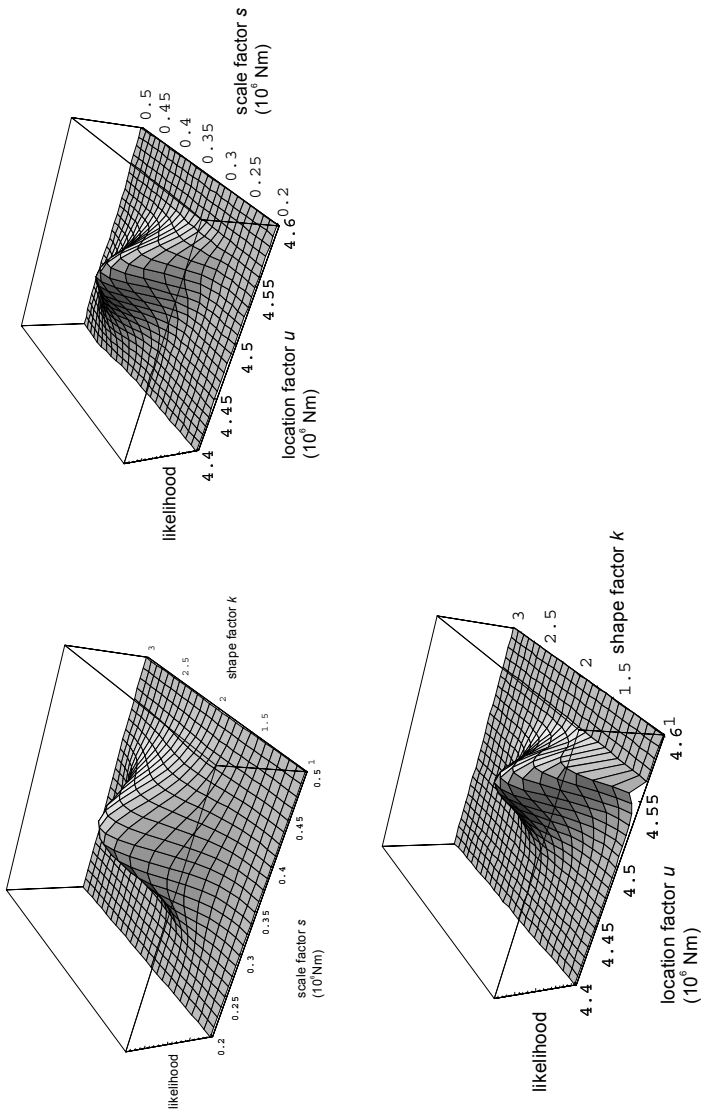

Figure 8.16: data likelihood functions of the maximum flap moment, at a mean wind speed of 15 m/s, with 50 maxima obtained from simulations, fitted with a 3 parameter Weibull distribution. upper left: k is constant; lower left: u is constant; lower right: s is constant.

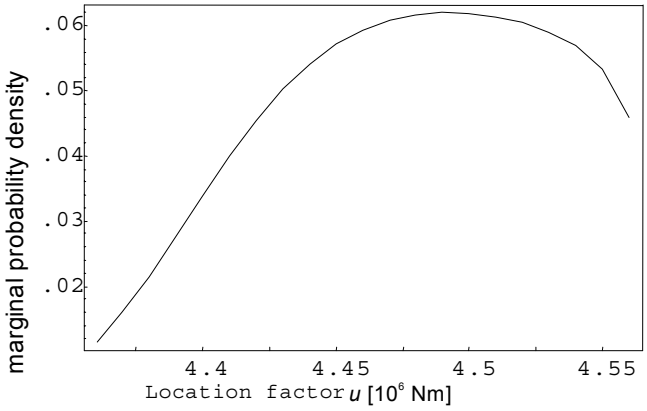

Figure 8.17: The marginal probability density of the location factor u of the distribution of the maximum flap moment.

Then, the Equation 8.5 is integrated over the domain of s and k. This yields the conditional probability density function (or the conditional quantile) that depends on the location factor u (Figure 8.18). Applying the total probability theorem again to the conditional quantile with the marginal distribution of the location parameter (Figure 8.17), the quantile value that takes into account the uncertainties of all the distribution parameters is obtained.

For the Weibull distribution the variation of the scale parameterand shape parameter has a larger impact on the estimate of the extreme response than the location parameter. While the location parameter u varies linearly with the physical variable ($x = u + s\tilde{x}$), the shape parameter k and the scale parameter s vary as a product (see Equation 8.2). Treating the location parameter u as a variable or a constant (estimated with MLE), the difference in the 99 percentiles of the distribution of the flap moment is less than one percent.

The same procedure that is applied to the Weibull distribution parameters is applied to the Gumbel and Normal distribution parameters. The quantile values that are representative for the extreme response with a 100 year return period are obtained[5]. The results are shown in Table 8.3

Clearly the spreading of the parameters does not have very strong effects on the estimate of the extreme response. The difference is no more than 2% for all the distributions. This leads to the assumption that the uncertainties of the distribution parameters do not considerably affect the estimate of the extreme flap response.

The effect of including the parameter uncertainties can be best explained with an example of a Normal distribution. Assuming that the data follow a

[5] The 100 year extreme response is obtained by considering only one conditional distribution and not all the conditional distributions. This simplification is done for the illustration of the Bayesian analysis.

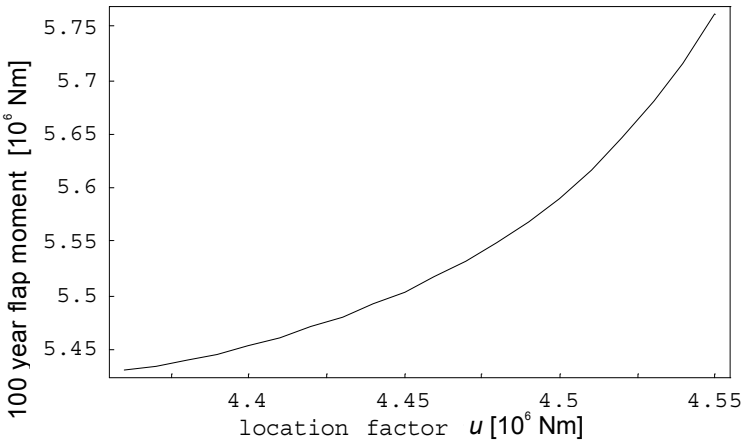

Figure 8.18: 100 year flap moment conditioned on the location factor u.

Table 8.3: 100 year return values with parameter uncertainties and without

Distribution function	**Bayesian estimate**	**least squares estimate**
Weibull	$5.57{\cdot}10^6 Nm$	$5.62{\cdot}10^6 Nm$
Gumbel	$6.21{\cdot}10^6 Nm$	$6.13{\cdot}10^6 Nm$
Normal	$5.45{\cdot}10^6 Nm$	$5.43{\cdot}10^6 Nm$

Normal distribution with the mean μ_x and the standard deviation σ_x. The uncertainty in the distribution parameter μ_x can be quantified with a prior that is also a Normal distribution with the mean μ_μ and standard deviation σ_μ (both the mean and the standard deviation are known). It has been shown that if a non-informative prior is used, i.e.$\sigma_\mu \gg \sigma_x$, then the distribution after the Bayesian analysis will assume the sample mean value and the increase of the standard deviation is $\sigma_x\sqrt{(1+1/n)}$, with n as the number of data [94]. For a sample size of 50, the increase of the standard deviation is less than 1%. In case the standard deviation is also unknown, then the Student-t distribution is used to define the variation of the mean. In this case, the uncertainty increases only slightly compared to the case of known standard deviation, assuming $n = 50$. As can be seen, a non-informative prior does not increase the estimate of the extreme response in a significant way when the likelihood function is dominant. This is usually the case when the number of data is sufficiently high.

However, one should keep in mind that the synthetic data set from simulations may present less variability than the real distribution (e.g. measurements). In that case the variability of the distribution of the extreme response maybe more significant.

8.3.3 Uncertainties of the choice of distribution

Different distribution models

The choice of distribution models is surrounded by subjective decisions. However, there are different diagnostical tools to distinguish those more likely ones from those less likely ones. But even these diagnostics are not always free of subjective elements. Before proceeding to the choice of the distribution function, one can have some statistical description of the data. Such statistical descriptors can be the mean, median, variance, skewness etc. This gives a general picture of the data. Here, a data set consisting of 50 maxima taken from 50 simulations of 10 minutes is used. The maxima are the extreme flap moment at the blade root and the different statistical descriptors are shown in Table 8.4.

One can see from Table 8.4 that the data has a coefficient of variation (i.e., the standard deviation divided by the mean value) and it is positively skewed. The kurtosis is less than 3 (Normal distribution), which may indicate a less fatter tail than the Gaussian distribution. First, it is fitted to 4 different distribution functions, the Normal distribution, the Gumbel distribution, the Frechét distribution and the Weibull distribution. The data are fitted with the least squares method. The data are also fitted to the Generalised Extreme Value (GEV) distribution. The fit yields a reverse Weibull distribution and this distribution is associated with a right end point. Considering that the response distribution will be extrapolated to a much longer period, this would present a serious limitation for the application. For this reason the GEV fit is discarded.

The test for the goodness of fit [28] is carried out for all the four distributions using the χ^2 test. For the present sample size of 50 data points, a bin size that is about $\sigma/3$ is chosen, where σ is the sample standard deviation. With a significance level of 5%, the null hypothesis can not be rejected for all the 4 distributions. However, as mentioned before, the bin size is a critical parameter for the χ^2 test. In case a larger bin size is chosen the test result can lead to the rejection of the null hypothesis for some of the distributions. There is also a recommendation about choosing the bin size in such way that at least 5 samples will fall into a bin or one can group the bins if the number of samples in the bin is too small.

Tests based on the empirical distribution function are also applied, the Kolmogorov-Smirnov (K-S) test and Anderson-Darling test (A-D). K-S test is recommended if the sample size is small. It measures the absolute deviation of the fitted distribution from the sample distribution. The A-D test measures the quadratic deviation of the fitted distribution to the sample distribution, with higher weighting factor for the tails.

According to the K-S and A-D tests, the null hypothesis can not be rejected for the chosen distribution functions. Figure 8.19 shows the empirical distribution function with fits of different parametric models using least squares fits. The Gumbel fit and the Frechét fit are almost identical, because the shape factor for the Frechét distribution is in the order of 10^8 and the Frechét distribution converges to a Gumbel distribution if the shape factor $\alpha \rightarrow \infty$. For this rea-

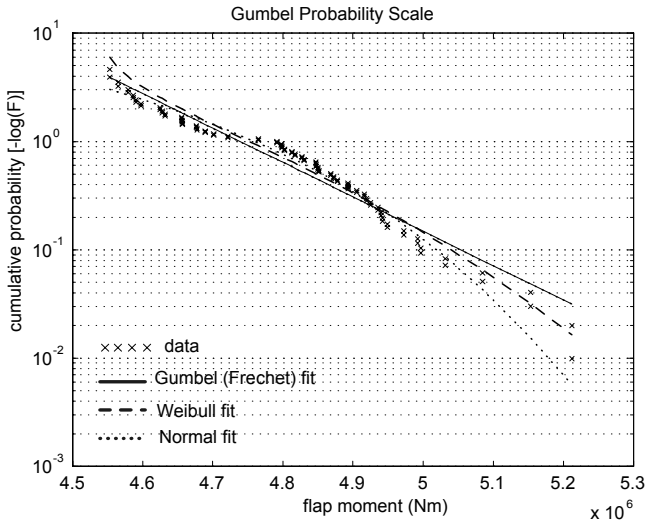

Figure 8.19: Maxima of the flap moment of the pitch regulated turbine from 50 simulations fitted to different distribution functions.

son there is no need to consider both distributions. Henceforth, the Gumbel distribution is used in place of Frechét.

It can be seen that the Gumbel distribution has the heaviest tail followed by the Weibull and Normal distribution. In this case a visual inspection is also carried out by plotting the data in the corresponding probability scales. Figure 8.20 shows the data plotted in a Normal, Weibull and Gumbel probability scale. It can be seen that the Normal and Weibull distribution have a poor fit of the lower tail of the data, while the Gumbel distribution may overestimate the upper tail. However, it is not easy to choose one of the distributions based on the visual inspection. Instead, the statistical descriptors of the distributions are compared to the statistical descriptors of the data. The mean and standard deviation of the Normal distribution are identical to the samples mean and standard deviation. The rest can be calculated from the distribution functions. Table 8.4 shows the first four descriptors of the distribution functions.

From Table 8.4 it can be seen that the mean and standard deviation are well approximated by all the distribution functions. The difference lies in the skewness and the kurtosis. The data suggest a slight positive skewness and a kurtosis that is below the kurtosis of the Normal distribution (i.e. 3). The Gumbel distribution has a positive skewness which is independent of the scale and location parameter. Since this skewness and kurtosis are much larger than the sample skewness, it can be expected that it will yield also a higher estimate. The Weibull distribution is a more flexible model, which can adjust the skewed sample data without producing a much heavier tail, due to the extra freedom of the shape parameter. The Normal distribution is also acceptable considering

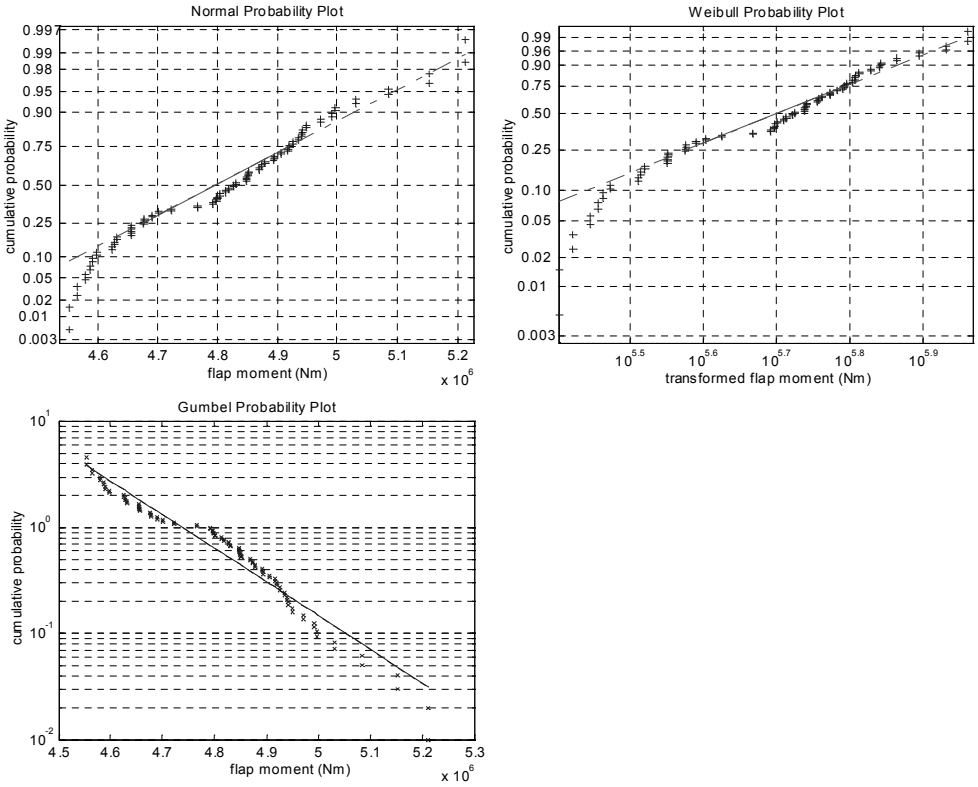

Figure 8.20: Maxima of the flap moments of the pitch regulated turbine plotted in three probability papers; for Gumbel probability plot, not the cumulative probability F but the -log(F) is shown.

Table 8.4: statistical descriptors of the sample data and distribution functions of the maxima of the flap moment

	Sample	**Weibull**	**Gumbel**	**Normal**
mean	$4.81{\cdot}10^6 Nm$	$4.82{\cdot}10^6 Nm$	$4.81{\cdot}10^6 Nm$	$4.81{\cdot}10^6 Nm$
standard dev.	$0.15{\cdot}10^6 Nm$	$0.15{\cdot}10^6 Nm$	$0.17{\cdot}10^6 Nm$	$0.15{\cdot}10^6 Nm$
skewness	0.22	0.69	1.13	0
kurtosis	2.58	3.2	5.4	3

Table 8.5: participation factors and fractile values of the distribution functions of the maxima of the flap moment in a Bayesian analysis

Distribution	**participation**	**99%**	**100 year**
Gumbel	14.6%	$5.36{\cdot}10^6 Nm$	$6.13{\cdot}10^6 Nm$
Normal	0.8%	$5.28{\cdot}10^6 Nm$	$5.61{\cdot}10^6 Nm$
Weibull	84.6%	$5.25{\cdot}10^6 Nm$	$5.62{\cdot}10^6 Nm$
Bayesian combination		$5.26{\cdot}10^6 Nm$	$5.93{\cdot}10^6 Nm$

the light tail of the sample data.

Bayesian analysis of the distribution choice

After the goodness of fit tests and comparison of the statistical moments, the choice of an appropriate distribution function still can not be made with certainty. One can evoke the Bayesian analysis to take the uncertainties into account. Using the procedure described in the previous section one can take the uncertainty of the distribution choice into account, in a semi-empirical way. The 3 distributions that have been tested before are chosen. The sample data are the maxima of the flap moment taken from 50 simulations with a mean wind speed of 15 m/s.

Table 8.5 shows the 99 percentiles of the distributions of the maximum flap moment for different distribution functions. It also shows the posterior probabilities of the distribution functions in percentage of the participation in the final distribution. The final result of a Bayesian analysis is a distribution composed of the chosen distributions with the corresponding participation factors. There is a distinct dominance of the Weibull distribution. Even though the Normal distribution gives very close estimates of the 99 percentile, slightly above the Weibull estimate, the contribution of the Normal distribution is insignificant. The difference between the 99 percentile estimates is less than 4%, with respect to the Weibull estimate. The difference between the different distribution models becomes larger when the estimates are extrapolated to a return period of 100 years.

Figure 8.21 shows the tail behavior of the different distributions. It can be seen that the Gumbel distribution gives the highest estimates due to the heavy tail. Weibull distribution and the Normal distribution have an overlapping tail for high fractiles up to 0.99999 (i.e. 10^{-5} in the logarithmic scale), then the

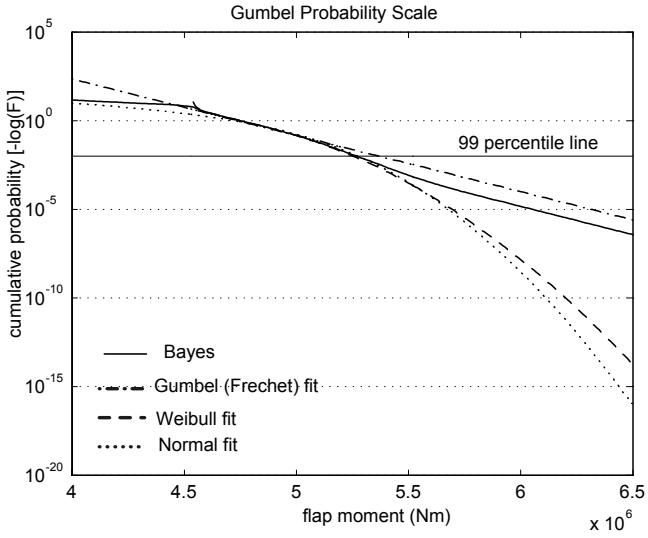

Figure 8.21: Cumulative probability of the extreme flap moment with different distribution models, the mean wind speed is 15 m/s.

tails diverge. The Normal distribution is the one with the lightest tail. Figure 8.21 also shows the Bayesian estimate of the distribution of the extreme flap moment. The Bayesian estimate of the 99 percentile of the flap moment is very close to the Weibull and Normal estimate. Further into the tail, the influence of the Gumbel distribution increases.

Table 8.5 shows the estimates of the extreme flap moment with a return period of 100 years. The difference between the distributions in the flap moment with a return period of 100 years increases considerably. The 100 year flap moment increases by 14% with respect to the 99 percentile for the Gumbel distribution, while for the Weibull and Normal distribution, this increase is about 7%. As can be seen the Bayesian analysis yields an estimate that is close to the average between the Weibull and Gumbel estimates. That means that at the tail region the influence of the Gumbel distribution increases eventhough the Bayesian factor remains the same.

It has to be said that there are two different manners of carrying out the extrapolation. One can apply the Bayesian factors either before or after the extrapolation. If the Bayesian factors are applied before the extrapolation, the 100 year estimate is higher than applying the Bayesian factors after the extrapolation. The extrapolation process favours the tail of the distribution, thus, before the extrapolation the contribution of the Gumbel distribution in percentage can be less than the contribution after the extrapolation because of the heavier tail.

In this case, the Bayesian factors are applied after the extrapolation. An-

other thing to be kept in mind is that the estimate is always bounded by the distributions that are included in the Bayesian analysis. For this reason it is always recommended to visualise the data in a probability plot together with the chosen distribution functions to ensure that the distribution functions cover the data reasonably.

8.3.4 Including the two types of statistical uncertainties in the estimates

Applying Bayesian analysis to include the uncertainties of the distribution types and uncertainties of the distribution parameters, the long-term estimate of the extreme flap moment can be determined. The 100 year return flap moment obtained in this manner is $5.65 \cdot 10^6 Nm$. This is less than one percent difference from the Weibull estimate without considering any uncertainties.

From a practical point of view one can say that analysis of the uncertainties contribute to the decision making process. The question of which distribution model to use is answered by the Bayesian analysis, which clearly favours the Weibull distribution. The evidence of the predominance of one distribution function make it often unnecessary to combine the different distributions. The influence of the uncertainties of the distribution parameters is less than expected. Normally, the inclusion of uncertainties would lead to a higher estimate of the extreme value. In the Weibull case, the inclusion of the parameter uncertainty lead to a lower estimate instead. This can be seen in the marginal distribution of the location parameter u (Figure 8.17). The probability that the location parameter is below the location parameter estimated with the least squares method is much higher. Hence, the long-term estimate becomes lower because integrating over the probability of u with the conditional quantile of the extreme response (Figure 8.18) yields a lower value.

Bayesian analysis offers a consistent approach to treat the statistical uncertainties that arise due to limited information. Using the Bayesian analysis one can determine the variablity of the estimate with more confidence.

8.3.5 Variation of the estimates caused by different fitting methods

The effect of the fitting method on the estimate of the extreme value is studied in the following section. There are three methods applied to the fitting of the data obtained by simulations. They are, the method of moments, the non-linear least squares and the maximum likelihood estimate. These methods were described in Section 7.3.1. The three methods are applied to fit the Gumbel and Weibull distribution[6]. The mean value of the maximum flap moment from 50 simulations of 10 minutes length, with a mean wind speed of 15 m/s is $\mu_y = 4.81 \cdot 10^6 Nm$ and the standard deviation is $\sigma_y = 0.15 \cdot 10^6 Nm$.

[6] Note that in order to preserve the assumptions of a constant standard deviation of residuals and randomness of residuals, it is necessary to transform the empirical CDF to Gumbel (Weibull) scale before the method of least squares can be applied.

The difference in the fitting method is usually not of concern if the number of samples is sufficient. The difference in the estimates will probably be of negligible magnitude, assuming that the distribution function chosen describes the behaviour of the data reasonably. The least squares fit is a minimisation method, finding a set of distribution parameters with a minimal deviation from the data. The maximum likelihood method finds the maximum of the likelihood function in the parameter space. As with all numerical problems, the maximum or minimum found is not necessarily global. The initial value for such problem can be important. Fortunately, the functions shown here are monotonous and continuous so that the choice of a numerical algorithm is usually not a problem. The 100 year flap moment obtained using different fitting methods to the Gumbel distribution is compared in Table 8.6.

Table 8.6: long-term estimates of the 100 year extreme flap moment obtained with different fitting methods (Gumbel distribution) cases

Fitting method	**100 year return value**
Moment of moments	$5.97 \cdot 10^6$ Nm
Non linear least squares	$6.13 \cdot 10^6$ Nm
Maximum likelihood estimate	$6.14 \cdot 10^6$ Nm

The sample skewness is 0.224, which suggests a slightly skewed distribution toward the positive end. The Gumbel distribution has a larger (fixed) skewness, this leads to a higher estimate in the tail region. With a more flexible distribution the sample skewness can be matched better. The three parameter Weibull distribution has one extra parameter to adjust the shape of the distribution. The three moments of the Weibull distribution (see Equations 7.12 to 7.14) can be used to match the first three sample moments and solving the three equations simultaneously one can obtain the estimates of the distribution parameters. The solution of these three equations is not as straightforward as for the Gumbel distribution, since three non-linear equations have to be solved. The comparison of the 100 year estimates using the Weibull distribution and different fitting methods is shown in 8.7.

Table 8.7: long-term estimates of the 100 year extreme flap moment obtained with different fitting methods (Weibull distribution) cases

Fitting method	**100 year return value**
Moment of moments	$5.45 \cdot 10^6$ Nm
Non linear least squares	$5.62 \cdot 10^6$ Nm
Maximum likelihood estimate	$5.58 \cdot 10^6$ Nm

The difference in the 100 year estimates between the least squares method and the maximum likelihood method is insignificant. The method of moments gives an estimate that is not far from the other two methods, about 3% lower. If the data set is homogeneous and no outliers are present then all the three

methods can be used. The difference in the estimates becomes significant if an outlier is present.

Therefore, an artificial outlier is introduced in the original data to study the effect of outliers. The outlier lies 5 standard deviations below the mean value. This distorted data set is fitted to a Weibull distribution. The least squares method and the MLE produce an estimate of the 100 year return value which differs about 2% from the original estimates without outlier. The method of moments fails to produce a solution to the non-linear equations that describe the statistical moments.

The reason is that the outlier deforms the sample statistical moments considerably. While the mean and standard deviation differ slightly from the original sample moments, the skewness has changed from 0.22 to -1.13. This makes it impossible to match the sample moments to the statistical moments of the distribution.

One may expect that an outlier on the lower part of the distribution does not change the estimates on the upper part of the distribution. Instead an outlier that is far above the mean value is introduced in the original data, 5 standard deviations above the mean value. Table 8.8 shows the influence of the outlier on the 100 year flap moment using different fitting methods. As expected, an outlier above the mean value exerts a considerable influence on the extreme value estimates, while an outlier below the mean value has nearly no influence. It can also be seen that the MLE is less susceptible to the presence of outliers.

The least squares is a sum based criterion, the deviation caused by the outlier is added to the rest of the deviation of the data. This portion can be quite considerable to the total deviation. The MLE is a product based criterion, the presence of an outlier would have less effect on parameters choice than the least squares method.

The use of MLE is recommended for fitting of the data to a distribution function. Although the least squares fit gives generally an adequate estimate of the distribution parameter as well. In many cases, outliers that emerge from abnormal simulations can be removed before proceeding to the fitting of a distribution model. The problem arises when one can not have the certainty of whether the outlier is an abnormal result or it is actually part of the population. In such case MLE is to be preferred because it is consistent with the Bayesian analysis of the statistical uncertainties.

Table 8.8: 100 year return value with outliers cases

Fitting method	**original data**	**-5 σ outlier**	**+5 σ outlier**
LSQ	$5.62 \cdot 10^6$ Nm	$5.53 \cdot 10^6$ Nm	$6.66 \cdot 10^6$ Nm
MLE	$5.58 \cdot 10^6$ Nm	$5.60 \cdot 10^6$ Nm	$6.00 \cdot 10^6$ Nm

LSQ: least squares
MLE: maximum likelihood estimate

8.4 Remarks on this chapter

In this thesis, the MAX method will be used as the reference method, thus the treatment of the statistical uncertainties is applied to the MAX estimate only. A comparison with the MAX estimate gives a picture of the variation of the estimate from POT and Process models with respect to the MAX estimate. Since it is an extensive chapter, it may be useful to condense some of the relevant results.

The following can be said from this chapter

- 50 simulations are regarded as sufficient for estimates of the response distribution.
- Longer simulation lengths are to be preferred to shorter simulation lengths. 40 minutes can be considered as adequate.
- Statistical uncertainties can be treated with Bayesian analysis; the uncertainties concerning the distribution parameters seem to have little effect on the estimates of the extreme responses. The uncertainties concerning the choice of distribution models are more considerable. In this case, Bayesian analysis gives automatically a choice of the distribution model: the 3 parameter Weibull distribution.
- The maximum likehood estimate of the distribution parameters is to be preferred, it is more robust for data sets with outliers. In case there are no outliers, the least squares method gives comparable estimates of the distribution parameters.
- The MAX estimate is not necessarily a better estimate than estimates from other methods. In this thesis, the MAX estimate is used as simply a reference value for comparison purposes, because the statistical uncertainties, the required number and length of simulations etc. are treated extensively for the MAX.

Chapter 9

Peak Over Threshold (POT) method

9.1 Summary

By restricting the data to the maximum of each simulation, only a small amount of the potentially useful information is utilised. This can be improved by incorporating more information in the analysis, by including the peaks above a certain chosen threshold. This increases the amount of information available for the statistical analysis. There are some 'subjective' choices that have to be made before. One of the choices is the threshold value. If the threshold value is high then the bias of the data can be large. On the other hand if the threshold is too low than the variance of the data can be considerable. Another issue of concern is the independence of the peak values. It can be an important parameter for the extrapolation of the peak distribution for a stationary period to the largest peak distribution for a longer period, say, 1 year.

The available POT models are described in Section 7.3. The peak flap moments of the OWT are fitted to POT models. The turbine used here is the pitch regulated turbine. The mean wind speed considered is *15 m/s*, the length of simulations is *40 minutes* and the turbulence intensity is *0.12*. Using the extrapolation procedure one can predict the distribution of the largest peak for a stationary period, given the number of independent peaks in a stationary period. It is expected that with the increase of information the number of simulations can be reduced. Effectively, one can divide the simulation into shorter pieces (shorter than the stationary length) and determine the maxima from the shorter pieces of the simulation. One can say that the shorter the simulation length, the less likely it is that these maxima are independent because these response maxima that are close to each other are likely to be the product of the same event, for example an extreme gust. The variation of the 99 percentile is also assessed for different numbers of simulations. The influence of the peak counting method on the response distribution is investigated. The results are compared

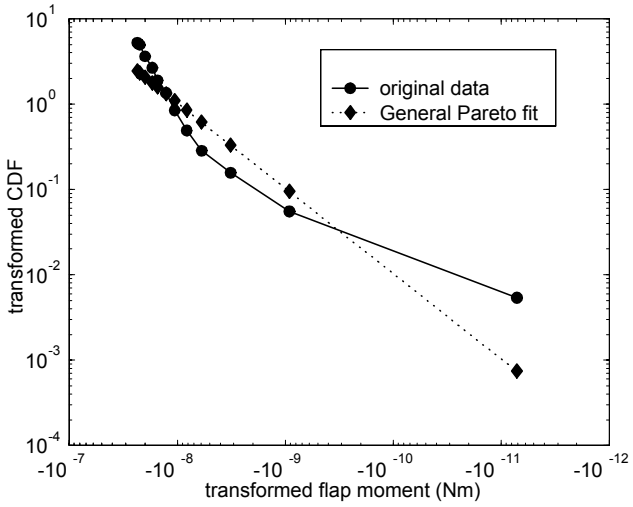

Figure 9.1: Least square fit of the Generalised Pareto distribution to the peaks of the flap moment.

with the estimates obtained with the MAX method.

9.2 Fitting of the data to POT distribution models

First, the GP distribution and the 3 parameter Weibull distribution are used to model the peak responses of the flap moment and the overturning moment. A peak is defined as the maximum between two mean up-crossings. In this way, the neighbouring peaks of high frequency components of the response around a local maxima can be eliminated, since these peaks are not independent. Figure 9.1 shows the flap moment in a Pareto probability plot with the fitted GP distribution. It can be seen that the GP distribution does not fit the flap moment satisfactorily because the data would appear as a straight line in a Pareto probability scale. The data suggest that the distribution is not as heavy tailed as the GP distribution. The same trend is observed for the overturning moment.

For this reason, the three parameter Weibull distribution is used. It can be seen in Figure 9.2 that the Weibull distribution offers a better fit to the flap moment than the GP distribution. Figure 9.3 shows the Weibull fit of the OTM. The data are plotted in a Weibull probability scale and can be approximated by a straight line. At lower fractiles, there is a strong deviation from the fitted distribution. The reason is that the threshold chosen may not be high enough so that peaks without influence on the extremes are included. This can be avoided

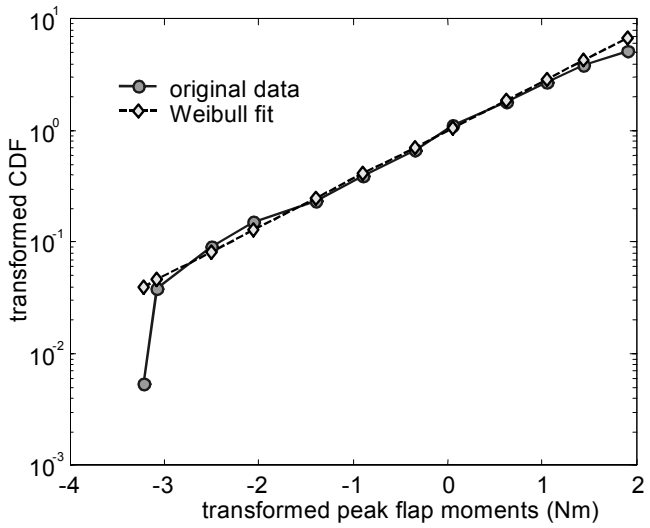

Figure 9.2: Fit of the Weibull distribution to the peak responses of the flap moment plotted in Weibull scale.

by increasing the threshold. However, the deviation in the lower tail region practically does not affect the upper tail behaviour of the Weibull distribution. It is to be noted that the 3 parameter Weibull distribution also includes the Exponential distribution, which is one of the POT distribution models.

9.3 Influence of the number of simulations on POT estimate

At this point, only peaks from one simulation run have been used to fit the response distribution. For the extrapolation of the peak response distribution of a stationary period, this may not be sufficient. Peaks of rare occurrence may not be present in the one simulation chosen for the analysis. For this reason, the effect of the number of simulations on the estimate of the peak response distribution need to be studied.

The peak distribution obtained here refers to a distribution when an arbitrary local maximum occurs within the simulation length. For the distribution of the largest peak that can occur during a stationary period, one need to extrapolate using Equation 9.1

$$F_T(m) = [W(m)]^{\lambda T} \tag{9.1}$$

where $F_T(m)$ is the probability distribution that the response m is not exceeded in a period of the length T. W is the POT distribution of the stochastic variable

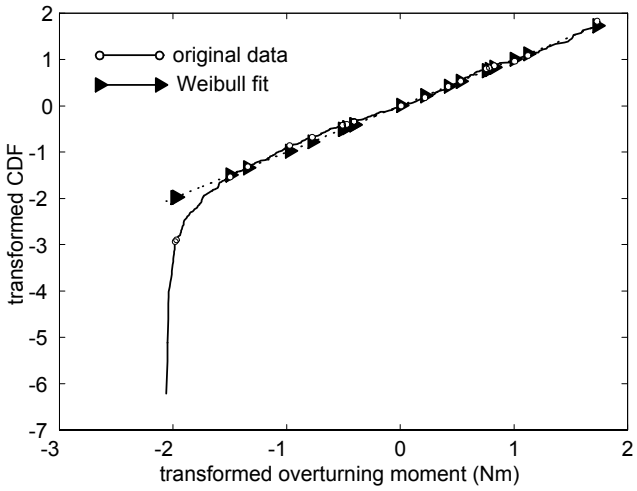

Figure 9.3: Fit of the Weibull distribution to the peak responses of the overturning moment plotted in Weibull scale.

of m. λ is the average number of peaks per time unit T. For the illustration purpose, the 100 year response is estimated from the peak distribution for only one mean wind speed. The 100 year response is obtained by extrapolating the peak response distribution $F_T(m)$ to the number of stationary periods in one year with that mean wind speed. The selected mean wind speed is 15 m/s (see also Equation 7.2).

The estimates of the 100 year flap moment for several simulations are plotted together with the maximum peak encountered in the corresponding simulation in Figure 9.4. It can be seen that there is a strong correlation between the extrapolated estimate of the 100 year flap moment and the maximum peak that is encountered in the simulation. Furthermore, the variation of the 100 year estimate of the flap moment is quite considerable, suggesting that using only one simulation, estimates of the response of long return periods can be largely uncertain. The question is how many simulations are necessary to achieve a reasonably accurate estimate.

To quantify the variation of the estimate, the MAX estimate is used as a reference value. One may expect that both methods should yield similar results. Moreover, it is assumed that with the POT method less simulations are required to achieve an estimate of the extreme response of comparable accuracy as estimated using the MAX method.

Random drawings of the simulations have been carried out to study the effect of the number of simulations on the POT estimate. The total number of simulations used is 50 and the sample size of the random drawing varies from 1 to 25. For every sample size 20 random drawings are performed. The mean upcrossing peaks from the randomly drawn simulations are fitted to a

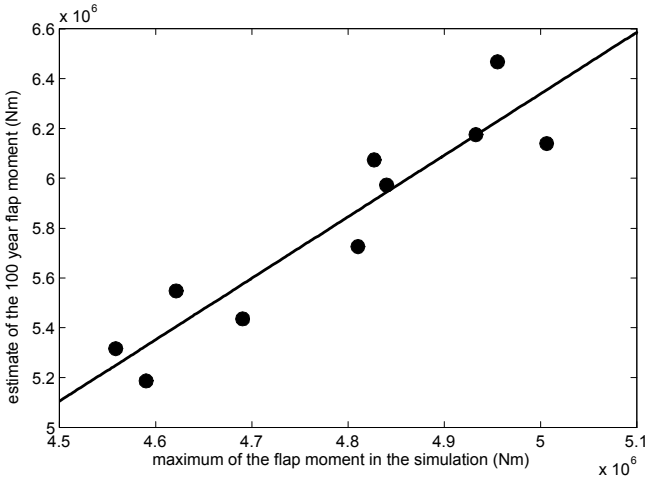

Figure 9.4: Scatter plot of the maximum flap moment of several simulations with the 100 year POT estimate of the flap moment from that simulation.

3 parameter Weibull distribution. From the fitted distribution the 100 year response is determined. Figure 9.5 shows the variation of the 100 year flap moment with different sample sizes. The mean deviation of the 100 year flap moment is reduced rapidly with the increase in the number of simulations. With 10 simulations and upwards, the mean estimate of the 100 year response reaches an asymptotic value, which is about 2% higher than the MAX estimate..

The spreadings of the 100 year flap moment for a given sample size are also shown in Figure 9.5. The spreading is shown as a two standard deviations bar from the mean value, i.e. two standard deviations above and below the mean value. It can be expected that the spreading will be reduced with the increase of the number of simulations. It can be seen that the POT method on average, gives a higher estimate of the 100 year flap moment compared to the MAX method[1]. The reduction of the standard deviation of the 100 year response decreases slowly after a sample size of 15 is reached. Weighing the computational efficiency against the reduction of the spreading, it would be advisable to choose a number of simulations around 15.

Figure 9.6 shows the same thing as in Figure 9.5 but for the overturning moment. The trend is comparable to that of the flap moment. Using very low number of simulations (e.g. 1 to 5), the spreading is lower than the spreading in the estimate of the 100 year flap moment. For a number of simulations of 10 and upwards, the difference in the spreading between the 100 year OTM and flap moment is insignificant. Also here it can be said that with 15 simulations

[1]The POT method does not necessarily provides a higher estimate of the maximum flap moment than the MAX method, it depends very much on the dataset, the choice of a threshold and the upper tail of the distribution.

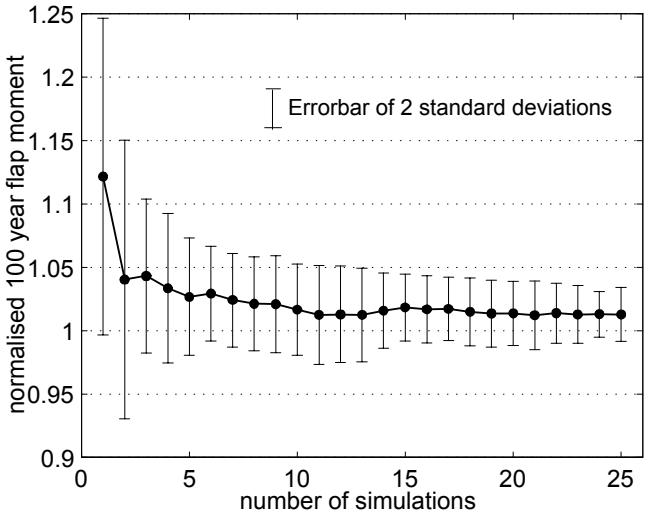

Figure 9.5: Variation of the 100 year flap moment estimated using different numbers of simulations.

one can obtain estimates that are comparable to that from the MAX method.

9.4 Selection of the threshold

The question that now arises is whether the fitted POT distribution is susceptible to the selection of thresholds. One may reason that the underlying assumption of independence between the peaks are more likely to be true for larger peaks. The effect of the choice of thresholds on the POT distribution is studied by choosing different threshold levels. Instead of specifying explicitly a threshold level, the peaks are ordered according to their magnitudes. Then, different percentages of the peaks are chosen, such as the highest 10% of the peaks. These different percentages of peaks are fitted to a 3 parameter Weibull distribution and the evolution of the 100 year response is examined.

Figure 9.7 shows the 100 year flap moment using different percentage of the peaks and different numbers of simulations. The figures are normalised with respect to the 100 year flap moment determined with the MAX method. As can be expected, if the number of simulations is small the spreading of the 100 year response is large for all the different percentages of peaks, especially for the case with the highest 10% of the peaks. The variation can be as much as 50%. However, this case has also the lowest spreading of the 100 year response for an increasing number of simulations.

The disadvantage of taking only the most extreme peaks is that there is a consistent overestimate of the 100 year response, although the spreading among

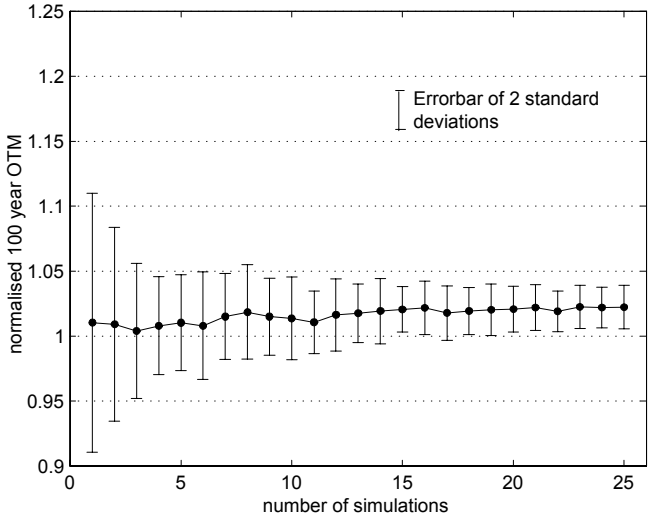

Figure 9.6: Variation of the 100 year overturning moment estimated using different numbers of simulations.

the estimates is the smallest. Increasing the percentage of peaks for the fitting, increases also the spreading of the estimates.

Defining the bias[2] (see Equation 9.2) as the ratio between the mean of the POT estimates of the largest peak $\bar{\mu}$ in a stationary period and the mean of 50 global maxima, $\bar{M}$, taken from 50 simulations

$$Bias = \frac{\bar{\mu}}{\bar{M}} \tag{9.2}$$

One can say that the bias decreases with the increase in the percentages of peaks taken into consideration, while the spreading of the estimates increases with the percentage of peaks (exceptions are the one sample estimates). The selection of a threshold becomes a less relevant issue if the number of simulations used is sufficiently large. With 10 simulations, the difference among the 100 year responses using different percentages of the peaks is less than 3%. Since 15 simulations were recommended, the choice of a threshold is only a real problem if one considers extremely few peaks from one simulation. For example, if one considers only 2 peaks per simulation and 15 simulations, there will be 30 data points for a POT fit. However, 30 peaks can be insufficient for a reliable fit of the POT distribution. For the OTM, the variation of the estimate is similar to that of the overturning moment. The choice of the threshold is not of concern if the number of simulation is sufficiently large, i.e. more than 10.

[2] Note that often bias has a statistical connotation as difference rather than ratio of two variables.

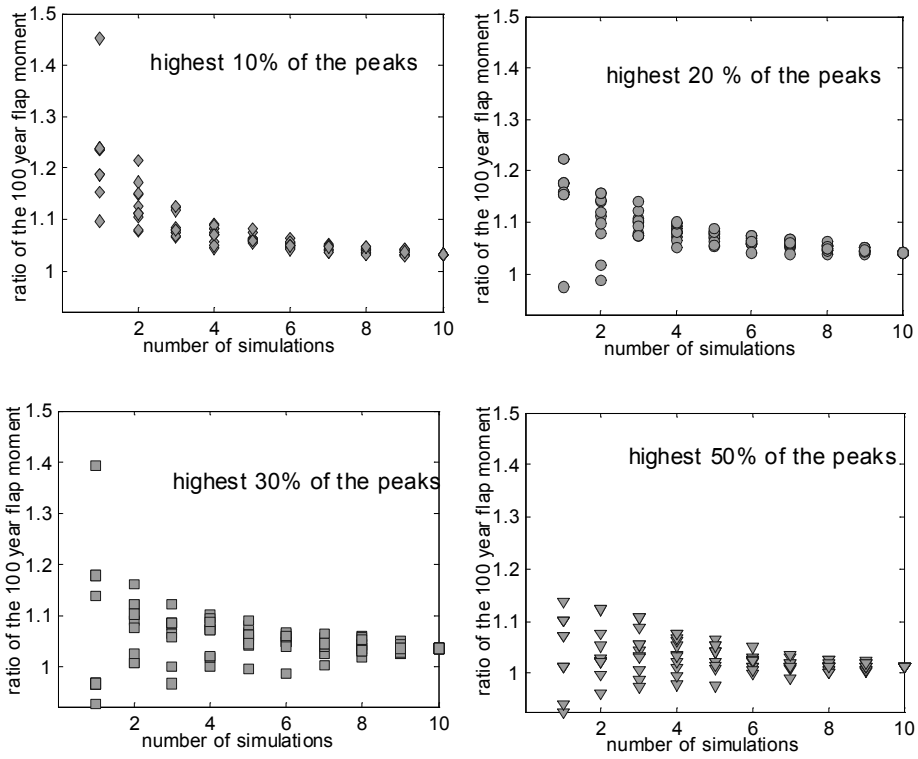

Figure 9.7: estimate of the 100 year flap moment with POT method using different percentages of the peaks.

9.5 Peak counting method

In the previous section, a peak is defined as the maximum between two mean upcrossings. Another way of defining the peaks is to give explicitly a threshold. If the threshold is the mean response, the number of local maxima is higher than the mean upcrossing peak definition because of high frequency fluctuation of the response [39].

The fact that more peaks are counted is reflected in the extrapolation of the extreme responses. The extrapolation of the response distribution for a random peak to the distribution of the largest peak in a stationary period T is carried out with Equation 9.1.

Even though the distribution is not affected by the extra number of peaks due to the counting method that includes all the peaks above the mean response, a higher estimate can still be expected due to the increase of λ, the average number of peaks per time unit. For this reason, this type of peak counting should not be applied.

Another way of removing the influence of high frequency components of the response is to define the peaks as the maximum value in one blade revolution. In this way, the number of peaks in a stationary period is no longer a variable.

To quantify the influence on the estimates between the peaks per blade revolution and peaks between two mean upcrossings, the bias is used. The bias is defined as the ratio of the mean of the POT distribution[3] and the mean of 50 maxima from 50 simulations (see Equation 9.2).

The different numbers of simulations are also taken into account by making 20 random drawings for each number of simulations. Figure 9.8 shows the bias of the flap moment using the peak per blade revolution counting and peak between mean upcrossings. The peak per blade revolution shows a significantly smaller bias of the mean estimate. The difference in the standard deviation of the estimates of the mean response is less noticeable between these two counting methods. For increasing number of data points (that i.e. number simulations), both give more or less the same standard deviation. Notice that the mean of the POT estimate is normalised with respect to the mean response estimated with the MAX method, the standard deviation is also normalised with respect to the mean response estimated with the MAX method (i.e. the COV).

In terms of the number of peaks, these two counting methods differ only slightly. The peak per revolution has in average about 10% more peaks than the peaks between two mean upcrossings. It seems like the periodic component of the blade response does influence the peak statistics. Given the result, the peak per blade revolution counting seems to achieve better estimates of the extreme responses using a POT model. Hence, the peak per blade revolution counting is recommended for the POT estimate of the flap moment.

Figure 9.9 shows the bias of the overturning moment using the peak per blade revolution counting and peak between mean upcrossings. The OTM is

[3] Note that the mean of the POT distribution refers to the mean of the largest peaks in a stationary period, ,thus, comparable with mean of the maxima.

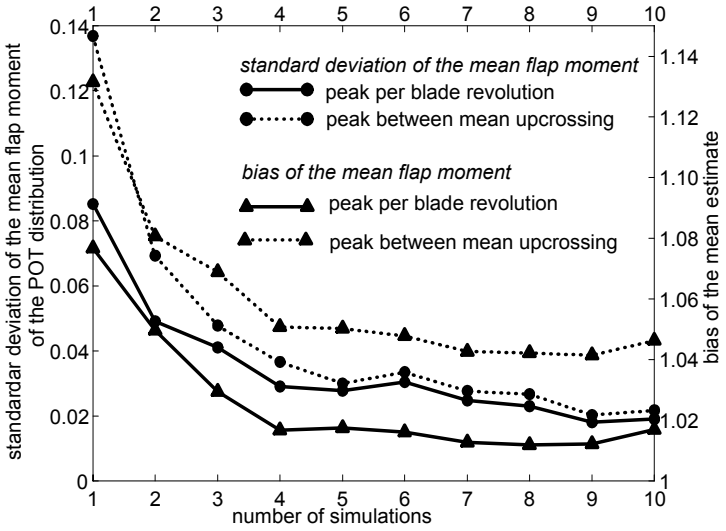

Figure 9.8: Bias of the mean estimate and the standard deviation of 100 year return value with different peak counting method

normalised with respect to the mean of the OTM's using MAX method. The bias is extremely small for both counting method, subsequently the standard deviation is also very small. Hence, both methods produce estimates with no discernible difference. One thing to be observed is that the peak per blade revolution counting can not be applied for a turbine in standstill. In this case the pitch regulated turbine is used. For this turbine, the extreme response occurs during the operation and it is clearly dominated by the aerodynamic loadings. For this reason the peaks per blade response works quite well. This is not necessarily the case for other types of turbines or where the hydrodynamic loading plays an important role. For this reason the mean upcrossing counting is to be preferred for the POT estimate of the overturning moment.

9.6 Uncertainties

9.6.1 Linear correlation of the neighbouring peaks

As can be seen before, the peak counting method can affect the extrapolation of POT distributions. The linear correlation of the peaks can be visualised by plotting the peak number N against the following peak $N + 1$. Figure 9.10 shows the scatter plots of the peaks of the flap moment using mean upcrossing counting and blade revolution counting. It can be seen that the mean upcrossing counting has a higher threshold than the peak per blade revolution counting because lower values of the peaks are discarded by the mean upcrossing counting.

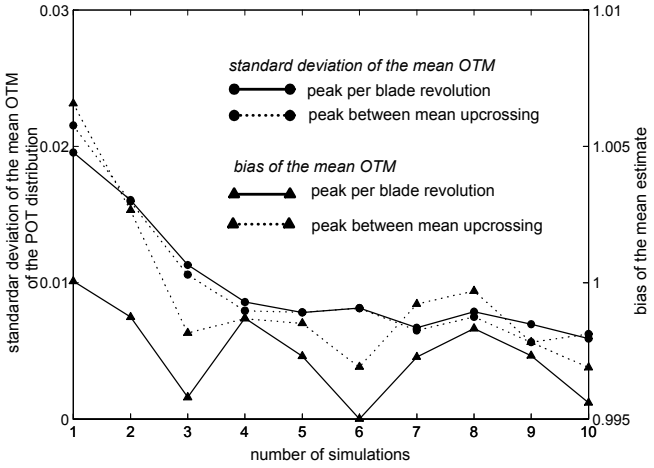

Figure 9.9: Bias and the standard deviation of the mean value of the POT distribution with different peak counting methods.

Effectively, the threshold for the mean upcrossing counting is the mean response level. There are numerous peaks during one blade revolution that are below the mean level of the flap moment. The linear correlation coefficient for the mean upcrossing counting is slightly lower than the blade revolution counting, 0.76 versus 0.82, respectively. Both counting counting methods show large linear correlation between two neighbouring peaks.

However, assuming that all the peaks are independent does not lead to an excessive overestimate of the extreme response. The 100 year responses determined with the POT method are simlar to the MAX estimate, given a sufficient number of simulations. Similar to the influence of the number of independent periods for the extrapolation of the extreme distribution in the MAX method, the sensitivity of the long-term response estimate to the number of independent peaks becomes smaller and less important when the POT distribution is used to predict upper tail realisations of the extremes. This is in the region where the distribution converges towards results for rare Poissonian events.

It is possible to take the correlation between the peaks into account when computing the POT estimates using the outcrossing method [32]. However, the POT estimate differs only slightly from the MAX for responses of long return period, hence the expected improvement is only marginal.

9.6.2 Combination of POT models with different peak counting methods

In the previous section, it was shown that the mean upcrossing counting has a higher bias in the flap moment estimate. It is possible that dropping the peak

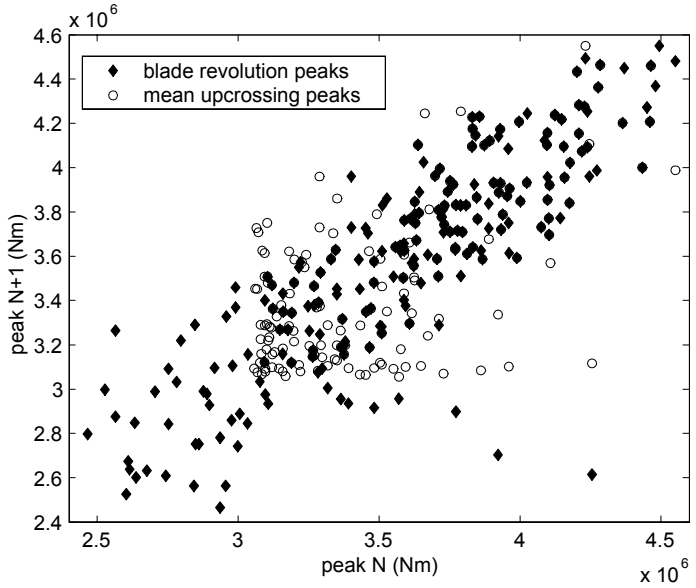

Figure 9.10: scatter plot of the peak N and the peak $N+1$ of the flap moment for different peak counting methods.

values below the mean level increases the estimate of the largest peak. Since the peaks below the mean level may belong to the same peak statistics. The peaks from one simulation using the two different counting methods are compared. These two sets of peaks are fitted to a 3 parameter Weibull distribution.

Figure 9.11 shows the mean upcrossing peaks fitted to two different distribution functions, a Weibull and a Generalised Pareto distribution. The distribution parameters are maximum likelihood estimates. The Weibull distribution has problems in fitting the lower tail of the mean upcrossing peaks constrained by the parameter choice. With the given sample size the K-S test rejects the Weibull distribution due to the deviation at the lower tail of the distribution. The Generalised Pareto distribution shows visually a better fit than the Weibull distribution and the K-S test does not reject it. However, the Generalised Pareto fit yields a negative shape parameter γ. This produces a right end point in the distribution, which presents a problem for the extrapolation.

In practice, if one ignores the deviation of the lower tail of the distribution from the empirical distribution and applies the K-S test to the remaining part of the distribution then the 3 parameter Weibull distribution will still pass the goodness of fit test. This is justified by the fact that the region of interests is on the upper tail region, hence deviation on the lower tail region can be disregarded.

Figure 9.12 shows the peaks of the flap moment per blade revolution fitted to

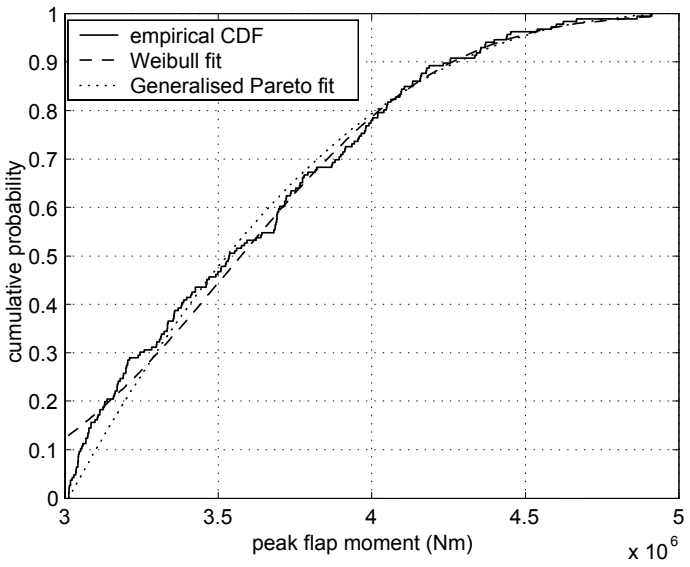

Figure 9.11: Weibull and Generalised Pareto fit of the empirical distribution function of the mean upcrossing peaks of the flap moment.

a Weibull distribution function. The Weibull distribution fits better the peaks per blade revolution. The numerical method used here to find a maximum likelihood estimate of the Generalised Pareto distribution does not converge within the given precision, thus, the GP distribution is not used. The fitted Weibull distribution has a longer lower tail and the left end point is usually lower than the smallest value in the sample, while the Generalised Pareto distribution usually has a left end point equal the smallest value in the sample. By increasing the threshold the distribution will be more 'Pareto like' but again the same problem with the right end point of the distribution emerges. The question here is whether the smaller peaks below the mean level can be regarded as a part of peak statistics. There is no direct justification for the inclusions of these peaks below the mean level.

However, using the Weibull distribution to fit the flap moment peaks per blade revolution does produce better fits than fitting the Weibull distribution to the the mean upcrossing peaks. The deviation of the lower tail does not lead to a rejection of the Weibull distribution using peaks per blade revolution counting method. Since GP is not suitable, the 3 parameter Weibull distribution is recommended for the fit of peaks. It is to be noted also that Weibull distribution also includes the Exponential distribution, which is another POT model. In conjunction with the Weibull distribution, the peak per blade revolution counting produces a lower bias of the estimate with respect to the response estimated from the MAX method.

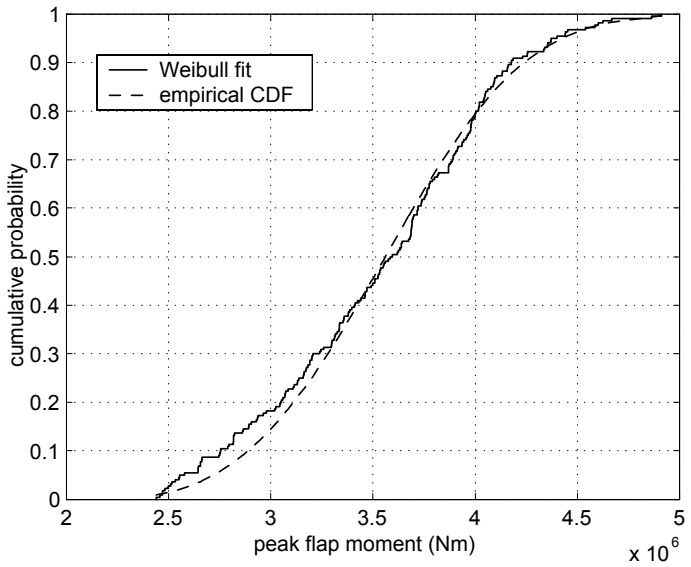

Figure 9.12: Weibull fit of the empirical distribution of the peaks per blade revolution for the flap moment.

Chapter 10

Time domain analysis using Process model

10.1 summary

In this chapter the random process model is analysed. The random process model uses the complete time series to estimate the distribution of the extremes, more specifically it uses the statistical moments of the time series. Theoretically such model uses the maximum amount of information, however, there are some difficulties associated with accurate estimation of the higher statistical moments from the time series. For a Gaussian process, the distribution of the local maxima has been extensively investigated in the past [30] [17]. The largest values of the local maxima follow asymptotically the extreme value distribution type I (Gumbel). For a non-Gaussian process, the higher statistical moments have to be taken into account as well. Usually a perturbation approach can be used to consider the deviations from the Gaussian skewness and kurtosis [65]. This can also be done with a Hermite transformation [99].

First, the different process models are applied to obtain the estimates of the extreme response of a pitch regulated wind turbine. The results are compared to the estimates using the MAX method. The extreme response distribution is determined using the statistical moments from the simulation time series. An advantage of this approach is that the use of statistical moments can be translated into less simulations because they characterise the process and all the data points are being taken into account. On the other hand the Gaussian model take only the first two statistical moments into account and while weakly non-Gaussian models consider the skewness and/or kurtosis of the process, these higher statistical moments are subject to a larger statistical variation than the first two moments, hence uncertainties of these parameters are also larger. Despite of the limitations and uncertainties it will be shown that the process model estimates are of comparable accuracy to the estimates of MAX and POT methods.

10.2 Gaussian model

Davenport [30] has shown that if the underlying parent distribution is Gaussian then the largest values will asymptotically follow a Gumbel distribution. The expectation values of the Gumbel distribution can be written as

$$\mu_{\max} = \mu + \sigma \left(\sqrt{2 \log N_0} + \frac{\gamma_e}{\sqrt{2 \log N_0}} \right) \tag{10.1}$$

$\mu_{\max}$ is the mean of the Gumbel distribution, μ and σ are the mean value and standard deviation of the process respectively. N_0 is the number of upcrossings and γ_e is the Euler's constant. The variance $\sigma^2_{\max}$ of the distribution is

$$\sigma^2_{\max} = \frac{\pi}{6} \frac{\sigma^2}{2 \log N_0} \tag{10.2}$$

where $\sigma_{\max}$ is the standard deviation of the Gumbel distribution. The mean and standard deviation of the Gumbel distribution can be calculated directly from Equations 10.1 and 10.2 using the process mean and standard deviation. The mean and standard deviation of the Gumbel distribution are related to the location and scaling parameters and they can be calculated using Equations 7.10 and 7.11.

50 simulations with a mean wind speed of 13 m/s and the corresponding wave parameters were carried out for the pitch regulated wind turbine. The simulation length is 10 minutes. From the 50 simulations, N simulations are randomly drawn, N varies from 1 to 10. The statistical moments from these N simulations are determined. For every N, 20 random drawings are performed so that the variation of the estimate for a given number of N simulations can be quantified. The variation of the statistical moments of the flap moment is depicted in Figure 10.1. The values are normalised with respect to the mean values of 10 simulations. In the figures an error bar of 1 standard deviation is also shown. Figure 10.1 (lower right) also shows the 99 percentile of the Gumbel distribution.

As can be seen the mean value has the smallest variation, while the variation of skewness is very large. There are samples that have very low skewness, near zero, and samples with small skewness in the order of 0.3. Thus, the relative variation is quite significant. In comparison, the kurtosis (not shown here) has larger absolute variation than the skewness, but the relative variation of the kurtosis with respect to the mean of the kurtosis from 10 simulations is limited, between 0.9 and 1.1 (with respect to the Gaussian kurtosis of 3). The relative variation of the kurtosis is higher than the variation of standard deviation. The 99 percentile of the distribution varies slightly more than the mean value but less than the other statistical moments. The 99 percentile of the distribution converges after 6 simulations. Adding more simulations to the statistical analysis brings no significant reduction to the estimate of the 99 percentile. In a Gaussian model, the skewness and the kurtosis are not taken into account. For this reason the variation of the 99 percentiles does not reflect the variation of the skewness and kurtosis.

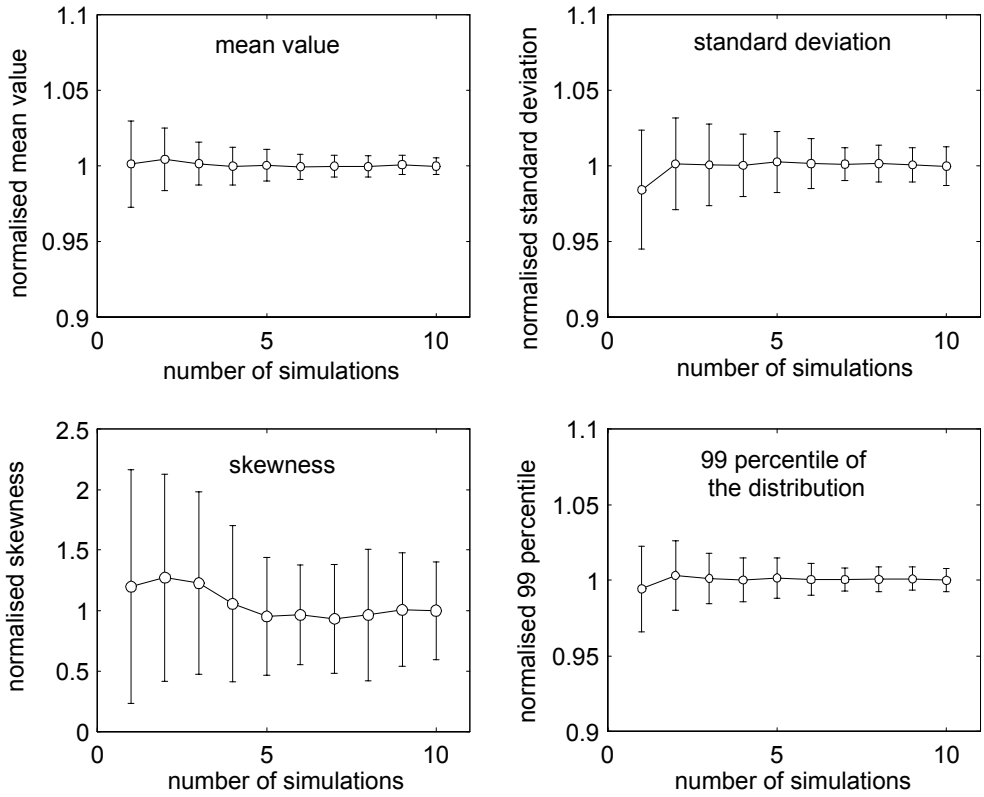

Figure 10.1: Mean value, standard deviation, skewness of the maximum flap moments and the 99 percentile of the distribution as function of the number of simulations; shown with errorbars of one standard deviation.

The variation of the statistical moments of the overturning moment shows very similar behaviour to the flap moment. The mean value has the lowest spreading followed by the 99 percentile of the Gumbel distribution. The skewness has only negative values with large relative variation, the values vary between -0.05 to -0.32. The kurtosis varies around 3, between 2.8 and 3.3. The 99 percentile of the Gumbel distribution of the OTM is not affected by the variation of the skewness and kurtosis due to the Gaussian assumption.

The Gaussian model makes use of the asymptotic behaviour of the distribution of the local maxima with a Normal distribution as parent distribution. The local maxima of a Gaussian process converges to a Gumbel distribution. This is valid for large values of the stochastic variable, in this case the extreme responses, and a large number of local maxima, N_m. Instead of using the asymptotic result, the analytical distribution of the local maxima can be used. This distribution is also known as the Rice distribution [63].

$$F_{rice}(\zeta) = \Phi\left(\frac{\zeta}{\sqrt{1-\alpha^2}}\right) - \alpha e^{\frac{\zeta^2}{2}}\Phi\left(\frac{\alpha\zeta}{\sqrt{1-\alpha^2}}\right) \tag{10.3}$$

where Φ is the standard Normal distribution and α is the regularity factor defined as the ratio between the number of mean upcrossings N_0 and the number of local maxima N_m. N_0 and N_m are calculated directly from the simulation time series by counting. The distribution of the largest value for an interval T (in which N_m is present) is

$$F_T(\zeta) = [F_{rice}(\zeta)]^{N_m} \tag{10.4}$$

From Equations 10.3 and 10.4, the 99 percentile of the distribution of the extreme flap moment for a period T can be determined. Comparison of the asymptotic result with the 'exact' result is given in Figure 10.2. It also shows the variation of the 99 percentile with the number of simulations. For each number of simulations 20 random drawings are performed. The spreading of the estimates is illustrated with errorbars of 1 standard deviation. The values are normalised with the 99 percentile estimated using the MAX method. As can be seen the asymptotic estimate is above the MAX estimate while the "exact" estimate lies in average 6% below it.

There are several explanations for this deviation. First, the asymptotic estimate is higher because it assumes that N_m is very large. Thus, the extrapolation will give a higher estimate. Another source of overestimation comes from the kurtosis. The Normal distribution has a kurtosis of 3, but some simulations have kurtosis slightly below 3. A larger kurtosis means a heavier tail than the Gaussian distribution. On the other hand, the positive skewness suggests that the distribution are skewed toward the upper tail. All these factors together make the Gaussian estimate of the extreme flap moment agrees reasonably well with the MAX estimate. The "exact" estimate considers the actual number of N_m, but lack the ability to correct the effects of a non-zero skewness and a kurtosis that is different than 3. This leads to an estimate below the asymptotic estimate using the Gumbel distribution.

Another conclusion that can be drawn is that the mean value of the estimate varies very little with the number of simulations. However, the increase of number of simulations does reduce the spreading of the estimates. This means that instead of grouping the simulations together one can use estimates from different simulations and takes the averaged values of the estimates. This is shown in Figure 10.3. The values are normalised with the 99 percentile from the MAX estimate. Notice also that these are random drawings from 50 simulations, for this reason the spreading of estimates for 10 simulations is not zero.

Grouping means that all the simulations are merged into one single time series and the statistical moments are obtained from the merged time series. Averaging means that the statistical moments are computed separately for each time series, then the 99 percentiles of the distribution are determined. The average value is taken from all the 99 percentiles. Obviously the spreading of the estimates decreases with the number of simulations for both procedures but in

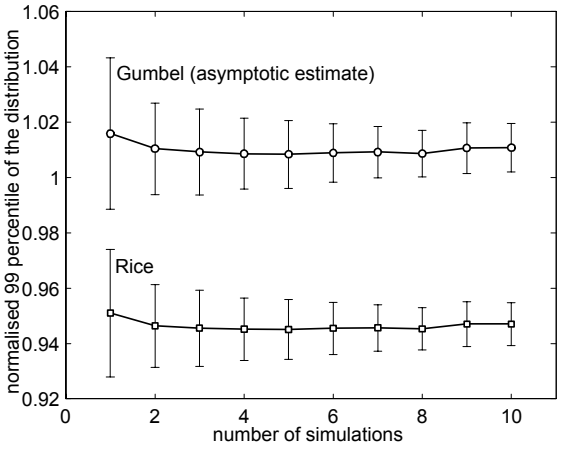

Figure 10.2: comparison of the 99 percentile of the distribution of the flap moment using the Gumbel asymptotic estimate and the Rice distribution; with errorbars of one standard deviation.

absolute term the 'Averaging' approach achieves a lower scatter. The spreading in estimates decreases rapidly, with more than 5 simulations the spreading of the estimates decreases very slowly. For the overturning moment the averaging procedure gives also smaller scatter than the grouping procedure.

10.3 Weakly non-Gaussian models applied to the flap moment

10.3.1 Weakly non-Gaussian model with skewness correction

As mentioned before the response time series are not strictly Gaussian. For this reason, models that include correction terms based on the skewness and the kurtosis [65] [99] were developed. The non-Gaussian process is written as

$$X(t) = \xi + \eta\left(\zeta(t) + \epsilon\zeta(t)^2\right) \tag{10.5}$$

where ζ is a standard Normal process, ξ and η are constants that are related to the process mean and standard deviation, ϵ is a correction factor for the non-Gaussian process. Equation 10.5 is usually used for small ϵ. The three parameters, ξ, η and ϵ, can be determined from the mean, standard deviation and skewness of the time series. The first order approximations are [65]

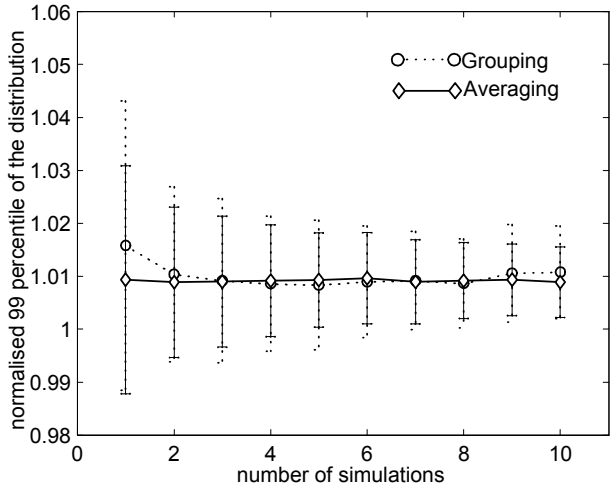

Figure 10.3: 99 percentile of the distribution of the flap moment using different number of simulations. The statistical moments are estimated by grouping or averaging; shown with errorbars of one standard deviation.

$$\xi \approx \mu_x - \epsilon\sigma_x \tag{10.6}$$

$$\eta \approx \sigma_x \tag{10.7}$$

$$\epsilon \approx \frac{\beta}{6} \tag{10.8}$$

where, μ_x is the mean of the sample, σ_x is the standard deviation and β is the skewness. Equation 10.5 is also valid for the maximum of the process so that

$$X_{\max}(t) = \xi + \eta\left(\zeta_{\max}(t) + \epsilon\zeta_{\max}(t)^2\right) \tag{10.9}$$

The relationship between $X_{\max}$ and $\zeta_{\max}$ is monotonic for small ϵ, that means that there is a one to one correspondence between $X_{\max}$ and $\zeta_{\max}$. The distribution for $X_{\max}$ can be written in terms of the distribution of $\zeta_{\max}$ through a functional transformation [1]

$$F_{X_{\max}} = F_{\zeta_{\max}} \cdot \left|\frac{d\zeta_{\max}}{dX_{\max}}\right| \tag{10.10}$$

The asymptotic distribution of $\zeta_{\max}$ is a Gumbel distribution with the mean and standard deviation as given in Equations 10.1 and 10.2. The resulting distribution of $F_{X_{\max}}$ is close to the Rice distribution if the parameter ϵ is small. The distribution of the largest values in a period T is then

$$F_T = \left(F_{\zeta_{\max}} \cdot \left| \frac{d\zeta_{\max}}{dX_{\max}} \right| \right)^{Nm} \tag{10.11}$$

This will converge to Gumbel distribution if $\frac{d\zeta_{\max}}{dX_{\max}}$ is nearly constant and the number of local maxima, N_m is large. If that is the case the mean and standard deviation of the Gumbel distribution F_T can be also approximated, see [65]. Figure 10.4.shows the 99 percentile of the extreme flap moment from different approximations of Equation 10.11. One of the possibilities is to use the Rice distribution as $F_{\zeta_{\max}}$, shown as 'Rice distribution' in the figure. The second choice is to approximate the term $(F_{\zeta_{\max}})^{Nm}$ using a Gumbel distribution, shown as 'Gumbel distribution' in the figure. The third possibility is to model the distribution F_T as a Gumbel distribution, shown as 'Approximated Gumbel distribution'. The 99 percentile of the distributions using different approximations are normalised with respect to the 99 percentile obtained with the MAX method.

As can be seen, the Rice distribution gives the closest estimates to the MAX estimate, considering that it is the theoretically exact distribution. Approaching the term $(F_{\zeta_{\max}})^{Nm}$ with a Gumbel distribution gives a slightly higher estimate of the 99 percentile, about 5% on average (shown as 'Gumbel distribution' in Figure 10.4). The approximation of the distribution F_T as a Gumbel distribution gives an estimate of the 99 percentile of the flap moment that is 30% above the MAX estimate, on average. Figure 10.4 also shows the spreading of the estimates determined by random drawings. For each number of simulations, 20 random drawings are carried out. The spreading is shown as errorbars of 1 standard deviation.

Using the Rice distribution with skewness correction the estimates are improved with respect to the Gaussian model, cf. Figure 10.2 Nevertheless, the Gaussian model using Gumbel distribution delivers an estimate that is very close to the estimate using the Rice distribution with skewness correction. The Rice estimate can be further extended with a kurtosis correction, however, the margin of improvement may be small because the deviation of the estimates with skewness correction is about 2% , on average (with respect to the MAX estimate).

It should be noted that the time series generated with a computer are strictly stationary. The wind input is Gaussian, thus the predicted estimates of the extreme response are quite close to the theoretical values predicted by a Gaussian model. For measured time series where the inputs are non-Gaussian and non-stationary, the improvement of the non-Gaussian model can be more significant. The approximation of the F_T with a Gumbel distribution can not be justified here because the overprediction is quite considerable.

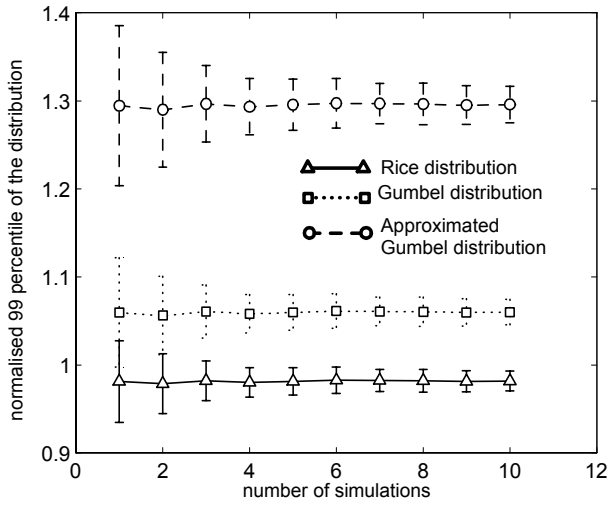

Figure 10.4: 99 percentile of the distribution of the maximum flap moment obtained using different distribution approximations as function of the number of simulations; shown with errorbars of one standard deviation.

10.3.2 Non-Gaussian model with skewness and kurtosis correction

Equations 10.5 and 10.9 can be further extended with the correction of the kurtosis of the data. This can be written in terms of a Hermite polynomials [101]

$$X(t) = \mu_x + \varphi\sigma_x \left(\zeta(t) + c_3(\zeta(t)^2 - 1) + c_4(\zeta(t)^3 - 3\zeta(t)\right) \tag{10.12}$$

μ_x and σ_x are the mean and standard deviation of the time series of the response, φ is a normalisation factor defined as

$$\varphi = \frac{1}{\sqrt{1 + 2c_3^2 + 6c_4^2}} \tag{10.13}$$

c_3 and c_4 are related to the skewness and kurtosis of the sample. They are chosen in such a way that the deviation of the skewness and kurtosis of the data to the skewness and kurtosis of the process is minimised The first order approximations are

$$c_3 = \frac{\beta}{6}; \quad c_4 = \frac{\kappa - 3}{24} \tag{10.14}$$

where κ is the kurtosis of the time series of the response. Equations 10.12 to 10.14 are valid for kurtosis larger than 3. For kurtosis smaller than 3 the transformation is

$$X(t) = \mu_x + \sigma_x \left(\left(\sqrt{\hat{\zeta}(t)^2 + \varphi} + \hat{\zeta}(t)^2 \right)^{1/3} - \left(\sqrt{\hat{\zeta}(t)^2 + \varphi} - \hat{\zeta}(t)^2 \right)^{1/3} - a) \right) \tag{10.15}$$

with

$$\begin{aligned} \hat{\zeta}(t) &= 1.5b(a + \zeta(t)) - a^3 \\ \varphi &= (b - 1 - a^2)^3 \\ a &= \frac{4}{3}\frac{\beta}{\kappa - 3}, \qquad b = -\frac{8}{\kappa - 3} \end{aligned} \tag{10.16}$$

In both cases, the transformation is monotonous. Analogously this can be applied to obtain the maxima of the process as described in the previous section. Since it is a monotonous transformation, the probabilities of the Gaussian process can be mapped accordingly to the probability of the non-Gaussian process (Equation 10.10 and 10.11).

Figure 10.5 shows the estimates of the 99 percentiles of the distribution of the extreme flap moment, with skewness and skewness-kurtosis correction. The result is normalised with the 99 percentile from the MAX estimate. It has to be kept in mind that the MAX estimate is also a stochastic estimate. The variation of the MAX estimate was quantified with a bootstrap procedure using 50 simulations. From these 50 simulations 1000 bootstraps are carried out. The bootstrap samples are fitted to a 3 parameter Weibull distribution and the 99 percentiles of the distributions are determined. The reference value of 1 is the mean value of the 99 percentiles (1000 values). The boundary of one standard deviation of the bootstrap estimates is shown in the figure as well.

As can be seen the variation of the MAX estimate quantified by the bootstrap is in general smaller than the spreading of the estimates of the non Gaussian models . The inclusion of the kurtosis leads to a lower estimate of the 99 percentile because the kurtosis of the time series are in many cases below the Gaussian kurtosis of 3. Due to a considerable spreading of the kurtosis, the spreading of the 99 percentiles is also larger.

The relative variation of the skewness is quite large, but in absolute terms the variation of the kurtosis is larger. Hence the correction brought by the kurtosis can fluctuate considerably, adding more spreading to the 99 percentile estimates. The skewness corrected estimate represents a quite good agreement with the MAX estimate. In general, estimates of higher statistical moments are associated with uncertainties that increase with the order of the statistical moment. The higher statistical moments are more susceptible to outliers and extreme values. For this reason, it can not always be expected that the inclusion of kurtosis will improve the estimates of the 99 percentiles. In this case a skewness correction is a better choice.

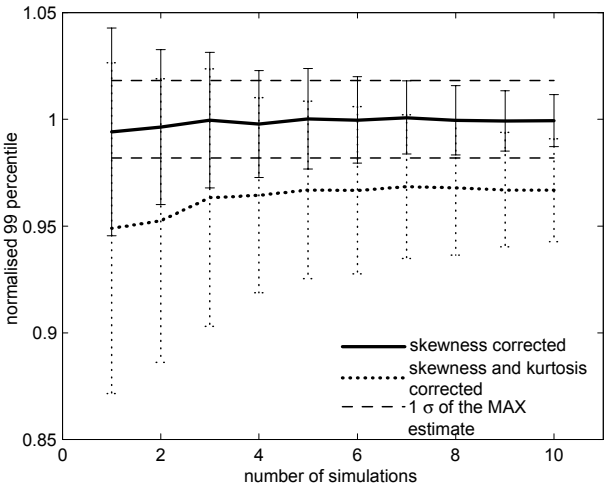

Figure 10.5: Estimates of the normalised 99 percentile of the extreme flap moment with skewness or skewness and kurtosis correction; shown with errorbars of one standard deviation.

10.4 Process models applied to the overturning moment

The Gaussian and weakly non-Gaussian models are applied to the time series of the overturning moment to determine the 99 percentile of the distributions of the maximum overturning moments. The 99 percentiles are normalised with respect to the 99 percentile estimated from the MAX method using 50 simulations. The variation of the MAX estimate is quantified with bootstraps. 1000 bootstraps are performed and the bootstrap samples are fitted to a 3 parameter Weibull distribution. The 99 percentiles of the distributions are determined. The variation of the 99 percentiles of the bootstrap samples is shown in Figure 10.6 as a rectangle, that contains one standard deviation below and above the mean value. Furthermore, for each number of simulations 20 random drawing are carried out and the spreading of estimates of the 99 percentiles is shown as errobars of 1 standard deviation.

The Gaussian model gives a 99 percentile that is about 5% above the MAX estimate, on average. Althought the spreading within the estimates is much lower than the non-Gaussian models. This is because the fluctuation of the mean and standard deviation from simulation to simulation is smaller compared to the fluctuation of the skewness and kurtosis.

The skewness corrected model gives an average estimate that is within one standard deviation from the MAX estimate. The mean deviation is about 2% below the MAX estimate. The variation of estimate of the 99 percentile within

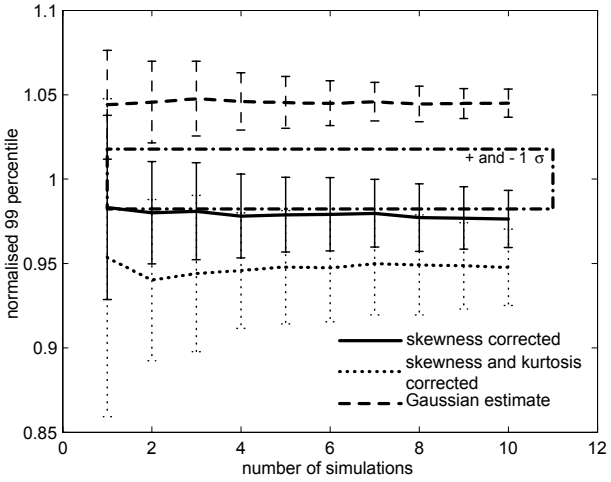

Figure 10.6: comparison of the estimate of the 99 percentile of the overturning moment with different process models. Normalised with MAX estimate; shown with errorbars of one standard deviation.

the number of simulations is larger than the Gaussian model, but still lower than the skewness-kurtosis corrected model.

The skewness and kurtosis corrected model does not perform better than the other models. The variation is very significant from one estimate to another. This has to do with the fact that the higher statistical moments are subject to larger variation when estimated from limited data. Thus, the large variation of the kurtosis propagates into the 99 percentile of the distribution. The asymptotic estimate used in [65] produces here also an estimate that is about 20% higher than the MAX estimate and it is not shown here.

10.5 Selection of the model

For both flap moment and OTM the Gaussian process model perform reasonably well. The asymptotic approximation using a Gumbel distribution does partially compensate the underestimate by disregarding the positive skewness of the time series.

For non-Gaussian models, it is recommended to use the Rice distribution directly to model the distribution of local maxima. The approximation of the distribution of the largest value in a non-Gaussian process using Gumbel distribution can lead to much higher estimate than the MAX model, about 20 to 30% on average.

The skewness correction gives a better estimate than the estimate of skewness-kurtosis correction. Moreover, the large variation of the kurtosis propagate

larger fluctuation to the estimates of 99 percentiles. For this reason the skewness correction is to be preferred.

Chapter 11

Long-term distributions

11.1 Relevant sea states for the long-term distribution

Until now only conditional distributions are analysed and in some cases the conditional distribution of one sea state is extrapolated to obtain extreme responses of a certain return period, e.g. 100 years. Theoretically, for a correct estimation of the extreme response one needs to take into account the contributions from all the conditional distributions, i.e. conditional distributions that correspond to different sea states.

According to Equation 7.1 all the conditional distributions for a given set of sea state parameters have to be considered to obtain the distribution of the extreme response for a random sea state. However, the upper tail of the distribution is unlikely to be influenced by the conditional distributions from 'mild' sea states. The question here is how many of the sea states in a scatter diagram need to be taken into account. First, it is necessary to identify the severe sea states that cause extreme responses.

The sea states are divided in three different operation modes.

1: Idle, with wind speeds below the cut-in wind speed. This operation mode is unlikely to trigger extreme responses, unless combined with other discrete extreme events.

2: Normal production, with wind speeds between the cut-in and cut-out wind speed. During this stage, energy is being extracted from the wind and thrust forces can be considerable, which can have significant influences on the tower bending. In this operating condition, the dominant forces are the aerodynamic forces.

3: Standstill, after the wind speed has reached the cut-out wind speed, the wind turbine is shut down and the blades turn to a parking position where the thrust forces are minimized[1]. The dominating loading here is the wave loading.

[1] This can vary from turbine to turbine. Some turbines have special manoeuvres to reduce the thrust forces (such as pitching or yawing) while other turbines may simply shut down

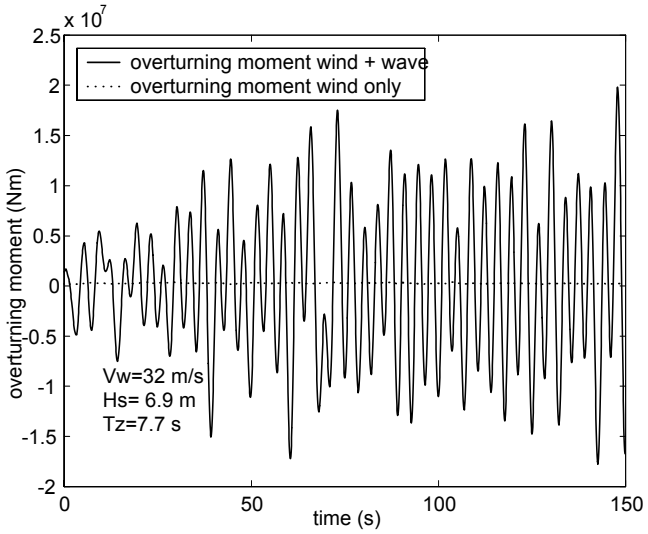

Figure 11.1: Overturning moment in an extreme sea state (standstill) with and without wave loads for the pitch regulated wind turbine.

Figure 11.1 shows the overturning moment of the pitch regulated turbine in an extreme sea state. The wind turbine is not operating and, as can be seen, the contribution of the wind forces to the overturning moment is insignificant. This is due to the fact that the blades are positioned in such a way as to minimise the drag force which contributes to the tower bending. For other turbines, such as stall controlled turbines where blade pitching is not possible, the contribution of the aerodynamic forces to the overturning moment can still be significant.

Figure 11.2 shows the flap moment ratio at the blade root for two different types of turbines. The flap moment is normalised with respect to the flap moment at a mean wind speed of 13 m/s. The most important load situations are around the rated wind speed (13.7 m/s) for the pitch regulated turbine. Around the rated wind speed, the maximum thrust is also reached, which contributes the most to the overturning moment. In contrast, the flap moment of a stall regulated turbine increases monotonically with the mean wind speed. For the stall regulated turbine, the extreme responses occur at extreme sea states with high mean wind speed and large significant wave height, rather than during the turbine operation.

In [24] the maximum overturning moment of the pitch controlled turbine at standstill has been studied. The wave load dictates the overturning moment and the base shear during storm situations. For the rotor blade, the flap moment is relatively small compared to the flap moment during the turbine operation. The OTM during operation is larger than the OTM during the most severe sea

without special load reducing measures.

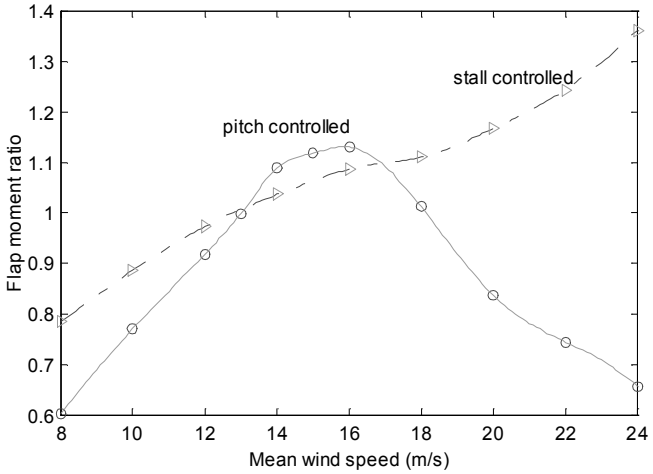

Figure 11.2: Maximum flap moment ratio for different wind speeds (turbine in operation)

state found in the hindcast data. The contribution of the blade forces to the OTM during operation exceed the contribution of the wave loads to the OTM during storms. For this reason, it is likely that the extreme responses of this turbine are to be expected during turbine operation.

The wave loads have practically no influence on the extreme flap moment of the blade. This is due to the low excitation frequency of wave load and the relatively high natural frequency of the rotor [58]. During the turbine operation, the different wave parameters that correspond to a given mean wind speed cause only small variations on the response of the support structure. One may expect that the wave parameters have more significant influence on the overturning moment of the support structure. This is, however, suppressed by the dominant contribution of the aerodynamic forces to the overturning moment. Also because at the rated wind speed, the wave conditions are rather harmless compared to the waves in a storm situation. For this reason it is not necessary to consider all the combinations of the significant wave height and wave periods for each mean wind speed since this variation is negligible for the pitch controlled wind turbine.

11.2 Contributions of the conditional distributions to the yearly extremes: pitch turbine

In the previous section, the sea states that are relevant for the extreme responses are identified for the pitch regulated wind turbines. The most severe extreme response distribution contributes the most to the long-term estimate of the

extreme responses. In this section an effort will be undertaken to quantify the participation of the different sea states in the estimation of the extreme response for a given return period, e.g. 100 year.

Five mean wind speeds around the rated mean wind speed have been selected, they represent the most severe load situations for the pitch regulated turbine (during operation). For these five mean wind speeds 50 simulations are carried out with a simulation length of 40 minutes. The 50 maxima of the flap moment and overturning moment are fitted to a 3 parameter Weibull distribution. The frequency of occurrence of these mean wind speeds (averaging period of 1 hour) are listed in Table 11.1

Table 11.1: frequency of occurrence of different mean wind speeds

Mean wind speed (m/s)	frequency	number of hours/year
13	0.048	421
14	0.041	360
15	0.031	278
16	0.028	253
17	0.008	76

Subsequently, N random drawings are performed on each of the conditional distributions of the response, where N is the number of occurrences in hours in one year (see Table 11.1). For example, the mean wind speed of 15 m/s has 278 hours of occurrences per year. Thus, 278 random numbers between 0 and 1 are drawn. Using the inverse function of the conditional distribution of the extreme flap moment for the mean wind speed of 15 m/s, one obtains 278 estimates of the extreme flap moment. This procedure is repeated for other mean wind speeds.

From all the random samples of the extreme responses from five mean wind speeds, the largest value represents the 1 year extreme response. Repeating this procedure for 100 times, one can obtain 100 extreme values which represent the 100 yearly maxima of the response. The most extreme response in one year does not necessarily come from the most severe mean wind speed, in this case 15 m/s. Although, the chance that this 1 year extreme response comes from that mean wind speed is larger than for the other mean wind speeds. Each of the mean wind speeds will contribute differently to the 100 yearly maxima of the extreme response.

Since the random drawing is a stochastic process, the number of contributions to the 100 yearly maxima of the extreme response will vary. For this reason, the random drawing is repeated for 1000 times to quantify the variation of the contribution of each mean wind speed to the yearly maxima.

The mean values and the standard deviation of the contributions to the 100 yearly maxima of the flap moment from the five mean wind speeds are shown in Table 11.2. It can be seen that the major contribution comes from the mean wind speed of 15 m/s. Basically, this mean wind speed delivers 60 yearly maxima (from a total of 100) on average. Figure 11.3 shows the variation of

Table 11.2: statistical parameters of the number of contributions to the 100 yearly maxima of the flap moment from different mean wind speeds

Mean wind speed (m/s)	Mean number of contributions	standard deviation
13	1.9	4.0
14	12.4	9.7
15	59.7	14.6
16	25.6	13.3
17	0.23	1.5

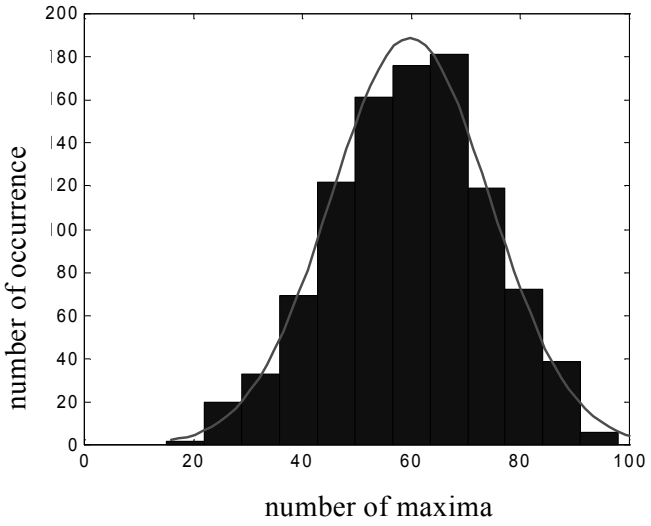

Figure 11.3: Variation of the number of contributions to the 100 maxima of the flap moment (year maxima) for the mean wind 15 m/s.

the contribution of the mean wind speed (15 m/s) to the total number of yearly maxima of the flap moment (100 maxima). The number of contributions can vary from as low as 20 to as much as 90.

The predominance of the most severe mean wind speed lies in the fact that it determines the tail of the distribution of the yearly maxima. Even if the contribution to the 100 yearly maxima is as low as 20, the randomly drawn maxima from the conditional distribution of this mean wind speed are usually not much lower than the maxima contributed by other mean wind speeds.

To illustrate the predominance of this mean wind speed, the randomly drawn 100 maxima (year maxima) of the flap moment are fitted to a Gumbel distribution. This is done for the 100 maxima contributed by all the mean wind speeds and the 100 maxima contributed by the mean wind speed of 15 m/s. The 100 year flap moment is estimated from the fitted Gumbel distribution. The results are shown in Table 11.3.

It shows that using only the most severe mean wind speed the estimates differ, in average, no more than 0.8% from the estimates using all the 5 mean wind speeds. Using only the most severe mean wind speed can give a slightly lower estimate than using all the mean wind speeds. From the 1000 randomly drawn samples of the 100 yearly maxima, the maximum difference in the 100 year response is merely 2.7%. From this one can conclude that for this pitch regulated wind turbine, using the most severe conditional distribution it is possible to obtain an accurate estimate of extreme values of long return periods.

Table 11.3: statistical parameters of the 100 year flap moment and OTM estimated from the most severe mean wind speed and from 5 mean wind speeds.

Data	mean	standard dev.
M_{flap} with all the U	$6.22{\cdot}10^6$ Nm	$0.06{\cdot}10^6$ Nm
M_{flap} with $\bar{U} = 15m/s$	$6.18{\cdot}10^6$ Nm	$0.06{\cdot}10^6$ Nm
OTM with all the U	$4.54{\cdot}10^7$Nm	$0.04{\cdot}10^7$Nm
OTM with $\bar{U} = 15m/s$	$4.51{\cdot}10^7$Nm	$0.04{\cdot}10^7$Nm

M_{flap} = flap moment
$\bar{U}$ = mean wind speed

11.3 Variation of the extrapolation parameters

It has been shown that for the pitch controlled turbine, the long-term response can be estimated accurately using the most severe sea state. The question is whether this can be assumed for different wind turbines with different response characteristics and external conditions. For this reason, the influence of several parameters on the extrapolation of the long-term response is studied. The turbine used now is the stall regulated turbine. The extreme response for this turbine occurs at extreme mean wind speeds beyond the cut-out wind speed. For this reason only the standstill condition is considered. It can be seen from the extrapolation equation (Equation 7.2) that the total number of the sea states[2], and the participations of these sea states have direct influence on the estimate of the long-term response. The purpose of this section is to show the qualitative influence of the parameters that influence the estimate of the long-term response, for this reason it is applied only to one turbine.

The base values used here to normalise the y-axis of the figures are the 100 year flap moment and the 100 year OTM obtained from considering all the sea states beyond the cut-out wind speed in the scatter diagram. Figure 11.4 shows the 100 year flap moment estimated from the most severe sea state where the total number of sea states is different. As can be seen, the variation of the total number of sea states has only a marginal effect for this turbine.

[2] The total number of sea states considered in the analysis, since it is usually not necessary to consider all the possible sea states for the extreme response distribution.

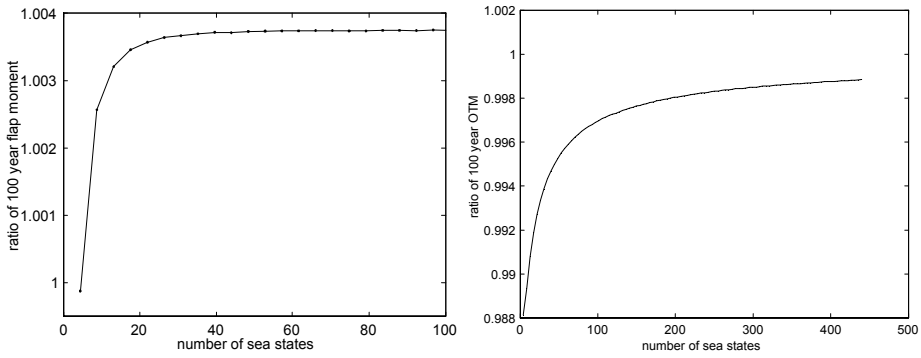

Figure 11.4: Influence of the total number of sea states on the long-term estimate of the stall regulated wind turbine. (left: flap moment, right: OTM); the ratio is between the most severe sea state and all the sea states.

The reason is that the increase in the total number of sea states, also increases the influence of the tail of the distribution, consequently the influence of the most severe sea state. A further increase in the number of sea states means that it is sufficient to take the conditional distribution of the most severe sea state into account to determine the long-term response. It can be expected that with a low number of sea states, using only the most severe sea state can lead to an underestimate of the long-term response (Figure 11.4 right), but again the order of underestimate is rather small.

The relative occurrence frequency[3] of the sea states plays also an important role on the outcome, they are the weighting factors of the different conditional distribution functions. The relative occurrence frequency of the most severe sea state in this case is about 0.005[4]. If the relative occurrence frequency of the most severe sea state increases, there is basically no need to take the other sea states into account. On the other hand, if the relative occurrence frequency of the most severe sea state decreases, the contribution of the other sea states to the long-term estimate becomes more significant. As a matter of fact, the estimate of the long-term response using only the most severe sea state becomes an overestimate. This can be seen in Figure **??**. The decrease or increase of the relative occurrence frequency of the most severe sea state is redistributed to the rest of the sea states so that the sum of the relative frequency remains 1. The normalisation factor is recalculated according to the new distribution of the relative occurrence frequencies.

[3] The relative occurrence frequency of a sea state refers to the ratio between the number of occurrences of that sea state to the total number of sea states. Note that this parameter depends on the specific location.

[4] This is the occurrence frequency of the sea states with a mean wind speed of 15 m/s, a significant wave height of 3.25 m and a zero upcrossing period of 6.25 s. The occurrence frequency of the sea states with a mean wind speed of 15 m/s (irrespectively of H_s and T_z) is 0.031.

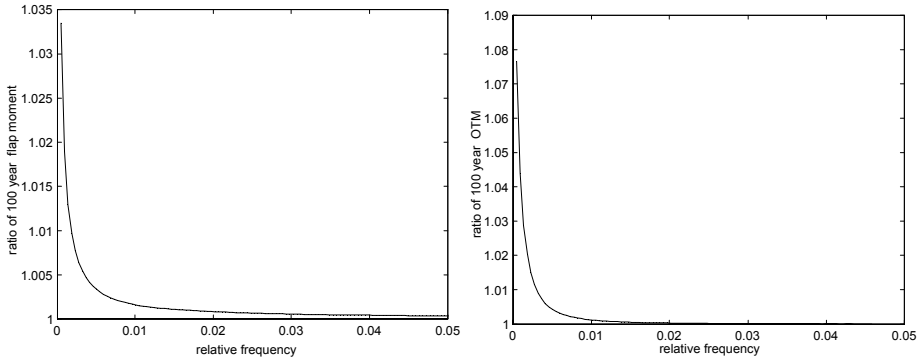

Figure 11.5: Influence of the relative occurrence frequency of the most severe sea state on the long-term estimate of the stall regulated wind turbine. (left: flap moment, right: OTM); the ratio is between the most severe sea state and all the sea states.

Needless to say, the distribution function itself has large influences on the estimate of the long-term response. In this case, the distribution functions have characteristic values (e.g. location factor) far away from each other. Thus, the dominance of one conditional distribution of the response can be such that the inclusion of other conditional distributions has no effect on the long-term distribution.

On the other hand, if the conditional distributions of the response are closer to each other, this may change the tail of the long-term distribution. Since the conditional distributions can only be known once they have been obtained through simulations or measurements, it is difficult to assess its influence. For this reason a fictitious sea state is added to the scatter diagram. The response distribution of the imaginary sea state is identical to that of the most severe sea state, only with a different location parameter. The relative occurrence frequency of this imaginary sea state is also taken as a variable.

Figure 11.6 shows the influence of this imaginary sea state on the estimate of the long-term response. It can be observed that if the conditional distributions are far away from each other (i.e., the location parameters of the distributions differ significantly), the presence of such sea state has basically no effect on the long-term distribution. However, if the distribution functions are close to each other, the influence of this fictitious sea state on the long-term distribution of the response becomes more significant. In the presence of such a fictitious sea state, using only the response distribution of the most severe sea state to determine the 100 year response will produce always an underestimate. This can be seen in Figure 11.6. Here, the location parameter varies from 70% to 90% of the location parameter of the distribution of the most severe sea state. With a location parameter that is 70% of the most severe one, there is basically no influence. With 90% the influence increases with the relative occurrence

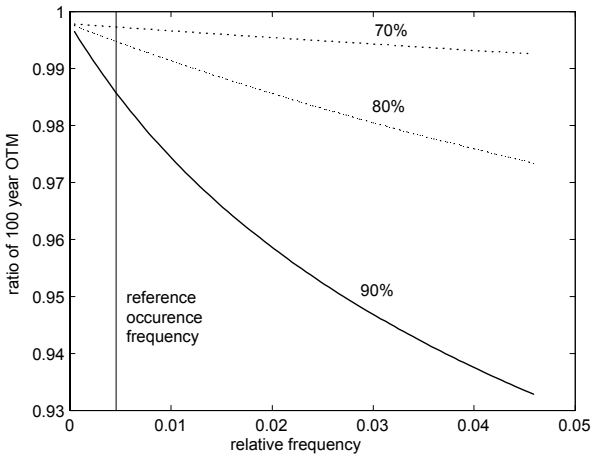

Figure 11.6: Influence of a fictitious response distribution whose location parameters have relative shifts to the location parameter of the overturning moment distribution of the most severe sea state; the ratio is between the most severe sea state and all the sea states.

frequency of the fictitious sea state. The reference occurrence frequency is the relative occurrence frequency of the most severe sea state.

It can be said that if there is only one dominating conditional distribution and the relative occurrence frequency of that sea state is not too low, then the long-term distribution of the extreme response can be determined with sufficient accuracy using the most severe sea state. However, to determine the most severe sea state, it is necessary to run simulations for all the sea states, although one can use the mean extreme response of the sea state as a representative measure for the severity of the sea state. As shown before, the mean of the maximum response can be determined with relatively few simulations, e.g. 5.

Chapter 12

Constrained simulation of extreme wind gust and wave

12.1 Introduction

In the previous chapters, the response based methods have been applied to obtain the extreme responses of a certain return period of an offshore wind turbine. However, the current design practice uses an external condition based approach. The external condition based approach determines the external condition of a given return period and determines the extreme response using that external condition.

One of the extreme load conditions is when an extreme gust reaches the wind turbine. On the other hand one can also expect that when an extreme wave hits the support structure, extreme responses can occur as well. These load cases have to be considered during the design process of the wind turbine. Current design codes, such as the IEC [53], describe the extreme gust in a deterministic way with a specified amplitude, shape and duration. The shape of the IEC gust resulted from analyses of the wind data. However, validation of the proposed gust shape with the theory was not present during the drafting of the code.

One of the objections to the deterministic gust shape is that it does not include the stochastic properties of the gusts. With constrained simulations, one can model the extreme wind gust with stochastic properties. The constrained simulation of the waves has been applied to offshore structures and the subject is treated in detail in [49]. For this reason the emphasis of this chapter is on the constrained wind gust. The main idea behind a constrained simulation is to impose a theoretically derived average form (e.g. an average gust shape) on a previously simulated signals (e.g. a stochastic wind field), so that a characteristic of the signals (in this case, a predetermined gust speed) can be obtained.

The pitch regulated turbine is used here. The flap moment at the blade root due to extreme gusts is studied using the constrained simulations. Different gust models and the influence of the gust centre on the blade response is investigated. The gust response is conditioned on the gust amplitude and the mean wind speed. The gust response distribution is determined using the conditional distribuitions of the gust response and the probability density distribution of the gust amplitude and of the mean wind speed.

The number of simulations that are required to achieve a reliable estimate of the conditional distribution of the gust response is also studied. The blade response obtained with the deterministic gust model is compared to the response obtained with constrained simulations.

The constrained simulations of the waves are applied to obtain the distribution of the overturning moment. In this case, no wind input is given. The response obtained using the constrained simulations is compared to the response obtained using the Stream functions.

Theoretically one can build the extreme response distribution based solely on the constrained simulations. However, the problem concerning the combination of constrained wind gusts and waves is not yet solved. The joint occurrence probability of the wind gust and extreme waves is not known. Moreover, it is necessary to carry out a large number of constrained simulations in order to obtain the conditional distributions of the response. Note that these distributions are conditioned on amplitudes (gust amplitudes, wave heights) as well as the mean wind speeds.

A promising application of the constrained simulation is to improve the current description of extreme wind gust and waves for response calculations. By carrying out a series of constrained simulations one can gain insight in the variation of the extreme responses. Given the fact that constrained simulations give a better description of the physical phenomena of the extreme wind gusts and extreme waves, it represents also a more realistic load description.

The combination of extreme wind gust and wave loading is explored with constrained simulations. The Turkstra's rule [64] is applied to combine the extreme gust and wave loadings. To investigate how the response varies if the maximum wind speed and the maximum wave height do not occur simultaneously, a time delay between the two maxima is introduced. The influence of the time delays on the extreme responses is studied.

12.2 Extreme gust response

12.2.1 General considerations

Although extreme gusts occur also in the conventional wind simulations, a long simulation length is usually required to obtain gusts of a large amplitude, because the probability of occurrence of such gusts is small. With the constrained simulation technique, it is possible to generate stochastic gusts with predefined amplitude, at a pre-selected location and point in time. The basic idea of con-

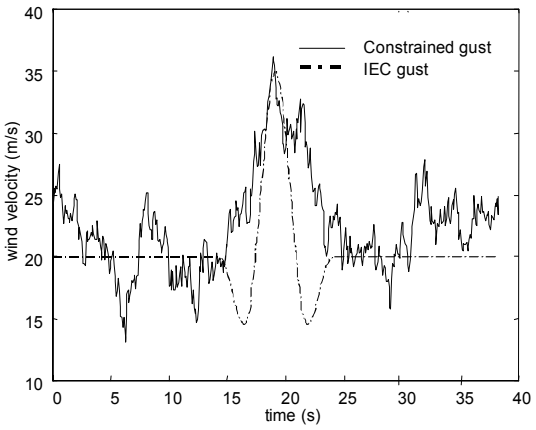

Figure 12.1: Stochastic and deterministic wind gusts, solid line is a constrained gust and the dash-dot line is the IEC gust.

strained simulations is to impose a theoretical gust shape on the (simulated) wind turbulence. This is done in such a way that the constrained gust is statistically equivalent to the gust of the same amplitude found in a long wind simulation.

Theoretically, the constraint should be applied to a three-dimensional turbulence wind field, given the fact that the 3D turbulence structure exerts an influence on the gust response. However, the emphasis here is on the methodology. For this reason only the horizontal along wind component of the wind speed is considered. A constrained gust is shown together with the IEC gust in Figure 12.1.

Two different gust models are compared, a uniform gust and a spatial gust. A uniform gust is stochastic in time but not in space. That means, the maximum wind speed is reached simultaneously over the whole rotor surface. A spatial gust has stochastic variations in space and in time. The spatial gust considers the cross correlation of the wind speeds at different locations.

One of the issues that arises from the application of the spatial gusts is the variation of the gust centre. The gust centre is a stochastic variable, whose distribution can not be determined without an extensive investigation. There is no clear indication how the gust centre is distributed in space. Hence a sensitivity study is carried out to quantify the variation of the blade responses due to changes in the gust centre.

The response resulting from a constrained simulation of the wind gust is different from simulations to simulations. Thus, using a certain number of simulations one can obtain the conditional distribution of the gust response. The conditional distributions of the gust response are fitted to different distribution models.

One of the questions raised when fitting the gust responses to a distribution

is the number of simulations required to obtain a reliable estimate of the distribution parameters. The spreading of the distribution parameters is studied with a bootstrap-like method [35]. This method consists of random drawing of gust responses that are obtained with constrained simulations. The randomly drawn responses are fitted to a 3 parameter Weibull distribution. The random drawing is performed many times to determine the variation of the distribution parameters. The confidence intervals of the parameter spreading are also determined.

To obtain the gust response distribution for a random mean wind speed, it is necessary to perform a convolution on the conditional distributions of the gust response with the PDF of the gust amplitudes and of the mean wind speeds.

12.2.2 Deterministic gust model

The IEC deterministic gust used for calculation of the extreme gust during operation is defined as

$$u(z,t) = \left\{ \begin{array}{cc} \bar{U}(z) - 0.37 u_{gustN} \cdot \sin(3\pi t/T)(1-\cos(2\pi t/T)) & 0 \leq t \leq T \\ u(z) = \bar{U}_{hub}\left(\frac{z}{z_{hub}}\right)^{\alpha} & 0 > t \text{ and } t > T \end{array} \right\} \tag{12.1}$$

The gust speed u_{gustN} is defined in terms of the standard deviation of the horizontal wind turbulence and a gust factor, which is related to a return period (see [53]). $\bar{U}(z)$ describes the height dependency of the mean wind speed, that is, the wind shear. It is described in Equation 3.4. The wind speed at the hub height is used as the reference value. One of the main purposes of the IEC gust is to determine the response of the wind turbine controller to a fast rising gust. It is not necessarily the most realistic representation of a wind gust.

12.2.3 Stochastic gust model

Recently efforts have been made to model extreme gusts that take into account the stochastic properties of the wind [9].

There are different definitions of a wind gust. In this thesis a gust is defined as a local maximum above a certain wind speed. 20 seconds are chosen as the duration of a wind gust[1], centred on the maximum wind speed. Note that different definitions of the gusts yield different statistics of the gusts. For example, one previous study of the wind gust statistics [19] defines a gust as the difference of two wind speeds at two different instances in time. The gust statistics obtained in this manner are fundamentally different than the gust statistics used in this work [8].

The shape of the averaged gust has been verified with wind measurements. Figure 12.2 shows the verification of the mean shape of the gust with measure-

[1] One can chose a longer gust duration but the constrained wind gust far from the time point of the constraint, t_0, will resemble that of the stochastic background.

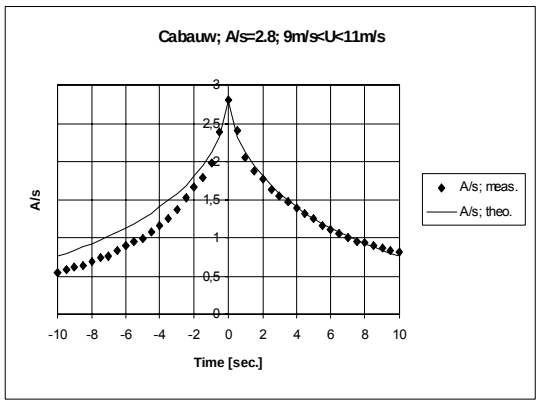

Figure 12.2: Measured (anemometer) and predicted average gust shapes based on 1335 gust observations corresponding to 10-minute mean wind speeds restricted to the range from 9 m/s to 11 m/s.

ments from wind database [89]. The PDF of the gust amplitude[2] is depicted in Figure 12.3. Both the shape and the statistics of the gust show a good agreement with the theoretical predictions. In few cases a smaller negative gust that precedes a larger positive gust (as specified in the IEC code) can be observed in the measurements. However, the amplitudes of the negative gusts are usually less than 10% of the positive gust.

For a single point in space the constrained wind signals are [9]

$$u_{cr}(t) = u(t) + R(t-t_0)(A - u(t_0)) + \frac{\dot{R}(t-t_0)\dot{u}(t)}{\dot{R}(t_0)} \tag{12.2}$$

$u(t)$ is the original wind signal, $R(t)$ is the auto correlation function, and A is the prescribed gust amplitude. t_0 is an arbitrarily chosen time point, where the prescribed gust amplitude occurs and t is simply the time. The influence of the term with the time derivative of the auto correlation function is neglected. This term ensures that the constrained gust is a local maximum with a slope of 0 at the time of the constraint. Theoretically, this term is close to a delta function and contributes only to the constrained gust amplitude at the time point t_0. Thus, the Equation used for the contrained wind gust is reduced to

$$u_{cr}(t) = u(t) + R(t-t_0)(A - u(t_0)) \tag{12.3}$$

As can be seen from Figure 12.1 the shape of the constrained gust resembles the auto correlation function in the neighborhood of the constrained point. As the gust amplitude A increases, the term with the auto correlation function in

[2] The negative gust level is because there are local maxima which are below the mean wind speed.

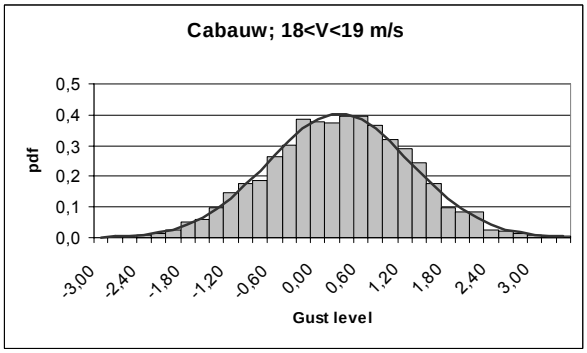

Figure 12.3: Measured and theoretical PDF of the gust amplitudes.

Equation 12.2 dominates and the effect of the second term can be neglected. With the decay of the auto correlation function, the constrained wind signals distant from the constraint point approach the original wind signals.

To create a constrained gust in time and space it is necessary to consider the cross correlation function and the time derivative of the cross correlation function, together they determine the 'deterministic' part of the spatial gust. The formulation is identical to Equation 12.2, by replacing the uniform formulation of the wind and correlation function with the spatial formulation of the wind and the cross correlation function. The deterministic part of a spatial gust is illustrated in Figure 12.4. In Figure 12.5 a spatial gust is shown for the time point when the maximum gust speed at the gust centre is reached. As it can be seen the gust dimension is considerably large, which could imply that the shift of the gust centre would have limited effects on the gust response.

12.2.4 Gust response variations due to different gust models

Uniform and deterministic gust responses

The responses of the blade to a deterministic and a stochastic (uniform) gust is illustrated in Figure 12.6. The response shown is the bending moment in the flap direction at the blade root. The pitch regulated wind turbine is used. The mean wind speeds are 13 m/s and 14 m/s. The controller is active after the rated mean wind speed (13.7 m/s) is reached. The gust amplitude is 10 m/s above the mean wind speed for both cases.

At a mean wind speed of 13 m/s, the stochastic gust noticeably contributes to the dynamic excitation of the wind turbine, producing higher mean response of the blade than the deterministic gust. The rotational effect can be seen in the flap moment of the deterministic gust, because of the constant wind speed assumed outside the gust duration T. The response peak occurs nearly

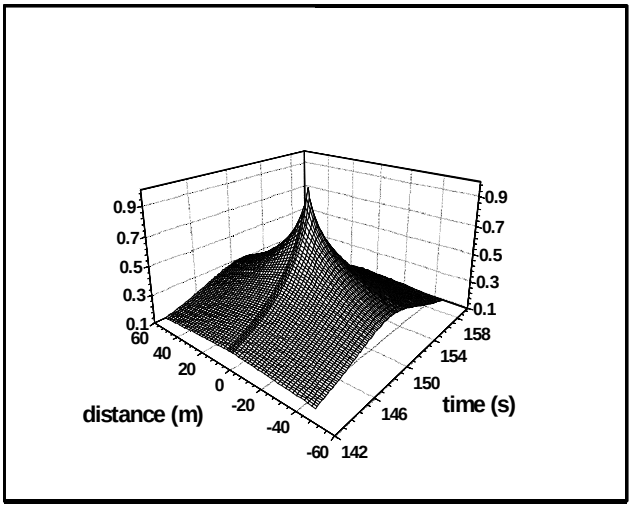

Figure 12.4: Spatial gust (deterministic part).

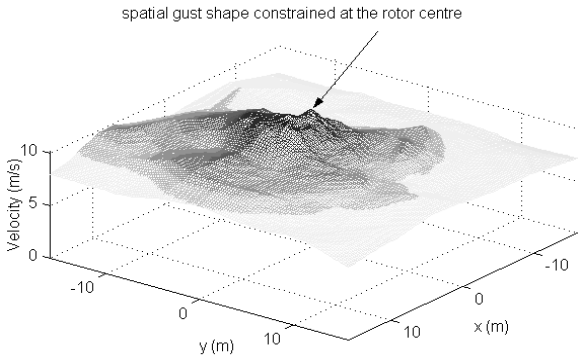

Figure 12.5: Constrained spatial gust

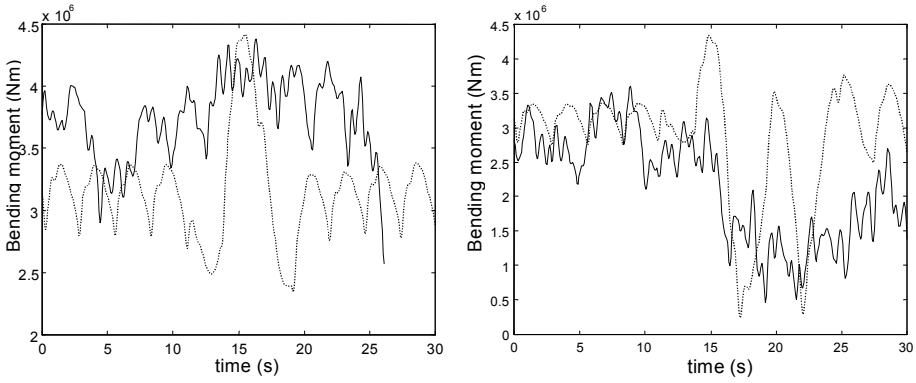

Figure 12.6: Flap moment at the blade root of the pitch regulated wind turbine at mean wind speeds of 13 m/s (left) and 14 m/s (right). Solid line is from constrained simulation and dashed line is from the IEC gust.

simultaneously with the gust peak in case of the deterministic gust. For the stochastic gust, the peak response occurs in the neighbourhood of the contraint. The maximum of the flap moment is similar for both gust models.

At a mean wind speed of 14 m/s, the response differs considerably. The activation of the controller leads to a reduction of the maximum blade response using the stochastic gust. As shown in Figure 12.6 (right), the controller is able to 'filter' the gust excitation. In this case, the gust does not effectively contribute to the increase of the blade response. In contrast, the deterministic gust produces a much higher blade response than the stochastic gust and the effect of the gust peak on the response can be clearly seen. The role of the controller is crucial, since it is unable to react to the IEC gust. For pitch regulated wind turbines, the IEC gust will produce a higher estimate of the peak flap moment. However, the controller is an integrated part of a wind turbine and the influence it exerts on the turbine response differs from turbine to turbine. It is not possible to determine quantitatively the influence of the controller from the study of a single controller.

The mean response of the flap moment increases with the gust amplitude for mean wind speeds below the rated wind speed. The standard deviation increases sharply for large gust amplitudes. The absolute wind speed difference that the wind turbine experiences (i.e. the difference between the maximum wind speed and the minimum wind speed in the neighbourhood of the constraint) differs from simulation to simulation because of the stochastic wind signals. This leads to a large spreading of the extreme flap moment even with the same constraint for all the simulations, namely the same maximum wind speed.

When the wind turbine operates with an active controller the mean and standard deviation of the peak flap moment remain approximately constant, due to the 'filtering' of gust loads by the controller. The variation of the peak

Table 12.1: Peak bending moment with the IEC gust and the mean value of the constrained simulations (mean wind speed = 13 m/s)

Gust amplitude above mean	**IEC gust (10^6Nm)**	**mean (10^6Nm)**
8 m/s	4.60	4.66
10 m/s	4.76	4.79
13 m/s	4.91	5.62
15 m/s	5.17	6.67

flap moment is limited within the 10% of the mean response [21].

In Table 12.1 the maximum of the flap moment at the blade root produced by deterministic gusts are listed together with the mean flap moment produced by constrained gusts of the same gust amplitude. For each amplitude 30 constrained simulations are carried out. The mean wind speed is 13 m/s.

For small amplitudes, the means of maximum flap moment are quite close to the peak flap moment of the deterministic gusts. The difference increases with increasing gust amplitudes. The stochastic gusts seem to produce higher responses.

In many cases, a local maximum near the time point of constraint is observed in the original wind signal. The superposition with the mean gust shape will shift this local maxima upwards. Thus, besides the principal gust peak defined by the constraint, there is another local maximum preceding it. This often leads to a higher gust response.

It can be seen that the deterministic gusts yield a lower estimate than the mean of the maximum flap moments using contrained simulations. However, it has to be noticed that the higher gust amplitudes given here have very low exceedence probability, which can be as much as 9 standard deviations away from the mean wind speed, given a turbulence intensity of 12%.

Above the rated wind speed, the IEC gust consistently delivers a higher estimate of the peak flap moment than the contrained gusts. Table 12.2 shows the maximum flap moment of the blade, with IEC deterministic gusts and the mean value of the maximum flap moments with uniform constrained gusts. The mean wind speed is 20 m/s. As mentioned before, the controller was not able to react to the IEC gust, thus, unable to reduce the blade response. The characteristic of this particular controller plays a crucial role in determining the peak response.

Uniform and spatial gust response

The uniform gust refers to a gust that is uniform across the rotor area (wind shear effect is included). However, a real wind gust has spatial variation as well. One can expect that these two gust models will produce different responses.

The difference in the blade response due to spatial gusts and uniform gusts is studied. The gust response increases monotonously with the gust amplitude.

Table 12.2: Maximum flap moment with the IEC gust and the mean value of the maximum flap moment with constrained gusts (mean wind speed = 20 m/s)

Gust amplitude above mean	**IEC (10^6Nm)**	**mean (10^6Nm)**
8 m/s	4.42	3.55
10 m/s	4.18	3.41
13 m/s	4.69	3.45
15 m/s	4.87	3.29

The uniform gust produces a consistently higher estimate of the peak response of the blade than the spatial gust. This can be attributed to the fact that the maximum gust speed occurs simultaneously at all locations in case of a uniform gust. The uniform gust produces an estimate of the peak blade responses that deviate at most 10% from the peak responses obtained by spatial gusts. Another consequence of using uniform gusts is that a uniform gust produces a much higher thrust to the tower due to the coherence of the gust. The tower thrust has an important contribution to the overturning moment of the support structure, hence the overturning moment is higher in case of a uniform gust. In the following sections, only the spatial gust is used in the constrained simulations.

Variation of the gust centre

In the previous calculations the gust centre is fixed in the middle of the rotor although the location of the gust centre is random. To study the influence of the gust centre on the blade response, gusts with different gust centres are constructed and the blade responses are determined. Two different mean wind speeds are selected, 13 m/s and 14 m/s. The gust amplitude is 7 m/s above the mean wind speed. The gust centres are positioned in five different blade locations for twelve azimuth angles. For each blade location 10 simulations have been carried out. The pitch regulated wind turbine is used.

Figure 12.7 shows the mean value of the maximum flap moment for mean wind speeds of 13 m/s (upper) and 14 m/s (lower) respectively at 3 different blade locations and 12 different radial positions. The blade locations are normalised with respect to the rotor radius R. The response is normalized to the maximum response calculated for the respective mean wind speed. The radius of the circle represents the normalised response ratio, varying from 0 to 1. However, the figures for mean wind speeds of 13 m/s and 14 m/s are not directly comparable because the maximum gust response of these two mean wind speeds differ considerably.

At 13 m/s the variation of the mean of the maximum responses can be quite considerable but the variation does not have a definite pattern, except that the maximum gust response is registered in the upper region of the rotor swept area. Even with a radial position of 0.035 (very close to the hub) the variation

of the response is still quite considerable. The maximum variation between the maximum gust responses is within the boundary of 25% of the maximum response registered for the mean wind speed of 13 m/s.

For 14 m/s the variation of the gust center has also impacts on the gust response. The activation of the controller reduces the gust response and the variation of the gust response is also reduced. The difference between the maximum and minimum of the mean of the maximum gust response for different gust centers is reduced to about 15 %. For a given azimuth position the variation of the gust response among different radial positions is, in general, also decreased compared to the same situation for the mean wind speed of 13 m/s.

The gust centre has definitely influence on the extreme flap moment. However, from the calculations performed here it can not be concluded that there is a correlation between the location of the gust centre and the increase of the maximum flap moment. Although, with 10 simulations, the stochastic variation among the simulations can be significant, but on the other hand the maximum variation of the peak response is not large (maximum 25%). This is partly due to the dimension of the gust, which is large compared to the dimension of the rotor. The present knowledge of the spatial gust does not allow a reliable treatment of the gust centre as a stochastic variable. For this reason, the gust centre is placed in the middle of the rotor in the following calculations.

12.2.5 Gust response distribution

The gust responses obtained by constrained simulations will be fitted to distribution models. The wind turbulence is generated using the wind field generator SWING4 [6], but the method can be adapted to any conventional wind field generator. The hub is chosen as the gust centre. The pitch regulated wind turbine is used and the turbulence intensity is 0.12. The 3 parameter Weibull distribution is used to fit 50 maxima of the flap moment from 50 constrained simulations.

To obtain the distribution of extreme gust response, it is necessary to determine the conditional distributions of the gust response for a given gust amplitude and a mean wind speed. Theoretically, the conditional distribution of the gust response needs to be determined for every mean wind speed. However, those mean wind speeds that do not deliver large gust responses, have insignificant contributions to the upper tail of the distribution. The reason is that when the distribution is extrapolated to a longer period using Equation 12.5, the tail of the distribution is determined by the conditional distributions of those wind speeds that produce large blade responses.

The extreme gust responses of the pitch regulated turbine are concentrated around the rated wind speed [23]. Four mean wind speeds, from 13 to 16 m/s, are chosen and the blade response to the stochastic gusts are studied for five different gust amplitudes, $1.5\ \sigma - 5.5\ \sigma$.,where σ is the standard deviation of the wind turbulence.

The statistical moments of the maximum gust responses from 50 constrained simulations are shown in Tables 12.3 and 12.4 for the mean wind speeds 13 and

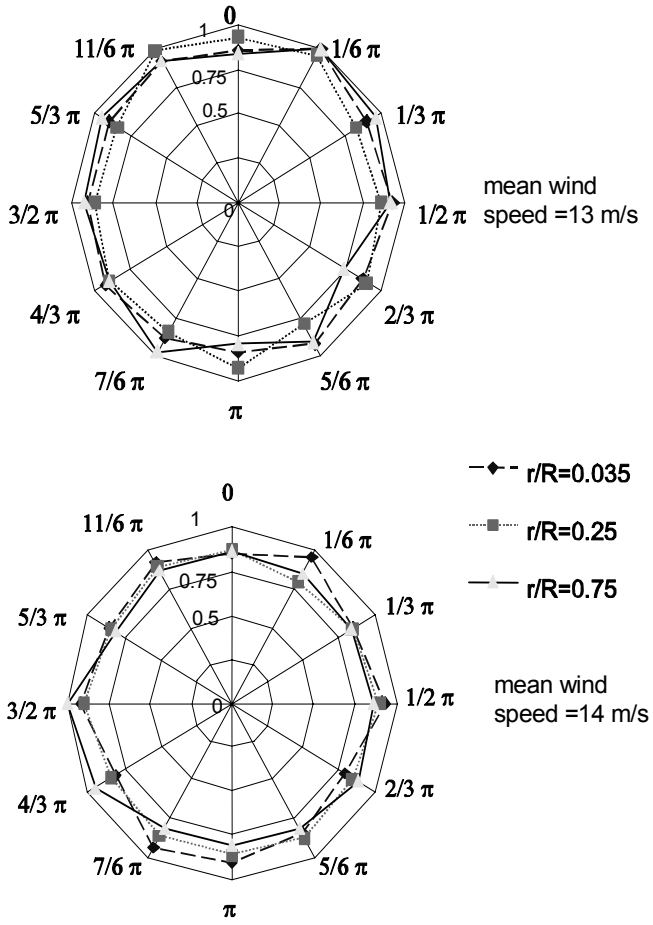

Figure 12.7: Mean peak moment for different locations of the gust center left:14m/s right:13m/s.

Table 12.3: Statistical moments of 50 maxima of the constrained gust responses of the pitch regulated wind turbine; for different gust amplitudes at a mean wind speed of 13m/s.

Gust amplitude above mean	**mean (10^6Nm)**	**standard dev. (10^6Nm)**	**skewness**
1.5 σ	4.02	0.127	0.31
2.5 σ	4.10	0.131	0.77
3.5 σ	4.24	0.121	-0.02
4.5 σ	4.39	0.120	-0.18
5.5 σ	4.49	0.085	0.62

Table 12.4: Statistical moments of 50 maxima of the constrained gust responses of the pitch regulated wind turbine; for different gust amplitudes at a mean wind speed of 14m/s.

Gust amplitude above mean	**mean (10^6Nm)**	**standard dev. (10^6Nm)**	**skewness**
1.5 σ	3.67	0.087	0.81
2.5 σ	3.66	0.085	0.98
3.5 σ	3.69	0.082	0.21
4.5 σ	3.63	0.118	-1.46
5.5 σ	3.64	0.087	0.82

14 m/s, respectively. The average of 50 maximum gust responses increases monotonously with the gust amplitude at a mean wind speed of 13 m/s. At this mean wind speed, the controller is not active; thus, increases in the wind speed are translated into increases of the blade response. However, the standard deviation of the gust response decreases slightly with the gust amplitude. This can be attributed to the fact that the gust amplitude dictates the extreme gust response at large gust amplitudes. Thus, the maximum gust response has a smaller spreading. At smaller gust amplitudes, the turbulent background can have considerable influence on the gust response. The distribution parameters of the maximum gust responses are shown in Table 12.5. As can be seen, the location parameter increases with the gust amplitude, which reflects the increase of the maximum gust response with the gust amplitude. It can be observed also that large values of the scale parameter are paired with large values of the shape parameter.

The response characteristics are very different at the mean wind speed of 14 m/s. The response is practically independent of the gust amplitude because the gust load is virtually filtered by the blade pitch controller. For the mean wind speeds 15 m/s and 16 m/s (not shown), the responses are lower, hence the contribution of these two wind mean speeds to the tail of the gust response distribution is limited.

At 14 m/s with a gust amplitude of 4.5 σ, the simulated gust response has

Table 12.5: The Weibull distribution parameters of the gust response distribution for different gust amplitudes at a mean wind speed of 13m/s; for the pitch regulated wind turbine.

Gust amplitude above mean	location parameter u ($\mathbf{10}^6$Nm)	scale parameter s ($\mathbf{10}^6$Nm)	shape k
1.5 σ	3.68	0.38	2.64
2.5 σ	3.91	0.20	1.38
3.5 σ	4.03	0.25	2.02
4.5 σ	4.09	0.33	2.66
5.5 σ	4.37	0.13	1.41

Table 12.6: Weibull distribution parameters of the gust response distribution for different gust amplitudes at a mean wind speed of 14m/s; for the pitch regulated wind turbine.

Gust amplitude above mean	location parameter u ($\mathbf{10}^6$Nm)	scale parameter s ($\mathbf{10}^6$Nm)	shape k
1.5 σ	3.54	0.15	1.41
2.5 σ	3.54	0.12	1.18
3.5 σ	3.55	0.16	1.81
4.5 σ	2.99	0.68	8.46
5.5 σ	3.52	0.13	1.28

a negative skewness and the distribution parameters deviate significantly from the rest. It is possible that the stochastic gusts have la arger rise time and the controller was able to limit the gust response or, it may be that these deviations are simply due to the presence of some outliers in the simulation result. However, a closer inspection of the data does not reveal any anomaly. This deviation of the distribution parameters, however, does not affect the tail of the distribution. Table 12.6 shows the distribution parameters of the 3 parameter Weibull distribution for the gust response of 14 m/s. The distribution parameters of the gust amplitude of 4.5 σ differ significantly from the others, with a large scale parameter and a large shape parameter.

The goodness of fit test was carried out for the fitted distributions. The Kolmogorov-Smirnov test is used with a significance level of 5%. The Weibull fits are shown in Figure 12.8 and Figure 12.9 for mean wind speeds of 13 m/s and 14 m/s, respectively. The upper tail of the extreme gust response distributions for 14 m/s is fairly independent of the gust amplitudes. This can be attributed to the influence of the pitch controller. Although the lower tail of the distributions does differ for different gust amplitudes. This is associated with the difficulty of identifying the extreme response caused by the extreme gust because not all the stochastic gusts manifest themselves in the response. The controller can suppress the gust load, hence the maximum response is not always a direct product of the extreme gust.

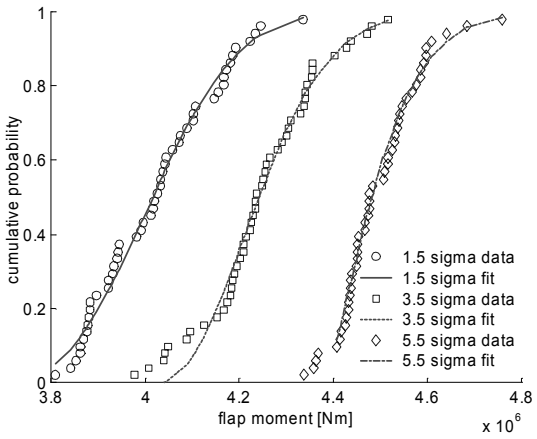

Figure 12.8: Weibull fit of the conditional distributions of the gust response for different gust amplitudes at a mean wind speed of 13 m/s.

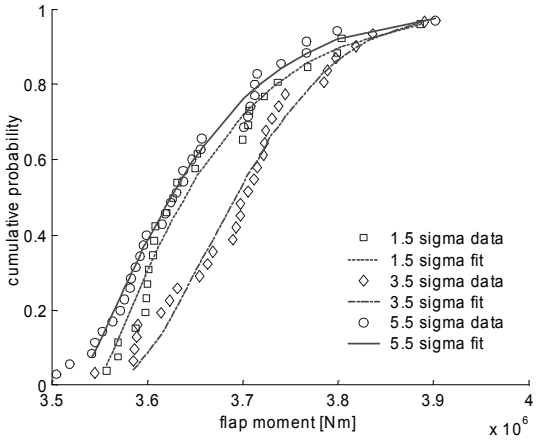

Figure 12.9: Weibull fit of the conditional distributions of the gust response for different gust amplitudes at a mean wind speed of 14 m/s.

Once the conditional distributions of the gust response for different gust amplitudes are established, the gust response for a given mean wind speed can be determined [49] according to the Equation 12.4, given the distribution of the gust amplitude $f_v(\sigma)$:

$$F_m(M) = \int F_m(M)|_\sigma \cdot f_v(\sigma) d\sigma \tag{12.4}$$

Here, F_m is the cumulative probability function of the peak flap moment and f_v is the probability density function of the gust amplitude in terms of the standard deviation σ and $F_m|_\sigma$ is the distribution of the peak flap moment conditioned on σ.

Assuming that a gust represents a positive local maximum, the theoretical distribution can be derived for a Normal process [17]. The local maxima of a Gaussian process follow the Rice distribution (see Equation 10.3); the Rice distribution depends on the spectral bandwidth of the process. In the limiting cases of a narrow and a wide band process, the distribution of the local maxima is the Rayleigh and the Normal distribution, respectively. The wind turbulence can be considered as a wide band process, with a spectral bandwidth parameter close to 1. Hence, the Normal distribution can be used to describe the distribution of the gust amplitude, in case an empirical distribution from measurements is not available.

In theory, the distribution of the gust amplitude is a continuous function. However, the simulation can deliver only conditional distributions for discrete gust amplitudes. Therefore, as a simplification, Equation12.4 is discretised for 5 amplitudes and the resulting distribution is the sum of the conditional distributions weighted with the occurrence probability of the gust amplitude range. One can also interpolate the distribution parameters to achieve a continuous description of the conditional distributions of the gust response, such as shown in the extrapolation of the joint probability of the sea state parameters (see Figure 3.3 and 3.4). However, a simple interpolation can not be used here because of the parameter correlation, which can yield meaningless parameter combinations (see for example the distribution parameters for 4.5 σ in Table 12.6).

Equation 12.4 represents the gust response distribution to a single gust. To predict the maximum gust response within a stationary period of 10 minutes, it is necessary to determine how many independent gusts can be expected. The estimate of gust number with the mean upcrossing frequency results in a large number of gusts. Furthermore, by assuming that all the gusts are independent, it will yield a conservative estimate of the gust response.

For this study, a practical measure following reference [4] is taken. It is assumed that in the interval, in which the normalised auto correlation function is higher than 0.5, only one independent gust exists. The maximum number of independent gusts can be calculated from this interval length. For the present purpose this practical measure of the correlation length is sufficient, given the presence of other uncertainties. Moreover, the influence of the number of independent gusts on the tail of the distribution becomes less significant when the distribution is extrapolated to a period T.

The distribution of the largest gust response in the 10-minute period can be extrapolated given the number of gusts N_{10}. The largest gust response distribution for the 10-minute period can be written as

$$F_{10}(M) = F_m(M)^{N_{10}} \tag{12.5}$$

$F_{10}(M)$ is the cumulative distribution of peak flap moment for a 10-minute period (a function of the mean wind speed) and $F_m(M)$ is the cumulative distribution of the peak flap moment for a single gust (the cumulative probability function obtained in Equation 12.4).

The distribution of the gust response during operation can be obtained by integrating the conditional distributions of the gust response between the cut-in and cut-out mean wind speeds.

$$F(M) = \int_{V_{cut-in}}^{V_{cut-out}} F_{10}(M)|_{\bar{U}_{10}} \cdot f(\bar{U}_{10}) d\bar{U}_{10} \tag{12.6}$$

$F_{10}(M)|_{\bar{U}_{10}}$ is the conditional distribution of the peak flap moment obtained in Equation 12.5 and $f(\bar{U}_{10})$ is the probability density function of the mean wind speed, usually a two parameter Weibull probability density function. In this case, only the mean wind speeds between 13 m/s and 16 m/s are considered because the other mean wind speeds do not contribute significantly to the upper tails of the distribution.

The distribution obtained with Equation 12.6 represents the response distribution for a random stationary period of 10 minutes. It can be extrapolated to distributions which represent the largest gust response in a period of 1 year, 20 years or 50 years etc. Following the same principle as described in Equation 12.5, the number of gusts N_{10} is replaced by the number of independent stationary periods. In this case, it is the number of stationary periods (of 10 minutes length) of the considered mean wind speeds. The extrapolated distributions are shown in Figure 12.10.

12.2.6 Number of constrained simulations

The gust response distribution was obtained with a limited number of simulations. Before the return periods of the gust response can be determined, it is necessary to consider the variation of the distribution parameters due to the limited number of simulations, since it will affect the estimate of the return period of the extreme gust response

The methodology used here is similar to the methodology employed to determine the required number of simulations for the MAX method. 500 constrained simulations with the mean wind speed of 13 m/s are carried out. The simulation length is 76 seconds and the gust amplitude is 3 σ. From the 500 simulations 500 maxima of the gust response are obtained. N random maxima are drawn each time. The set of random maxima is fitted to a 3 parameter Weibull distribution. This process is repeated 100 times with different N.

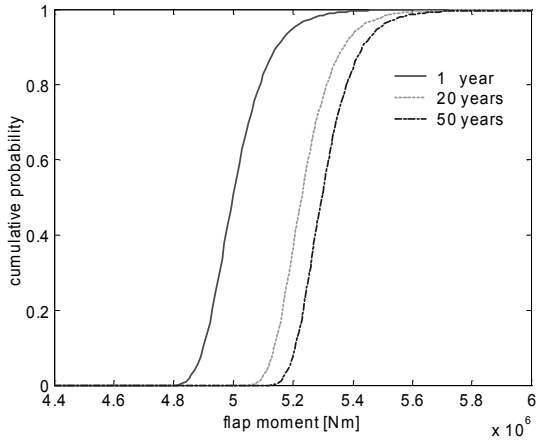

Figure 12.10: Long-term distribution of the gust response distribution function for different periods.

The variations of the distribution parameters u, s and k are presented in Figures 12.11 to 12.14. The distribution parameters obtained from the fitting of the 500 maxima are used to normalise the values (on the y axis). The 99 percentile of the distribution obtained with the reference distribution parameters is used to normalise Figure 12.14.

The upper boundary of the location parameter u is very close to the reference value using 500 simulations. Practically, it does not change with the number of simulations because the location parameter determines the left end point of the distribution and it can not be much larger than the minmum gust response in the data, while it can be much smaller than the minimum gust response. As can be seen, the lower boundary of the location parameter is subject to a larger fluctuation.

The scale parameter s and the shape parameter k have a fluctuating upper boundary. The variation of these two parameters with the number of simulations is quite similar. This can be attributed to the correlation between the two distribution parameters (see also Figure 8.12).

However, the predicted 99 percentiles of the distribution parameters have a much smaller variation. Since these are the values that are relevant for the extrapolation of the long-term extreme response, it can be said that the predicted 99 percentiles can be used as a criterion to choose the required number of simulations. The 99 percentile of the distribution is shown in Figure 12.14.

From Figure 12.14 it can be seen that the 99 percentile of the distribution converges rapidly util it reaches 100 simulations. From there the increase of the number of simulations contributes marginally to an estimate closer to the reference value (from 500 simulations). With 50 simulations, the spreading of the 99 percentiles is about plus and minus 5% from the reference value.

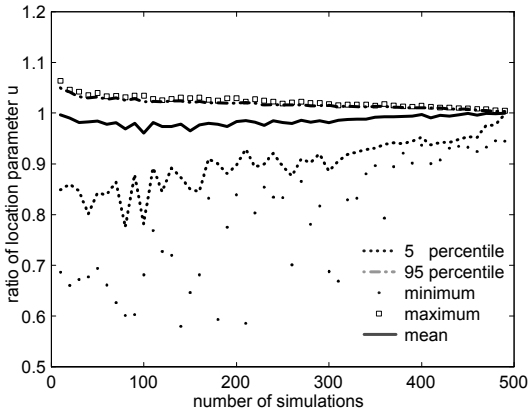

Figure 12.11: Variation of the location parameter u of the Weibull distribution of the maximum gust response (flap moment) for different numbers of simulations.

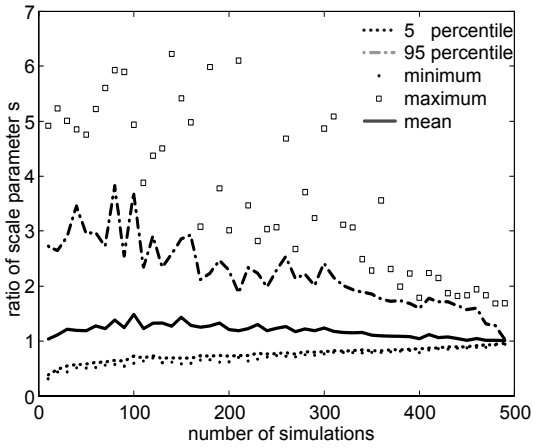

Figure 12.12: Variation of the scale parameter s of the Weibull distribution of the maximum gust response (flap moment) for different numbers of simulations.

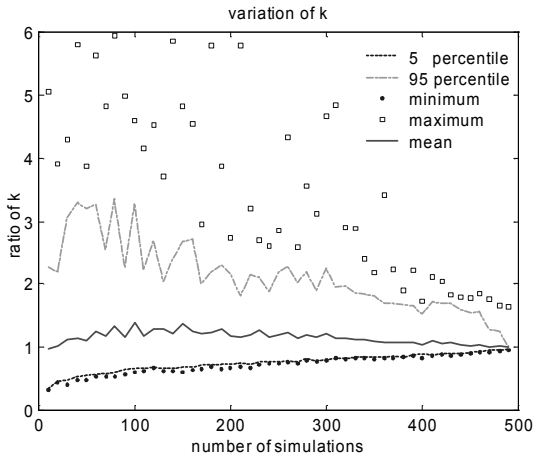

Figure 12.13: Variation of the shape parameter k of the Weibull distribution of the maximum gust response (flap moment) for different numbers of simulations.

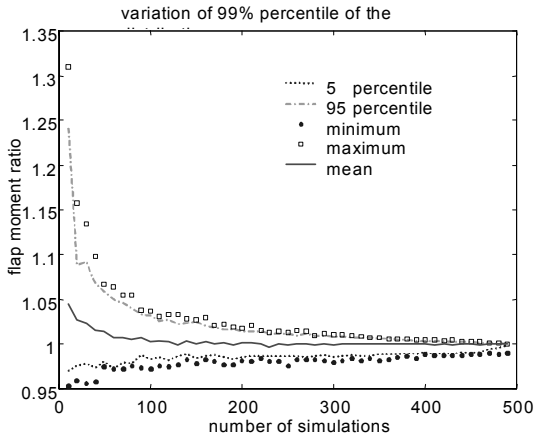

Figure 12.14: Variation of the 99 percentiles of the Weibull distribution of the maximum gust response (flap moment) for different simulation numbers.

Table 12.7: Variation of the distribution parameters from 100 bootstraps (mean wind speed 13 m/s)

Gust amplitude in σ	**mean μ (10^6Nm)**	**stand. dev. σ (10^6Nm)**	**skewness**
u	3.79	0.21	-2.09
s	0.43	0.21	2.06
$k*$	3.66	1.67	1.97
99 percentile of the flap moment distribution	4.59	0.03	0.10

* the unit does not apply for k

Furthermore, with a smaller number of simulations, the prediction of extremes tends to be above the reference value. Even with only 10 simulations the lower limit of the 99 percentile is merely 5% from the reference value. From the study of the parameter variation with the number of simulations, it can be concluded that 50-100 simulations would suffice for a reliable estimate of the gust response distribution.

The conclusion drawn above was based on the assumption that 500 simulations are representative for the gust response, it is necessary to investigate the variation of the distribution parameters given 500 simulations. The traditional bootstrap method with replacement is used to generate artificial results. The bootstrap has been done 1000 times. The variation of the distribution parameters are given in Table 12.7

The variation of the location parameter u is limited and negatively skewed because the upper limit of the location parameter is more or less determined by the minimum gust response in the data. The scale and shape parameter have larger variations. However, the 99 percentiles have a rather small variation. This effect was already illustrated previously by the correlation of these two distribution parameters. If the 99 percentile of the flap moment is normalised with the mean value of the 99 percentile estimates from the 1000 bootstraps, then it can be seen that the two standard deviation is about plus or minus one percent. It can be said that the variation of the 99 percentiles given 500 simulations is not significant.

12.2.7 Choice of distribution functions

To determine the gust response of a longer return period one needs to extrapolate the gust response distribution. The extrapolation depends on the distribution model used. Three different distribution models are used to determine to which extent the choice of distribution models can affect the prediction of the extreme response of long return periods.

The three distribution functions are, the 3 parameter Weibull, Gumbel and Rayleigh distribution. The 3 parameter Weibull is chosen due to the versatility

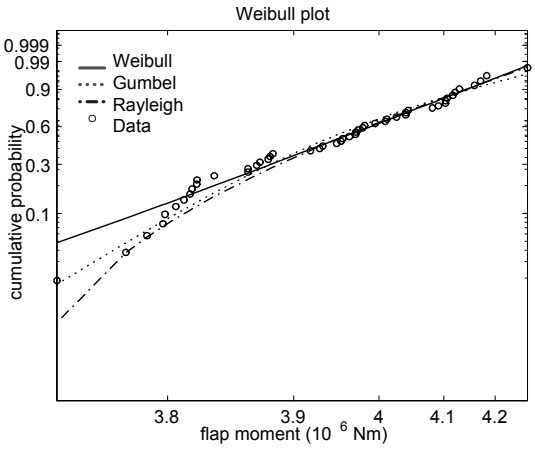

Figure 12.15: Distribution of the gust response fitted with different distribution functions conditioned on the gust amplitude of 1.5σ and mean wind speed of 13 m/s. (Weibull scale)

it has shown in the fitting of response maxima in the MAX method. The Gumbel distribution is a commonly used distribution to model extremes and theoretically, the Rayleigh distribution is included in the Weibull distribution, however, the constraint of the shape parameter gives a different fit than the Weibull distribution. The K-S goodness of fit test does not reject the Rayleigh fit.

Figure 12.15 shows the fit of the gust response to different distribution functions; the gust amplitude is 1.5 σ and the mean wind speed is 13 m/s. All the three distribution functions pass the K-S goodness of fit. The test is only applied to the upper tail, which is the region of interest, although the deviation in the lower tail can be quite significant. Nevertheless, all the three distributions model the upper tail reasonably well.

Figure 12.16 shows the conditional distribution of the gust response obtained from Equation 12.4 with a mean wind speed of 13 m/s.

The difference in the estimates of the 99 percentile can be considerable depending on the choice of the distribution model. The Weibull and the Rayleigh distributions give a very similar estimate. Obviously, the small difference is because the Rayleigh distribution is closely related to the Weibull distribution. However, in the lower exceedence probability region (upper tail)of the response, the Weibull distribution has a heavier tail than the Rayleigh distribution.

The highest estimate of the 99 percentile comes from the Gumbel distribution. The extrapolation carried out in Equation 12.5 amplifies the difference in the tail regions of the different distribution functions (see Figure 12.16). Numerically, the 99 percentile of the Gumbel fit is approximately 10% higher than the Weibull fit.

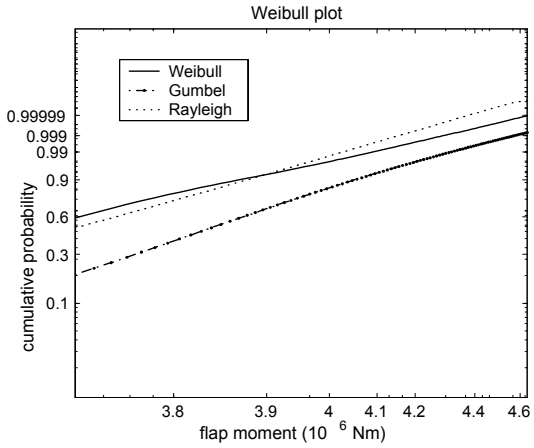

Figure 12.16: Distribution of the gust response fitted with different distribution functions conditioned on mean wind speed of 13 m/s. (Weibull scale)

To obtain a better fit of the tail of the distributions, one can use only gust responses above a certain threshold. However, that will cause the uncertainty of the estimated parameter to increase due to the fact that fewer data are available. In the present analysis, the difference of the 99 percentile of the gust response using the different distributions is within a limit of 10 percent. The three parameter Weibull distribution is a reasonable choice for the present purpose, since it offers more flexibility than the Rayleigh and Gumbel distributions. The uncertainty of the distribution choice can be taken into account by applying a Bayesian analysis, described in Section 8.3.

12.3 Extreme wave response distribution

12.3.1 Deterministic models of extreme wave

The current design of OWT uses deterministic wave models to model the extreme wave loads. There are several non-linear wave models that can be used to calculate the structural response due to extreme waves. A commonly used one is the Stokes wave. It incorporates higher order waves in order to satisfy the non-linear boundary conditions. The inclusion of the higher order waves leads to an asymmetrical wave profile. The crest becomes larger than the trough. The wave forces of non-linear waves are higher than the wave forces of the linear wave theory, partly because of the higher particle velocity predicted by the non-linear wave theory. Stokes waves are suitable for description of ocean waves in deep waters or in waters of a intermediate depth. In the near future, it is very likely that most of the OWT's will be situated in shallow waters. For this reason, Stokes waves do not describe appropriately the kinematics for extreme

wave forces in shallow water regions.

In the simulation code DUWECS[102], the stream function is implemented. the non-linear wave from Stream functions are more suitable for describing waves in shallow waters. The basic thought behind the stream functions is to use wave functions of higher orders to fulfil the non-linear boundary conditions. The coefficients of the stream function are chosen such that the errors in the non-linear boundary conditions are minimised. As with the deterministic gust model, the disadvantage of the deterministic waves is that it does not take into account the stochastic properties of the waves.

The non-linear waves yield higher wave loads than the linear waves. In a stochastic environment, there are non-linear phenomena that can yield extreme structural responses, for example the breaking waves. Breaking waves are a stochastic phenomenon that still needs further investigations, especially in the region of shallow waters. For the moment being, the influence of the breaking waves on the distribution of the extreme response is excluded.

Figure 12.17 shows the response of a monopile to an extreme wave using 10^{th} order Stream functions. The turbine used here is the stall regulated wind turbine. The natural period of the support structure can be found in Appendix C. No aerodynamic loading is present. The wave height in the simulation represents the extreme wave height of a return period of 50 years specified in the Opti-OWECS study(12.8 m). The wave period corresponding to this wave height is 9.5 s. It can be seen that the Stream function does not produce a sinusoidal wave and the fundametal frequency of the monopile can be observed clearly in the response time series of the monopile.

12.3.2 Stochastic model of extreme waves

From statistical studies, it has been shown that the expected shape in the neighbourhood of a local maximum of a Gaussian process can be described analytically. This has been applied to the ocean waves. Considering an extreme wave as a local maximum, the average shape of an extreme wave in a random Gaussian sea can be expressed analytically in terms of the auto correlation function. This leads to the formulation of New Wave [87], which can be used as a design wave. Embedding the New Wave in a random wave field, one can produce a constrained wave of predefined crest height. This constrained wave represents an extreme wave with stochastic properties, which is, statistically speaking, indistinguishable from an extreme wave obtained from a long simulation of random waves.

How does the response of the support structure to constrained waves compare to the response from deterministic non-linear waves ? To answer this question, a number of simulations with constrained waves has been carried out. In each constrained wave simulation the maximum crest height at the time point of contraint is specified. In contrast, the Stream function uses the maximum wave height as an input parameter. Using the 50 year return sea state specified in the Opti-OWECS study, the maximum wave height of the design wave is 12.8 m. The stall regulated wind turbine is used and the number of simulation is

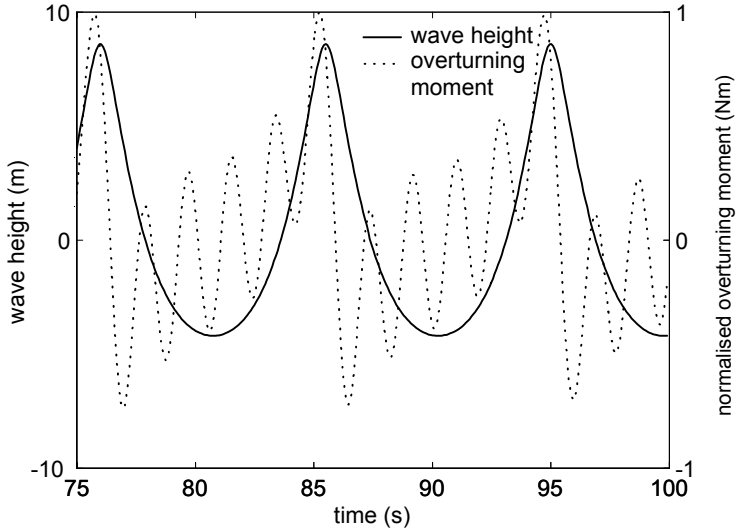

Figure 12.17: Overturning moment of an extreme wave of 50 year return period using Stream Function

50. The significant wave height for the random simulation is 6.9 m and the zero upcrossing period is 7.7 s [38].

In order to compare the overturning moment from constrained wave simulation and from Stream function, an equivalent wave height is defined for the constrained wave simulations. The equivalent wave height is defined as the difference between the local minimum and the local maximum where the wave constraint is defined. This is to be justified by the fact that near the constraint point the deterministic shape of the wave (the mean shape of the wave) dominates, see Figure 12.18.

Since every simulation is random, the equivalent wave height of the constrained waves will fluctuate from simulation to simulation. Only those simulations whose equivalent wave height does not deviate more than plus or minus 5% percent from the maximum wave height of the stream function, are chosen. The maximum response of each simulation is plotted in an empirical distribution function normalised with the maximum response obtained using the Stream functions, see Figure 12.19.

As it can be seen the variation of the maximum overturning moment is quite considerable, varying from 30% to 90% of the extreme response determined using the Stream function. This implies also that the equivalent wave height has a rather weak correlation with the maximum response of constrained simulations because the equivalent wave height is kept more or less constant. None of the maximum overturning moments due to constrained waves reaches the level of the maximum response obtained using Stream function waves. The maximum

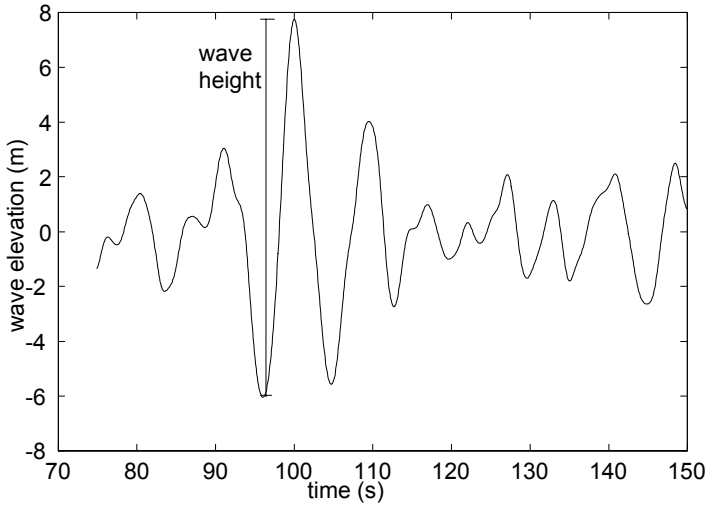

Figure 12.18: A constrained wave with the definition of the equivalent wave height

overturning moment from 50 constrained waves is about 90% of the maximum Stream function response. However, a direct comparison can be quite misleading, because one may directly conclude that the deterministic non-linear wave yields a more conservative estimate of the extreme response.

One has to be aware that the constrained wave is based on the linear wave theory and the water particle kinematics predicted is lower than the non-linear wave theory. This means that the linear wave theory gives a lower estimate of wave loads. If one takes the non-linearity of the waves into account for the constrained waves, the Stream Function estimate of the extreme response may not be necessarily higher than the extreme response predicted using constrained simulations.

Figure 12.19 shows also that the variation of the structural response due to a random wave field can be considerable and this is not taken into account by the deterministic waves. On the other hand the non-linearity of the wave is not taken into account by the constrained waves. A second order hybrid wave model, that satisfies the nonlinear boundary conditions up to the second order has been applied to determine the structural response of fixed offshore structures. It has been concluded that the hybrid wave model yields smaller structural response than the linear wave theory and the difference between these two theories is not very considerable [25]. However, the structural response compared in the mentioned study is taken from an offshore structure in deep waters. The effect of the non-linear wave loading at the surface is negligible for a fixed offshore structure in deep to intermediate water depth. Furthermore, the fixed offshore structures in deep waters respond to the wave loading in a quasi-static way.

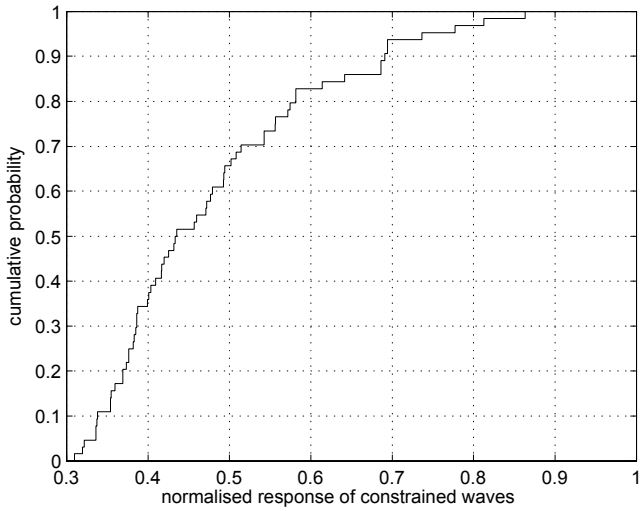

Figure 12.19: The CDF of the overturning moment from 60 constrained waves

Hence the dynamic response constitutes a smaller part of the total response Therefore results from deep water offshore structure design can not be directly translated to the design of the support structures in shallow waters. In the future, one may need to account for the non-linear waves in shallow waters to obtain a more accurate description of the extreme response. For the present it is assumed that the linear theory produces an adequate estimate of the extreme structural response.

12.4 Combination of extreme wave and extreme gust

12.4.1 Combination of the extreme wind gust and waves

In the previous sections of this chapter, the extreme gust loading and extreme wave loading are treated as separate loads. In a real situation both wind and wave loads occur simultaneously. The combination of wind and wave loading is an important aspect of the design when using an external condition based approach. Several combinations of extreme gust and wave loadings are analysed here.

Two of the extreme load combinations specified in the GL design code for offshore wind turbines concern the combined loads of extreme wind and waves. These two extreme load combinations are shown in Table 3.2. The first load case has a 3 second gust speed, with a reduced wave height. The second one has a larger wave with 1 minute gust speed. The 50 year mean wind speed

and significant wave height are determined from the marginal distributions of the mean wind speed and significant wave height, respectively. The turbulence intensity is 0.12. The zero upcrossing period is determined using Equation 3.11. Load combination 1 is studied because it is assumed here that it produces the most extreme response.

It has been shown that the load conditions specified in the Table 3.2 do not produce the maximum response for the pitch regulated turbine. For this reason, the stall regulated turbine is studied because these load combinations are more likely to produce extreme responses for this type of turbines.

The extreme response will be determined using the deterministic IEC gust model and non-linear stream function waves. The extreme responses are also calculated with constrained gust and waves using the wave heights and gust speeds

12.4.2 Comparison of different load combinations

Different combinations of the constrained wave and constrained wind gust are carried out to study the influence of the different combination possibilities on the extreme response of the OWT. The four combinations considered here and the corresponding parameters are

1. A constrained wind with constrained wave with the maxima occurring simultaneously ($\bar{U} = 34$ m/s, $H_s = 6.2$ m, $T_Z = 7.7$ s, $U_{gust} = 46.2$ m/s, $H_{\max} = 8.2$ m).

2. Constrained wind and stochastic waves ($\bar{U} = 34$ m/s, $H_s = 6.2$ m, $T_Z = 7.7$ s, $U_{gust} = 46.2$ m/s).

3. Constrained wave and stochastic wind ($\bar{U} = 34$ m/s, $H_s = 6.2$ m, $T_Z = 7.7$ s, $H_{\max} = 8.2$ m).

4. Constrained wind and no wave ($\bar{U} = 34$ m/s, $U_{gust} = 46.2$ m/s).

U_{gust} is the maximum gust speed and $H_{\max}$ is maximum wave height. For these 4 combinations 50 simulations are performed. The statistical descriptors of the overturning moment at sea bottom are shown in Table 12.8. The different combination criteria have no effect on the flap moment of the blade, hence it is not shown here. The mean is the mean value of the maximum overturning moments from 50 constrained simulations. Accordingly, the standard deviation is the standard deviation of the maximum overturning moments.

As can be expected, the combination of the constrained wind and waves results in the highest OTM. From the fourth combination case, only constrained wind, it can be seen that the wind is a major load source, compared to the load combination of constrained wind with stochastic wave, or constrained wave with stochastic wind, there is a slight difference in the response of about 5%. The load combinations 2 and 3 can be regarded as an application of the Turkstra's rule to the external load conditions. In case 2 one can consider the wind load

Table 12.8: Statistics of the overturning moment for different combinations of constrained simulations

Combination	**Mean** (10^7Nm)	**Standard dev.** (10^7Nm)	**Maximum** (10^7Nm)
Constrained wind Constrained wave	3.31	0.43	4.14
Constrained wind Stochastic wave	2.71	0.31	3.53
Stochastic wind Constrained wave	2.87	0.35	3.75
Constrained wind	2.53	0.24	3.28

Table 12.9: Extreme load cases specified in GL design codes

OTM (10^7Nm)	**Flap moment (10^6Nm)**	**Delay (s)**
3.24	0.99	4.20 second (out of phase)
3.20	1.12	3.20
3.30	1.10	2.20
4.03	0.92	1.20
4.07	1.09	0 (in phase)
3.47	1.04	1.20
3.40	1.01	2.20
3.34	0.96	3.20

as the principal load and the wave load as a secondary load and vice versa in case 3. It can be seen that assuming concurrence of the two extreme loads yield responses that are about 20% higher, on average, than the combinations suggested by the Turkstra's rule.

12.4.3 Time dealy between the extreme gust and extreme wave

Until now the maximum of the wind gust and the maximum of the wave height are assumed to occur simultaneously. This is rarely the case in reality. To investigate the effect of the non simultaneous occurrence of the wind gust and extreme wave, a time lag is introduced between the two maxima.

The distance between the two constrained signals varies from 0 to 20 seconds. 50 simulations are performed for each delay time step of 2 seconds. The maxima of the overturning moments are taken from each constrained simulation. The mean value of the maxima of the OTM is plotted against the time difference between the two constrained signals in Figure 12.20. Errorbars of one standard deviation is also shown.

It can be seen that the simultaneous occurrence gives the highest estimate. The mean of the maximum overturning moment decreases slowly with an increasing distance between the two maxima of the constrained wind and wave. Considering the stochastic fluctuations of the simulations, the maximum response converges slowly toward the load combinations 3 of Table 12.8. This combination is a constrained wave with a stochastic wind. At a time difference

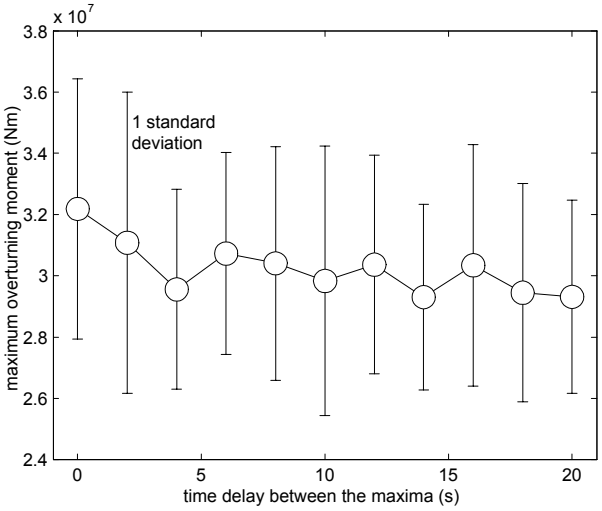

Figure 12.20: Mean and one standard deviation of the maximum overturning moment with different delays between constrained wind and wave.

of 20 seconds between the peak of wind speed and wave height, the mean value of the maximum overturning moment is about 3% higher than that of the case 3 and about 8% higher than the case 2.

For comparison purposes, the effect of a time delay between the maxima of the wind gust and wave height on the turbine response is also studied with the deterministic load models. The parameters used for the deterministic models are identical to those of the combination 1 in Section 12.4.2 For the stream function wave the individual wave period is 9.2 s. Table 12.9 shows the extreme flap moment and the OTM for different time delays between the maxima of wind gust and waves. It can be seen that the delay has basically no influence on the flap moment of the blade. For the OTM the increase of the maximum response is very sharp when the delay between the maxima of the wind gust and the wave approaches zero. Also the difference in the response for different time delays is quite considerable, which can differ up to 25%.

Comparing the overturning moments from contrained simulations and deterministic models (both with a time delay), it can be seen that the mean values of maximum response using contrained models are much lower, especially for simultaneous occurrence of the extreme wind gust and wave. For other time delays, the deterministic models give an estimate that is about 10% higher than the mean values of the maxima obtained with the constrained models. However, one should be aware of the stochastic character of the response, since the values compared here are the means of the maximum responses. The maximum of the 50 maxima of the OTM obtained with constrained simulation is slightly higher than the maximum OTM determined using the deterministic models. However,

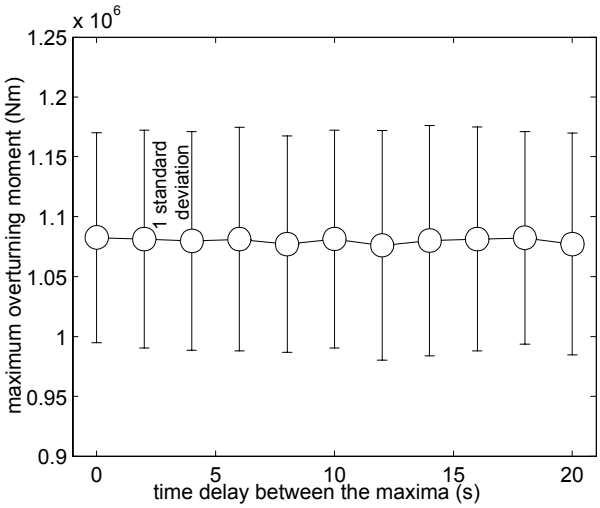

Figure 12.21: Mean and one standard deviation of the maximum flap moment with different delays between constrained wind and wave.

using the maximum of 50 contrained simulations as design value would be too conservative, given the fact that the constrained gust and wave correspond to a 50 year event, and if this event occurs the probability that the maximum value (from 50 constrained simulations) will be exceeded is very small.

For the blade, the issue of the combinations of constrained wave and constrained gust is not relevant since the influence of the wave on the blade response is insignificant. This can be seen in Figure 12.21. It shows that the mean and one standard deviation of the maximum flap moments for different delays between the extreme wind gust and wave. The variation with the time delay is insignificant.

The maximum flap moment obtained using the deterministic IEC gust has a similar value as the mean of the maximum flap moments using 50 constrained gust simulations.

The maximum overturning moment using the deterministic gust and wave models is considerably higher than the mean value of the maximum overturning moments obtained using 50 constrained simulations of wind gusts and extreme waves. The OTM obtained using deterministic models is about 2 standard deviations above the mean of the maximum OTM obtained from 50 simulations of constrained gusts and waves. However, the maximum overturning moment from all the maxima of the OTM using 50 constrained simulations is slightly higher than the OTM calculated using the deterministic models, about 2%.

12.5 Application of the constrained simulations

The constrained gust simulation is applied to the pitch regulated wind turbine but the operating condition of a stall controlled turbine is similar to the pitch regulated wind turbine when the pitch controller is not active. In this case it means the mean wind speed is below the rated wind speed. Thus, the conclusion drawn for the pitch regulated wind turbine at 13 m/s can be applied to the stall regulated wind turbine. The gust response of a stall regulated wind turbine will increase with the gust amplitude and the mean wind speed. The most severe gust loading will occur at wind speeds near the cut-out wind speed.

For pitch regulated wind turbines, the short duration gusts can be of more relevance. For stall regulated wind turbines, the gusts amplitude will be more dominant.

Using the constrained simulation one can obtain a long-term distribution of the gust response. This distribution should be very similar to the long-term response distribution determined by the MAX method, if wind gusts are the principal mechanism that causes the extreme response in the wind turbulence. However, this is not the case here. The gust response predicts a lower 99 percentile than the MAX method. Apparently there are other characteristics of the wind turbulence that can cause extreme responses.

Furthermore it is a time consuming process to determine the distribution of the extreme gust responses. Using 100 simulations of 60 seconds, 5 amplitudes for each mean wind speed, the simulation time is not different than the required simulation time for the MAX method. For this reason, it is better to use the constrained gust model to improve the modelling of the extreme wind gust in the external condition based method.

For a purely hydrodynamic loading environment, the constrained simulation can represent a more time efficient method to obtain the extreme response distribution due to extreme waves because the stationary period of the wave is considerably longer than that of the wind. However, for a wind turbine the wind can have a considerable contribution to the extreme response of the support structure. The combination of both contrained processes means an even larger number of simulations. Hence, the constrained simulation technique can be applied to improve the current deterministic modellings of extreme gusts and waves used in the external condition based design, since it includes stochastic properties of the process which are not taken into account in the deterministic models.

Chapter 13

Application of the methods

13.1 Introduction

In this chapter the response based approach and the external condition based approach are applied to two types of wind turbines in an offshore environment, one with a pitch control and the other one with a stall control (see also Sections 4.4. and 4.5). Using time domain simulations the responses of the offshore wind turbines are obtained. Two responses are analysed here, the flap moment at the blade root and the overturning moment of the support structure. The 100 year response is determined using three response based methods (MAX, POT and Process models). The MAX method uses the maximum of each simulation, the POT methods uses peaks of each simulation and the Process model uses the statistical moments to predict the maxima of the response (see also Chapters 8, 9 and 10). The response obtained using the MAX method is used as the reference value, to which the responses obtained using other methods are compared.

The uncertainty concerning the choice of distribution functions is taken into account with a Bayesian analysis. This is applied to the responses of the pitch regulated and stall regulated wind turbines. The uncertainty of the distribution parameters is not taken into account because the influence of this uncertainty is considerably less significant than the choice of distribution.

The external condition based approach is applied to the two types of wind turbines as well. The extreme wind events are modelled with a steady wind, an IEC extreme operating gust, or constrained wind gusts (Section 12.2). The extreme waves are modelled with stream functions and constrained waves (Section 12.3). For the pitch regulated turbine, the extreme wave condition is replaced by random waves because the extreme response for this turbine occurs at low significant wave heights. Different combinations of the extreme wind and waves are studied. The extreme responses determined with the external condition based approach are compared with the responses obtained by the MAX method.

For an overview of the applications carried out here see Figure 13.1.

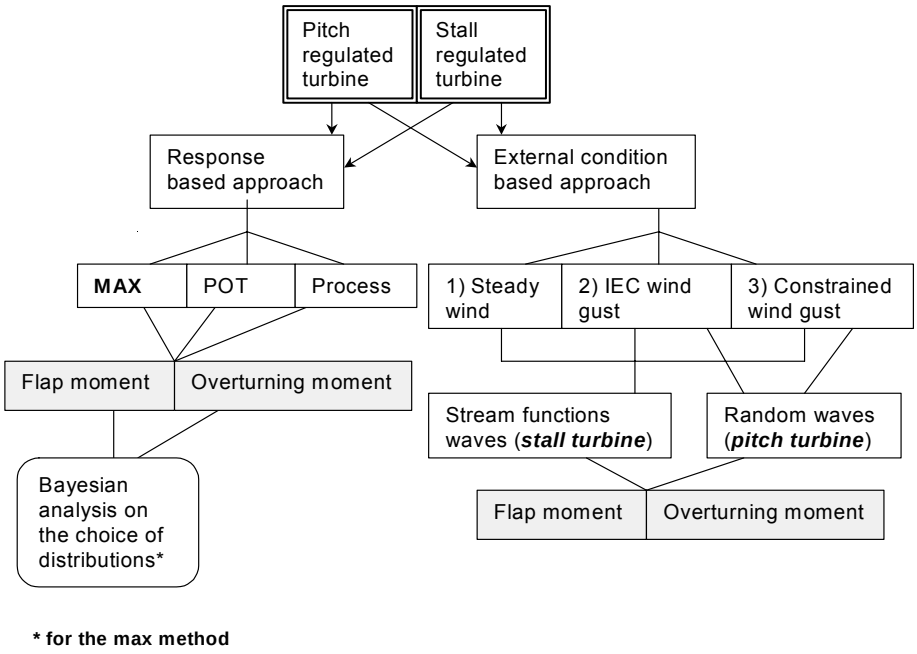

Figure 13.1: Overview of the applications of the response based and external condition based approaches.

13.2 Response based models

13.2.1 Pitch controlled turbine

The extreme responses of this turbine occur around the rated mean wind speed (13.7 m/s) [23]. For this reason not all the mean wind speeds need to be analysed (Chapter 11). The number of mean wind speeds is reduced to the most severe six for this pitch controlled turbine [20], ranging from 13 m/s to 18 m/s. For the MAX method 50 simulations are carried out for each sea state, for the POT method, 10 simulations and for the Process model, 5 simulations. All the simulations have a length of 40 minutes. The different methods have different requirements for the number of simulation and this has been analysed in Chapter 8, 9 and 10.

There are different combinations of the significant wave height and wave periods for a given mean wind speed. From the selected mean wind speeds, different combinations of wave parameters taken from the scatter diagram are studied. The scatter diagram for the reference location is made from the data of the NESS/NEXT hindcast database [72].

50 maxima of the maximum flap moments and overturning moments are obtained from 50 simulations. This has been done for all the combinations of $\bar{U}$, H_s and T_z. The mean values of these 50 maxima of the flap moment and overturning moment are shown in Figure 13.2). The mean values of the 50 maxima of the flap moment and OTM are normalised with respect to the largest mean value of the 50 maxima from all the sea states. In this case the largest mean of the response maxima occurs at a mean wind speed of 15 m/s. The vertical variation of the response for a given mean wind speed represents different combinations of wave parameters.

It can be seen from Figure 13.2 that the maxima of the flap moments is hardly influenced by the variations of the significant wave heights and wave periods, while the maxima of the overturning moment does vary with the wave parameters. Nevertheless, the variation of the OTM in percentage is rather small. This is due to the low mean wind speeds, where the significant wave height is not large. For every sea state (defined by a mean wind speed, a significant wave height and a wave period), a conditional distribution of the maximum response is obtained. The number of different sea states that needs to be taken into account for the long-term distribution of the maximum response can be further reduced, due to the small variation of the maximum response with the wave parameters.

For each mean wind speed the combination of wave parameters that produces the highest response is used to compute the long-term distribution of the maximum response. In this case there are 6 conditional distributions. This reduction will introduce a slight overestimate in the long-term distribution of the maximum response, although it will be insignificant because the response variation for different waves parameters at a given mean wind speed is small (shown in Figure 13.2). The number of independent sea states used to extrapolate the maximum response distribution to a period of one year is the number of hours

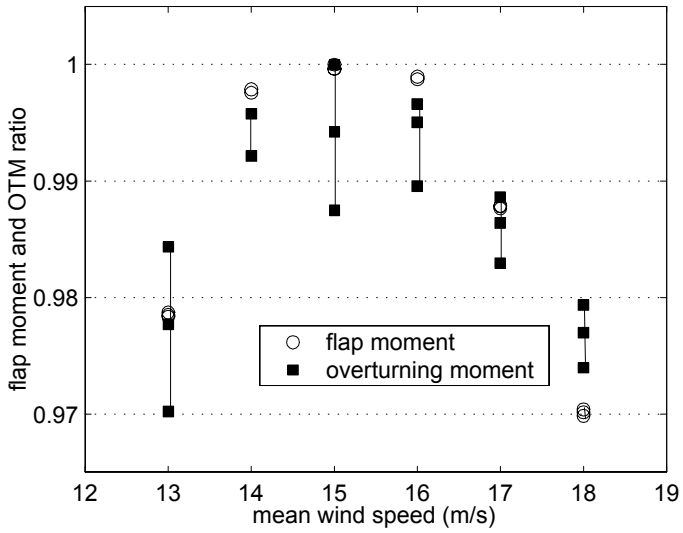

Figure 13.2: Mean of the maximum responses of the pitch turbine for different sea states (every point represents a combination of the mean wind speed, the significant wave height and the zero upcrossing period); normalised with respect to the maximum mean value at 15 m/s.

of occurrence of the sea states between the mean wind speed of 13 m/s and 18 m/s in one year.

The 3 parameter Weibull distribution is used to fit the maxima of the response for the MAX method and the peaks for the POT method. The peak per blade revolution counting is applied to the flap moment and the mean upcrossing counting is applied to the OTM (Section 9.5).

The maximum response with a 100 year return period is determined from the long-term distribution of the maximum response. The 100 year responses are normalised with respect to the MAX estimate (see Table 13.1).

All the three response based methods give similar estimates with differences that vary between 2% to 6%. The deviation in the 100 year flap moment is slightly smaller than for the OTM.

Considering the fact that 50 simulations are used for the MAX estimate, 10 simulations for the POT estimates and 5 simulations for the Process models, it is more likely that the MAX estimates have a slight advantage to capture rare extremes that do not occur in 10 or 5 simulations. However, using the statistics of local maxima (POT and Process models) one can still predict reasonably the maximum response with a return period of 100 year. Moreover, the saving on the simulation time by applying the POT and Process model is quite considerable and 6% deviation can still be regarded as acceptable.

Within the Process method, the Gaussian model gives a quite close estimate

Table 13.1: 100 year flap moment and overturning moment of the pitch regulated wind turbine obtained with different response based methods, normalised with the MAX estimate

	100 year flap moment	**100 year OTM**
MAX	1.00	1.00
POT	0.98	0.95
Process (Gaussian)	1.01	0.98
Process (non-Gaussian)	0.98	0.94

with respect to the MAX estimate. The Gaussian model predicts an estimate closer to the MAX estimate, compared with the non-Gaussian model with skewness correction (Section 10.3). It is to be noticed that the Gaussian model uses the Gumbel distribution to approximate the distribution of the largest response, while the non-Gaussian model uses the Rice distribution. Gumbel distribution produces a higher estimate than the Rice distribution and this does compensate the correction of the positive skewness (which is taken into account in the non-Gaussian model but not in the Gaussian model). The non-Gaussian model with skewness and kurtosis is not applied because the variation of the kurtosis is rather significant. A reliable estimate of the kurtosis is not guaranteed and this can lead to large variation in the estimate of the maximum responses.

The extreme response of this pitch regulated wind turbine occurs during operation. The maximum response of the wind turbine at standstill above the cut-out wind speed is less than the maximum response during the operation. However, one should be aware that the extrapolation of the extreme response during standstill to a return period of e.g. 100 year can be larger than the extrapolation of the extreme response during the operation. Although, it does not apply to this turbine here, one should always consider the extreme responses during standstill because different response characteristics and different external conditions can make the extreme responses during standstill higher than during operation.

13.2.2 Stall controlled turbine

For the stall controlled wind turbine the same number of simulations are carried out to obtain the structural responses: 50 simulations for the MAX method, 10 for the POT and 5 for the Process model. The maximum response of this turbine does not occur during the turbine operation but beyond the cut-out wind speed. Using the scatter diagram, the sea states with wind speeds above the cut-out wind speeds are selected, with mean wind speeds varying from 24 m/s to 34 m/s. For each mean wind speed, the response due to different combinations of the significant wave heights and wave periods are analysed. For the stall regulated wind turbine the same reference location as the pitch regulated wind turbine is used.

From the 50 simulations, 50 maxima of the flap moment and OTM are

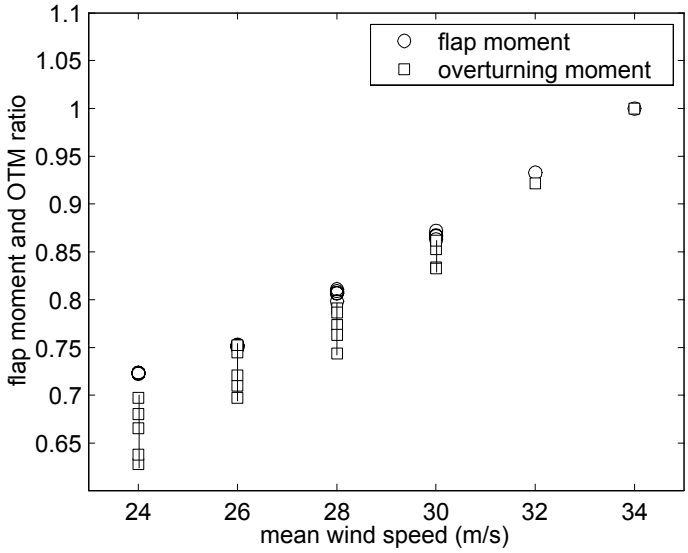

Figure 13.3: Mean response of the stall turbine for different sea states (every point represents a combination of the mean wind speed, the significant wave height and the zero upcrossing period);normalised with respect to the maximum mean value at 34 m/s.

obtained. Figure 13.3 shows the mean values of the the maxima of the flap moment and of the OTM. The mean of the maximum responses are normalised with the largest mean value of the maximum responses from all the considered sea states. In this case the largest mean value of the maximum response comes from the mean wind speed of 34 m/s. The variation of the mean of the maximum response for a given mean wind speed represents different combinations of significant wave heights and wave periods.

As can be seen, the variation of the mean flap moment is not sensitive to the variation of the significant wave heights and wave periods. Due to the larger range of the mean wind speeds that are taken into account (24-34 m/s compared to 13-18m/s), the variation of the responses is also much larger than the variation of the responses shown for the pitch regulated turbine (see Figure 13.2), since the thrust forces increase quadratically with the mean wind speed. Also note that the sea states considered here have considerably lower occurrence frequencies than the occurrence frequencies of the sea states considered for the pitch regulated turbine. This means also that one may need to take a closer look at the conditional distributions of the response because the number of sea states N has an influence on the determination of the long-term distribution (see Section 11.3).

The maximum responses with a return period of 100 year are determined

Table 13.2: 100 year flap moment and overturning moment of the stall regulated wind turbine, obtained with different response based methods, normalised with the MAX estimate

	100 year flap moment	**100 year OTM**
MAX	1.00	1.00
POT	0.98	0.94
Process (Gaussian)	1.04	1.05
Process (non-Gaussian)	1.01	0.96

with different response based methods. The 3 parameter Weibull distribution is used to fit the maxima and peaks of the response. The peak per blade revolution counting is applied to the flap moment and the mean upcrossing counting is applied to the OTM for a sea state. For every sea state, a conditional distribution of the maximum response is determined. Taking the occurrence frequencies of these sea states into account, the long-term distribution of the maximum response can be calculated. The number of independent sea states is equal to the hours of occurrence of the sea states considered in the analysis, i.e. all the sea states are independent. The number of independent sea states is then used to extrapolate the maximum response distribution to a period of 1 year.

Two process models are used, the Gaussian model and the non-Gaussian model with skewness correction. The 100 year responses obtained using different response based methods are shown in Table 13.2.

For this stall regulated turbine, the variation of the estimates of the 100 year flap moment and OTM is not much different than for the pitch regulated wind turbine, varying from 2% to 5% with respect to the MAX estimates. In this case it can be seen that the MAX estimate does not necessarily give the highest estimate.

The low number of simulations (5) and the large variation of the higher statistical moments can have considerable influence on the long-term estimates using the Process method. When the non-Gaussian model with a skewness and kurtosis correction is applied, this model gives an estimate of the 100 year flap moment that is about 10% above the MAX estimate. For the 100 year OTM, the skewness-kurtosis corrected model yields an estimate that is about 2% below the MAX estimate, which is closer to the MAX estimate than the skewness corrected model.

13.2.3 Choice of Distributions/ Bayesian analysis

Pitch regulated turbine

It has been shown that the uncertainties concerning the distribution types is larger than the uncertainties concerning the distribution parameters (Section 8.3). The uncertainties of the choice of distribution has been studied for the pitch regulated wind turbine using 3 distributions, the Weibull, Gumbel and

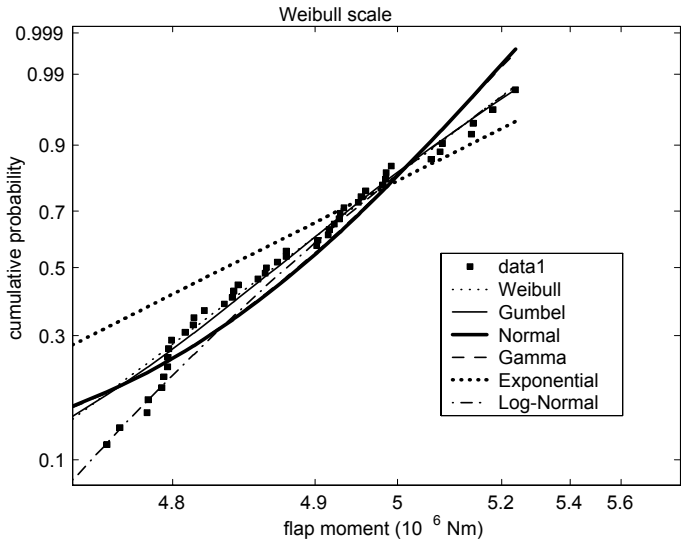

Figure 13.4: Fit of the maxima of the flap moment of the pitch regulated turbine with 6 distribution functions.

the Normal distribution. To ensure that these distributions cover reasonably the data in the probability space, additional distributions are used. The added distributions are the Log-Normal, 3 parameter Gamma and the Exponential distribution (see Appendix A for a list of the distribution functions). The 50 maxima of the flap moment and overturning moments are used. The least squares method is applied to fit the cumulative distribution functions.

Figure 13.4 shows the maxima of the flap moment of the most severe sea state fitted to 6 different distributions plotted in a Weibull probability scale. It can be seen that the chosen distributions cover the data reasonably well. It is important to choose the distribution functions such that the probability of the data are covered from both sides[1]. Three distinct groups can be observed. The Normal and Log-Normal distribution differ only slightly from each other and belong to the light tail distributions. The Weibull, Gamma and Gumbel distributions form the group that capture the tail of the data satisfactorily. The Exponential distribution has the heaviest tail of all the distributions and it has a poor fit. Inspecting the Figure 13.4 visually, one can see that the Weibull, Gamma and Gumbel distributions are more likely to represent the distribution of the maxima of the flap moment.

Figure 13.5 shows the same distribution functions extrapolated beyond the data range of the maximum flap moment obtained by simulations. It can be seen that the 3 parameter Gamma, Weibull and the Gumbel distribution are

[1] In Figure 13.4, the Exponential distribution covers the data from below and the Normal distribution covers the data from above in the tail region.

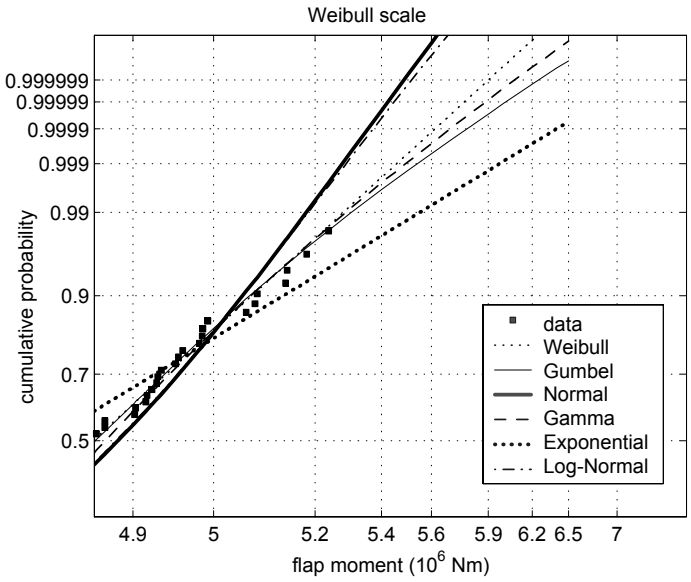

Figure 13.5: Tails of the fits of the maxima of the flap moment of the pitch regulated turbine with 6 distribution functions.

almost identical up to a cumulative probability of 0.99. From there the tails of these 3 distributions start to diverge. The Gumbel distribution gives a slightly higher estimate of the 100 year flap moment than the Weibull and Gamma distribution. The Exponential distribution has the heaviest tail. The Normal distribution family gives the lowest estimates. Goodness of fit tests are applied to check whether the chosen distributions fit the data in a reasonable way. The K-S and A-D tests (see Section 7.3.2) are applied to the upper part of the distributions with a cumulative probability of more than 0.5. This limit is chosen to avoid the rejection of the distribution by the goodness of fit tests, since the deviation at the lower part of the distributions can be quite considerable. This can be justified by the fact that the area of interest is the upper part of the distributions. The distributions are not rejected by the goodness of fit tests with a significance level of 5%.

To take into account the uncertainty of the distribution functions, the Bayesian analysis is applied. The Bayesian weights of the different distribution functions are calculated and shown in Table 13.3. The 100 year flap moments are normalised with respect to the Weibull estimate. It can be seen that the large part of the probability rests on the Weibull and Gamma distributions, Gumbel takes a smaller part of the probability, while the rest of the distributions has practically no influence on the long-term estimate. The Bayesian estimate is virtually identical to the Weibull estimate. In this case, the outcome of the Bayesian analysis confirms to a large extent the conclusion of the visual inspection.

Table 13.3: participation factors and 100 year return values of the distribution functions of the flap moment of the pitch regulated turbine using Bayesian analysis

Distribution	**participation**	**100 year**
Gumbel	15%	1.03
Normal	0.7%	0.93
Weibull	34.2%	1.00
Gamma	48.6%	1.01
Exponential	0 %	1.08
Lognormal	1.2%	0.94
Bayes		1.005

Table 13.4: participation factors and 100 year return values of the distribution functions of the overturning moment of the pitch regulated turbine using Bayesian analysis

Distribution	**participation**	**100 year**
Gumbel	2%	1.05
Normal	0.3%	0.93
Weibull	10.3%	1.00
Gamma	86.6%	1.00
Exponential	0 %	1.12
Lognormal	0.5%	0.94
Bayes		0.997

Table 13.4 shows the result for the OTM for the same wind turbine. The overturning moments are normalised with respect to the Weibull estimate. Again, the dominance of the Weibull and Gamma distribution can be clearly observed. The 100 year OTM is almost identical to the Weibull estimate. As can be seen the Bayesian analysis provides directly a formal selection criterion of the distribution functions. In these cases using the Weibull distribution to obtain the estimates of the 100 year responses is sufficient, taking other distributions into account will not affect the estimates of the 100 year responses. Even so, the Gumbel, Gamma and Weibull distribution give very different estimates at the low exceedence probability region, the difference becomes significant only at a very large cumulative probability (for example, 0.999999, which represents a return period of ca. 4000 years, in Figure 13.5) and this cumulative probability corresponds to a return period much larger than the return period used for design purposes, e.g. 100 years. However, this can not be generalised and a Bayesian analysis of the distributional choice is always recommended.

Stall regulated turbine

The Bayesian analysis is applied to the uncertainty of the choice of the distributions for the maxima of the flap moment and overturning moment of the

Table 13.5: participation factors and the 100 year flap moment using Bayesian analysis; stall regulated turbine

Distribution	**participation**	**100 year**
Gumbel	1%	1.01
Normal	0.2%	0.98
Weibull	78%	1.00
Gamma	20%	1.02
Exponential	0 %	1.09
Lognormal	0.8%	0.98
Bayes		1.009

stall regulated wind turbine. 50 maxima are obtained through time domain simulations and the following sea state parameters, the mean wind speed is 34 m/s, the significant wave height is 5.75 m and the zero upcrossing period is 7.31 s. The six distributions used here are the Normal, Log-Normal, 3 parameter Weibull, 3 parameter Gamma, Gumbel and the Exponential distribution Table 13.5 shows the 100 year flap moment estimated using different distribution functions and the Bayesian estimate. The values are normalised with the 100 year flap moment determined by the Weibull distribution.

As can be seen the Weibull and Gamma distribution have taken the majority of the contribution to the Bayesian estimate. The influence of the rest of the distributions is insignificant. The K-S and A-D goodness of fit tests are applied to all the distributions with a significance level of 5%. The Exponential distribution is rejected by the goodness of fit tests. Nevertheless it is included in the Bayesian analysis for the sake of completeness and indeed the Bayesian analysis regards the Exponential distribution as an unlikely distribution to describe the maxima of the flap moments.

The dominance of the Weibull and Gamma distribution can be also observed for the 100 year overturning moment, shown in Table 13.6. In this case, a visual inspection shows that the Weibull and Gamma distributions fit the data reasonably well (not shown here). The A-D and KS reject the Exponential distribution as a likely distribution for the maxima of the overturning moment.

An advantage of applying a Bayesian analysis is that the unprobable distributions, such as the Exponential distribution, are automatically disregarded by the Bayesian analysis. In such case, the Bayesian analysis acts like a built-in quantitative goodness of fit test without incurring extra computational efforts.

13.3 External condition based models

13.3.1 External conditions: GL approach

The response based approach proposes a more rational methodology for the determination of the extreme responses in the design process of an offshore wind turbine. The response based approach is indeed a logical step toward a prob-

Table 13.6: participation factors and 100 year overturning moment using Bayesian analysis; stall regulated turbine

Distribution	**participation**	**100 year**
Gumbel	0.5%	0.99
Normal	0%	0.93
Weibull	54%	1.00
Gamma	45%	1.00
Exponential	0 %	1.04
Lognormal	0.5%	0.94
Bayes		1.00

abilistic design, however, it requires a detailed knowledge of the offshore wind turbine, in order to determine correctly the response. This may present a problem for the response calculation in the early design stage where such information is simply not available. Furthermore, the computational effort required for the response based approach represents an obstacle hindering a wider acceptance of the response based methods. For these reasons, the design codes usually specify the external conditions, which are assumed to induce extreme responses. In this section, the external conditions approach is applied to the two wind turbines. The extreme response determined with the external condition approach is compared with the extreme response obtained by the MAX method.

Sea state parameters: $\bar{U}$, H_s and T_z

The external condition based approach starts with the specification of the environmental conditions in which extreme responses will occur. The environmental condition is specified by three sea state parameters, the mean wind speed $\bar{U}$, the significant wave height H_s and the zero upcrossing period T_z. For the pitch regulated wind turbine the extreme response occurs during the turbine in operation, while for the stall regulated turbine, the extreme response occurs in the extreme wind situations with the turbine in standstill. Hence, the mean wind speeds defined for these two turbines are different. For the pitch regulated wind turbine the mean wind speed used is 13 m/s. This is the mean wind speed where the extreme gusts produce the maximum response. For the stall regulated wind turbine, the extreme mean wind speed with a 100 year return period is used. The 100 year mean wind speed is given for different wind turbine classes in the GL design code [43]. The turbine class I is chosen for the stall regulated turbine. The 50 year extreme mean wind speed[2] for the turbine class I is 50 m/s.

The significant wave height and the zero upcrossing period have to be determined for the external condition based approach as well. GL does not specify a distribution for the significant wave height and the zero upcrossing period. For the pitch regulated turbine the wave parameters are taken from the scatter diagram. From all the sea states with a mean wind speed of 13 m/s, the one

[2] A 100 year wind speed can be converted to a 50 year wind speed by reducing the speed by 3% [43]. Conversely a 50 year wind speed can be converted to a 100 year wind speed.

Table 13.7: Different models of extreme gusts and extreme waves for the external condition based approach; load combination 1

	pitch regulated turbine	**stall regulated turbine**
model 1	X	Steady wind (coherent) ($U_{gust} = 63.3\ m/s$)
	X	Stream functions ($H_{\max} = 8.3\ m$, $T_{wave} = 9.22\ s$)
model 2	IEC gust (coherent) ($\bar{U} = 13\ m/s$, $U_{gust} = 23\ m/s$) Random wave ($H_s = 2.5\ m$, $T_z = 5.5\ s$)	IEC gust (coherent) ($\bar{U} = 50\ m/s$, $U_{gust} = 63.3\ m/s$) Stream functions ($H_{\max} = 8.3\ m$, $T_{wave} = 9.22\ s$)
model 3	Constrained gust (not coherent) ($\bar{U} = 13\ m/s$, $U_{gust} = 23\ m/s$) Random wave ($H_s = 2.5\ m$, $T_z = 5.5\ s$)	Constrained gust (not coherent) ($\bar{U} = 50\ m/s$, $U_{gust} = 63.3\ m/s$) Constrained wave ($H_s = 6.3\ m$, $H_{\max} = 8.3\ m$, $T_z = 7.7\ s$)
	U =mean wind speed U_{gust} =maximum gust speed T_z =zero upcrossing period	H_s =significant wave height $H_{\max}$ =maximum wave height T_{wave} = individual wave period

with the highest significant wave height is selected. For the stall regulated wind turbine, the 100 year significant wave height is determined from the marginal distribution of the significant wave heights. The zero upcrossing period can be determined with Equation 3.11. The problem for this equation is the choice of the mean wind speed. As shown in Section 3.5, the 100 year mean wind speed from the GL guideline is much larger than the 100 year mean wind speed from the environmental contour line. Using the GL extreme mean wind speed in combination with Equation 3.11 would result in a larger wave period. For this reason the wave period is calculated with Equation 3.11 using the 100 year mean wind speed with the 100 year significant wave height (see first line of Table 3.1).

Maximum values: $H_{\max}$, T_{wave} and U_{gust}

From the mean wind speed, significant wave height and the zero upcrossing period one can arrive at a gust speed U_{gust} averaged over a short period, for example 3 seconds, and a maximum wave height $H_{\max}$. In the GL guideline [43] two combinations of the wind gust with the maximum wave height are given. The individual wave period associated with a deterministic wave[3] is calculated using Equation 3.17. The turbulence intensity is 0.12 according to GL. The two extreme load combinations are given in Table 3.2 and the numerical values are given in Table 3.3. This table is valid for the stall regulated wind turbine. Load

[3] In the load combinations of the GL guideline the zero upcrossing period is not specified but an individual wave period is given, T_{wave}=$11.1 \cdot \sqrt{\frac{H_{\max}}{g}}$; $H_{\max}$ is the maximum individual wave height and g is the earth acceleration of gravity. This formula is not used in this study, because it applies to deep water waves.

Table 13.8: 50 year responses of the pitch regulated wind turbine with GL combinations of extreme external conditions , normalised with the MAX estimates

Pitch turbine	**load combination 1**	
	Flap moment ratio	Overturning moment ratio
model 1	X	X
model 2	0.80	1.2
model 3	0.81	0.82

combination 1 refers to the 3 second gust speed with a reduced extreme wave height, while load combination 2 refers to a higher extreme wave height with 1 minute gust speed. The maximum response from the two load combinations is analysed. One needs to take into account these two combinations because it can not be determined beforehand which combination will give the most extreme response.

For the pitch regulated wind turbine, an alternative extreme external condition is defined. As mentioned before, the chosen mean wind speed is 13 m/s, the turbulence intensity is 0.12. The extreme external condition here is the 50 year operating gust using the IEC gust model[4] [53]. The wave condition at the given mean wind speed has only marginal influence on the response, for this reason random wave simulations are combined with the 50 year extreme operating gust. The response of the extreme operating gust is compared to the 50 year extreme response obtained with the MAX method.

Three different models of the extreme gust speed and extreme waves are applied to the pitch and stall regulated wind turbines. These models are summarised in Table 13.7 for the load combination 1. There is no model 1 for the pitch regulated wind turbine because this load combination is not relevant for the pitch regulated turbine. The maximum response due to a steady wind is much lower than due to an extreme operating gust because the controller is able to adjust to the constant gust wind speed. For this reason this model can be disregarded. Load combination 2 is not shown because the results show that the maximum response from load combination 2 is always lower than the maximum response from load combination 1. Notice also that the constrained simulation is applied to the maximum value and not to other characteristics of the wind gust or waves, e.g. rise time.

The extreme responses obtained using the different models are shown in Table 13.8 and Table 13.9, for the pitch controlled and stall controlled wind turbine, respectively. Only the load combination 1 is shown here. The results shown in the tables will be discussed in detail in the following sub-sections.

[4] To calculate the gust speed U_{gust} one needs to know the turbulence intensity. IEC does no have a specification for the turbulence intensity of offshore locations, thus the GL turbulence intensity for offshore locations is used (0.12).

Table 13.9: 100 year responses of the stall regulated wind turbine with GL combinations of extreme external conditions , normalised with the MAX estimates

Stall turbine	**load combination 1**	
	Flap moment ratio	Overturning moment ratio
model 1	1.12	1.53
model 2	1.41	1.94
model 3	1.18	1.36

13.3.2 Model 1/ steady wind

Stall controlled wind turbine

The first line of Table 13.9 shows response ratios for the the load combination 1.The values are normalised with respect to the MAX estimates. The extreme flap moment determined from a 3 second wind gust with a reduced wave height is 12% higher than the MAX estimate, while the OTM is about 50% higher

One can say that the dynamic response plays an important role in the extreme response, taken into account that the most severe mean wind speed is 34 m/s in the MAX estimate. The 50 year mean wind speed of 50 m/s specified for the wind turbine class 1 is almost 50% higher, while the extreme flap moment to the steady wind model is only about 12% higher than the MAX estimate. The 1 minute gust speed (load combination 2) is irrelevant because it produces lower extreme response than the load combination 1 and is not analysed here.

The magnitude of variations for the overturning moment is in the same order as that of the flap moment. The MAX estimate of the OTM is considerably lower than those of the GL load cases. One of the reasons is that a uniform wind field produces a larger thrust to the tower and since this thrust force contributes significantly to the OTM, it produces also a larger OTM.

13.3.3 Model 2/ IEC gust

Pitch controlled wind turbine

The 50 year extreme operating gust produces an extreme flap moment in the wind turbine, although this extreme flap moment is lower than the maximum flap moment estimated with the MAX method. The ratio between the two estimates is 0.80 (see the second line of Table 13.8). Observe that the maximum response to the wind gust occurs at a mean wind speed of 13 m/s, while for the response based approach the most severe mean wind speed is 15 m/s. Apparently, there are other stochastic properties of the wind that can produce higher responses and these properties are not captured by the extreme operating gust, neither the deterministic nor the constrained gust models (model 3).

The OTM predicted in this case is considerably larger than the MAX estimate, the ratio between them is 1.2. The reason is that a coherent IEC gust produces a higher thrust. This thrust force contributes considerably to the overturning moment. The second load combination (extreme wave with a one

minute gust speed) is not relevant for this wind turbine, since the wave condition is mild at the given mean wind speed of 13 m/s.

Stall controlled wind turbine

In this model, the steady wind is replaced with the deterministic gust model from the IEC with a maximum wind speed equal to the 3 second gust speed. The mean wind speed is the 100 year mean wind speed from the wind turbine class one.

For the load combination 1, the ratio of the OTM responses between the deterministic gust model and the MAX estimate is 1.94. For the flap moment the ratio is 1.41 (see second line of Table 13.9). As can be seen the combination of the deterministic gust and stream function waves leads to a considerably higher estimate of the OTM response than the MAX method. It is to be noticed that the IEC gust uses a coherent wind over the height, thus the tower thrust is higher than in a spatially stochastic wind field. This higher thrust leads also to a higher OTM.

Load combination 2 gives lower responses for the flap moment and OTM than the load combination 1, thus it need not to be considered here.

13.3.4 Model 3/ constrained gust

Pitch controlled wind turbine

For the pitch controlled turbine, a constrained wind gust is combined with a random wave loading. 50 constrained simulations are carried out. The constrained wave is not applied due to the low significant wave height. Moreover, the contribution of the wave loading to the overturning moment is insignificant at a mean wind speed of 13 m/s.

This model yields a blade response that is lower than the MAX estimate. The ratio between the mean of 50 maxima of the flap moment from 50 constrained gust simulations and the MAX estimate is 0.81 (see third line of Table 13.8). As observed already in the previous section with the deterministic gust, the extreme gust response occurs at a mean wind speed[5] of 13 m/s. Apparently, there are other stochastic properties of the wind that can produce higher response in the blade and these properties can not be reproduced solely by the constrained gusts (on the maximum value). One of the possible explanations is that the pitch controlled turbines are more vulnerable to gusts with short rise time, while the mean gust shape used here has a rather long rise time. Hence, the controller has enough time to filter the gust loading.

The OTM predicted in this case is also lower than the MAX estimate, the ratio between the mean of the 50 maxima of the OTM obtained from 50 constrained simulations and the MAX estimate is 0.82. As mentioned, the tower

[5] The maximum response of the pitch regulated wind turbine occurs at a mean wind speed of 13 m/s using contrained gusts as input, while using the stochastic wind field simulations the maximum response occurs at a mean wind speed of 15 m/s.

thrust for spatial gusts is significantly lower than, for example, the deterministic IEC gust which is a coherent gust. Load combination 2 is not analysed because it is not relevant for this pitch regulated wind turbine.

Stall controlled wind turbine

50 constrained simulations of extreme wind gusts and extreme waves are carried out. For the load combination 1, the ratio between the mean of the maximum flap moments of the contrained simulations to the MAX estimate is 1.18. The ratio between the mean of the maximum overturning moments to the MAX estimate is 1.36 (see third line of Table 13.9). The higher estimate of the extreme response of the external condition based approach is due to the higher mean wind speed prescribed by the GL guideline for the turbine class 1.

The constrained simulations are comparable to short pieces of random simulations, with the exception that the maximum of the wind speed and wave height can be determined beforehand. The stochastic properties of the load signals are reproduced, if the number of constrained simulations is large enough. In the case of the stall regulated turbine, the sea state with the highest mean wind speed determines the 100 year response. With 50 constrained simulations the stochastics of the external loads are partially reproduced giving an estimate of the flap moment that is closer to the MAX estimate than the deterministic IEC gust models. For the wave loads, 50 simulations may not be sufficient because the stationary period of waves is longer than the stationary period of winds.

The load combination 2 is insignificant because it does not produce a higher response than the load combination 1 and is not analysed here.

13.3.5 Comparisons of the response based and external condition based approaches

The extreme response from using the different models of extreme winds and waves are shown in an overview figure. The load combination 1 is considered, that is, a 3 second gust with a reduced wave height. The load combination 2 gives always a lower estimate of the extreme response, hence it does not need to be analysed here. Figure 13.6 shows the extreme flap moment, normalised with the MAX estimate and Figure 13.7 shows the OTM, also normalised with the MAX estimate.

As far as the flap moment is concerned, it can be seen that the external condition based approach gives the stall regulated wind turbine overall higher response than the response based approach of the MAX method. This is mostly due to the higher mean wind speed as well as the gust speeds assigned by the GL design code to the wind turbine class 1. With the constrained wind gust and waves, the estimates are closer to the MAX estimates partly because constrained simulations contain stochastic background which represents a more realistic external load condition. The steady wind approach of the Model 1 gives also an estimate that is very close to the MAX estimate, despite the large difference in the wind speed.

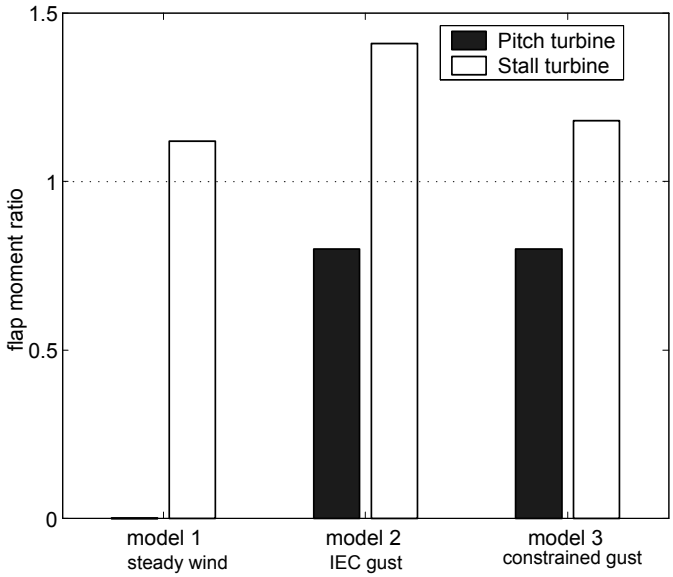

Figure 13.6: Ratio of the extreme flap moment obtained with different extreme gust and wave models. (normalised with the MAX estimate).

As can be seen also in Figure 13.6, the external condition based approach does not always give a more conservative estimate as generally believed. The extreme flap moment determined by the external condition approach lies 20% below the MAX estimate, for the deterministic and stochastic gust models. The response characteristics play an important role in the determination of the extreme responses. For wind turbines, the influence of the controller on the response is crucial and needs to be taken into account accordingly.

The coherent models of the wind gust (model 1 and 2) produce a much higher response ratio for the OTM than for the flap moment (compared to the MAX estimate). The difference in the estimate of the extreme OTM is quite considerable for the stall regulated turbine. The OTM of the external condition based approach can be twice as much as the MAX estimate. Notably, the external condition based approach using constrained gusts does not give a higher response than the MAX method for the pitch controlled turbine. This is due to the smaller contribution of the blade to the thrust on the tower. The IEC gust induces a higher OTM of the pitch regulated turbine than the MAX estimate because the coherence of the gust produces a higher thrust.

As mentioned before the gust response for the pitch controlled wind turbine may be less relevant because of the ability of the controller to filter the gusts. Hence, the response based approach seems to be more suitable to determine the extreme response because the stochastic properties of the wind that lead to extreme responses may not be fully reproduced by the gusts constrained on the

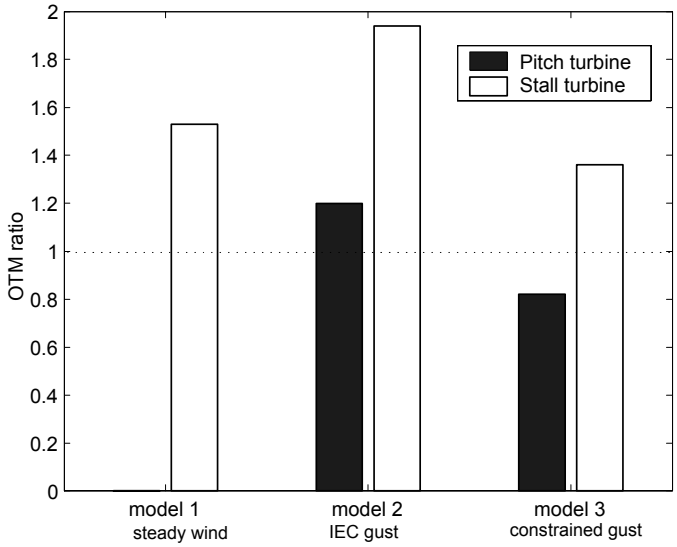

Figure 13.7: Ratio of the extreme OTM obtained with different extreme gust and wave models. (normalised with the MAX estimate).

maximum value. Although, it has to be noted that the constraint is imposed on the maximum value.

The difference in the computational effort between the two approaches is very significant. Response based approach requires a large number of simulations and the simulation length is also considerably longer than the simulation length required for the external condition based approach. The external condition based approach is suitable for the preliminary design stage, while the response based approach is recommended for the final design stage.

Chapter 14

Conclusions

14.1 General conclusions

The current approach to determine the extreme response of an offshore wind turbine is based on specifying the extreme external conditions. As has been shown, an extreme external conditon does not necessarily lead to an extreme response of the wind turbine.

Physically speaking, the response based method should be preferred because it is a consistent approach which treats external conditions without making any assumption on the response. However, the computational effort is considerable for the response based approach because of the large number of external conditions. Moreover, it is difficult to specify this method universally in a design guideline because the response characteristics of the wind turbines are very diverse. An advantage that the external condition based approach enjoys is that it can be formulated independently of the wind turbines.

However, it is not necessary to take all the external conditions into account since the region of interest is the upper tail of the distributions. Furthermore, applying the response based approach one can achieve a more efficient structural design of an offshore wind turbine.

The current design practice uses deterministic models of an extreme wind gust and extreme waves to determine the exteme responses. The disadvantage of the deterministic models is that they do not include the stochastics of the process. Stochastic models of the extreme wind gust and extreme waves are introduced to improve the modelling of the wind gust and extreme waves. Verification with measurements has shown a good agreement with the theoretical models.

The stochastic models generally give a lower estimate of the extreme response than the deterministic models. This is partly due to the fact that the deterministic gust model assumes a total coherence of the wind speed for the whole rotor swept area, while the stochastic gust model takes into account the spatial variation of the wind speeds at different locations. However, the vari-

ation of the extreme response depends strongly on the control concept of the wind turbine.

A direct comparison between the response based method and the external condition based method has to be done with caution because the extreme responses estimated by these two approaches are fundamentally different. Quantitatively, the external condition based approach generally yields a higher extreme response than the response based approach, for the stall regulated wind turbine. For the pitch regulated wind turbine, the external condition based approach gives an estimate of the extreme response that is generally lower than the response based methods. The controller plays an important role. The most severe load situation occurs during the operation with an active controller for the pitch regulated turbine. For the stall regulated wind turbine, the most severe load situation is at standstill with high mean wind speeds.

The general conclusions drawn above should be judged in light of the assumptions and limitations described in Chapter 2. The variation of the data obtained using simulations may have considerably smaller variation than the real data from measurements. Note also that in the real loading situation, many extreme responses arise in non-stationary conditions. The main objective of this thesis is to provide a general methodology for a more efficient structural design of an offshore wind turbine. The methods described here can be extended to include more stochastic parameters such as the turbulence intensity or other extreme load cases.

14.2 Specific conclusions

In this section specific conclusions are drawn for different subjects treated in this thesis.

External conditions

The hindcast data provides a useful source of information which can be used for the estimation of the environmental contour and a scatter diagram. One can apply the joint probability approach to determine the extreme mean wind speed, the extreme significant wave heights and the wave period. However, the estimates of the 100 year wind and waves using joint statistics or marginal statistics show insignificant difference for this data set (see Table 3.1).

The number of stochastic variables are reduced after a sensitivity study. The mean wind speed, the significant wave height and the zero upcrossing period are chosen as stochastic variables. Although, the variation of the turbulence intensity has also a considerable influence on the rotor response, it is not taken as a stochastic variable because the hindcast data do not have any information on the variation of the turbulence intensity for the chosen location.

MAX, POT and Process methods

The MAX method is used as a reference value for the POT and Process methods. Applying the MAX method, 50 simulations can be regarded as sufficient for the estimate of the extreme response distribution. The simulation length can vary, depending on which process determines the extreme response.

40 minutes is regarded as an acceptable simulation length to account for the load variations of the wind and the waves.

The POT model and Process model show results within a maximum variation of around 10% of the refence MAX estimate (using 50 simulations). The recommended number of simulations for the POT method is 10-15 and for the Process method is 5-10 in order to reach a similar degree of accuracy as the MAX estimate.

For the blade response, the peak per blade revolution counting is to be preferred to the mean upcrossing counting while for the response of the support structure the mean upcrossing counting is to be preferred. The three parameter Weibull distribution is suitable to model both the maxima of the simulations as well as the POT of the simulations.

For the response considered in this study, the flap moment at the blade root and the overturning moment at the base of the tower, the Gaussian process model gives an estimate of the extreme responses with less than 5% difference to the MAX estimate. This is because the Gumbel distribution is the asymptotic approximation of the Rice distribution for a large number of maxima. The use of the Gumbel distribution compensates the underestimate due to the positive skewness, which is not taken into account in the Gaussian model. In the non-Gaussian models a correction for the skewness and kurtosis is applied. The skewness correction improves the predicted estimate of the extreme response, i.e. a smaller difference to the MAX estimate. The inclusion of the kurtosis correction does not necessarily bring the estimate closer to the MAX estimate, due to the larger variation of the kurtosis of the response time series.

Extrapolation

For the extrapolation of the response distribution, the issue of the independence of the sea states is not significant, if the response of interest has a return period of, say, more than 20 years. The response of a much shorter return period will be overestimated if the independence of the sea states is assumed.

It is not necessary to take all the sea states into account to determine the long-term distribution of the response. In the presence of few dominating conditional distributions, the conditional distributions from mild sea states will have no effects on the tail of the extrapolated distribution. If the distance between the conditional distributions is large (e.g. the location parameters are far away from each other), it is even sufficient to take into account only the most severe conditional distribution.

Constrained simulations

The constrained gust does not necessarily produce an extreme response on the pitch regulated turbine when the controller is active, because the controller can filter the gust loads. The centre of gusts has some influences on the blade response (maximum variation $\sim 25\%$). However, the distribution of the gust centre in a spatial gust remains largely unknown. Hence, the influence of the gust centre of a spatial gust on the response can not be taken into account properly yet. The verification of the mean shape of the one point gust, i.e. the deterministic part of the constrained gusts, with measurements is very satisfactory.

Load combinations

A time delay between the maximum of the wind gust speed and the extreme wave height decreases the maximum response (assuming that the maximum wind speed and the maximum wave height are the governing parameters of the external loadings). This decrease is very sharp for the deterministic models of the extreme wind gust and extreme waves.

For a time delay between a constrained wind gust and wave, the decrease of the response is less significant (20%, on average). After 20 seconds of delay between the maximum wind gust and the maximum wave, the maximum response approaches the value obtained by applying the Turkstra's rule for a load combination. Thus, one can choose the simultaneous occurrence of the constrained wind and wave maxima without incurring too much conservatism in the design.

Statistical uncertainties

The statistical uncertainties of the extreme responses are taken into account with a Bayesian analysis. In this case, the effect of the uncertainties of the distribution parameters in the long-term distribution is marginal using a non-informative prior in a Bayesian analysis. The choice of distribution models has a much more significant effect on the long-term distribution. One can use visual inspections by plotting the data in different probability scales and use formal goodness of fit tests to select the suitable distributions, although it is not always possible to make an unambiguous choice of the distribution model. In that case, a Bayesian analysis can be applied to take the uncertainty of the choice of distribution models into account.

The distribution parameters determined using the Maximum Likelihood Estimate is less susceptible to outliers. Before fitting the data to distribution models, they should be checked for outliers (e.g. due to simulation error) because it can have considerable influence on the estimates of the skewness and kurtosis, affecting the fit of the distribution function and the estimates of the Process method.

14.3 A proposed approach

Based on this study one can formulate the following approach to be applied to determine the distribution of the extreme response of an offshore wind turbine.

Response based methods

The stochastic parameters that should be taken into account are the mean wind speed, significant wave height and the wave period. The conditional distribution of the response can be obtained using the Process method with 6 simulations and a non-Gaussian model using a skewness correction. A simulation length of 40 minutes should be used. The distribution of the local maxima is modelled by the Rice distribution.

The advantage of the Process method is that one does not need to consider the choice of the distribution model because the distribution of the local maxima is derived from a theoretical basis.

The number of sea states that needs to be taken into account for the long-term distribution of the response depends on the response characteristics of the turbine. One should carry out simulations for the sea states that can lead to extreme responses of the turbine, and based on the mean of the maximum response the 3 most severe distributions can be selected. This is usually sufficient since the region of interest is the tail of the distribution.

The response method is recommended for final design of a wind turbine.

External condition based methods

For the external condition based approach, constrained simulations represent a more realistic load representation than the deterministic models, for the stall regulated wind turbine. 50 constrained simulations of wind gust and extreme waves of simultaneous occurrence should be carried out. The mean value of the extreme response obtained by 50 simulations can be used to represent the design response (with a return period of the given external condition).

For the pitch regulated wind turbine it is not recommended to use the external condition based approach, since the wind characteristics that can lead to extreme responses of the wind turbine may not be fully represented in simulations with the constraint on the maximum value. If the external condition based approach is to be applied, one should use deterministic gust models and stream functions to determine the extreme response. The external condition based approach is more suitable for the preliminary design stage.

14.4 Recommendation for future research

The following issues can be carried out to enhance the methodology treated in this thesis. They are not ordered according to their relevance. However, the verification with measurements can be placed at the top of the priorities.

The methodology should be applied to data obtained from measurements, to verify the accuracy of the response estimate, since it was assumed from the beginning that the simulation code can predict the turbine response accurately. Moreover, it can also be verified if the Process and POT method require less amount of measurement data than the MAX method to estimate the extreme response distribution.

The conclusions show that it is only necessary to account for few sea states for the estimate of the extreme response distribution; one can include other critical load situations or stochastic parameters, for example the turbulence intensity. The inclusion of other load situations would expand the scope of the method because one of the limitations of the method is that it considers only extreme responses of normal production states and standstill.

The constraint of the wind gust is applied to the maximum wind gust speed. For the pitch regulated wind turbine this does not necessarily give a severe response. One may apply the constraint to the rise time of the gust, which can be more detrimental to the pitch regulated wind turbine, because the controller can not react indefinitely fast to the rapid change of the wind speed.

The required number of simulations are determined empirically. This can

be improved using theoretical analysis to determine the limit by studying the characteristics of the process, i.e. wind turbulence and waves.

The joint statistics of wind and waves used here does not give a very different estimate of the extreme wind and waves. Other models of joint statistics with different correlation structures should be applied to see whether the difference of the estimates (or the lack of it) is due to the statistical models or is inherent to the hindcast data used here.

The non-linearity of waves may become more relevant for shallow water locations. The improvement of non-linear random waves will contribute to a better estimate of the extreme wave loads. The influence of breaking waves on the extreme response is also another issue to be studied.

In this study the focus is on the response, however, for a full reliability approach one also needs to take into account the variation of the structural strength. This should be done in order to assess the failure probability of the structure. Another reason why the strength should be modelled as a stochastic variable is that in some structural reliability problems (e.g. the foundation) the uncertainty of the strength may actually be larger than the uncertainty of the loads.

Bibliography

[1] A.-S. Ang and W. Tang. *Probability Concepts in Engineering Planning and Design*. John Wiley, New York, 1975.

[2] ANSYS Inc. Ansys command reference manual, release 5.5, 10th edition. Technical report, ANSYS Inc., 1998.

[3] N. Barltrop and A. Adams. *Dynamics of Fixed Marine Structures*. Butterworth-Heinemann, Oxford, 1991.

[4] H. Bergström. Distribution of extreme wind speed. Technical report, Wind Energy Report WE92:2, Dept. of Meteorology Uppsala University, 1992.

[5] W. Bierbooms. Swing3: users manual. Technical report, Institute for Wind Energy, DUT, 1996.

[6] W. Bierbooms. Swing4: users manual. Technical report, Institute for Wind Energy, DUT, 2000.

[7] W. Bierbooms. Determination of wind and wave design conditions based on the NESS/NEXT database. In *Proceeding of the Offshore Wind Energy Special Topic Conference*, Brussels, 2001. European Wind Energy Association, EWEA.

[8] W. Bierbooms, P. Cheng, G. Larsen, and B. Pedersen. Modelling of extreme gusts for design calculations - newgust final report jor3-ct98-0239. Technical report, Institute for Wind Energy, DUT, 2000.

[9] W. Bierbooms and J. Dragt. Stochatic model for extreme loading of wind turbine. In *Proceeding of the European Wind Energy Conference*, Goterborg, 1996. European Wind Energy Association, Stephen and sons.

[10] E. M. Bitner-Gregersen. Joint environmental model for reliability calculations. In *Proceeding of the 1st ISOPE conference*, Edinburgh, 1991. International Society of Offshore and Polar Engineering, ISOPE.

[11] L. Borgman. Spectral analysis of ocean wave forces on piling. *Journal of the Waterways and Harbors Division*, 93:129–156, 1967.

[12] L. Borgman. Techniques for computer simulation of ocean waves. In A. Osborne and P. Rizzoli, editors, *Topics in Ocean Physics*, pages 387–417. NHPC, Amsterdam, 1982.

[13] G. Box and G. Tiao. *Bayesian Inference in Statistical Analysis*. John Wiley, New York, 1992.

[14] H. Braam. Reliability analysis tool: Prodeto. Technical report, ECN, 2000.

[15] M. Buhl Jr., A. Wright, and K. Pierce. Wind turbine design codes: A comparison of the structural response. In *Proceeding of the ASME Wind Energy Symposium*, Reno, 2000. American Society of Mechanical Engineers, ASME.

[16] T. Burton, D. Sharpe, N. Jenkins, and E. Bossanyi. *Wind Energy Handbook*. John Wiley, West Sussex, 2001.

[17] D. Cartwright and M. Longuet-Higgins. The statistical distribution of the maxima of a random function. *Proceeding of the Royal Society of London*, pages 212–232, 1956.

[18] S. Chakrabarti. *Hydrodynamics of Offshore Structures*. WIT Press, Southampton, 1987.

[19] P. Chaviaropoulos. Probabilistic analysis of extreme wind events. *Wind Engineering*, 21(3), 1997.

[20] P. Cheng. Probabilistic design method applied to extreme response of offshore wind energy converters. Technical report, Section Wind Energy Report: Delft University of Technology, 2001.

[21] P. Cheng and W. Bierbooms. Statistic of extreme loads for wind turbines. In *Proceeding of the ICWE conference*, Copenhagen, 1999. Danish Wind Engineering Society, Balkema.

[22] P. Cheng and W. Bierbooms. Extreme gust loading for wind turbines during operation. *Journal of Solar Energy Engineering*, 123(4):356–363, 2001.

[23] P. Cheng and G. van Bussel. Extreme loading of offshore wind turbines using constrained simulations. In *Proceeding of the OWEMES conference*, Siracusa, 2000. ENEA, ENEA.

[24] P. Cheng and G. van Bussel. A probabilistic approach to extreme loading of an offshore wind energy system. In *Proceeding of the 8th International Conference on Structural Safety and Reliability*, Los Angeles, 2001. International Association for Structural Safety and Reliability (IASSAR), IASSAR.

[25] J. Conte and A. Couch. Field verification of linear and nonlinear hybrid wave models for offshore tower response prediction. In *Proceeding of the Conference of Offshore Mechanics and Artic Engineering*, Florence, 1996. ASME.

[26] N. Cook. Towards better estimation of extreme winds. *Journal of Wind Engineering and Industrial Aerodynamics*, 9:295–323, 1982.

[27] N. Cook. Discussion on modern estimation of the parameters of the weibull wind speed distribution for wind speed energy analysis by J.V. Seguro, T.W. Lambert. *Journal of Wind Engineering and Industrial Aerodynamics*, 89:867–869, 2001.

[28] R. D'Agostino and M. Stephens(eds). *Goodness-of-Fit Techniques*. Dekker, New York, 1986.

[29] Danish Energy Agency. Recommendation for technical approval of offshore wind turbines. Technical report, Danish Energy Agency, 2001.

[30] A. Davenport. Note on the distribution of the largest value of a random function with application to gust loading. *Proceeding of the Institution of Civil Engineering*, 28:187–195, 1964.

[31] R. Dean. Stream function representation of non-linear ocean waves. *Journal of Geophysical Research*, 70(18):4561–72, 1965.

[32] O. Ditlevsen and H. Madsen. *Structural Reliability Methods*. John Wiley, New York, 1996.

[33] DNV. Guideline for offshore structural reliability analysis - general. Technical report, Det Norske Verita, 1995.

[34] DNV/Risø. *Guidelines for Design of Wind Turbines*. DNV/Risø, Roskilde, 2001.

[35] B. Efron and R. Tibshirani. *An Itroduction to the Bootstrap*. Chapman and Hall, New York, 1993.

[36] M. Efthymiou, J. van de Graaf, P. Tromans, and I. Hines. Reliability-based criteria for fixed steel offshore platforms. *Journal of Offshore Mechanics and Arctic Engineering*, 119(2):120–124, 1997.

[37] ESDU. Esdu volume 1c:aerodynamics. Technical report, ESDU, 1992.

[38] M. Ferguson(ed), M. Kühn, G. van Bussel, W. Bierbooms, T. Cockerill, B. Goeransson, L. Harland, J. Vugts, and R.Hes. *Opti-OWECS Final Report Vol. 4: A Typical Design Solution for an Offshore Wind Energy Conversion System*. Delft University of Technology, Delft, 1998.

[39] L. Fitzwater and S. Winterstein. Predicting wind turbine loads from limited data:comparing random process and random peak models. In *Proceeding of the ASME Wind Energy Symposium*, Reno, 2001. American Society of Mechanical Engineers, ASME.

[40] G. Forristal. On the statistical distribution of wave height in a storm. *Journal of Geophysical Research*, 83, 1978.

[41] L. Freris. *Wind Energy Conversion System.* Prentice Hall International, Cambridge, 1990.

[42] P. Friis-Hansen and L. Nielsen. On the new wave model for the kinematics of large ocean waves. In *Proceeding of the Conference of Offshore Mechanics and Artic Engineering*, Copenhagen, 1995. ASME.

[43] Germanische Lloyd. *Regulation for the Certification of Offshore Wind Energy Conversion System.* Germanische Lloyd, Hamburg, 1995.

[44] Germanische Lloyd. *Regulation for the Certification of Wind Energy Conversion System.* Germanische Lloyd, Hamburg, 1999.

[45] I. Gringorten. A plotting rule for extreme probability paper. *Journal of Geophysics Research*, 68:813–814, 1963.

[46] A. Halfpenny. *Dynamic Analysis of Both On and Offshore Wind Turbines in The Frequency Domain.* PhD thesis, UCL, 1998.

[47] K. Hansen, G. Larsen, and M. Courtney. Database on wind characteristics. In *Proceeding of the European Wind Energy Conference*, Copenhagen, 2001. European Wind Energy Association, EWEA.

[48] L. Harland, P. Taylor, and J. Vugts. The extreme force on an offshore structure and its variability. *Applied Ocean Research*, 20(1):3–14, 1998.

[49] L. Harland, J. Vugts, P. Jonathan, and P. Taylor. Extreme response of non-linear dynamic systems using constrained simulations. In *Proceeding of the Conference of Offshore Mechanics and Artic Engineering*, Florence, 1996. ASME.

[50] R. Harris. Gumbel re-visited - a new look at extreme value statistics applied to wind speeds. *Journal of Wind Engineering and Industrial Aerodynamics*, 59:1–22, 1996.

[51] J. Hojstrup, K. Hansen, B. Pedersen, and M. Nielsen. Non-gaussian turbulence. In *Proceeding of the European Wind Energy Conference*, Nice, 1999. European Wind Energy Association, James and James.

[52] S. Hsu. *Coastal Meteorology.* Academic Press, San Diego, 1988.

[53] IEC-TC88. *Safety of Wind Turbine Generator Systems (Draft).* IEC, Geneva, 1997.

[54] JCSS. Jcss probabilistic model code part 2: Loads. Technical report, JCSS, 2000.

[55] A. Jha. *Nonlinear Stochastic Models for Ocean Wave Loads and Responses of Offshore Structures and Vessels*. PhD thesis, Stanford University, Department of Civil Engineering, 1997.

[56] K. Johannessen, T. Meling, and S. Haver. Joint distribution for wind and waves in the northern north sea. In *Proceeding of the 11th ISOPE conference*, Stavanger, 2001. International Society of Offshore and Polar Engineering, ISOPE.

[57] M. Kühn. *Dynamics and Design Optimisation of Offshore Wind Energy Conversion System*. PhD thesis, Delft University of Technology, Section Wind Energy. Department of Civil Engineering, 2001.

[58] M. Kühn(ed), T. Cockerill, L. Harland, R. Harrison, C. Schöntag, G. van Bussel, and J. Vugts. *Opti-OWECS Final Report Vol. 2:Methods Assisting the Design of Offshore Wind Energy Conversion Systems*. Delft University of Technology, Delft, 1998.

[59] C. Lange. *Probabilistic Fatigue Methodology and Wind Turbine Reliability*. PhD thesis, Stanford University, Department of Civil Engineering, 1996.

[60] G. Larsen and S. Petersen. Experimental investigation of ultimate loads. In *Proceeding of the European Wind Energy Conference*, Copenhagen, 2001. European Wind Energy Association, James and James.

[61] A. Law and W. Kelton. *Simulation Modeling and Analysis*. McGrawhill Inc., New York, 1991.

[62] H. Madsen. Omission sensitivity factors. *Structural Safety*, 5, 1988.

[63] H. Madsen, S. Krenk, and N. Lind. *Methods of Structural Safety*. Prentice Hall Inc., Englewood Cliffs NJ., 1986.

[64] H. Madsen and C. Turkstra. Load combinations in codified structural design. *Journal of the Structural Division*, 132:2527–2543, 1980.

[65] P. Madsen, K. Pierce, and M. Buhl. Predicting ultimate loads for for wind turbines design. In *Proceeding of the ASME Wind Energy Symposium*, Reno, 1999. American Society of Mechanical Engineers, ASME.

[66] H. Matthies, A. Garrad, and M. S. et al. *Study of Offshore Wind Energy in the EC*. Verlag Natuerliche Energie, Brekendorf, 1995.

[67] R. Melchers. *Structural Reliability: Analysis and Prediction*. Ellis Harwood, Chichester, 1987.

[68] D. Molenaar and S. Dijkstra. State-of-the-art of wind turbine desing codes: Main features overview for cost-effective generation. *Wind Engineering*, 23(5):295–311, 1999.

[69] G. Neumann and W. Pierson. *Principle of Physical Oceanography*. Prentice Hall International, Cambridge, 1963.

[70] T. Onoufriou. Overview of advanced structural and reliability techniques for optimum design of fixed offshore platforms. *Journal of Constructional Steel Research*, 44(3):181–201, 1997.

[71] D. Oscar and T. Paez. Analysis of wind turbines on offshore support structures excited by random wind and random waves. Technical report, Sandia National Laboratories Report SAND87-1689, 1988.

[72] D. Peters, C. Shaw, C. Grant, J. Heidemanand, and D. Szabo. Modelling the north sea through the north european storm study. In *Proceeding of the 25th Offshore Technology Conference*, Houston, 1993.

[73] S. Petersen, G. Larsen, I. Antoniou, S. Lind, and M. Courtney. Experimental investigation of ultimate loads. In *Proceeding of the European Wind Energy Conference*, Nice, 1999. European Wind Energy Association, James and James.

[74] J. Pickands. Statistical interference using order statistics. *Annals of Mathematical Statistics*, (3):119–131, 1975.

[75] R. Reiss and M. Thomas. *Statistical Analysis of Extreme Values*. Birhaeuser Verlag, Basel, 1997.

[76] K. Ronold and G.C.Larsen. Reliability-based design of wind-turbine rotor blades against failure in ultimate loading. *Journal of Engineering Structures*, 22:565–574, 2000.

[77] M. Rosenblatt. Remarks on a multivariate transformation. *Annals of Statistics*, 23:470–472, 1952.

[78] T. Sarpakaya and M. Isaacson. *Mechanics of Wave Forces on Offshore Structures*. Van Nostrand Reinhold, New York, 1981.

[79] H. Schaub. *Probabilistische Sicherheitsanalyse Turmartiger Bauwerke unter Aerodynamischer Beanspruchung*. PhD thesis, Bochum University, Department of Civil Engineering, 1981.

[80] J. Schepers et. al. Verification of european wind turbine design codes. In *Proceeding of the European Wind Energy Conference*, Copenhagen, 2001. European Wind Energy Association, EWEA.

[81] M. Shinozuka and C. Jan. Digital simulation of random processes and its application. *Journal of Sound and Vibration*, 25(1):111–128, 1972.

[82] H. Snel. Sectional prediction of lift coefficients on rotating wind turbine blades in stall. Technical report, ECN:ECN-C-93-052, 1994.

[83] H. Snel. Review of the present status of rotor aerodynamics. *Wind Energy*, 1:46–69, 1998.

[84] P. Soerensen. Frequency domain modelling of wind turbine structures. Technical report, Risoe report R749(EN), 1995.

[85] M. Tayfun. Joint distributions of large wave heights and associated periods. *Journal of the Waterways and Harbors Division*, 119(3):261–273, 1993.

[86] W. Timmer. Measured section performance of rotating blades as input to the design of inboard airfoils. In *Proceeding of the European Wind Energy Conference*, Nice, 1999. European Wind Energy Association, James and James.

[87] P. Tromans, A. Anaturk, and P. Hagemeijer. A new model for the kinematics of large ocean waves-application as a design wave. In *Proceeding of the 1st ISOPE conference*, Edinburgh, 1991. International Society of Offshore and Polar Engineering, ISOPE.

[88] P. Tromans and L. Vanderschuren. Response based design method in the north sea: Application of a new method. In *Proceeding of the 27th Offshore Technology Conference*, Houston, 1995.

[89] Unknown. www.windatabse.com. Technical report, Risoe report R749(EN), 1995.

[90] B. van den Horn, L. Rademakers, and T. Verbruggen. Reliability analysis and design review of the newecs-45 part 2: Probabilistic fatigue analyses. Technical report, ECN, 1994.

[91] P. van Gelder, J. van Noortwijk, and M. Duits. Selection of probability distributions with a case study on extreme oder river discharges. *Safety and Reliability*, 2, 1999.

[92] R. van Rooij. Terminology, reference systems and conventions. Technical report, Delft University Wind Energy Research Institute, DUT, 2001.

[93] A. van Wijk, A. Beljaars, A. Holtslag, and W. Turkenburg. Evaluation of stability correction in wind speed profiles over the north sea. *Journal of Wind Engineering and Industrial Aerodynamics*, 33:551–566, 1990.

[94] A. Vrouwenvelder and J. Vrijling. *Probabilistisch Ontwerpen*. Delft University of Technology, Delft, 1993. Lecture Note in Ducth.

[95] M. Wastling, D. Quarton, J. Wei, H. Matthies, and T. Schellin. Study of offshore wind energy in the ec vol.4 the dynamic loading of offshore wind turbines. Technical report, Garrad Hassan and Partners Germanischer Lloyd, 1993.

[96] J. Wheeler. Method of calculating forces produced by irregular waves. *Journal of Petroleum Technology*, 22:359–367, 1970.

[97] J. Wieringa. Gust factor over open water and built up country. *Boundary Layer Meteorology*, 3:424–441, 1973.

[98] R. Wilson and P. L. et.al. Aerodynamic performance of wind turbines. Technical report, U.S. Department of Energy:ERDA/NSF/04014-76/1, 1995.

[99] S. Winterstein. Nonlinear vibration models for extremes and fatigue. *Journal of Engineering Mechanics*, 114(10):1772–1790, 1988.

[100] S. Winterstein, T. Ude, and G. Kleiven. Spring and slow-drift responses: Predicted extremes vs. simulation. In *Proceeding of the Behaviour of Offshore Structures Conference*, MIT Cambridge, 1994.

[101] S. Winterstein, T. Ude, and T. Marthinsen. Volterra models of ocean structures: Extreme and fatigue reliability. *Journal of Engineering Mechanics*, 120(6):1369–1385, 1994.

[102] M. Zaaijer. Duwecs reference guide. Technical report, Institute for Wind Energy, DUT, 1999.

[103] M. Zaaijer and J. Vugts. Sensitivity of dynamics of fixed offshore support structures to foundation and soil properties. In *Proceeding of the European Wind Energy Conference*, Copenhagen, 2001. European Wind Energy Association, EWEA.

[104] S. Zachary, G. Feld, G. Ward, and J. Wolfram. Multivariate extrapolation in the offshore environment. *Applied Ocean Research*, 20(3):273–295, 1998.

Appendix A

Appendix

List of Distribution functions used PDF

- Normal $f(x) = \frac{1}{\sqrt{2\pi\sigma^2}} e^{-\frac{(x-\mu)^2}{2\sigma^2}}$
- Log-Normal $f(x) = \frac{1}{x\sqrt{2\pi\sigma^2}} e^{-\frac{(\ln x-\mu)^2}{2\sigma^2}}$
- Exponential $f(x) = \frac{1}{s} e^{-\frac{x-u}{s}}$
- Gamma $f(x) = \frac{s^{-k}(x-u)^{k-1}e^{-\frac{x-u}{s}}}{\Gamma(k)}$
- Weibull $f(x) = \frac{k}{s}\left(\frac{x-u}{s}\right)^{k-1} e^{-\left(\frac{x-u}{s}\right)^k}$
- Gumbel $f(x) = \frac{e^{-\left(\frac{x-u}{s}\right)} e^{-e^{\left(\frac{x-u}{s}\right)}}}{s}$
- GEV $f(x) = e^{-(1+\gamma\frac{(x-u)}{\sigma})^{-\frac{1}{\gamma}}}(1+\gamma\frac{(x-u)}{\sigma})^{-\frac{1}{\gamma}-1}, \quad 1+\gamma(x-u)/\sigma > 0,\ \gamma \neq 0.$
- GP $f(x) = (1+\gamma\left(\frac{x-\mu}{s}\right))^{-(1+\frac{1}{\gamma})}$ for $\left\{ \begin{array}{c} x \geq 0,\ \gamma > 0 \\ \frac{1}{|\gamma|} > x \geq 0,\ \gamma < 0 \end{array} \right\}$

List of Distribution functions used CDF

- Normal $F(x) = \Phi\left(\frac{x-\mu}{\sigma}\right)$
- Log-Normal $F(x) = \Phi\left(\frac{\ln x - \mu_{\ln x}}{\sigma_{\ln x}}\right)$
- Exponential $F(x) = 1 - e^{-\left(\frac{x-u}{s}\right)}$
- Gamma $F(x) = \frac{s^{-k}}{\Gamma(k)} \int_0^x (x-u)^{k-1} e^{-\frac{x-u}{s}} dt$
- Weibull $F(x) = 1 - e^{-\left(\frac{x-u}{s}\right)^k}$

- Gumbel $F(x) = e^{-e^{-\left(\frac{x-u}{s}\right)}}$
- GEV $F(x) = e^{-(1+\gamma\frac{(x-u)}{\sigma})^{-\frac{1}{\gamma}}}, \quad 1+\gamma(x-u)/\sigma > 0,\ \gamma \neq 0.$
- GP $F(x) = 1-(1+\gamma\left(\frac{x-\mu}{s}\right))^{-\frac{1}{\gamma}}$ for $\left\{ \begin{array}{c} x \geq 0,\ \gamma > 0 \\ \frac{1}{|\gamma|} > x \geq 0,\ \gamma < 0 \end{array} \right\}$

Appendix B

Structural response of an OWT in the frequency domain

B.1 Methodology

A short description of the methodology to quantify the extreme response of an offshore wind turbine in the frequency domain using linear models is given

For the frequency domain analysis, a stall controlled wind turbine is used (see Chapter 4). It is assumed for this wind turbine that the extreme responses (flap moment and OTM) occur during standstill, unlike the pitch controlled wind turbine, for which the extreme responses occur during turbine operation. To obtain the response spectrum of a rotating wind turbine one needs special programs (see [46] and [84]) to deal with the rotational effects. But the methodology remains essentially the same.

Figure B.1 illustrates the main steps of the frequency domain calculation. First, a quantitative description of the external conditions is required. This can be a scatter diagram or a joint distribution of the sea state parameters (including the mean wind speed). The short-term description of the environment can be expressed in a spectral form, such as a wind speed spectrum or a wave elevation spectrum. The wind load spectrum is obtained by multiplying a load transfer function with the wind speed spectrum. The load models describe how the external condition is transferred to external loads. For large structures, where local load variations exist, the cross load spectrum needs to be determined, for example the aerodynamic loads on the rotor.

The wave load calculated with the Morison equation is inherently non-linear. To apply the frequency domain approach one needs to linearise the drag term [11]. The spatial variation of the wave load in the horizontal direction can be neglected for the monotower because the diameter of the pile is small compared

to the wave length, but not for tripod or lattice type structures.

Once the load spectrum is known, the response spectrum can be obtained by means of a response transfer function between response and loads. This response transfer function corresponds to the impulse response function in the time domain. The area under the response spectrum represents the variance of the process. Hence, the standard deviation of the (Gaussian) response can be determined.

For the flap moment, it is necessary to determine also the mean response as a consequence of the mean wind speed. The conditional response distribution for the given external conditions can be described with a Normal distribution with the mean and the standard deviation obtained above. The convolution with the probability of all possible sea states or relevant sea states yield the response distribution of a random sea state. Extrapolating it to a yearly distribution can be done by applying the Equation B.1.

$$P_a^N = [F(m = a)_{\mathrm{rand\,om}}]^N \tag{B.1}$$

where, the probability of non-exceedence P_a^N for a given value $m = a$ and for a period of N sea states is given.

B.2 Application

B.2.1 External conditions

The frequency domain method is applied to determine the response distribution of a stall controlled OWT. The operating condition considered is the standstill during extreme wind conditions, that is, wind speeds above the cut-out wind speed. The models used in the calculation are given in the Table B.1. The mean wind speeds considered here are all above the cut-out wind speed, hence an extreme wind speed distribution can be applied.

The turbulence intensity is 12% for all the mean wind speeds as specified in the GL standard for OWT. The exponential coherence model describes the cross correlation of the wind speed spectra at different locations, which is necessary to obtain the cross load spectra. The significant wave height and the mean upcrossing period are coupled to the mean wind speed using the empirical relation suggested in [69]. This is strictly speaking not correct as explained in the description of the offshore environment conditions (see Chapter 3). There is a significant scatter between the mean wind speed, the significant wave height and mean upcrossing period of the waves.

As mentioned in the Chapter Wind Turbine Concepts, the water depth for the stall regulated turbine is 20 m. For this shallow water location, the empirical relation predicts a significant wave height that is twice as much as the 100 year significant wave height estimated from the joint probability density distribution (see Table 3.1). The predicted zero upcrossing period is also much larger than the zero upcrossing period given by the scatter diagram for this location. This

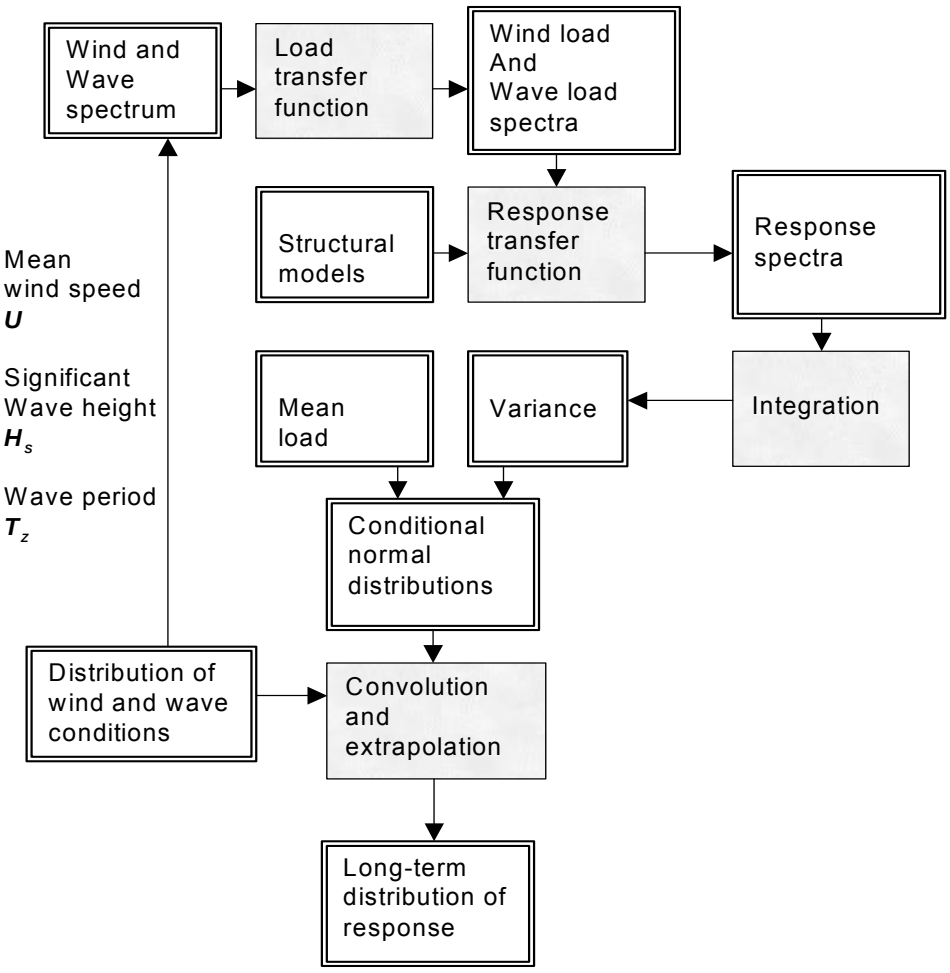

Figure B.1: General description of a frequency domain analysis for the response calculation.

Table B.1: Models used in the Frequency domain calculation

Models	
mean wind speed distribution	Gumbel
turbulence spectrum	von Karman
turbulence intensity	0.12
coherence model	Exponential
wave elevation spectrum	JONSWAP

can lead to an overestimate of the quasi-static part of the wave loading but also to an underestimation of the dynamic part of the wave loading.

However, the empirical relation between the mean wind speed, the significant wave height and wave period is used in this frequency domain study for the sake of reducing the number of required calculations. In the time domain analysis, a three parameter scatter diagram is used.

B.2.2 Load and response

The wind and wave spectra are converted into load spectra via a load transfer function. The load models for wind and waves are described in the previous chapter. The loads are essentially non-linear and need to be linearised. The linearisation of the Morison equation can be found in [11] and the linearisation of the wind load in [79].

Modal analysis is applied to calculate the response spectra. The advantage is that the structural continuum is discretised into orthogonal modes and every mode can be dealt with as a simple mass-spring system. The structural response is then the superposition of the individual responses of each mode. The blade and tower modes are calculated using the finite element program ANSYS [2]. The first 3 blade modes in the flap direction are shown in Figure B.2 and Figure B.3 shows the corresponding flap moments.

It has to be noticed that the modal decomposition is efficient for calculation of dynamic response. The structural response due to wave loading has a considerable quasi-static part. In the time domain calculation, this is partly taken into account by adding higher modes as static modes in the calculation.

In this case, 5 modes are being used in the response analysis. This will certainly underestimate the quasi-static response but this calculation is aimed at a demonstration of the probabilistic approach rather than accurate response calculation, for this reason one will bear this imperfection of the response calculation in mind.

By integrating the product of the response transfer function and the cross load spectra along the length of the blade, the response spectrum for a given location is obtained

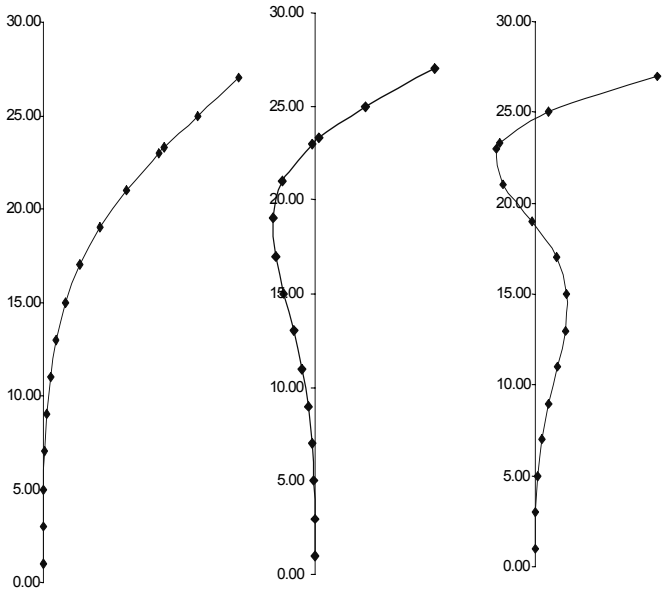

Figure B.2: The first three modes of the blade in the flap direction. The maximum displacement is normalised to 1.

B.2.3 Response distributions

The load input is Gaussian, the response model is linear, hence the response is also Gaussian. The mean value of the response is the static response of the structure to the mean wind speed. The standard deviation of the response is derived from the variance of the response, which is the area under the response spectrum. The distribution parameters of the flap moment at the blade root are shown in Figure B.4.

It can be seen that the mean value of the distribution increases quadratically with the mean wind speed in accordance with the quadratic increase of the wind load with the mean wind speed. The standard deviation of the flap moment increases much less rapidly with the mean wind speed than the mean flap moment. The fluctuating part of the wind load is also proportional to the square of the mean wind speed and to the turbulence intensity. Since the turbulence intensity is rather low, 0.12, the quadratic increase with the mean wind speed is less pronounced for the standard deviation of the wind load than for the mean value of the wind load. This can be seen for the flap moment as well.

For the support structure the overturning moment at the sea bottom is determined. The aerodynamic loads from the blades are transformed into a single force on the tower top. The wind loads are superimposed with the wave loads. The two load processes are considered to be not correlated in the short-term. The standard deviation of the overturning moment is shown in Figure

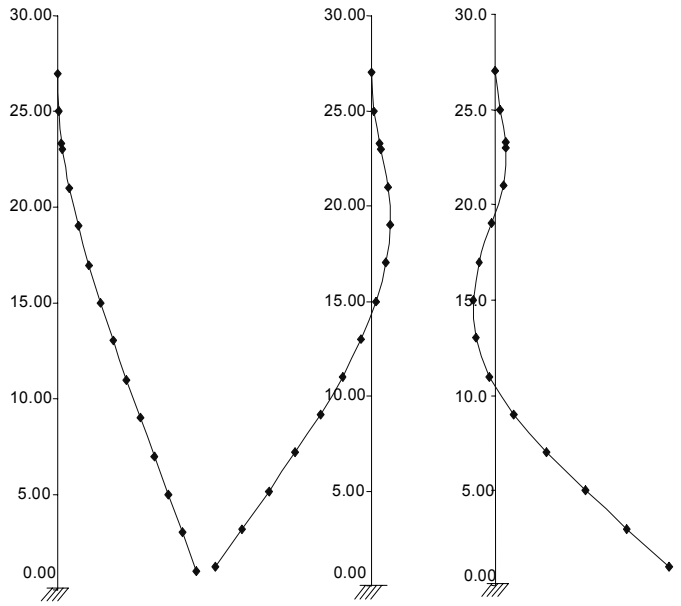

Figure B.3: The flap moments corresponding to the first three flap modes. The horizontal scale is not shown because the difference in the magnitudes differ considerably from mode to mode.

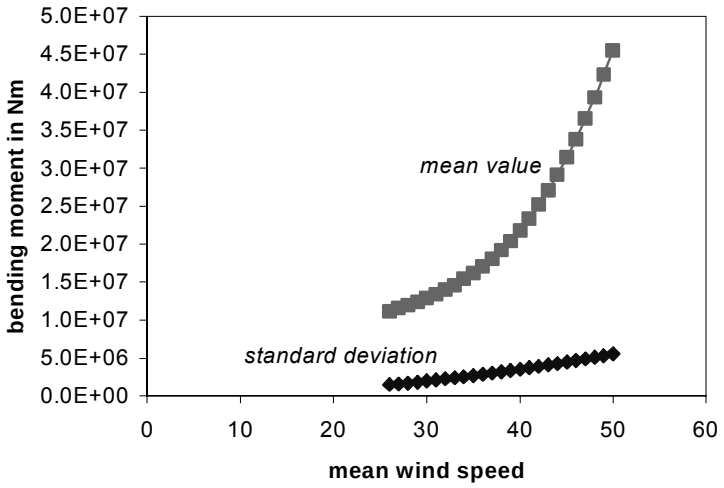

Figure B.4: Mean and standard deviation of the blade root flap moment for variable mean wind speeds.

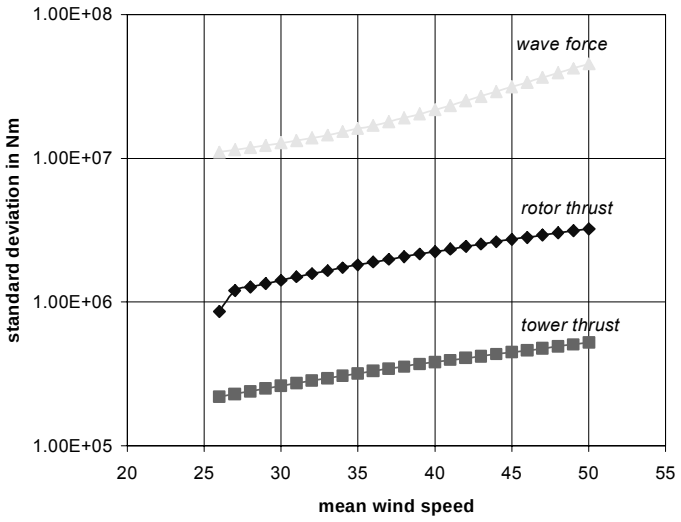

Figure B.5: Standard deviation of the Overturning moment from different load sources as function of the mean wind speed.

B.5.

The wave loads contribute the most to the standard deviation of the OTM, followed by the thrust force from the blade. The aerodynamic loads contribute to the mean value of the OTM. It has to be pointed out that the calculated wave load using the empirical relationship between the mean wind speed and the significant wave height from [69] is very large because of the overestimate of the significant wave height. The significant wave height corresponding to the maximum mean wind speed in the scatter diagram is about 1/2 of the significant wave height predicted using the empirical relationship. Again, it shows that the use of the empirical coupling of the mean wind speed and the significant wave height is not appropriate. In the statistical analysis of the results obtained by time domain simulations, a three parameter scatter diagram is used.

These conditional distributions have to be convoluted with the distribution of the extreme mean wind speed. The result is the response distribution for a random (extreme) mean wind speed. This distribution can be extrapolated to a longer period T using Equation B.1. The number N of independent sea states is the number of hours in the period of T years where the mean wind speed is above cut-out wind speed. The distribution for different periods T is illustrated in Figure B.6. This figure shows the distribution of the flap moment in a stationary period of 10 minutes for different periods T, and not the largest flap moment.

The convolution with the Gumbel distribution has influences on the long-term distribution of the response. It can be seen that the long-term distribution has a positive skewness and the kurtosis is higher than the kurtosis of the

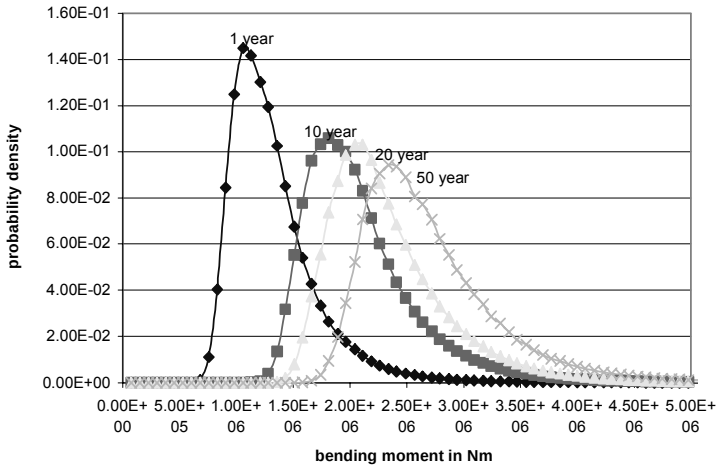

Figure B.6: Distribution of the extreme blade root flap moment for different periods T.

Gaussian distribution of the conditional distributions. Through the extrapolation of the distribution, the heavier tail of the Gumbel distribution becomes more explicit.

B.2.4 Frequency Domain or Time Domain method

The question here is whether the FD or TD method should be used. The FD method can be easily implemented and the computational effort is considerably less than the TD method. However, there are some issues that can not be taken into account with the FD method. For example, it is known that the foundation properties can influence the structural response significantly and the characteristics of the foundation are essentially non-linear and this can not be taken into account with the conventional FD method. In practice, it depends on how the non-linearities affect the response characteristics and the type of calculations. For early design stages, FD method is still an attractive option.

Furthermore, the external loads of wind and wave also require linearisation. The formulation of the frequency method becomes more complicated for a rotating structure. There are programs available that can calculate the response of a rotating blade. Theoretically one can use the thrust force from the rotor to calculate the contribution of the wind to the OTM, though the interaction of the blade and support structure is not taken into account. The dynamics of the blades deliver an important portion of aerodynamic damping to the support structure and this has to be considered.

It can be said that the presented level of the modelling for wind turbines in frequency domain is not sufficient for an accurate calculation of the extreme responses. If the interest lies in the determination of accurate structural responses,

then TD method is to be preferred.

The statistics of the response treated here are the total response during a stationary period. This means, it is not a distribution about the maxima. Although, the probability distribution of the maximum response can be determined from the distribution parameters of the conditional distribution using the methodology supplied in the Chapter Process Model, assuming that the response process is Gaussian.

The main part of this thesis is dedicated to the TD methods which constitute the principal focus of the research. Nevertheless, for fast estimate of the extreme response one can still use the FD method, provided that accurate models are available.

Appendix C

Main data of the two reference offshore wind turbines

The main data of the pitch regulated is shown in Table C.1 and for the stall regulated turbine they are listed in Table C.2. Table C.3 contains the parameters of the time domain simulations. These parameters are used if they are not explicitly specified in the text.

Table C.1: Main data of the pitch regulated offshore wind turbine

Pitch regulated offshore wind turbine WTS-80	
Rotor diameter	80 m
Rated power	3 MW
Number of blades	2
Hub height	78 m
Operating range	5-25 m/s
Rated wind speed	13.7 m/s
Power control	full span pitch
Support structure	piled monotower
Water depth	20 m
Maximum diameter of the pile	3.5 m
First natural frequency of the support structure	0.278 Hz

Table C.2: Main data of the stall regulated offshore wind turbine

Stall regulated offshore wind turbine	
Rotor diameter	54 m
Rated power	1 MW
Number of blades	3
Hub height	48 m
Operating range	3.5-25 m/s
Rated wind speed	16 m/s
Power control	fixed blade pitch
Support structure	piled monotower
Water depth	20 m
Maximum diameter of the pile	3 m
First natural frequency of the support structure	0.54 Hz

Table C.3: Main parameters of the time domain simulations

parameter of the time domain simulations	
Turbulence intensity	12%
Wind spectrum	von Karman
Wind shear power law exponent	0.11
Coherence function	IEC standard[53]
Wave spectrum	Pierson-Moskowitz
Sea currents	0 m/s

Samenvatting (Dutch)

Windenergie buitengaats maakt momenteel een snelle ontwikkeling door. Het wordt gezien als een belangrijke aanvulling voor windenergie op land. Grootschalige windparken buitengaats zullen een aanzienlijke aandeel vormen van de totale duurzame energie opwekking.

Het ontwerp van windturbines op zee geeft ook nieuwe uitdagingen vanwege de omgevingscondities in de Noordzee. De hydrodynamische belastingen leiden tot extra belasting op de constructie en de gecombineerde extreme wind en golf belastingen kunnen een belangrijke onderdeel van het ontwerp van de windturbine uitmaken. Extreme omgevingscondities hoeven niet automatisch tot extreme responsies van de windturbine te leiden, daarom wordt in deze studie de responsie van de windturbine buitengaats beschouwd.

De omgevingscondities van de betreffende locatie van de windturbine kan beschreven worden met een gezamenlijke verdeling van de windsnelheid, significante golfhoogte en de golfperiode. Uit deze verdeling kan men een contour van, bijvoorbeeld, 100 jaar bepalen. Uit deze contourlijn volgt de extreme condities van wind en golven.

De extreme responsie van een windturbine buitengaats kan berekend worden in frequentie of tijddomein. De tijddomein methode wordt hier toegepast omdat de windturbine een niet-lineair responsie gedrag heeft. De resultaten van de simulaties worden op verschillende manieren geanalyseerd. De MAX methode gebruikt de maximale waarde van elke simulatie. De POT methode gebruikt de locale maxima boven een gedefinieerde drempel, en de Proces methode maakt gebruik van de statistische momenten van de tijdreeks van de responsie. Met deze drie methoden kan de verdeling van de extreme responsie van de windturbine bepaald worden.

Omdat het aantal benodigde simulaties exponentieel stijgt met het aantal stochastische variabelen moet dat aantal beperkt blijven. Op basis van een gevoeligheidsanalyse zijn de volgende drie variabelen gekozen: de gemiddelde windsnelheid, de significante golfhoogte en de (positieve) nuldoorgangperiode. Het vereiste aantal simulaties en de lengte van de simulaties zijn bestudeerd. Voor de MAX methode worden 50 simulaties van 40 minuten elk aanbevolen. De resultaten met de MAX methode worden gebruikt als vergelijkingswaarde voor de POT en Proces schattingen. Om een schatting van de responsie verdeling te krijgen, die vergelijkbaar is met de schatting van de MAX methode, zijn voor

de POT en Proces methoden minder aantal simulaties nodig.

De onzekerheden omtrent de verdelingsfuncties en de verdelingsparameters worden in rekening gebracht met een Bayesiaanse analyse. De invloed van de onzekerheden van de verdelingsparameters is in dit geval niet significant. De variatie van de schatting die veroorzaakt wordt door de verschillende verdelingsfuncties is aanzienlijk groter. De Bayesiaanse analyse levert een formeel criterium voor het kiezen van een verdelingsfunctie.

In theorie dragen alle voorwaardelijke verdelingen bij aan de lange termijn verdeling. Echter, het is niet noodzakelijk om alle verdelingen mee te nemen omdat de staart van de lange termijn verdeling in dit geval wordt bepaald door een paar verdelingen. Daarom het is toereikend alleen die zeetoestanden mee te nemen, die de extreme responsies van een windturbine veroorzaken.

De drie methoden die hier zijn behandeld berekenen de verdeling van de responsie waaruit de responsie met een bepaalde terugkeertijd, bijvoorbeeld 100 jaar, volgt. In de praktijk worden vaak de 100 jaar externe conditie bepaald en wordt aangenomen dat de bijbehorende responsie ook een terugkeertijd van 100 jaar heeft. De twee benaderingen gebaseerd op de responsie en de externe conditie zijn toepast op twee voorbeeld windturbines, een met overtrekregeling en een andere met bladhoekregeling.

Een van de extreme condities die beschouwd is, is een windvlaag met een extreme golf. De huidige ontwerpcodes beschrijven de extreme windvlaag en extreme golven met deterministische modellen. Met de zogenoemde 'Constrained' simulatie kan men ook stochastische modellen van extreme windvlagen en golven construeren. Voor de windturbine met bladhoekregeling is de windvlaag uit 'constrained' simulatie niet maatgevend omdat de regelaar de windvlaag weg kan regelen. Voor de windturbine met overtrekregeling leiden de deterministische en stochastische windvlagen tot soortgelijke extreme responsies.

Een ander punt van discussie is het gelijktijdig optreden van een extreme windvlaag en extreme golf. In werkelijkheid treedt een extreme windvlaag en een extreme golf niet tegelijkertijd op en daarom wordt een bepaald tijdverschil aangenomen tussen de maxima van wind en golven. Voor de deterministische modellen neemt de extreme responsie heel snel af met het tijdverschil, terwijl de afname van de maximale responsie voor de 'constrained' modellen meer geleidelijk is. Dit tijdverschil tussen de maxima heeft een duidelijke invloed op de extreme responsie van de ondersteuningsconstructie maar niet voor de blad responsie.

De methode gebaseerd op de externe conditie geeft een heel andere schatting dan de methoden die gebaseerd zijn op de responsie, omdat de extreme responsie niet altijd correspondeert met de extreme externe condities. Voor de overtrekturbine, is er een duidelijk verband tussen de extreme responsie en de extreme externe condities maar niet voor de bladhoekgeregelde turbine.

De extreme responsie die hier zijn behandeld treden op onder normale operationele condities. Er zijn andere situaties die resulteren in extreme responsies, bijvoorbeeld het falen van de bladhoekregeling, scheve aanstroming enz. Op deze bijzondere situaties wordt in deze studie niet ingegaan. De conclusies zijn in principe geldig voor de gekozen turbine configuraties en de gekozen locatie,

maar de methodologie is algemeen toepasbaar op andere turbine typen, andere locaties en andere extreme situaties kunnen meegenomen worden.

About the author

Po Wen Cheng was born on November the 17th, 1970, in Chang-Hua, Taiwan. He completed secondary school in Buenos Aires in 1988. He spent the following three years studying medicine, architecture and civil engineering in three different universities before taking the entry exam to the German universities in 1991 He was admitted to the Technische Universität Berlin, Faculty of Mechanical Engineering. He graduated in 1997 from the Faculty of Aeronautics and Aerospace Engineering.

In 1996 he received a scholarship from the Berliner Senate which enabled him to undertake the master thesis 'Optimisation of Rotor Blades for Offshore Wind Turbines' at the Institute for Wind Energy, Delft University of Technology.

Between 1997 and 2002, he has been employed as a research assistant at the Institute for Wind Energy, working on this Ph.D. thesis as well as on national and EU funded projects.

He spends his summers in Scandinavia attending summer schools, on a broad range of subjects, from energy planning, Swedish language to neoliberalism. In autumn 2000 he completed an internship at the branch of Energy and Transport, at the headquarter of the United Nations, New York, assisting projects assessment.